

# The role of glial cells in a mouse model of inherited retinal dystrophies

**Yingdi Chen**

**Institute of Neuroscience  
Faculty of Medical Sciences  
Newcastle University**

Thesis submitted for the degree of Doctor of Philosophy at  
Newcastle University December 2018

The Candidate confirms that the work submitted is her own  
that appropriate credit has been made to the work of others

This copy has been supplied on the understanding that it is  
copyright material and that no quotation from the thesis may  
be published without proper acknowledgement



## Abstract

Inherited retinal dystrophies are a heterogeneous group of degenerative disorders characterised by genetically induced photoreceptor loss, leading to vision loss. Despite their genetic and clinical complexity, most inherited retinal dystrophies follow a common pathological pathway characterised by photoreceptor death and glial activation. Although glial activation has been widely reported in retinal degenerative diseases, the underlying mechanisms involved in the neuron-glia interaction and the role of glial activation in the degenerative process remain unclear. In this thesis, investigation of the relationship between glial activation and photoreceptor loss was conducted using a mouse model of Leber congenital amaurosis, the cone-rod homeobox (Crx) knockout mouse. The first part of the study aimed to establish a framework of photoreceptor death and glial activity during the degeneration process. Thinning of the outer nuclear layer suggested that, in the Crx retina, photoreceptors do not die at a constant rate, but occurred mostly during two rapid degeneration periods. Analysis of the glial activities revealed that changes in both microglial activity and Müller activity are highly correlated with the two waves of photoreceptor death. The second part of the study investigated the role of microglial activation in the photoreceptor degeneration process using a microglial inhibitor, Neurostatin. The results suggest that microglial activation accelerates photoreceptor loss and that inhibiting microglial activity could slow the process down.

These findings demonstrate a spatiotemporal relationship between microglial activity and photoreceptor degeneration, indicating a possible contribution of microglial cells towards photoreceptor loss. Taken together, these observations suggest that microglial inhibition is a promising strategy for visual restoration in retinal degeneration and provides important insights for future studies on microglial activation in retinal diseases.

## Acknowledgements

Firstly, I would like to thank my primary supervisor Prof. Evelyne Sernagor for taking me as her Ph.D student in the first place, giving me the opportunity to study in the UK and see more possibility of my life. Her continuous guidance has supported me throughout my Ph.D research from the very beginning of the project to the final thesis proofreading. I would also like to thank my second supervisor Mr. David Steel for his training on the surgical procedure and the guidance in all the time of research and writing of this thesis. David has been very helpful, providing direction, advice from the clinical aspect, and was always available when needed. Thanks also go to my assessors, Pr Majilinda Lako and Dr. Sasha Gartside, who has been incredibly helpful throughout my Ph.D and provide valuable insights on improving my research.

I would especially like to thank everyone I have worked alongside in Evelyne' s lab. A special mention must go to Dr. John Barrett, who has been a great friend but also been incredibly helpful on teaching me both Matlab coding and English, and to Dr. Gerrit Hilgen for his great support and advice in the lab and also been a source of life experience and enlightening discussions.

I would like to Dr. Trevor Booth and Dr. Alex Laude for sharing their experience in imaging. Thanks to everyone from CBC who have assist me in amending the project license and the surgical procedures.

Thanks to everyone who has been a great friend to me during my Ph.D and supported me through the highs and lows of my Ph,D. I thank Dr. Fiona LeBeau for being such a great coordinator and for great chats, Dr. Elizabeth Stoll for sharing valuable experiences as a senior researcher. I thank Dr. Felix Chan for organising all the dark side Christmas party and for being a good listener whenever needed, Dr. Thomas Hall for being a great teacher on English and British culture, Dr. Clare Tweedy for great nights out and organising all the activities that help me to fit in, Anderson Brito da Silva for sharing the knowledge of Brazilian culture, Dr. Sabine Gretenkord and Dr.

Katherine Newling for taking care of me during my first year, Dr. Reem Bsuodan for all the delightful discussion on immunohistochemistry and life, Dr. Bas Olthof for all the knowledge about baking and healthy lifestyle, to everyone in the IT service desk, who have been extremely nice to me and also allow me to experience a life outside academia.

I also want to take this opportunity to thank my family for their continual support throughout my Ph.D. In particular, I would like to thank my parents who have been very supportive, encouraging me to pursue my dream.

Finally, I would like to express my great gratitude to my partner Mosi Li for all his support and encouragement throughout my Ph.D. This could not have been done without you.

Chapter 1. Introduction .....	1
1. Overview .....	3
2. Retinal anatomy and physiology.....	3
3. Photoreceptors in the healthy retina.....	5
4. Hereditary Retinal Dystrophies.....	9
5. Microglia in the Healthy and Diseased CNS.....	19
6. Müller cells in healthy and diseased retina .....	30
7. Aims and hypothesis .....	32
Chapter 2. Materials and Methods.....	35
1. Animals and Surgical Procedures.....	37
2. Immunohistochemistry .....	38
3. Microscopy and Image Analysis .....	40
4. Data Processing and Statistical Analysis .....	43
Chapter 3. Photoreceptor Degeneration in Rd1 and Crx Retina .....	45
1. Introduction .....	47
2. Specific Methods.....	48
3. Results .....	48
4. Discussion.....	77
5. Conclusion.....	79
Chapter 4. Glial activity is correlated with the fast photoreceptor degenerating phases .....	81
1. Introduction .....	83
2. Specific Methods.....	84
3. Results .....	86
4. Discussion.....	107
5. Conclusion.....	112
Chapter 5. Pharmacological Inhibition of Microglia Cells in Isolated Retina.....	115
1. Introduction .....	117
2. Specific Methods.....	118

3. Results .....	119
4. Discussion:.....	130
5. Conclusion.....	133
Chapter 6. The Effect of Neurostatin on Microglial Activation and Photoreceptor Survival in Crx Retina	135
1. Introduction .....	137
2. Specific Methods:.....	138
3. Results .....	140
4. Discussion.....	163
5. Conclusion.....	167
Chapter 7. General Discussion .....	169
1. Glial activity during photoreceptor degeneration .....	171
2. Future implications and potential therapeutic strategies .....	172
References: .....	175
Table of Figures	
Figure 1-1 Schematic diagram of retinal anatomy.....	4
Figure 1-2 Schematic representation of phototransduction cascade (From dark to light states).....	7
Figure 1-3 Diagram summarizing the genetic overlap between RP and other inherited retinal dystrophies by S.K. Verbakel et.al.....	10
Figure 1-4 The prevalence of functional process affected by RP mutations. ....	12
Figure 1-5 Schematic diagram of retinal degeneration progression. ....	16
Figure 1-6 Schematic representation of phototransduction cascade phototransduction in RP photoreceptors .....	17
Figure 1-7 Proposed mechanisms involved in photoreceptor death in RP .....	18
Figure 1-8 Phenotypic alteration of microglial cells .....	21
Figure 1-9 Proposed mechanism of microglial intracellular cascade induced by LPS. (2011).....	26
Figure 2-1 Schematic graph of tissue preparation.....	38
Figure 2-2 Laminated retinal structure visualised by DAPI staining. ....	42
Figure 3-1 Fluorescence micrographs showing the change of ONL thickness against age in rd1 retina. ....	50
Figure 3-2 The changes of ONL thickness and ONL ratio against age.....	51

Figure 3-3 The fluorescent micrographs of apoptotic cells in P50 Crx retina.....	53
Figure 3-4 Fluorescent micrographs of TUNEL cells (green) in vertical sections of rd1 retina.....	54
Figure 3-5 Bar chart showing the change of ONL thickness and apoptosis against age in rd1 retina..	55
Figure 3-6 Fluorescent micrographs of Rhodopsin in vertical sections of rd1 retina.....	57
Figure 3-7 Fluorescent micrographs of S opsin in the vertical sections of rd1 retina. ....	58
Figure 3-8 Fluorescent micrographs of rhodopsin on wholemount retina .....	60
Figure 3-9 Fluorescence micrographs showing the change of ONL thickness against age in Crx retina. .....	61
Figure 3-10 Line graph showing group data for the changes of ONL thickness and ONL ratio against age in Crx retina. ....	62
Figure 3-11 Change in the density of TUNEL+ cells in retinal sections of Crx mice against age.....	65
Figure 3-12 Fluorescent micrographs showing focal areas of thinning on retinal section of Crx retina. .....	67
Figure 3-13 Fluorescent micrographs of rhodopsin (A-C ) and S opsin (D-F) in Crx retina.....	69
Figure 3-14 Fluorescent micrographs of rhodopsin on whole mount retina of Crx mice. Grey: Rhodopsin. ....	71
Figure 3-15 Fluorescent micrographs of rhodopsin and S opsin in the inner retina of rd1 mouse.....	72
Figure 3-16 Comparison of the time course of apoptotic activity and ONL ratio against age in rd1 and Crx retina.....	73
Figure 3-17 Representative images showing the localization of apoptotic cells in rd1 and Crx retina	74
Figure 3-18 The distribution of apoptotic cells in wholemount Crx retina.....	75
Figure 3-19 The correlation between ONL thickness and ONL nuclei counts in different strains.....	76
Figure 4-1 Thresholding methods for GFAP filament counts.....	85
Figure 4-2 Fluorescence micrographs showing the expression of iba1 in WT retinal sections.....	87
Figure 4-3 Fluorescent micrograph showing the remodelling of Müller cells in Crx retina .....	88
Figure 4-4 Clusters of GFAP+ filaments in the later stages of retinal degeneration in Crx retina.....	89
Figure 4-5 Changes in the number of GFAP+ filament against age in Crx and WT retina. ....	90
Figure 4-6 Fluorescent micrographs showing the remodelling of Müller cells into the photoreceptors holes.....	92
Figure 4-7 Fluorescent micrograph showing microglial activation in Crx retina .....	93
Figure 4-8 Representative micrographs of microglial cells in WT and Crx retina.....	95
Figure 4-9 Changes in iba1+ cell density with age in Crx and WT retina .....	97
Figure 4-10 Change in iba1+ cell density in the inner Crx and WT retina with age after correction by area size. ....	99

Figure 4-11 Change in iba1+ cell density in the outer Crx and WT retina with age after correction by area size. ....	100
Figure 4-12 The changes in the number of iba1+ cells in the subretinal space.....	102
Figure 4-13 Correlation between ONL thinning and microglial activation during retinal degeneration. ....	104
Figure 4-14 Correlation between ONL thinning and gliosis during retinal degeneration. ....	105
Figure 4-15 Correlation between microglial activity and gliosis during retinal degeneration. ....	106
Figure 4-16 Pathological events during photoreceptor degeneration in the Crx retina .....	113
Figure 5-1 Fluorescent micrographs showing the changes in glial cells in the WT retina with/without incubation and in the Crx retina without incubation. Scale bar: 50µm.....	120
Figure 5-2 The changes of glial cells at different retinal eccentricities with and without incubation. ....	121
Figure 5-3 The effect of Neurostatin on iba1+ expression in P10 inner Crx retina .....	123
Figure 5-4 The effect of Neurostatin on GFAP expression in P10 inner Crx retina.....	125
Figure 5-5 The effect of Neurostatin on iba1+ cells in P40 Crx retina .....	126
Figure 5-6 The effect of Neurostatin on GFAP in P40 Crx retina .....	128
Figure 6-1 Schematic diagram of the events during photoreceptor degeneration in the Crx retina. ....	138
Figure 6-2 Schematic graph of intravitreal injection and fundus image of mouse eye.....	140
Figure 6-3 Fluorescent micrographs of glial cells following Neurostatin treatment in early stages ..	142
Figure 6-4 Fluorescent micrographs of glial cells following Neurostatin treatment in later stages...	143
Figure 6-5 Fluorescent micrographs of iba1+ cells in the outer most of ONL following intravitreal injection. ....	144
Figure 6-6 Changes of iba1+ cell density in the inner retina over time following treatment with Neurostatin. ....	145
Figure 6-7 Changes of iba1+ cell density in the outer retina over time following treatment with Neurostatin. ....	147
Figure 6-8 Changes of the number of GFAP+ filaments following treatment with Neurostatin. ....	149
Figure 6-9 Changes in ONL thickness over time following treatment with Neurostatin. ....	151
Figure 6-10 Effect of Neurostatin treatment on photoreceptor death .....	154
Figure 6-11 Fluorescent micrographs of glial cells following treatment with Neurostatin during the second activation wave.....	156
Figure 6-12 Bar chart showing the density changes of iba1+ cells in the inner retina following Neurostatin treatment during the second activation wave. ....	157

Figure 6-13 Changes in iba1+ cells density in the outer retina following Neurostatin treatment during the second activation wave. ....	158
Figure 6-14 Changes in GFAP filament number following Neurostatin treatment during the second activation wave. ....	159
Figure 6-15 The change of ONL thickness after treated with Neurostatin at the second activation wave. ....	161
Figure 6-16 Bar chart showing the comparison of the effect on the iba1+ cells and ONL between P25-60DPI and P55-30DPI. ....	163

Table of tables

Table 1-1 Differential diagnoses for non-syndromic retinitis pigmentosa by S.K. Verbakel et.al .....	11
Table 1-2 Markers on microglial cells. ....	29
Table 2-1 Primary antibodies used in this study.....	40
Table 2-2 Secondary Antibodies used in This Study .....	40
Table 3-1 Changes of ONL thickness, ONL ratio and numbers of photoreceptor nuclei against age... 52	
Table 3-2 Changes of ONL thickness, ONL ratio and numbers of photoreceptor nuclei against age... 63	
Table 3-3 The density of TUNEL+ cells in the ONL at different retinal eccentricities .....	66
Table 4-1 The changes of GFAP filament density over age.....	91
Table 4-2 Density of iba1+ cells in the inner retina of Crx and WT retina .....	98
Table 4-3 Density of iba1+ cells in the outer Crx retina.....	98
Table 4-4 Density of iba1+ cells in the inner retina of Crx and WT retina after correction.....	100
Table 4-5 The density of iba1+ cells in the outer retina of Crx miceafter correction.....	101
Table 4-6 The number of iba1+ cells in the subretinal space in Crx retina.....	103
Table 5-1 Changes of glial cells at different retinal eccentricities after treatment .....	122
Table 5-2 The effect of Neurostatin on iba1+ density in P10 Crx retina.....	124
Table 5-3 The effect of Neurostatin on GFAP filaments in P10 Crx retina .....	125
Table 5-4 The effect of Neurostatin on iba1+ cell density in P40 Crx retina .....	127
Table 5-5 The number of GFAP filaments in P40 Crx retina .....	128
Table 5-6 Summary of the responses toward treatment. ....	129
Table 6-1 Changes of iba1+ cell density in the inner retina over time following treatment with Neurostatin .....	146
Table 6-2 Changes of iba1+ cell density in the outer retina over time following treatment with Neurostatin. ....	148
Table 6-3 Changes of the number of GFAP+ filaments following treatment with Neurostatin. ....	150
Table 6-4 Changes in ONL thickness over time following treatment with Neurostatin. ....	152
Table 6-5 The effect of Neurostatin on TUNEL+ cell density at P25-30DPI .....	154
Table 6-6 The effect of Neurostatin on iba1+ cells in the inner retina at the second activation wave. ....	157
Table 6-7 The effect of Neurostatin on iba1+ cells in the outer retina at the second activation wave .....	158
Table 6-8 The effect of Neurostatin on GFAP filaments at the second activation wave.....	159
Table 6-9 The effect of Neurostatin on ONL thickness in the second activation wave.....	161

# **Chapter 1. Introduction**



## 1. Overview

Hereditary retinal dystrophies are a group of degenerative disorders of the outer retina with heterogeneous clinical patterns and severities. They are one of the leading causes of untreatable blindness. The prevalence of retinitis pigmentosa, the most common form of hereditary retinal dystrophy, is 1 in 3000 individuals (Francis, 2006). Currently, none of the therapeutic approaches can successfully stop the progress of these diseases.

So far, over 100 genes and multiple biochemical pathways have been found to be affected in retinal dystrophies. This genetic complexity makes it difficult for gene replacement strategies. However, despite such genetic and clinical heterogeneity, most hereditary retinal dystrophies follow a common pathological pathway characterized by progressive photoreceptor loss concomitant with glial activation.

Recent evidence has shown that glial cells do not act as simple bystanders of retinal degeneration, but may make a primary contribution to the neuronal loss (Ransohoff, 2016, Karlstetter et al., 2015). Hence, being able to control the level of glial activation during the degenerative process may be a potential target for improving photoreceptor survival.

This thesis focuses on the interaction between glial activation and photoreceptor degeneration in inherited retinal dystrophies, and the contribution of glial activation to photoreceptor survival.

## 2. Retinal anatomy and physiology

As the light transduction organ of the visual system, the retina converts light into electrical signals and performs all the initial processing of information about the visual scene. The cellular architecture of the retina is highly organized, consisting of nine layers, each of which has its own distinct cellular constitution (Figure 1-1).

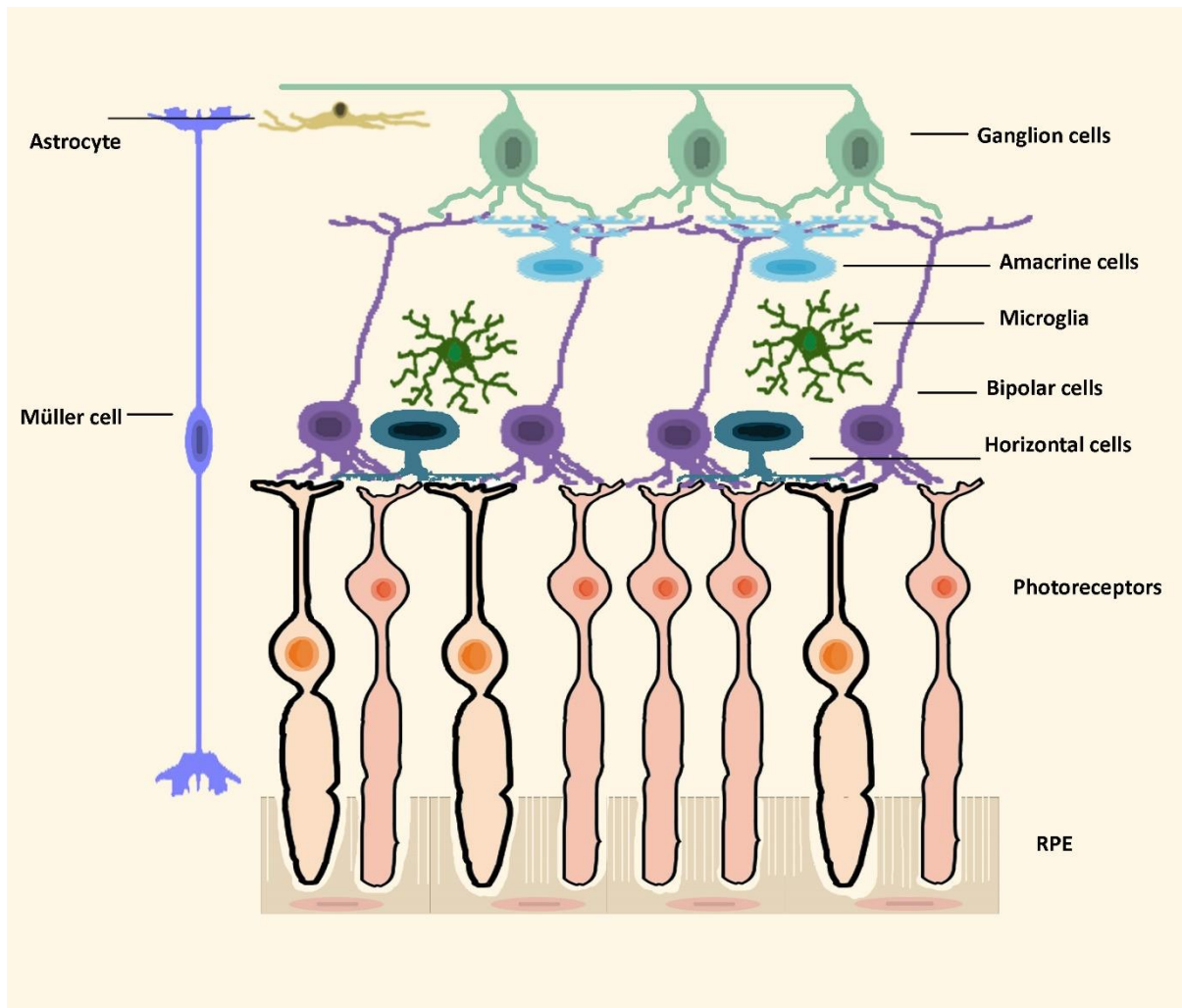


Figure 1-1 Schematic diagram of retinal anatomy

The diagram highlights the principle cells in the mammalian retina and the organization of neural retina. The retina comprises five types of neurons and three types of glial cells. The neurons are arrayed across the retina. The photoreceptors are neatly packed in the ONL, while the nucleus of bipolar cells, horizontal cells and amacrine cells reside in the INL. The ganglion cells are in the inner surface of the retina. As the scaffold of the retina, Müller cells span all the retinal layers from the inner surface to the outer limiting membrane. The astrocytes are mostly located in the nerve fibre layer with an intimate relationship with retinal vessels, while the microglial cells distribute across the inner retina in a dynamic manner.

There are over 60 distinct types of neurons in the retina, which can be sub-divided into five classes: photoreceptors (PRs), bipolar cells (BCs), horizontal cells (HCs), amacrine cells (ACs) and ganglion cells (GCs) (Masland, 2012). The ability of the retina to respond to visual stimuli in a highly specialized fashion is facilitated by its complex laminar structure.

PRs respond to light through phototransduction, which occurs in their outer segments (OS). The OS, in close apposition with the inner surface of the retinal pigment epithelium (RPE), are where the photons are captured and converted into neural signals, while PR cell bodies are in the outer nuclear layer (ONL). PR synaptic terminals are in the outer plexiform layer (OPL), where they form functional contacts with BCs and HCs. BCs, HCs, and ACs have their cell bodies in the inner nuclear layer (INL).

The BCs process the signals from PRs and transmit them to the GCs via synaptic contacts in the inner plexiform layer (IPL), where the responses are modulated by lateral interactions originating from ACs. The GCs encode the output of information from the entire network, generating spike trains that are conveyed to the visual centres of the brain via the optic nerve (Masland, 2012, Sernagor, 2006).

The mammalian retina has three types of glial cells: Müller cells (MGs), astrocytes and microglia. As the main macroglial cells in the retina, MGs span the entire thickness of the neural retina, ensheathing neurons to generate columns, which anatomically supports retinal neurons, and ensures the metabolic symbiosis between MGs and neurons. MGs supply oxygen and nutrients for neurons and remove neuronal metabolic waste (Bringmann et al., 2006), as well as acting in the isomerisation of cone retinoids and neurotransmitter recycling.

The other retinal macroglial cell is the astrocyte, which is responsible for retinal vascularization during development. Astrocytes are found in the nerve fibre layer (NFL) which covers the GC layer and blood vessels (Provis, 2001).

As the innate immune cells in the central nervous system (CNS), microglial cells are normally located in the inner retina, performing a surveillance function against insults and changes in physiological environment (Hamel, 2006).

### 3. Photoreceptors in the healthy retina

#### 3.1 The anatomy of the photoreceptor

As the first cell of the visual pathway, photoreceptors are highly specialised cells, responsible for phototransduction. Each photoreceptor consists of an outer segment, an inner segment, a cell body that contains the nucleus, and a large presynaptic terminal complex. The outer segment, where phototransduction occurs, is formed from stacks of tightly-packed disc-shaped membranes filled with photopigments (rhodopsin or cone opsins). The inner segment, which is the energy conversion and protein synthesis centre, connects to the outer segment via a cilium. The inner side of the inner segment connects to the cell body. The synaptic terminal (cone pedicle or rod spherule) is located on the innermost part of the cell, in the OPL, where it releases glutamate onto BCs and HCs.

PRs are classified into two types, based on their function and the morphology of their OS. (1) Rods, which are very sensitive to dim light, and are responsible for dark vision (scotopic vision), have long, cylinder shaped OS, formed by a stack of discs with no connection to the plasma membrane. (2) Cones, which possess shorter and tapering outer segments, with the disc stack connected to the plasma membrane, are sensitive to a much broader range of brighter light (photopic vision) and

have different types of photopigments, with different peak absorption, enabling colour vision (Hildebrand and Fielder, 2011).

Another feature that distinguishes rods from cones is the photopigments in the cells. Rods only contain one kind of photopigment, called rhodopsin, which resides almost exclusively in the outer segments, but is absent from anywhere else in the rods. Rhodopsin is highly efficient in absorbing light and also contributes to the morphogenesis of the outer segments. It is made up of opsin and a chromophore, 11-*cis*-retinal. Upon photon absorption, as the first step of the visual cycle, light triggers the isomerisation of 11-*cis*-retinal into all-*trans*-retinal, which activates rhodopsin to transfer into the “active” state (metarhodopsin 2).

By contrast, there are different types of cones, depending on the photopigment they express. Human cones are classified into three types: S (short wavelength, blue light) cones, M (medium wavelength, green light) cones, and L (long wavelength, red light) cones. The lack of a particular type of cone (most commonly, M or L cones) results in ‘colour blindness’.

### 3.2 The phototransduction cascade

Phototransduction in rods and cones follows a classic G-protein signalling pathway. Following photon absorption, the activated rhodopsin protein catalyses the activation of the G-protein transducin, which sequentially activates phosphodiesterase (PDE). PDE decreases the concentration of cytoplasmic free cyclic guanosine monophosphate (cGMP) by hydrolysis, which results in the closure of the cGMP-gated Na<sup>+</sup> channels, resulting in hyperpolarization of the plasma membrane (Figure 1-2) (Fu, 1995). The cGMP-gated Na<sup>+</sup> channels are responsible for the influx of Ca<sup>2+</sup> in the outer segments, while the clearance of Ca<sup>2+</sup> is done by the Na/Ca-K exchanger, which continuously extrude Ca<sup>2+</sup> to the extracellular space. The steady state of Ca<sup>2+</sup> level in the OS, which relies on the balance between the influx via the cGMP-gated Na<sup>+</sup> channels and the extrusion of Na/Ca-K exchanger, is the basis of phototransduction.

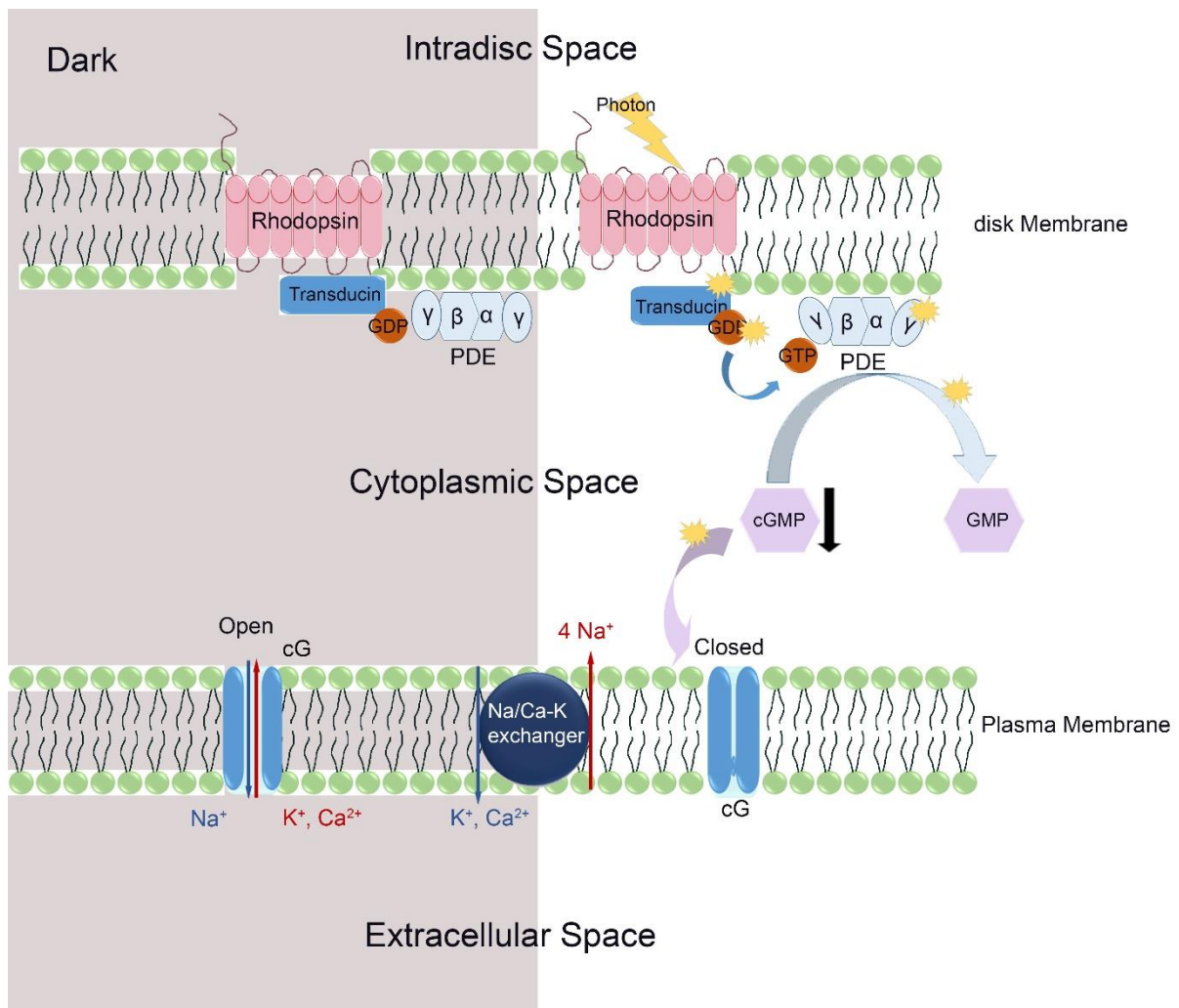


Figure 1-2 Schematic representation of phototransduction cascade (From dark to light states)

The activation of rod phototransduction pathway following photo absorption. The phototransduction cascade results in the closure of cGMP-gated channels. The phototransduction process begins with the capture of photons by rhodopsin. Following that, the G-protein transducin activates, which sequentially activates PDE. The activation of PDE causes in a decrease of cGMP, which results in the closure of cGMP-gated Na<sup>+</sup> channels.

The functionality of the phototransduction pathway and the fast recovery of visual pigments are both essential for visual function, as well as for the survival of photoreceptors. Defects involving any part of the pathway or the metabolism of visual pigments, will not only lead to visual loss, but also result in photoreceptor death.

The recovery of bleached opsins following phototransduction occurs in the RPE, where all-*trans*-retinol is converted back into 11-*cis*-retinol, and then hydrolysed to 11-*cis*-retinal before being transported back to the photoreceptor outer segment.

### 3.3 Photoreceptor metabolism

Whilst only 2% of human body weight, CNS takes up 20% of overall oxygen consumption and 25% of glucose uptake. Within CNS, retina ranks amongst the most energy-consuming systems (German et al., 2015, Wong-Riley, 2010).

The phototransduction cascade, as well as protein synthesis and transport, are highly energy-dependent. This means that photoreceptors are very sensitive to any disruption of energy metabolism, for example, due to blood supply, glucose uptake, or oxidative stress.

Glycolysis in the cytosol and aerobic respiration (oxidative phosphorylation) in the mitochondria both contribute to energy (adenosine triphosphate, ATP) production, although the efficiency of glycolysis outweighs oxidation (Wong-Riley, 2010). In photoreceptors, glucose uptake is highly active in the outer segments, as light transduction relies on a high concentration of ATP. By contrast, energy consumption for protein synthesis and transport in the inner segments largely relies on aerobic respiration, which is facilitated by the high expression of cytochrome c oxidase and high concentration of mitochondria in the inner segments.

Another factor that is essential for the function and survival of photoreceptors is the precise balance of the retinal microenvironment. RPE cells constantly remove metabolic waste (such as waste products of respiration) via phagocytosis. Furthermore, although photoreceptors are categorized as permanent cells, the outer segments undergo continuous renewal throughout the lifetime of the cell. The RPE cells contribute to phagocytosis of the discs (disc shedding), allowing the outer segments to maintain a relatively constant length. Overgrowth of outer segments triggers photoreceptor degeneration (Schietroma et al., 2017, Kevany and Palczewski, 2010).

### 3.4 Distribution of photoreceptors in the retina

There is much heterogeneity in the distribution of photoreceptors between human and rodents, due to the different demands on vision. Humans are diurnal, hence their vision relies on photopic vision (high acuity, chromatic), mediated by cones in the macula. Rodents, on the other hand, are nocturnal, with their vision relying on rods which are distributed throughout the retina (they have no fovea). In the mouse retina, rods account for 97.2% of the photoreceptor population, taking the dominant responsibility for phototransduction, whereas cones make up only 2.8% of the photoreceptor population (Jeon et al., 1998).

Although in rodents, the distribution of rods and cones is almost symmetric between the ventral retina and dorsal retina, the density of photoreceptors is not evenly distributed, showing a

decreasing gradient from the perioptic nerve area to the periphery (Jeon et al., 1998). In the mouse retina, there are only two types of cones, UV (S) and green (M) cones. M cones are previously reported to locate predominantly in dorsal retina (Szel et al., 1992, Applebury et al., 2000). However, results from a later study with larger sample size suggested that the M cones are evenly distributed across the retina (Ortin-Martinez et al., 2014). By contrast, the S cones are more abundant in the ventral area and rare in the far periphery of the dorsal retina (Ortin-Martinez et al., 2014).

## 4. Hereditary Retinal Dystrophies

### 4.1 Retinitis pigmentosa

#### 4.1.1 General view

RP is the generic name given to the most common phenotype of retinal dystrophies with a global prevalence of 1 in 3000 individuals (Francis, 2006). Clinical symptoms typically start with night blindness and impairment of peripheral vision (characteristic of rod degeneration), and in advanced cases, it leads to cone degeneration and ensuing blindness. The genes affected in RP are most commonly rod-specific, and cause malfunction in the phototransduction pathways which then triggers rod apoptosis. By contrast, cones are usually unaffected by these mutations, and cone death in RP is usually secondary to rod loss, due to oxidative stress.

The mutations that lead to RP are remarkably heterogeneous (Figure 1-3). Over 150 mapped chromosomal loci and one hundred genes are known to be responsible for the phenotype [<http://www.sph.uth.tmc.edu/RetNet/>]. Autosomal recessive (ar) mutations account for the majority of the defined RP mutations, but some are also autosomal dominant (ad) and X linked. Table 1-1 shows the differential diagnoses for RP (Ferrari et al., 2011, Verbakel et al., 2018)

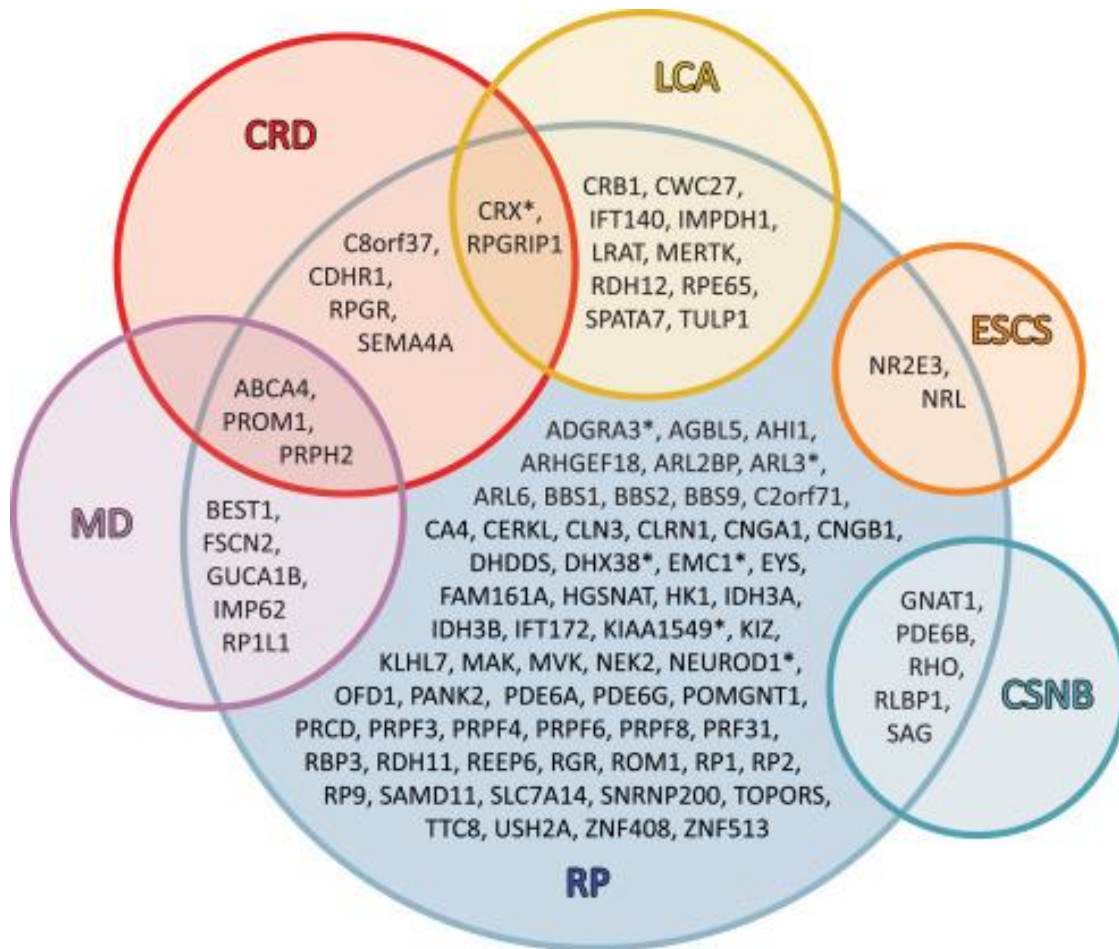


Figure 1-3 Diagram summarizing the genetic overlap between RP and other inherited retinal dystrophies by S.K. Verbakel et.al.

Downloaded from <https://www.sciencedirect.com/science/article/pii/S1350946217300721#fig1>. Licensed under the Creative Commons Attribution. Original Caption: Venn diagram summarizing the genetic overlap between RP and other inherited retinal dystrophies. Modified from S.K. Verbakel et.al (2018). The circle represents a condition of inherited retinal dystrophy. The gene names in the overlapped areas indicate that these mutations can lead to different phenotypes. \*: mutations for non-syndromic RP. MD: macular dystrophy; CRD: cone-rod dystrophy; LCA: leber congenital amaurosis; ESCS: enhanced S-cone syndrome; CSNB: congenital stationary night blindness.

Table 1-1 Differential diagnoses for non-syndromic retinitis pigmentosa by S.K. Verbakel et al

Inherited retinal dystrophies	Syndromic forms of retinitis pigmentosa	Pseudoretinitis pigmentosa
<b>Progressive retinal dystrophies</b>	<b>Ciliopathies</b>	<b>Durg-induced</b>
<ul style="list-style-type: none"> <li>• Cone-rod dystrophy</li> <li>• Cone dystrophy</li> <li>• Leber congenital amaurosis</li> <li>• Bietti crystalline corneoretinal dystrophy</li> <li>• Late-onset retinal degeneration</li> <li>• Macular dystrophy (Stargardt disease, Sorsby fundus dystrophy)</li> </ul>	<ul style="list-style-type: none"> <li>• Usher syndrome</li> <li>• Bardet-Biedl syndrome</li> <li>• Cohen syndrome</li> <li>• Joubert syndrome</li> <li>• Senior-Løken syndrome</li> <li>• Sensenbrenner syndrome (cranioectodermal dysplasia)</li> <li>• Short-rib thoracic dysplasia with or without polydactyly (includes Jeune, Mainzer-Saidino, Ellis-Van Creveld and short-rib polydactyly syndrome)</li> </ul>	<ul style="list-style-type: none"> <li>• Thioridazine and chlorpromazine</li> <li>• Quinolines (e.g.: (Hydroxy) chloroquine)</li> </ul>
<b>Stationary retinal disease</b>		<b>Chorioretinal infections</b>
<ul style="list-style-type: none"> <li>• Congenital stationary night blindness (including fundus albipunctatus and Oguchi disease)</li> </ul>	<b>Metabolic disorders</b>	<ul style="list-style-type: none"> <li>• Syphilis, Lyme disease, acute retinal necrosis and other viral infections (rubella, chicken pox, measles, cytomegalovirus)</li> </ul>
<b>Inherited vitreoretinopathies</b>		<b>Sequela of inflammatory disease</b>
<ul style="list-style-type: none"> <li>• X-linked juvenile retinoschisis</li> <li>• Ebgabcd S-cone syndrome/Goldmann-Fevre syndrome</li> <li>• Wagner syndrome/erosive vitreoretinopathy</li> <li>• Snowflake vitreoretinopathy</li> </ul>	<ul style="list-style-type: none"> <li>• Alfa-tocopherol transfer protein deficiency (familial isolated vitamin E deficiency)</li> <li>• Bassen-Kornzweig syndrome (abetalipoproteinemia)</li> <li>• Mucopolysaccharidoses</li> <li>• Neuronal ceroid-lipofuscinoses, childhood onset (Batten disease)</li> <li>• Refsum disease (phytanic acid oxidase deficiency)</li> <li>• Mevalonate kinase deficiency</li> <li>• HARP syndrome (hypoprebetalipoproteinemia, acanthocytosis, RP and pallidal degeneration)</li> <li>• PHARC syndrome (polyneuropathy, hearing loss, ataxia, RP, and cataract)</li> </ul>	<ul style="list-style-type: none"> <li>• Sarcoidosis</li> <li>• Acute posterior multifocal placoid pigment epitheliopathy</li> <li>• Birdshot chorioretinopathy</li> <li>• Serpiginous choroidopathy</li> <li>• Diffuse unilateral subacute neuroretinitis</li> <li>• Systemic lupus erythematosus</li> </ul>
<b>Chorioretinal dystrophies</b>		<b>Miscellaneous</b>
<ul style="list-style-type: none"> <li>• Chorioderemia</li> <li>• Gyrate atrophy</li> <li>• Helicoid peripapillary chorioretinal degeneration (Sveinsson chorioretinal atrophy)</li> <li>• Progressive bifocal chorioretinal atrophy</li> </ul>	<b>Mitochondrial disorders</b>	<ul style="list-style-type: none"> <li>• Vitamin A deficiency</li> <li>• Paraneoplastic</li> <li>• Trauma</li> <li>• Siderosis bulbi</li> <li>• Old retinal detachment</li> <li>• Pigmented paravenous retinochoroidal atrophy</li> <li>• Acute zonal occult outer retinopathy</li> </ul>
<b>Female carriers of inherited retinal dystrophies</b>		
<ul style="list-style-type: none"> <li>• Retinitis pigmentosa</li> <li>• Choroideremia</li> <li>• Ocular albinism</li> </ul>	<ul style="list-style-type: none"> <li>• Kearn-Sayre syndrome</li> <li>• NARP syndrome (neuropathy, ataxia, and RP)</li> </ul>	

Modified from S.K. Verbakel et al (2018).

<https://www.sciencedirect.com/science/article/pii/S1350946217300721?via%3Dihub#tbl1>. Licensed under the Creative Commons Attribution. Original Caption: Differential diagnoses for non-syndromic retinitis pigmentosa.

RP related mutations may affect different steps of the visual cycle which lead to different pathological outcomes (Figure 1-4). Rhodopsin (*RHO*) gene was the first identified RP gene, in which various mutations make up for 30-40% of adRP. Mutations in *RHO* gene can affect protein folding, 11-cis retinal chromophore binding, G protein coupling, cellular trafficking of rhodopsin proteins. Retinitis pigmentosa 1 (*RP1*) is expressed in the photoreceptors and involved in correct stacking of outer segment discs including orientation and higher order structure. Mutations in *RP1* account for about 5-10% of adRP. The retinal pigment epithelium 65 (*RPE65*) gene is expressed in the RPE and is crucial for pigment recycling for both cone and rod function. Mutations in *RPE65* accounts for 2% of recessive RP patients and 16% of LCA patients.

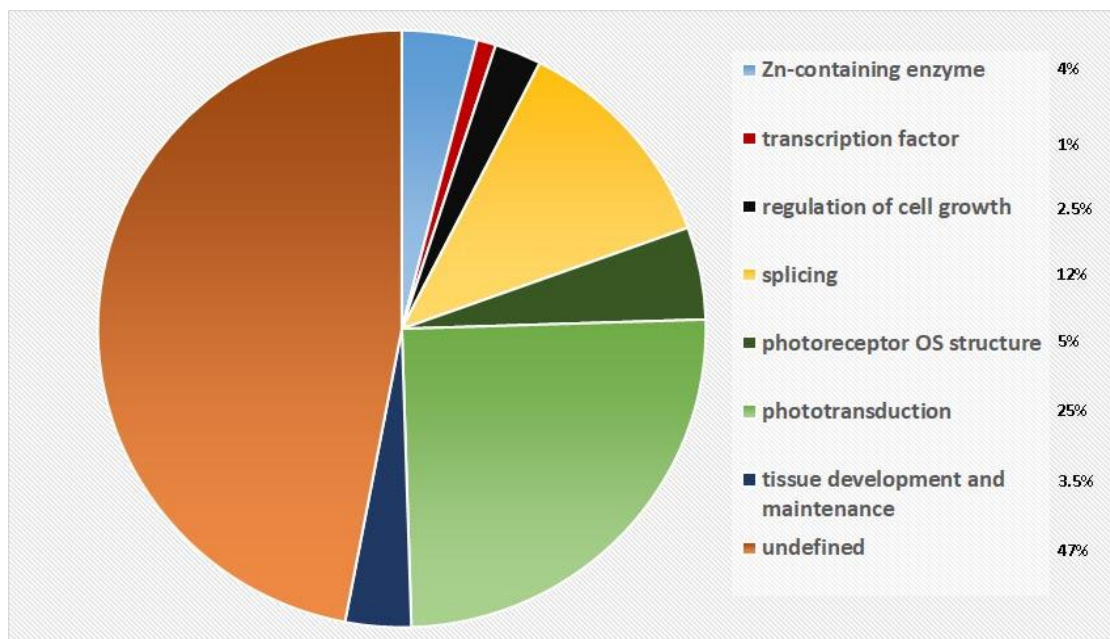


Figure 1-4 The prevalence of functional process affected by RP mutations.

*RP related mutations may affect a range of different genes affecting several different pathways. Although the majority remain to be defined, several have been identified to be affected. A quarter of the mutations are involved in phototransduction, and the second most prevalent mutations identified affect pre-mRNA splicing. Zn-containing enzymes, transcription factors, cell growth regulation, photoreceptor OS structure ('ciliopathies') as well as those affecting tissue development and maintenance are also identified to be affected by the RP related mutations. Summarized from Ferrari et al. (2011)*

#### 4.1.2 Animal models

As RP encompasses genetically diverse diseases, a large number of animal models of RP have been developed or discovered over the years. The rd1 mouse, also known as "rd" (retinal degeneration), is one of the most common RP models. The rd1 mice are substrains of the C3H mice, which are homozygous for the retinal degeneration 1 mutation. The mutation is on the gene which is responsible for encoding the rod cGMP-PDE6 $\beta$  subunit (Bowes et al., 1990). The defect in this gene induces malfunction of cGMP cycling, which in turn triggers the rod apoptotic cascade. The rd1

mouse retina undergoes a fast degenerating process, with rod death occurring between postnatal (P) day 10 and P21. Cones remain unaffected at the rod apoptosis stage, but they start degenerating secondarily with rod depletion during the fourth postnatal week. The PDE6 $\beta$  mutation is also observed in human autosomal recessive RP, which undergoes a similar degenerating process as rd1 (Bayes et al., 1995). Thus, the well-documented rd1 mouse is a good model to study human RP. However, in addition to the PDE6 $\beta$  mutation, another mutation in Gpr179 allele has recently been identified in many of the strains from the C3H background (Balmer et al., 2013, Nishiguchi et al., 2015, Chang, 2015). The Gpr179 mutation is responsible for the depletion of b wave and the depolarization of bipolar cells, but this phenotype can be masked with the presence of rd1 mutation. Considering the impact of the Gpr179 mutation on the retinal function, the possible presence of this mutation needs to be taken into account when conducting functional test using mice models from C3H strains.

There are also slow degeneration models of RP, such as rd2. Rd2 mice suffer from mutations in the gene Prph2, which is responsible for the maintenance of the outer segments discs. Although the abnormality of outer segments develops as early as P7, the photoreceptors in rd2 retina survive for up to a year (Chang et al., 2002).

Rd10 mice suffer from the mutation on the same gene as rd1, but present in a slower progression phenotype. Indeed, the retinal degeneration in the rd10 retina is caused by a missense mutation in exon 13 of the beta subunit (Chang et al., 2002). Anatomical signs of degeneration emerge at P16 in the rd10 retina, and degeneration is completed by P30 (Chang et al., 2007). The slower and milder degenerating process in the rd10 mice makes it a better model than rd1 mice for pharmacological intervention. (Gargini et al., 2007, Pennesi et al., 2012)

## 4.2 Leber congenital amaurosis

### 4.2.1 General view

LCA is a severe phenotype of retinal dystrophy with a prevalence of 1 in 40000 individuals (van Huet et al., 2013). Affected individuals typically present with early onset blindness, wandering nystagmus, and a pigmentary retinopathy (Koenekoop, 2004).

LCA is highly clinically and genetically heterogeneous. Histo-pathological studies of LCA cases suggest three possible disease categories: Degenerative (cases with progressive atrophy in the photoreceptors and RPE, and sometimes in the inner retina), Aplasic (cases that fail to form photoreceptors from early developmental stages), and Dysfunctional (cases with intact retinal

anatomy but manifesting biochemical dysfunction) (Porto et al., 2002, Porto et al., 2003, Koenekoop, 2004).

Mutations have been found in six genes, affecting a wide range of retinal pathways including retinoid metabolism (*RPE65*), photoreceptor outer segment development (*CRX*), Phototransduction (*GUCY2D*), zonula adherens formation (*CRB1*), cell-cycle progression (*AIPL1*) and disk morphogenesis (*RPGRIP1*) (Koenekoop, 2004).

Unlike RP, the mutations in LCA often lead to abnormalities equally in rods and cones in both developing and adult retina. Individuals with *GUCY2D* mutations have a reduced ability to produce cGMP (Tucker et al., 2004), which manifests as a cone dystrophy. The *RPE65* gene encodes for retinal pigment epithelial protein-65, RPE65, which is responsible for pigment recycling (Redmond et al., 1998) in the RPE. Defects on this gene can develop early onset severe rod-cone dystrophy (Lorenz et al., 2000). *CRX* refers to a class of genes that encode the cone-rod homeobox protein. Individuals who have mutations in *CRX* will not only fail to form outer segments from development, but also develop an early onset form of cone-rod degeneration.

The *AIPL1* gene encodes the Aryl hydrocarbon receptor-interacting protein-like 1 (*AIPL1*), which is specifically expressed in the photoreceptors and pineal gland. A defect in this gene results in a reduction in rod cGMP phosphodiesterase (PDE) levels (Liu et al., 2004), leading to phenotypes that are similar to RP. The *RPGRIP-1* and *CRB1* genes encode the proteins that are essential for photoreceptor morphogenesis (Zhao et al., 2003, Pellikka et al., 2002). Mutation in these genes results in abnormalities in photoreceptors such as oversized outer segments and develop into severe retinal degeneration.

#### 4.2.2 Animal models

Several animal models have been developed to study the pathological process of LCA. The biochemical dysfunction caused by LCA related mutations tends to be more severe than RP. In most LCA animal models, although photoreceptor degeneration is slow, retinas are often characterised by a complete inability to generate light responses from the earliest developmental stages.

The *Crx* knockout mouse model carries a targeted disruption of the *CRX* homeobox gene (Furukawa et al., 1999). Although cones and rods are present during early postnatal life, their outer segments exhibit severe atrophy from the onset, and they cannot generate responses to light. Photoreceptor degeneration starts at P30 in the *Crx* mouse, presenting a concomitant loss of cones and rods. The ONL decreases from 8-10 to only 1-3 rows within 5 months. The *Crx* mouse represents a good model for human LCA with aplasia followed by a cone-rod degeneration.

In the *RPE65* knockout mouse model, although rods and cones maintain intact outer segments until 15 postnatal weeks, rods cannot generate responses to light from the onset because there is no functional rhodopsin. *RPE65* mice exhibit a late onset photoreceptor degeneration. The ONL thinning starts from 15 weeks and declines from 10-11 layers to 7 layers at 28 weeks. The *RPE65* mouse is thus a good model for human LCA with a rod-cone degeneration.

There are also naturally occurring LCA animal models such as *RPE65* dog (which exhibits an initial normal gross retinal anatomy, but with no photoreceptor activity) and *RetGC-1* bird (early onset of photoreceptor degeneration and RPE dystrophy). In these models, the mutations cause a similar degenerative process as in human LCA, providing the opportunity to study pathological processes and attempt rescue strategies.

### 4.3 The pathology of hereditary retinal dystrophies

Despite being a polygenic disorder with many possible different origins, the pathological changes seen in retinal dystrophies are always characterised by different degrees of photoreceptor death concomitant with activation of glial cells. Inner retinal neurons such as BCs, ACs or RGCs survive the degeneration process, but undergo profound neural remodelling. The progression of retinal degeneration in hereditary retinal dystrophies can be classified into three pathological phases: phase 1, photoreceptor stress; phase 2, photoreceptor death; phase 3 neural remodelling (Figure 1-5) (Jones and Marc, 2005).

In the photoreceptor stress phase, the mutations interrupt encoding of essential proteins in the visual cycle, which commonly lead to accumulation of their metabolic products. The resultant metabolic stress induces the deconstruction of photoreceptors in terms of shortening the rods or cones (Jones and Marc, 2005). Furthermore, metabolic stress may also lead to the exposure of surface proteins such as phospholipid PS (known as “eat me signal” ) and triggers early microglial activation (Zhao et al., 2015), which sequentially mediates the activation of Müller cells (Figure 1-5B).

In phase 2, the retina undergoes progressive photoreceptor loss. The mechanisms involved may include primary cell death induced by metabolic stress (Chang et al., 1993), but they may also include non-cell autonomous processes such as autophagy and/or phagoptosis (Koenekoop, 2009, Zhao et al., 2015). Although the mechanisms of neuron-glial communication during this phase are as yet unclear, microglial cells are actively engaged throughout this phase, as indicated by microglial cells reaching peak density during that phase and maintained until the end of photoreceptor depletion (Noailles et al., 2016, Zeng et al., 2005). Meanwhile, Müller cells undergo profound

morphological changes and form a glial seal around the neural retina, resulting in separation from the RPE (Jones and Marc, 2005) (Figure 1-5 C).

With the depletion of photoreceptors, inner retinal “rewiring” is triggered. Neighbouring Müller cells hypertrophy and coalesce into large vertical columns and separate the retina into new vertically segregated domains. Meanwhile, the neurons including ACs, HCs, as well as BCs undergo morphological remodelling such as dendritic loss and sprouting of ectopic processes, and they migrate into the GCL. These cells together with RGC processes tangle together to form microneuromas (Jones and Marc, 2005) (Figure 1-5 D).

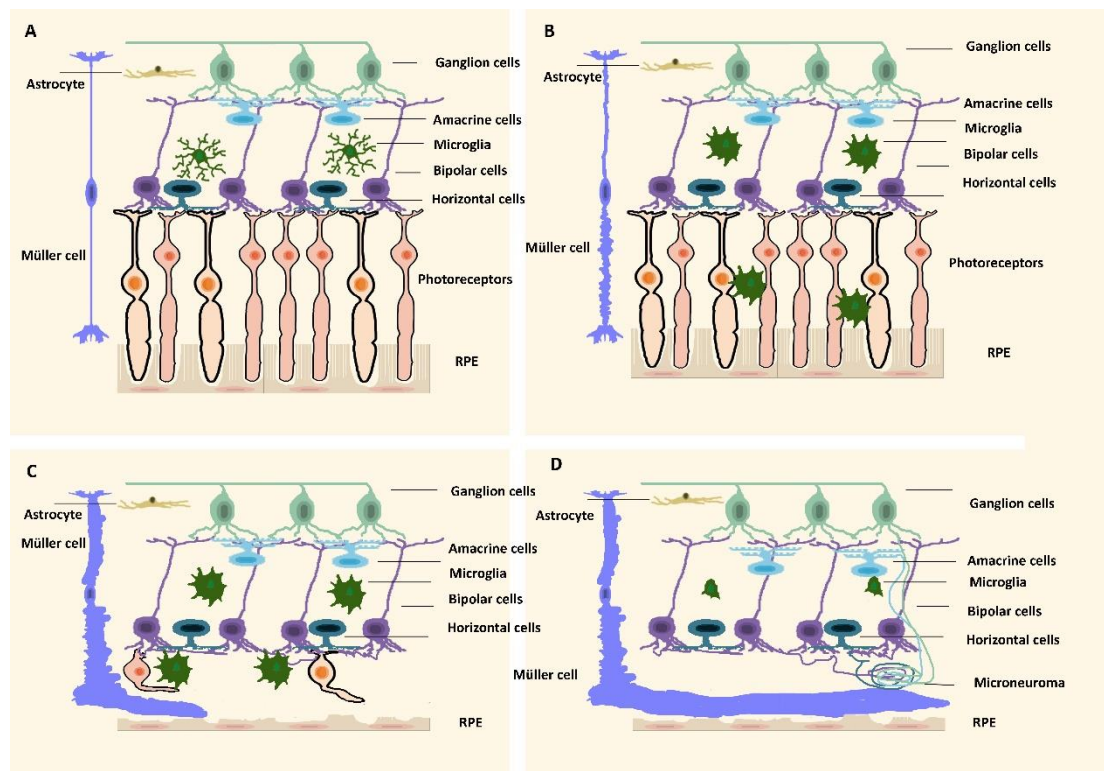


Figure 1-5 Schematic diagram of retinal degeneration progression.

A: shows the normal lamination of a healthy retina; B: shows stage 1 of retinal degeneration: the photoreceptor stress phase; C: Stage 2 of retinal degeneration: the photoreceptor death phase; D: Stage 3 of retinal degeneration: The “rewiring” phase.

#### 4.4 Mechanisms for photoreceptor death in hereditary retinal dystrophies

The survival of photoreceptors relies on the precise regulation of metabolic homeostasis and visual pigment recycling. In RP, apoptosis is the main cause that attributes to photoreceptor loss. Evidence has shown that apoptosis in RP follows a common downstream pathway regardless of the mutation. The mutations that trigger photoreceptor degeneration usually disrupt either the phototransduction cascade or the pigment cycle. In rd1 retina, the mutations result in defects in the cGMP-PDE6 $\beta$  subunit, leading to excessive accumulation of metabolic products such as cGMP (Figure 1-6 red

square). This causes a persistent opening of cGMP-gated  $\text{Na}^+$  channels, resulting in dysregulation of intracellular calcium (Chang et al., 1993, Rohrer et al., 2004) (Figure 1-6 red oval).

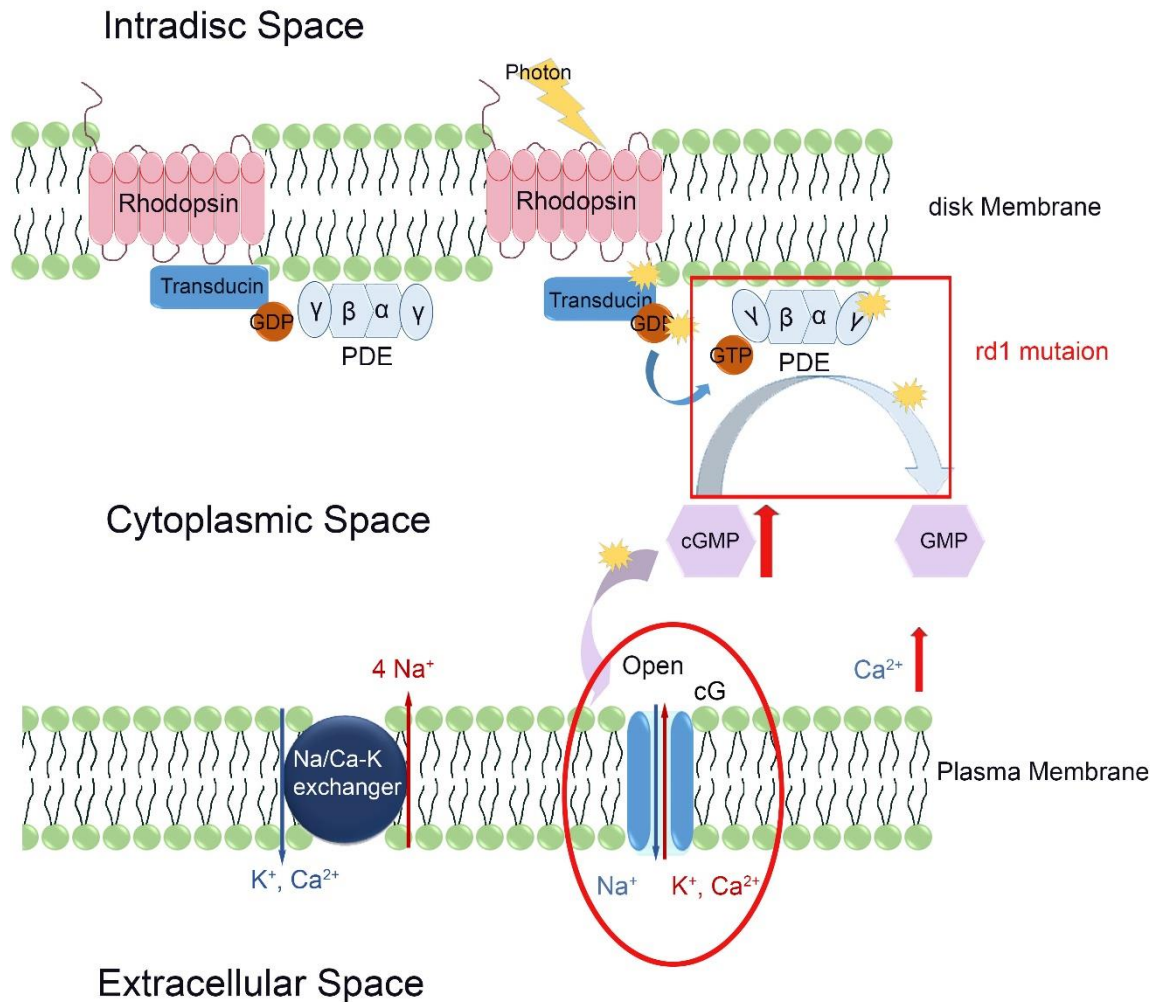


Figure 1-6 Schematic representation of phototransduction cascade phototransduction in RP photoreceptors

The RP-related mutations commonly affect the cGMP-PDE6 $\beta$  subunit which leads to the accumulation of cytoplasmic cGMP. This sequentially causes the persistent opening of the cGMP-gated  $\text{Na}^+$  channels and results in the increase of cytoplasmic  $\text{Ca}^{2+}$  level.

The homeostasis of intracellular calcium is essential to oxidative metabolism and hence increased calcium results in a rise of oxidative activity and ER stress, which sequentially lead to mitochondrial energy depletion and the production of ROS (Figure 1-7). The upregulation of calcium level also contributes to the mediation of Calpain activation. The activation of Calpain together with overproduction of ROS and ATP causes mitochondrial membrane permeabilization (MMP), the process of releasing the pro-apoptotic factors into the mitochondrial intermembrane space such as

cytochrome c, apoptotic inducing factor (AIF) and procaspases into the cytosol (Ferri and Kroemer, 2001). Meanwhile, the stimuli that cause MMP will also trigger lysosomal membrane permeabilization (LMP), the mechanism that is responsible for the release of cathepsins. These cytoplasmic pro-apoptotic factors eventually induce the apoptotic process (Johansson et al., 2010).

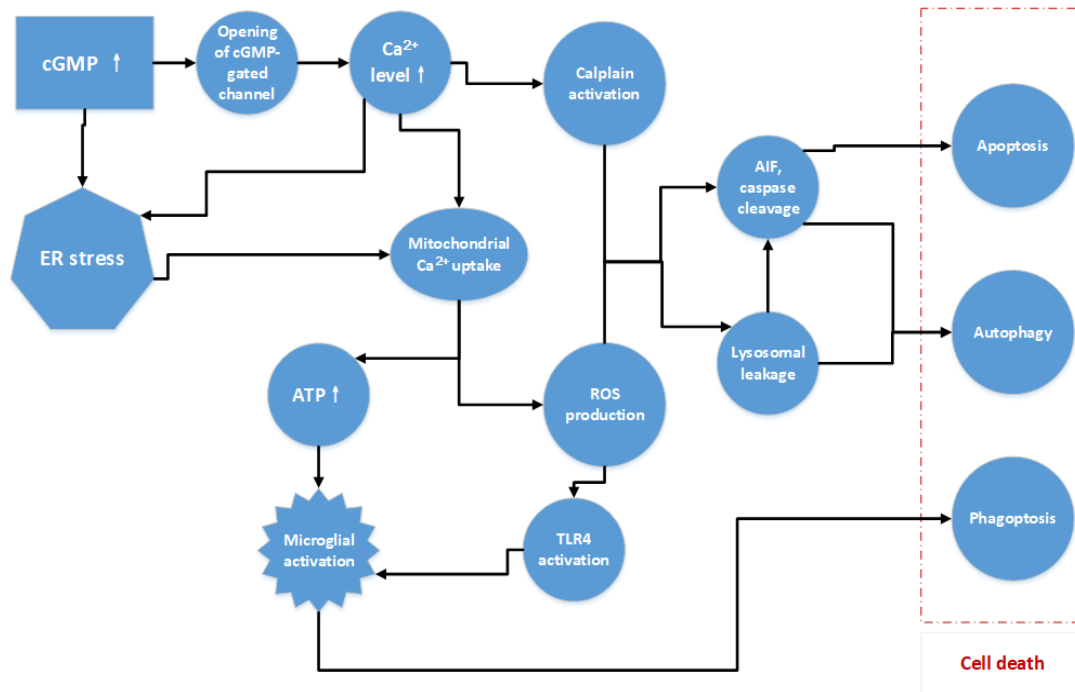


Figure 1-7 Proposed mechanisms involved in photoreceptor death in RP

The metabolic dysfunction caused by RP-related mutations usually begin with the upregulation of cGMP, which leads to the opening of cGMP-gated channel and ER stress. Following that, the increase of Ca<sup>2+</sup> level and ER stress will trigger Calpain activation, microglial activation and upregulation of ROS production. These events will eventually lead to apoptosis, autophagy, and phagoptosis (phagocytosing photoreceptor alive), which contribute to photoreceptor loss.

Although mutations in RP are usually rod specific, cones are not immune from degeneration, suggesting the involvement of non-cell autonomous death. Cone death in RP may be caused by endotoxins released by the degenerating rods, the loss of anatomical organization, and oxidative damage caused by rod death (Koenekoop, 2009, Punzo et al., 2009).

In retinal dystrophies such as LCA, the pathways that are affected by mutations are more heterogeneous. The degenerative process in LCA can follow an opposite sequence of events, as primary cone death or concomitant cone and rod loss may happen due to the mutation. Nevertheless, disruption of the phototransduction cascade and pigment cycle is still considered to be the main cause of primary photoreceptor death (Roosing et al., 2014).

## 5. Microglia in the Healthy and Diseased CNS

### 5.1 Microglia and brain macrophages

#### 5.1.1 The myeloid cells in the brain

For a long time, the brain has been referred as an immune privileged site, which is devoid of lymphatic leakage. However, recent evidence suggested that there is a broad spectrum of innate myeloid cells in the brain, including parenchymal macrophages, namely microglia, and non-parenchymal macrophages, such as perivascular macrophages, meningeal macrophages and choroid-plexus macrophages (Prinz et al., 2017).

The classification of CNS macrophages is mainly based on their location, morphology and expression of surface markers. Despite all CNS myeloid cells sharing surface markers such as *iba-1*, *F4/80*, *CD11b* and *CX3CR1*, expression of MHC II is low in microglia in contrast to the high expression in non-parenchymal macrophages. In addition, microglia exhibit a unique ramified structure surrounded by neurons, astrocytes and oligodendrocytes, whereas non-parenchymal macrophages are found in the interface between the circulation and parenchyma (Li and Barres, 2018).

#### 5.1.2 The ontogeny of myeloid cells

As the myeloid cells in the CNS, the origin of microglia and macrophages is hematopoietic. The most widely accepted hypothesis of the resident microglial origin is a yolk sac (YS) origin (Kierdorf and Prinz, 2017, Alliot et al., 1999). During embryonic development, the early wave of the erythro-myeloid progenitors (EMPs) in the YS generate the primitive microglial cells, which sequentially enter the CNS and become the major source of resident microglial cells (Ginhoux et al., 2010, Hoeffel et al., 2015). Foetal monocytes, which also arise from the EMPs during the later wave, contribute to the rest of the resident microglial cells (Hoeffel et al., 2015).

Although bone marrow (BM) derived cells are the reservoir that contributes to microglial cells proliferation under pathological condition (Xu et al., 2007), recent evidence suggests that maintenance of the microglial population in the healthy CNS may be independent from BM derived cells, and instead, relies on self-renewal of proliferating intrinsic microglial cells (Gomez-Nicola and Perry, 2015).

While the steps of the non-parenchymal macrophages origin remain to be elucidated, the previously proposed ontogeny that the non-parenchymal macrophages are initially derived from EMPs and then constantly replenished by BM derived cells is also being challenged by the recent evidence from fate-mapping experiments (Goldmann et al., 2016). Although the choroid-plexus macrophages are

partially differentiated from BM derived monocytes, the maintenance of the perivascular and meningeal macrophages is exclusively via self-renewal.

During the embryonic phase, microglial progenitors migrate into the retina via two sources: through the retinal margins and optic nerve, and via blood vessels in the ciliary and retinal circulation (Jin et al., 2016, Santos et al., 2008). The location of these cells can be identified by macrophage/microglial markers. Another wave of microglial cells entering the retina from the vitreous occurs at the end of the first postnatal week and is complete by the end of the second postnatal week. From then on, microglial cells present similar characteristics as they do in the mature retina. They are distributed across all retinal layers except for the ONL and outer segments and exhibit ramified processes (Santos et al., 2008). Similarly, to the microglia in CNS, although there is no anatomical barrier, BM derived cells do not migrate into the retina under normal physiological conditions. Instead, they reside in the optic nerve and in the blood vessels of the ciliary body, which allows them to differentiate into microglial cells and enter the retina immediately following retinal damage (Kaneko et al., 2008).

## 5.2 The function of microglial cells in the healthy and diseased CNS

Microglial cells have been referred to as the bodyguards of the CNS. They respond to any kind of chronic or acute insult to the retinal microenvironment. The status of microglial cells can be classified into two phenotypes; resting microglia, and activated microglia. The function of each is reflected by their morphology (Figure 1-8).

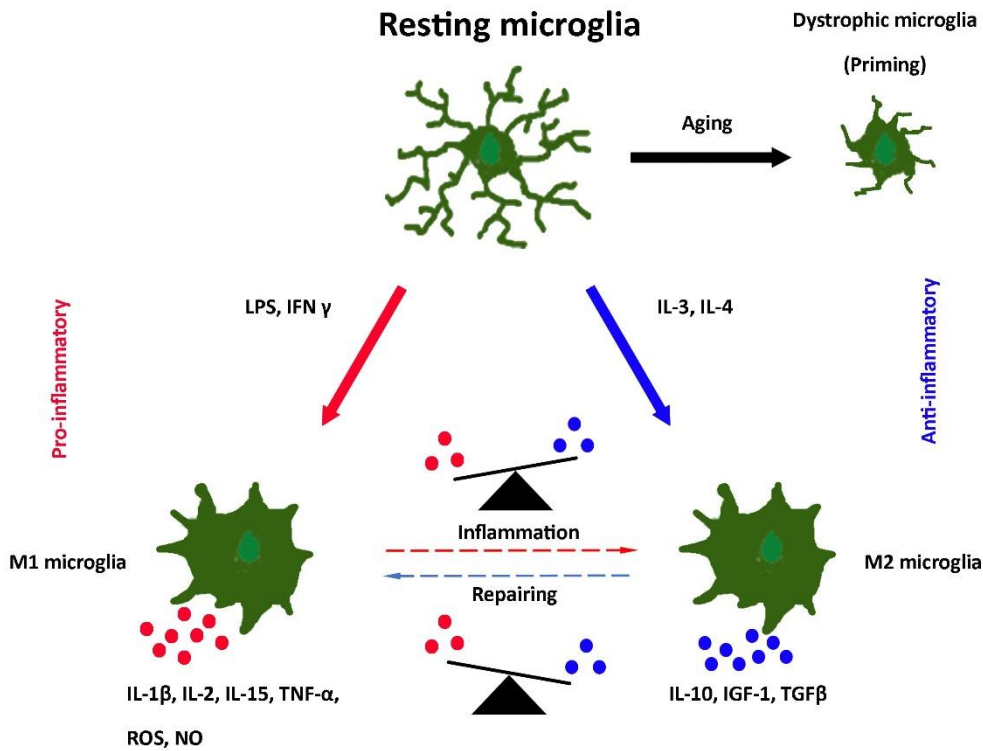


Figure 1-8 Phenotypic alteration of microglial cells

The alteration of microglial profile under different conditions. The status of microglia can be identified by their morphology. M1 and M2 microglia interact with each other, and their overall effect determines the outcome

## 5.2.1 The function of resting microglia

Resting microglial cells have a distinct ramified structure with a tiny soma and numerous long branching processes. The term resting was originally used to define the status of microglial cells in healthy tissue, which assumed that those cells were functionally dormant in normal physiological conditions. Later evidence from time-lapse imaging appears to contradict this finding. Although there are no signs of migration, microglial cells in the healthy CNS are highly dynamic. Their processes are remarkably motile, efficiently monitoring the surrounding environment, capable of quickly clearing metabolic products to prevent their accumulation (Nimmerjahn et al., 2005, Tremblay et al., 2010).

Evidence has also shown that resting microglia play an important role in supporting the development of neuronal connections and maintaining the functional integrity of mature tissue.

### 5.2.1.1 Resting microglia and synaptic connectivity

The dynamics of resting microglia are crucial for the establishment of neuronal connectivity. During synaptogenesis, microglial cells regulate developing synaptic connectivity by either reinforcing or

eliminating specific subsets of synapses via engulfment of perisynaptic processes based on the feedback from neural inputs such as visual experience. Microglial cells also sculpt the synaptic cleft via secretion of various proteases which can degrade extracellular proteins and in turn decrease the peri-synaptic extracellular space (Tremblay et al., 2010). The engulfment of synaptic processes by microglia during postnatal synaptic pruning is regulated by the complement signalling cascade CR3/C3. The synapses with weaker inputs are first identified by activated C3 and then eliminated by microglial engulfment, whilst the synapses with stronger inputs are retained and strengthened (Schafer et al., 2012). Furthermore, the anti-inflammatory cytokine TGF –  $\beta$  is also known to contribute to microglia-mediated synaptic refinement via regulating the expression of the complement component C1q during development (Bialas and Stevens, 2013).

Meanwhile, microglial cells play an indispensable role in the maintenance of synaptic function in the adult retina. Sustained depletion of these cells can lead to a progressive functional defect in retinal light responses (Wang et al., 2016).

#### 5.2.1.2 Resting microglia in vascular formation

Although microglial cells are not involved in the vascular pattern in mature CNS, lack of microglial cells during development will lead to failure of the vascular formation (Arnold and Betsholtz, 2013). In the developing CNS, microglial cells are associated with astrocytes, pericytes and endothelial cells to shape vascular sprouting (Rymo et al., 2011).

In the retina, resident microglial cells, which arrive prior to angiogenesis, rather than circulating macrophages and monocytes, play the main role in vascular formation (Greenberg and Jin, 2005, Santos et al., 2008). Arnold and Betsholtz (2013) proposed that microglial cells may also contribute to facilitating vascular branching during vascular development in the CNS, and reduced vascular branching points were observed in microglia-deficiency retina in mouse.

#### 5.2.2 Microglial activation in the diseased CNS

Under pathological conditions, microglial cells leave their resting mode and switch to a reactive status. Morphologically, they lose their ramified structure and transform into an amoeboid structure with enlarged soma and shortened processes. Associated with this morphological transformation, they undergo pronounced functional changes.

## 5.2.2.1 The main function of activated microglial cells

### 5.2.2.1.1 Phagocytosis

The main function of activated microglial cells is phagocytosis. Similar to phagocytosis in developing and healthy tissue, microglial cells actively engage in engulfing pathogens, apoptotic cells, as well as degenerated neurites. This process is considered to be secondary to cell-autonomous mechanisms triggered by mutations or other stimuli.

However, evidence has shown that activated microglial cells can also contribute to neuronal loss by phagocytosing viable neurons. This process, as part of the non-cell autonomous neuronal death during degeneration, has been termed “phagoptosis” (Brown and Neher, 2012). Phagoptosis has been reported in multiple neurodegenerative diseases, including in the retina (Zabel et al., 2016, Zhao et al., 2015, Brown and Neher, 2014).

Phagoptosis is caused by the imbalance of a variety of cell signals which have collectively been termed “eat-me” and “don’t eat me”. The “eat-me” signals include exposure of surface protein phospholipid (PS) (Brown and Neher, 2012), and calreticulin (CRT), which can activate phagocytosis via binding with lipoprotein receptor-related protein (LRP). The “don’t eat me signals”, on the other hand, can block phagocytosis via exposure of CD47 and sialic acid residues. The initialization of phagoptosis is usually a result of the overall effect of the presence of “eat-me” signals and the loss of “don’t eat me” signals (Brown and Neher, 2012).

### 5.2.2.1.2 Antigen presentation

Another important function of microglia is antigen presentation. Microglial cells are considered to be a major part of the antigen presenting cell (APC) population. The APCs are a group of immune cells that process and present surface antigens. These surface antigens can be recognized by receptors on T cells, triggering the adaptive immune response.

In conditions presenting endogenous or exogenous stimuli, T cells cannot recognize and respond to “free” or soluble antigens primarily. Instead, following phagocytosis, APCs, process phagocytosed antigens, and then, by expressing carrier molecules like major histocompatibility complex (MHC), trigger T cell activation (Mantegazza et al., 2013). There are two classes of MHC molecules. The MHC class I can be recognized by cytotoxic T cells and stimulate cytotoxic T cell activation leading to T cell proliferation, while MHC II are recognized by T helper cells and trigger T helper cell activation that in turn, release substances to attract macrophages (Jakubzick et al., 2017).

### 5.2.2.2 Reactive phenotypes of Microglia.

The concept of macrophage polarization was first brought up with the discovery of the different response of macrophages induced by cytokine IL-4. In contrast to the classical activation induced by lipopolysaccharides (LPS) and interferon- $\gamma$  (IFN  $\gamma$ ), IL-4 stimuli trigger a different series of macrophage gene expression, which was originally termed as “alternative activation” (Martinez and Gordon, 2014). The polarization of macrophage towards different stimuli was later termed as M1 and M2 activation (Mills et al., 2000).

In this concept, M1 activation is considered to be pro-inflammatory, with cytotoxic properties, while M2 activation is considered to be anti-inflammatory with regenerative properties. There are two subsets of the M2 phenotype: M2a is involved in repair and regeneration and M2b is involved in immunoregulation (Chhor et al., 2013).

M1 activation, which is also called “classical” activation, can be experimentally induced by exposing macrophages to LPS and IFN  $\gamma$  in *ex vivo* conditions. M1 activation follows a Type I inflammatory pathway, which is widely observed during bacterial and viral infection. Activated macrophages boost the release of pro-inflammatory cytokines, which aggravate inflammation (Gordon, 2007).

M2 activation is also called “alternative” activation, which can be experimentally achieved by exposure to the T helper type 2 (Th2) cytokines IL-4 and IL-3 (Gordon, 2003). M2 activation promotes tissue repair and cell proliferation, which are commonly seen in allergic conditions such as asthma as well as acute neuro-inflammation such as traumatic brain injury (Cherry et al., 2014).

However, it should be noted that, the grouping of M1 and M2 activation is determined by their ability of either presenting inflammatory response or anti-inflammatory response, whilst the source, role and signalling pathways of the macrophages may be substantially different.

Martinez and Gordon (2014) proposed that the occurrence of M1 and M2 activation is not mutually exclusive, and that the states overlap with each other. The mixed phenotype is determined by the balance of activatory and inhibitory activities under different circumstances. Accordingly, the complexity of activation states results in the diversity of microglial responses and underlies the dual role of microglial activation from pathological insults (Gomes-Leal, 2012). In acute diseases like infection and trauma, the function of microglial cells is dominated by repair and regeneration. The timely removal of toxic factors is also important for protecting neurons from further damage. Hence, the contribution of microglial cells during the early stage is considered to be protective (Davalos et al., 2005), but it is considered to be harmful in chronic conditions, as the pro-inflammatory profile usually outweighs the anti-inflammatory one in the long term.

### 5.2.2.3 Microglial activation in neurological disorders

Microglial activation is found in almost all types of neurological disorders. Although the common pathological changes in these diseases are always the expansion of microglial population and microglial infiltration around the lesion, the origin of the microglial population and the pathways involved vary significantly amongst different diseases (Dheen et al., 2007).

In acute diseases such as traumatic brain injury (TBI) and ischemic brain injury (IBI), BM derived cells enter the CNS and differentiate into microglial cells. These cells, together with the resident microglia, contribute to expanding the microglial population and to microglial infiltration into the lesion site. (Ziebell and Morganti-Kossmann, 2010, Patel et al., 2013). By contrast, in chronic conditions such as Alzheimer's disease (AD) and amyotrophic lateral sclerosis (ALS), the expansion of the microglial population is exclusively attributed to innate microglial cells. (Dheen et al., 2007).

### 5.2.2.4 Microglial cells in inherited retinal degeneration

In the healthy retina, microglial cells reside across all retinal layers except in the ONL. They exhibit a ramified structure, monitoring the microenvironment of the retina. The hallmarks of microglial activation upon photoreceptor degeneration are microglial proliferation and morphological transformation, as well as microglial infiltration into the ONL.

There are two sources that may contribute to the infiltrated microglial population in the ONL: microglial cells migrated from the GCL, and microglial cells that have differentiated from BM derived cells. The migration of microglial cells from GCL into the ONL following photoreceptor dystrophy has been well documented in the RCS retina (Thanos, 1992, Thanos and Richter, 1993, Ebert et al., 2009). Recruitment of BM derived cells into the ONL has also been observed from the beginning of photoreceptor degeneration in the rd1 retina (Sasahara et al., 2008).

Microglial activation is not merely a temporal response in retinal degeneration. Instead, the involvement of microglial-mediated process has been found throughout the degenerating phase in RP. The upregulation of microglial-specific transcripts has been detected prior to the onset of apoptosis or degeneration (Gehrig et al., 2007). In addition, the migration of microglial cells into the ONL has been observed at the very beginning of photoreceptor degeneration in several RP animal models (Zeng et al., 2005, Sasahara et al., 2008), suggesting that microglial cells may contribute to the initial pathological events of photoreceptor degeneration.

A sustained activation status of microglial cells is also observed during the advanced stage of photoreceptor degeneration in rodent RP models such as rd1 mouse and P23H rat. In the P23H

retina, increased pro-inflammatory cytokines were found in the end phase of photoreceptor degeneration (Yoshida et al., 2013, Noailles et al., 2016).

### 5.2.2.5 Mechanism involved in microglial activation

The exact mechanisms that underlie the initiation of microglial activation in retinal dystrophies are still unknown. However, several pathways have been reported to contribute to trigger it.

Toll-like receptors (TLRs) pathway has previously been reported to be involved in neuroinflammation and microglial activation. The TLRs are a family of pattern recognition receptors (PRR) expressed on the innate immune cells including microglial cells for recognising the molecular motif of a wide range of pathogens (Kielian, 2006). Previous work has shown that TLR4 activation is involved in several neurological diseases including ischemic brain injury and neurodegeneration. In retinal degeneration, evidence has also shown that delayed clearance of all-*trans*-retinal due to the disruption of RPE phagocytosis may trigger microglial activation via TLR4s (Kohno et al., 2013). The mechanism of TLR4 in microglial activation has been proposed using the classic inflammatory model, the LPS induced inflammation (Kacimi et al., 2011) (Figure 1-9).

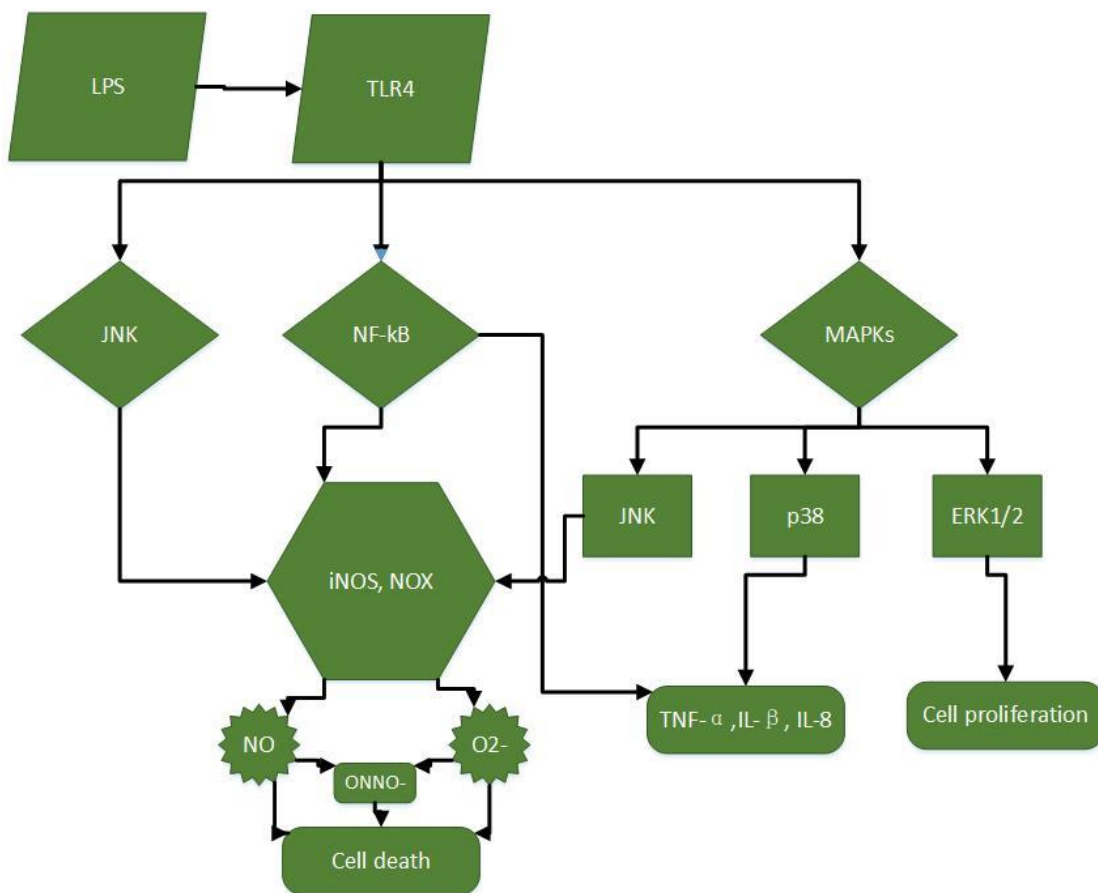


Figure 1-9 Proposed mechanism of microglial intracellular cascade induced by LPS. (2011)

*LPS binds to TLR4 on the surface of microglial cells and triggers the microglial intracellular cascade, leading to the activation of several pathways (JNK, NF- $\kappa$ B, MAPK). Adapted from Kacimi et al*

The fractalkine/CX3CR1 pathway is known to regulate  $\beta$  cell function and insulin secretion (Lee et al., 2013). However, recent studies have shown that, fractalkine/CX3CR1 signalling may contribute to modulating microglial activation (Arnoux and Audinat, 2015). Soluble fractalkine is able to ameliorate the microglial activation and reduced proinflammatory cytokine release in a drug-induced Parkinson's disease model (Morganti et al., 2012). The neuroprotective effect of fractalkine/CX3CR1 signalling has also been documented in animal models of amyotrophic lateral sclerosis and stroke. Nonetheless, the cytotoxic effect of fractalkine/CX3CR1 signalling has also been reported in several animal models of neurodegenerative diseases (Arnoux and Audinat, 2015), suggesting the neuroprotective and neurotoxic effect of the fractalkine/CX3CR1 signalling may depend on the pathological context.

The colony-stimulating factor-1 (CSF-1), also known as macrophage-CSF(M-CSF), influences the proliferation and survival of microglial cells via an adaptor protein called DNAX activation protein of 12kDa (DAP12). Furthermore, the activity of DAP12 is relied on the transcription factor PU.1. The upregulation of DAP12 and PU.1 expression have been found in microglial cells from the RP retina (Otero et al., 2009, Weigelt et al., 2007).

#### 5.2.2.6 Primed microglial cells in ageing and degenerative diseases

Previous work has shown that microglial cells in the CNS undergo alteration of their morphology with age, characterised by shortening and branch pruning of their processes (Streit et al., 2004). These ageing cells have been referred to as “dystrophic microglia” (Figure 1-8).

However, functional investigation of microglial cells in ageing CNS has revealed that their state actually shifts into an enhanced inflammatory status, in which the microglial cells:

- 1) present increased sensitivity at baseline level, with a lower threshold to become activated;
- 2) respond exaggeratedly towards immune challenges with increased production of pro-inflammatory factors like IL-1 $\beta$ , cytokines (Godbout et al., 2005) (Norden et al., 2015).

This process has been recently termed “priming” (Norden et al., 2015). Primed microglial cells have been found in ageing, albeit healthy neural tissue, in the chronic phase after traumatic brain injury (TBI), and in neurodegenerative diseases. The cause that underlies priming is still unclear. Possible mechanisms may be associated with various typical hallmarks of ageing including an increase in oxidative stress, as well as the increase of inflammasome activity (Fenn et al., 2013, Youm et al., 2013).

### 5.2.2.7 Functional diversity of homogeneous microglia

Microglial cells make up to 5-12% of the total cell population in the CNS (Lawson et al., 1990). Whilst our understanding of the function of different neuron subtypes has vastly improved over recent decades (Masland, 2012), a detailed knowledge of the components of the microglial population is still unclear.

Currently, there is a consensus on the dual role of microglia; neuroprotective and cytotoxic (Jin et al., 2016, Ferreira and Bernardino, 2015, Patel et al., 2013). However it is also clear that these cells should not be treated as a functional uniform population, instead, their functional diversity may be the result of differences of unknown functional subsets (Gomez-Nicola and Perry, 2015, Hanisch, 2013).

These authors have suggested that specific cytokines such as tumour necrosis factor  $\alpha$  (TNF $\alpha$ ) initially trigger the activation of a master subset of microglial cells. These 'master' cells then mediate the activity of neighbouring cells. Hence, the reactive phenotypes and their associated functions could be a reflection of different responding sets of microglial cells, instead of an overall effect of the entire microglial population.

This concept is yet to be confirmed by more experimental validation. However, the differential expression of surface protein such as MHC I and MHC II on microglial cells may support the existence of these functional subsets. Considering the diversity of the sequential pathways that lead to completely different outcomes, a better understanding of the classification of these subsets and their function during the course of neuropathology may provide promising therapeutic targets.

## 5.3 Microglial cell markers

As 'the macrophage' of the CNS, microglial cells have been found to express most of the known macrophage-associated markers, which can facilitate their characterization. Ionized calcium binding adaptor molecule-1 (iba1) is considered to be the most reliable marker for microglial cells, and it is specifically expressed in both amoeboid (activated) and ramified (resting) microglial cells in the CNS from embryonic stages to adulthood (Ito et al., 1998, Santos et al., 2008). Other markers such as CD11b, CD45, CD68 are also expressed in both resting and activated microglial cells, which also can be used to label the overall microglial population.

The hallmark of microglial activation is the transformation from ramified to amoeboid structure. However, practically, classification based on morphology can be subjective and ambiguous. Although none of the available markers are able to accurately differentiate activated from resting microglia, a

few biomarkers for the functional status have been used to broadly identify the involved subsets (Table 1-2).

Table 1-2 Markers on microglial cells.

Resting (ramified) microglia	activated (amoeboid) microglia
iba1	iba1
CD11a, CD11b, CD11c	CD11a, CD11b, CD11c
MHC I	MHC I
	MHC II
F4/80 (Only during embryonic period )	F4/80
	CD64, CD36
CX3Cr1	CX3Cr1
CD45	CD45
CD68	CD68
Isolectin B4	Isolectin B4
Mac-1	Mac-1
CD18	CD18
OX42	OX42
	TSPO
RMG-1	RMG-1
RMG-2	
LN-1	LN-1
OX6,OX3,OX18	OX6,OX3,OX18

Summarized from Li et al (2015) and Greter et al (2015)

The F4/80 antigen is a member of the macrophage- specific adhesion-GPCR family (Lin et al., 2010). The expression of F4/80 is similar to iba-1 in the developing retina, but it decreases after birth. In the adult retina, F4/80 is highly expressed in the amoeboid microglia, which can be used as a marker to identify microglial phagocytosis (Table 1-2). However, as expression of F4/80 decreases dramatically after birth, the sensitivity of F4/80 on detecting microglial cells in adult CNS is relatively low. Hence, it may be ideal to be used as a complementary marker rather than being used alone.

As APCs, the expression of major histocompatibility complex MHC class I and class II are also found in microglial cells under pathological conditions (Penfold et al., 1997, Akaishi et al., 1998, Noailles et al., 2014). The differential expression of MHC classes on microglial cells may assist in distinguishing the population that contributes to downstream T cell activation. Furthermore, MHC II + cells are widely observed in aged CNS, and are considered to be a sign of priming (Perry and Teeling, 2013).

The translocator protein (18kDa) (TSPO) is also highly expressed in reactive rodent and human retinal microglial cells, but it is weakly expressed in the healthy retina (Karlstetter et al., 2014), and therefore it is regarded as a reliable biomarker of neuroinflammation and gliosis (Karlstetter et al.,

2015). CD64, a high affinity Fc gamma receptor, and CD36, a class B scavenger receptor, are also both known to have increased expression in phagocytic microglia (Indik et al., 1994, Martin et al., 2007).

Nevertheless, despite the numerous markers available, none of them are able to differentiate between resident microglia and BM derived microglia. One solution to this problem is to use a chimeric bone-marrow (BM) transplant model. This chimeric model is made by transplanting GFP+ bone marrow of a donor mouse into an irradiated mouse. Hence, the extrinsic microglial cells can be identified because they are GFP+, whereas intrinsic cells are GFP-.

## 6. Müller cells in healthy and diseased retina

### 6.1 The anatomy and physiology of Müller cells

As the main glia cell in the vertebrate retina, the MGs span across the entire retinal thickness, with its cell body residing in the INL and two trunks processing towards the outer and inner surface of the retina where the trunks expand into endfeet and form the OLM and the inner limiting membrane(ILM). The important anatomical and metabolic functions played by MGs are reflected in their unique anatomical design.

#### 6.1.1 The anatomical homeostasis

Acting as scaffolds spanning the entire retina thickness, MGs present a unique biomechanical character. These mechanical properties of MGs are confirmed via a technique called scan force microscope(SFM) measurement. It shows that MGs possess a softer property, especially in their processes, when compared to neurons(Lu et al., 2006). This viscoelastic characteristic of MGs allows more flexibility while neurites grow and branch during development(Lu et al., 2013). It also protects neurons from mechanical pressure(Lindqvist et al., 2010). Notably, this viscoelastic property undergoes alterations in pathological conditions. In an ischemic model, the MGs became stiff in accordance with the upregulation of the intermediate filaments(IFs) such as glial fibrillary acidic Protein(GFAP). Although IFs are not the main contributor to the viscoelastic behaviour of MGs in physiological conditions, overexpressed IFs are responsible for the stiffness behaviour of activated MGs. In an ischemic model, MGs from GFAP knock-out mice retain their softness whereas MGs from wild-type mice become activated and stiffer(Lu et al., 2011); (Lu et al., 2006).

#### 6.1.2 Metabolic homeostasis

Neurons are highly vulnerable to oxidative stress, energetic deficiency and osmotic changes, whereas MGs are known to be relatively more resistant to oxygen and glucose deficiency. Such resistance to metabolic stress may allow MGs to spare oxygen and glucose for the neurons in their

vicinity, especially during ischemia and hypoglycemia(Winkler et al., 2000). On the other hand, MGs also provide crucial neurotrophic function for the survival of photoreceptors by releasing antioxidant such as glutathione and neuroprotective factors such as bFGF to increase the viability of photoreceptors(Harada et al., 2000, Penn et al., 1987). Transgenic ablation of MGs in a rat model of retinal dystrophy induces massive photoreceptor death(Shen et al., 2012).

Water and potassium accumulate in the retinal extracellular space due to the constant oxidative activities and neuronal activity. MGs express high density of aquaporin-4 water channels and several types of membrane potassium channels, maintaining the balance of spatial K<sup>+</sup> buffering for neural activity. These channels also facilitate water redistribution in the inner retina, supporting water homeostasis in the retina and the RPE and keeping neurons from swelling. (Bringmann et al., 2004).

### 6.1.3 Neurotransmitter recycling

Another important contribution MGs make to the balance of neural activity is the recycling of neurotransmitters. MGs express transporters for the uptake of glutamate and  $\gamma$ -aminobutyric acid(GABA)(Biedermann et al., 2002, Bringmann et al., 2013). Glutamate is released from the terminals of PRs and BCs. MGs take up glutamate and GABA from the extracellular space and transform them into glutamine via the glutamine synthetase(GS) pathway. Glutamine will then be released back to neurons as a precursor for GABA and glutamate synthesis. The fast synaptic transmitter clearance function of MGs is necessary for the maintenance of excitatory synaptic function and neurotoxic prevention(Barnett et al., 2000).

## 6.2 Activation of Müller cells in retinal degeneration

Although photoreceptor apoptosis is considered to be the beginning of degeneration in RP, activated MGs have been reported at the early stage of the degenerative process in many RP animal models(Chua et al., 2013, Vogler et al., 2013). The activation of MGs goes in concert with PR degeneration. As an indicator of "retinal stress"(Lewis and Fisher, 2003, Bringmann and Wiedemann, 2012), GFAP expression in MGs remains low during the rod degenerating phase, undergoing significant upregulation later on, at the beginning of the cone degeneration phase. GFAP expression decreases once both rods and cones photoreceptors have died (Chua et al., 2013). As mentioned above, GFAP overexpression causes alteration of viscoelastic properties in activated MGs. The processes of MGs become stiffer and this could help the PRs structural integrity when the cell number decreases during degeneration. The activation process of MGs is considered to be neuroprotective at the beginning of degeneration because of its contribution to anatomical support and neurotrophic factors releasing (Lu et al., 2011). However, in the longer term it will have toxic

effects by inducing the migration of cone cells, and by inhibiting the growth of neurites and regeneration.

Notably, an alteration of glutamate uptake and degradation has been observed even before the onset of photoreceptor death, which indicates that the malfunction of MGs may play a role in the aetiology of retinal degeneration (Fletcher and Kalloniatis, 1996).

Activation of MGs is non-proliferative before the onset of photoreceptor death, but it becomes proliferative once PRs begin to die. The potassium channels expressed in MGs commonly remain normal during the entire photoreceptor degeneration phase in the rd mouse model (Chua et al., 2013). In Royal College of Surgeons (RCS) rats, another model of retinal dystrophy, potassium currents change at very late stage of degeneration (Zhao et al., 2012).

In addition, as the major source of inflammatory mediator, MGs are also known to play an important role in the inflammatory process in the retina. A wide range of inflammatory mediators such as IL-6, TLRs, which can be mediated by microglial cells, are found to be expressed by MGs (Liu et al., 2015). Upon an insult, MGs are able to respond towards changes of the inflammatory factor IL-1 $\beta$  by modulating production of IL-6 through the p38 MAPK/NF- $\kappa$ B pathway (Liu et al., 2015). Evidence has also suggested that there is a bidirectional interaction between microglial cells and MGs through which activated microglial cells are able to influence MGs directly and initiate adaptive responses of both cells towards insults. Meanwhile, the inflammatory mediators expressed by MGs and the MG processes can facilitate the intraretinal migration of microglial cells. Hence, a better understanding of the role of microglial-Müller cells would provide potential therapeutic targets for diseases such as retinal degeneration.

## 7. Aims and hypothesis

The evidence presented above suggests that glial activation may contribute to exacerbating photoreceptor loss during retinal degeneration by:

- 1) Developing a reactive phenotype related to the onset of photoreceptor degeneration and subsequently releasing inflammatory factors that lead to photoreceptor death.
- 2) Primarily phagocytosing viable photoreceptors due to the imbalance of the “eat me” and “don’t eat me” signals.

As noted in section 5.2.2, microglial activation occurs in heterogeneous states during the degeneration process. The overall effect of activation states is highly dynamic, and relies on the balance of micro-environmental change as well as the genetic defects albeit to a lesser. Hence, we

hypothesised that the status of microglial activation may change during the process of photoreceptor degeneration and may vary with the causative mutation, which may sequentially affect the response of MGs. Furthermore, we also hypothesised that regulating microglial activation may improve photoreceptor survival by reducing microglial-mediated cell death.



## **Chapter 2. Materials and Methods**



# 1. Animals and Surgical Procedures

## 1.1 Animals

Three strains of mice were used: C3H/HeNHsd (also known as rd1) and *Crx*<sup>-/-</sup> (cone rod homeobox) were used to study the time course of retinal degeneration in a fast and a slow model respectively; C57BL/6 was used as wild-type (WT) control. C3H/HeNHsd was obtained from Harlan Laboratories (Indianapolis, USA) and bred in house. These mice were homozygous for the *Pde6brd1* allele. The naturally occurring mutation results in abnormality of rod photoreceptor cGMP- phosphodiesterase, leading to an early onset of retinal degeneration (Bowes et al., 1990). The *Crx*<sup>-/-</sup> mice originated from our in-house colony, originally acquired from Connie Cepko (Harvard University). The *Crx* gene acts as the upstream gene for a series of outer segment-specific genes. Disruption of the *Crx* gene results in reduced expression of genes encoding for rhodopsin, opsin, recoverin, etc. Although the outer segments do not form normally in the first place, the *Crx* retina undergoes a relatively slow degeneration process, which takes 7 months for the ONL to decrease from over 12 rows to 1~2 rows (Pignatelli et al., 2004). Mice were aged from P10 to P240 in order to obtain a comprehensive overview of the retinal degenerative process in both strains. All mice were kept under 12 hours light/dark cycle with unrestricted food and water. All procedures on animals were conducted in accordance with the Animals (Scientific Procedures) Act 1986 issued by the UK Home Office.

## 1.2 Drug preparation

The lyophilized solid of Neurostatin (Disialoganglioside GD1b from bovine brain (Sigma) was firstly dissolved in CHCl<sub>3</sub> and then aliquoted into 100µg per sample. The solution was then placed in a film hub, and the powder was collected after the liquid had evaporated and stored at -20°C.

## 2. Immunohistochemistry

### 2.1 Tissue preparation

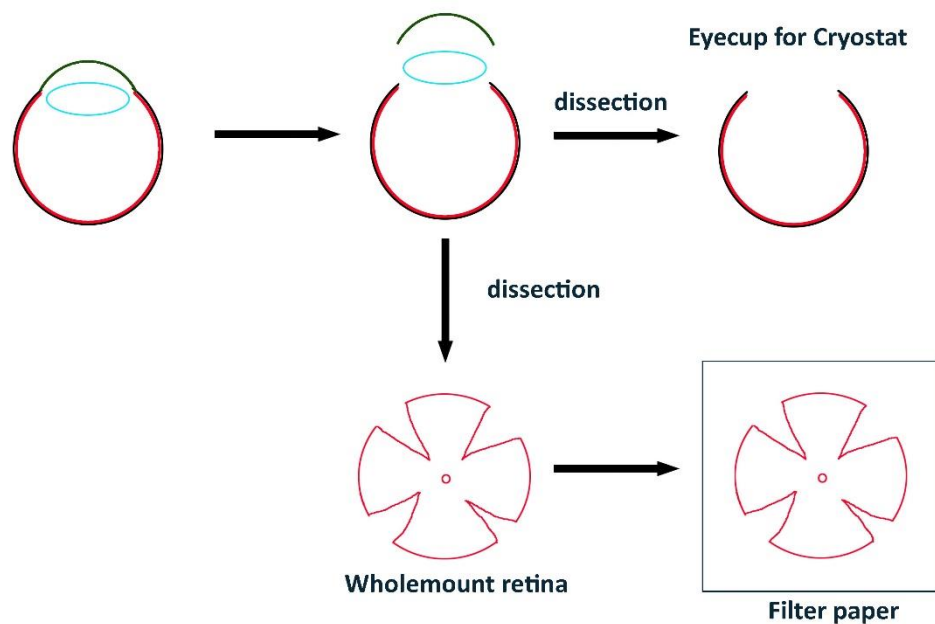


Figure 2-1 Schematic graph of tissue preparation

Schematic graphs showing how the retinal tissues were prepared for cryostat section and wholemount retina. Black line: sclera; Red line: retina; Light blue line: lens; Green line: cornea.

Mice were sacrificed by cervical dislocation. For wholemount studies, the eyes were enucleated quickly and then transferred to carboxygenated artificial cerebrospinal fluid (aCSF). The anterior chamber was removed, and the sclera and choroid were gently peeled off. The isolated retina wholemount was then mounted on filter paper (Figure 2-1). The whole-mount retinas were fixed in 4% paraformaldehyde (PFA) with 200mM sucrose in 0.1M PB (1×, PH7.4) for 1 hour and then collected for immunohistochemistry.

For cryostat sections, after enucleation, the anterior chamber and vitreous body were removed (Figure 2-1). The eyecups were then immersed in 4% PFA with 200mM sucrose in 0.1M PB(1×, PH7.4), fixed for 1 hour at room temperature, and then transferred to sucrose solution in 0.1M PB (PH 7.4) for dehydration. The eyecups were kept in 10% sucrose for 1h, 20% sucrose for 1h, and then 30% sucrose overnight. The eyecups were then embedded in OCT compound medium (Tissue-Tek, Elkhart, IN) and sectioned for immunohistochemistry (Bright OTF 5000 Cryostat, The United Kingdom). Sections within 400-600  $\mu\text{m}$  (based on the

age of the mice) from the optic nerve on both sides were collected on gelatin-coated slices (MENZEL-GLÄSER, Germany) and stored at -20° C until used.

## 2.2 Immunohistochemistry for wholemount

Following fixation, retinas were transferred into 1.8 ml tubes for the following steps. They were washed with 0.1M PB for 30 min, and then incubated with primary antibodies for 72 h at 4° C. After incubation, retinas were rinsed with 0.1M PB for 30 min and then incubated with a secondary antibody with 5% serum and 0.3% TritonX-100 in 0.1M PB in dark at room temperature for 1.5 h. Retinas were then washed with 0.1M PB for another 30 min and then transferred to gelatine-coated slides with photoreceptors side up. The filter paper was gently removed, and retinas were flattened before adding antifade mounting medium (with DAPI) (Vectashield). Slides were stored at -20° C until observation.

## 2.3 Immunohistochemistry for vertical sections

For each antibody, three non-consecutive slices per mouse were selected for staining. The labelling for cryostat sections was similar to the procedure described above except that the incubation time for primary antibodies was shorter, lasting only 12 h.

For terminal deoxynucleotidyl transferase dUTP nick end labelling (TUNEL) assay, the samples were incubated with freshly prepared permeabilization solution (0.1% TritonX-100 and 0.1% sodium citrate) at 4° C for 10 min, followed by rinsing for 30 min with 0.1M PB. The samples were then incubated with freshly prepared TUNEL cocktail (labelling solution: enzyme solution = 9:1) (In Situ Cell Death Detection Kit, Roche Life Science) for 1h at 37° C. No secondary antibodies were required for TUNEL assay.

Antibodies and serum used are summarized in Table 2-1 and Table 2-2.

Table 2-1 Primary antibodies used in this study

Antigen	Antibody(clone)	Dilution	Source
Rhodopsin(1D4)	Mouse monoclonal [1D4] to Rhodopsin	1:200	Abcam
S Opsin	Goat polyclonal to S Opsin	1:150	Santa Cruz
Iba1	Goat polyclonal to Iba1	1:500	Abcam
Glial fibrillary acidic protein (GFAP)	Mouse monoclonal to GFAP	1:400	Sigma
Glutamine synthetase (GS)	Rabbit polyclonal to Glutamine Synthetase	1:1000	Abcam

Table 2-2 Secondary Antibodies used in This Study

Antibody	Host	Dilution	Source
Anti-goat IgG(H+L), Alexa Fluor 586	Donkey	1:150	Thermo Fisher Scientific
Anti-mouse IgG, FITC	Donkey	1:400	Jackson ImmunoResearch
Anti-mouse IgG(H+L), Cy3	Goat	1:400	Jackson ImmunoResearch
Anti-rabbit IgG(H+L), Alexa Fluor 488	Donkey	1:200	Thermo Fisher Scientific
Anti-rabbit IgG, FITC	Goat	1:150	Sigma-Aldrich

### 3. Microscopy and Image Analysis

#### 3.1 Microscopy and image processing

For wholemount retinas, images were scanned using either Nikon TE2000 Invert fluorescence microscope with 20× magnification or Zeiss AxioImager with apotome (Zeiss, Germany) with 10× magnification. The Zeiss AxioImager widefield technique was used to capture images of widefield whole-mount retinas and tiled together automatically. The apotome mode was used to obtain confocal-like Z stack images. Each field was scanned from top to bottom to cover the entire thickness of the retina with an interval of 3µm.

For 20µm cryostat sections, images were acquired using Nikon TE2000 Invert fluorescence microscope with 20× objective (Nikon, Japan). Each slice was scanned systematically from dorsal to ventral ora serrata. For 30µm cryostat sections, images were acquired using Nikon

NiE upright fluorescence semi-automated microscope with 40× oil objective. Slices were scanned following the same protocol, except that each field of the images was scanned from the top to the bottom using automated Z drive platform with an interval of 3µm. All raw images were then processed using ImageJ to enhance the quality.

### 3.2 Numbering for blind observation

Each eye was randomly assigned an integer between 1 and 600. The randomization was done in Microsoft Excel. After randomization, the images were masked by a second person, and the observer for cell counting had no access to the specimen information of the images.

### 3.3 Cell counting

Following image enhancement, images were manually analysed using ImageJ cell counter. Each slice was divided into six equidistant areas from the dorsal to ventral ora serrata (two periphery, two medium, and two peri optic nerve). The density of cells was determined by the numbers of cells in each defined area divided by the length of the defined area measured at the GCL.

### 3.4 Thickness of Outer Nuclear Layer

The evaluation of the survival photoreceptors was conducted by the assessment of the thickness of the ONL. To analyse the ONL thickness, five positions were randomly selected in each image with an interval of 50-70µm to offset the uneven distribution of ONL thickness. Intervals were consistent within each image and were determined by the length of the retina in the image. The ONL thickness was measured on images labelled with DAPI at each selected position (Figure 2-2, black line), while the thickness of the retina was determined by measuring the distance between the outer edge to inner edge at each corresponding position in the same image (Figure 2-2, white line). The ONL ratio (ONL thickness/ retinal thickness) was also used to compensate for the bias of retinal thickness caused by sectioning.

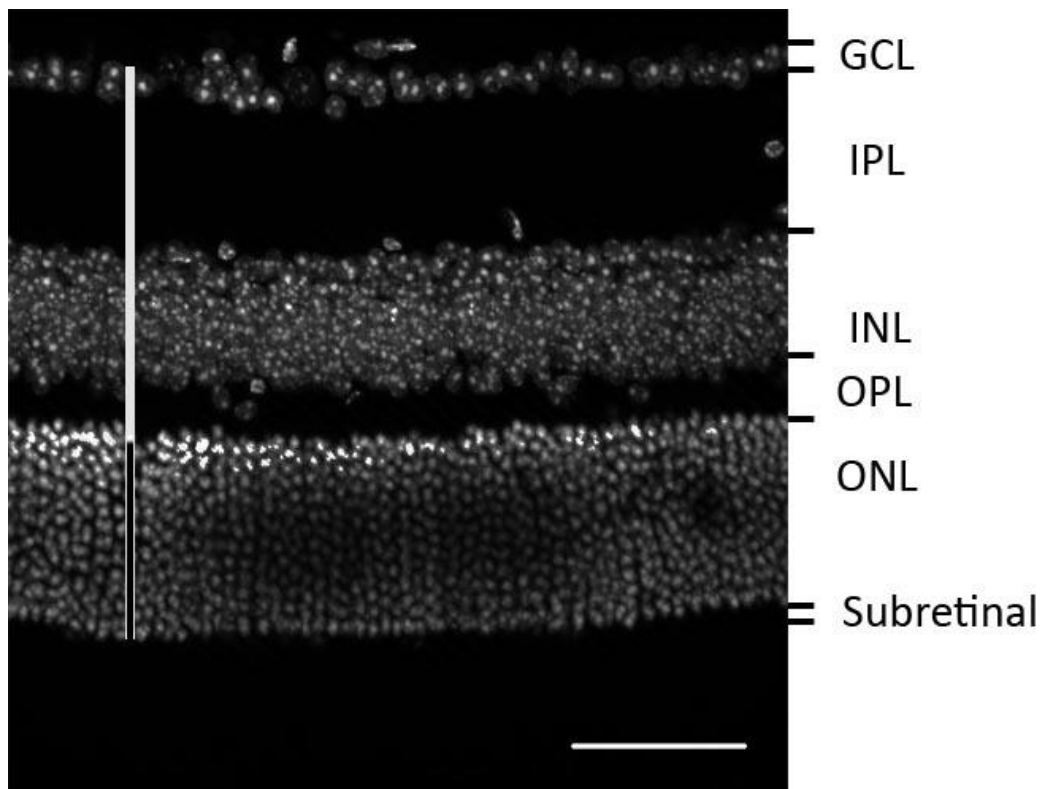


*Figure 2-2 Laminated retinal structure visualised by DAPI staining.*

*Representative images showing how retinal thickness and ONL thickness were measured. White line defines the retinal thickness, and the black line defines the ONL thickness. Scale bar: 50  $\mu$ m. Image was taken from the central area of the retina of a P100 WT mouse.*

### 3.5 Iba1

To evaluate the phenotype and location of microglia cells during retinal degeneration, ionized calcium binding adapter molecule 1 (iba1) was used to stain microglia. iba1 is recognised as a marker expressed in macrophages/microglia. A positive microglial cell was defined as a cell with the soma labelled by iba1 and the nucleus labelled by DAPI. Staining of cell processes but not the cell soma was not included. Based on their location, iba1+ cells were then differentiated into five categories according to the layers defined by DAPI staining (as shown in Figure 2-2). The position of microglial cells was determined by the location of their somata.

### 3.6 GFAP

To assess the activation of MGs, glial fibrillary acidic protein (GFAP) was used to stain activated MGs and astrocytes. Due to the unique distribution of MGs and astrocytes, These two cells are distinguishable using GFAP staining. Astrocytes are confined within NFL, whilst MGs spans across the entire thickness of the retina. GFAP is considered as a stress marker in CNS system. As opposed to the physiological status in which GFAP expression is confined

within NFL, activated MGs are defined as GFAP+ filaments extending towards outer retina. The filaments that passes half of the retinal thickness are counted as GFAP+ filaments.

### 3.7 Apoptotic cells

TUNEL assay was used to detect the presence of apoptotic cells by labelling the terminal end of nucleic acids on the DNA fragments. An apoptotic cell was determined by the presence of positive TUNEL staining overlapped with DAPI staining. The numbers of cells in the ONL and the areas proximally to ONL were recorded respectively.

## 4. Data Processing and Statistical Analysis

Statistical analysis was carried out using Matlab 2016b Statistics Toolbox (The Mathworks, Inc.). Data were shown as mean  $\pm$  standard error. The Spearman's rank correlation test was used to identify possible relationship between the iba1 positive cells in each layer and: i) thickness of ONL; ii) numbers of GFAP positive cells; numbers of TUNEL positive cells. The same correlation was performed to determine: i) the relationship of the iba1 positive cells in different retinal layers; ii) the relationship between ONL thickness and TUNEL positive cells. Repeated ANOVA was used to compare the changes in numbers of each cell type with age. Each cell type was analysed separately. Two way ANOVA was used to compare of the cells numbers and ONL thickness at different days post injection with/without drug.



## **Chapter 3. Photoreceptor Degeneration in Rd1 and Crx Retina**



## 1. Introduction

A common feature of hereditary retinal degenerations is photoreceptor depletion. However, despite the fact that there is no difference in the terminal stages of degeneration, the mechanisms that will eventually lead to photoreceptor death may vary across different gene mutations, allowing potential specific targets for preventing photoreceptor loss.

Apoptosis is considered to be the cardinal feature of photoreceptor degeneration in RP (Cottet and Schorderet, 2009), where rod apoptosis is most prevalent, caused by rod specific mutations that disturb either the pigment cycle or phototransduction cascade (Cottet and Schorderet, 2009, Chang et al., 1993). Additionally, non-autonomous cell death such as autophagy, phagoptosis, have also been implicated during photoreceptor degeneration (Punzo et al., 2009).

Although cones are not affected by mutations in RP, they eventually die as a result of the changes in the glucose level caused by rod death (Koenekoop, 2009), and also because of autophagy triggered by rod loss (Punzo et al., 2009).

In other retinal dystrophies, however, such as Leber's congenital amaurosis (LCA), which is related to mutations in several genes including RP65, CRX, CRB1 (den Hollander et al., 2001, Hamel, 2007, Furukawa et al., 1997), cone loss can be primary and events can follow the opposite sequence (cone to rod), or in the most severe cases, manifest as concomitant cone and rod loss.

Rd1 mice, the most popular animal model for retinitis pigmentosa, undergo a fast degenerative process (Bowes et al., 1990). The time course of photoreceptor degeneration in rd1 retina has been well defined, due to rod apoptosis, while ensuing cone loss results from non-cell-autonomous mechanisms (Punzo and Cepko, 2007, Zeng et al., 2005).

Unlike the single pathway affected in the rd1 retina, the Crx homeobox gene is expressed exclusively in photoreceptors and contributes to regulating the expression of other photoreceptor genes. The Crx retina is characterised by atrophied photoreceptor morphogenesis during the first three postnatal weeks, affecting both rods and cones. The defects not only lead to complete atrophy of outer segments, but also to extremely short inner segments. In addition to the abnormal formation of the inner and outer segments, other features have been noted including the presence of an unknown extracellular matrix material, displaced nuclei in the outer segments layer, and numerous vesicles with 100-200 nm diameter in the inner segment layer (Morrow et al., 2005). Hence, different mechanisms may be involved during the degenerating process.

Nevertheless, the late onset of photoreceptor degeneration and slow degenerative process make the Crx retina a useful model to study the consequences of photoreceptor loss. Furthermore, the

absence of outer segments and the complete lack of a light response make it ideal to investigate cell interactions without the interference of retinal damage caused by light exposure.

It has been previously demonstrated that the onset of photoreceptor loss starts from P30 and lasts for six months in the Crx retina (Furukawa et al., 1999). However, the kinetics of photoreceptor degeneration during the process and how apoptosis contributes to the photoreceptor loss remain unclear. The aim of this chapter was therefore to investigate the kinetics of photoreceptor degeneration in Crx retina and compare it with the well-defined rd1 mouse model in order to set up a basis for the following studies of glial activation.

## 2. Specific Methods

### 2.1 Animals

To investigate the time course of retinal degeneration, a cohort of Crx mice were sacrificed from P10 to P150, at 10 days intervals before P100, and then collected at P130 and P150. As the rd1 retina follows a fast degenerating process, rd1 retinas were harvested at initially shorter intervals, P10, P15, P20, P30, P60, and P110. Wild-type retinas were collected at P10, P20, P30, P80, and P100 for comparison. No less than three mice (one eye from each) from each strain were included in each time point.

### 2.2 Tissue collection and immunohistochemistry

The retinas were harvested and stored following the procedures described in Chapter 2, except that the thickness of the cryostat sections for TUNEL assay was 20 $\mu$ m. Immunohistochemistry used the protocol described in Chapter 2.

Rhodopsin was used to label rods, while S opsin was used to label red/green cones. TUNEL assay was used to identify apoptotic cells.

### 2.3 Microscopy

Cryostat sections were scanned using a Nikon TE2000 Invert fluorescence microscope with 20 $\times$  objective (with 10 $\times$  eyepiece and 1 $\times$ intermediate magnification) at a 1344  $\times$  1024 pixel resolution. Each slice was scanned systematically from the dorsal to ventral ora serrata with only one single image in each field.

Image processing, cell counting, data analysis and statistics used the same procedures as described in Chapter 2.

## 3. Results

### 3.1 Photoreceptor degeneration in rd1 retina

#### 3.1.1 The depletion of Photoreceptors occurs during the first postnatal month in rd1 retina.

To validate the time course of photoreceptor degeneration in rd1 retina, the cryostat retinal sections were examined to compare the ONL thickness at different ages in rd1 retina. In WT retina, the alignment of photoreceptor nuclei was consistent with that observed across different ages with a highly organized arrangement in the ONL (Figure 3-1 A and B). By contrast, although the photoreceptor nuclei were orderly arranged in the ONL and evenly distributed throughout the entire retinal length at P10, the ONL thickness was slightly reduced to approximately 12-15 layers of nuclei in the perioptic nerve area and 9-12 layers of cells in the peripheral area (Figure 3-1 C). At P15, the ONL started to lose its alignment and the ONL thickness was significantly reduced. By P20, there was only one layer of photoreceptor nuclei left, and these nuclei were still detectable at P30, but at a lower density, with gaps present between nuclei (Figure 3-1 F).

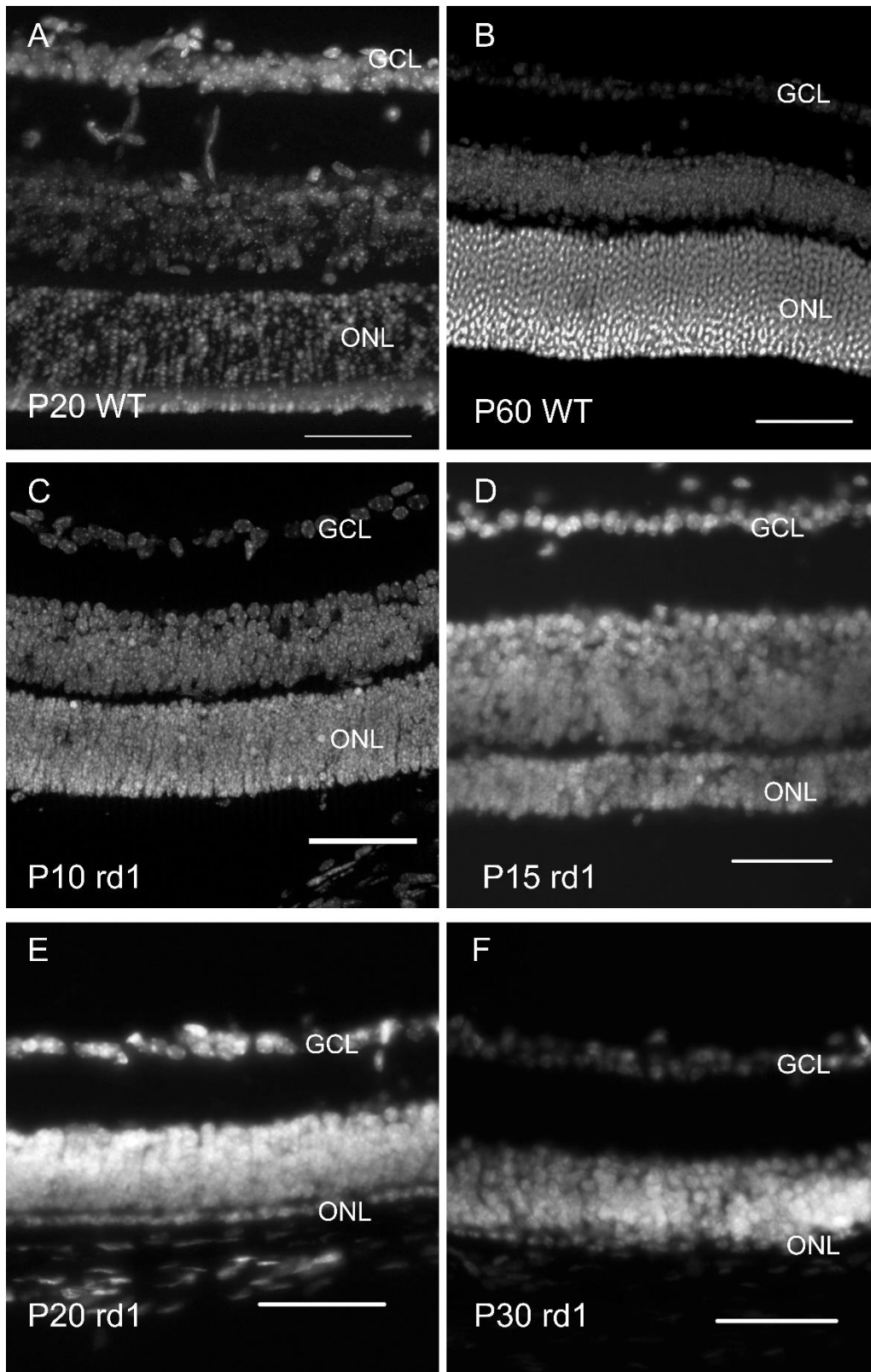


Figure 3-1 Fluorescence micrographs showing the change of ONL thickness against age in rd1 retina.

A-B: DAPI stained retinal sections from developing retina (A) and adult retina (B) of WT mouse. In the healthy state, the photoreceptor nuclei maintained a regular appearance with organized alignment throughout all ages. C-F: DAPI stained retinal sections from rd1 retina between P10-30. In rd1 retina, the photoreceptor nuclei remain clearly aligned at P10, while the ONL is slightly thinner than in WT (C). The ONL thickness is sharply reduced by P15, and alignment of the cell nuclei becomes less organised (D). By P20, there is only one layer of photoreceptors left (E). Photoreceptors are still detectable at

P30, however, discontinuities in the ONL are widely observed (F). Images were taken from the central retina. Scale bar: 50 $\mu$ m.

To quantify changes in ONL thickness in the rd1 retina over time, we measured the thickness of the ONL and of the entire retina (the ratio between these two metrics was defined as the ONL ratio) and counted photoreceptor nuclei (Figure 3-2). Our results were in accordance with previous studies (Pennesi et al., 2012). Compared to the WT retina, there was a slight reduction in the ONL thickness at P10, and by P20, the ONL thickness had already decreased to less than 20% of its initial value. The largest drop occurred between P15 and P20. The ONL ratio and the number of photoreceptor nuclei were consistent with the ONL thickness. From P10 to P20, the ONL ratio decreased from 0.325 to 0.069, while the numbers of nuclei decreased from 11 to 1 cell. By contrast, in the WT retina, the ONL thickness remained relatively stable between P10-30, with a mean thickness of 55 $\mu$ m, 0.36 for ONL ratio and 13 nuclei.

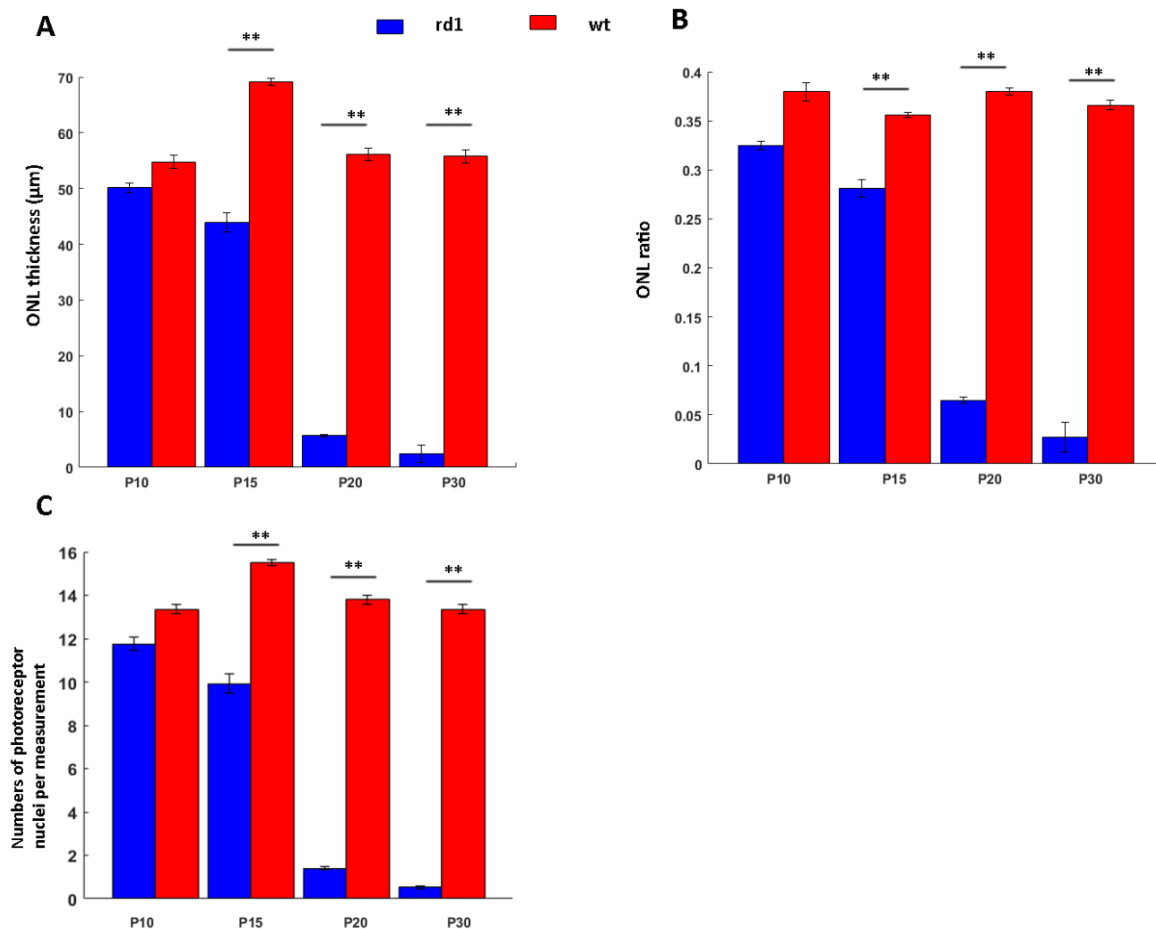


Figure 3-2 The changes of ONL thickness and ONL ratio against age

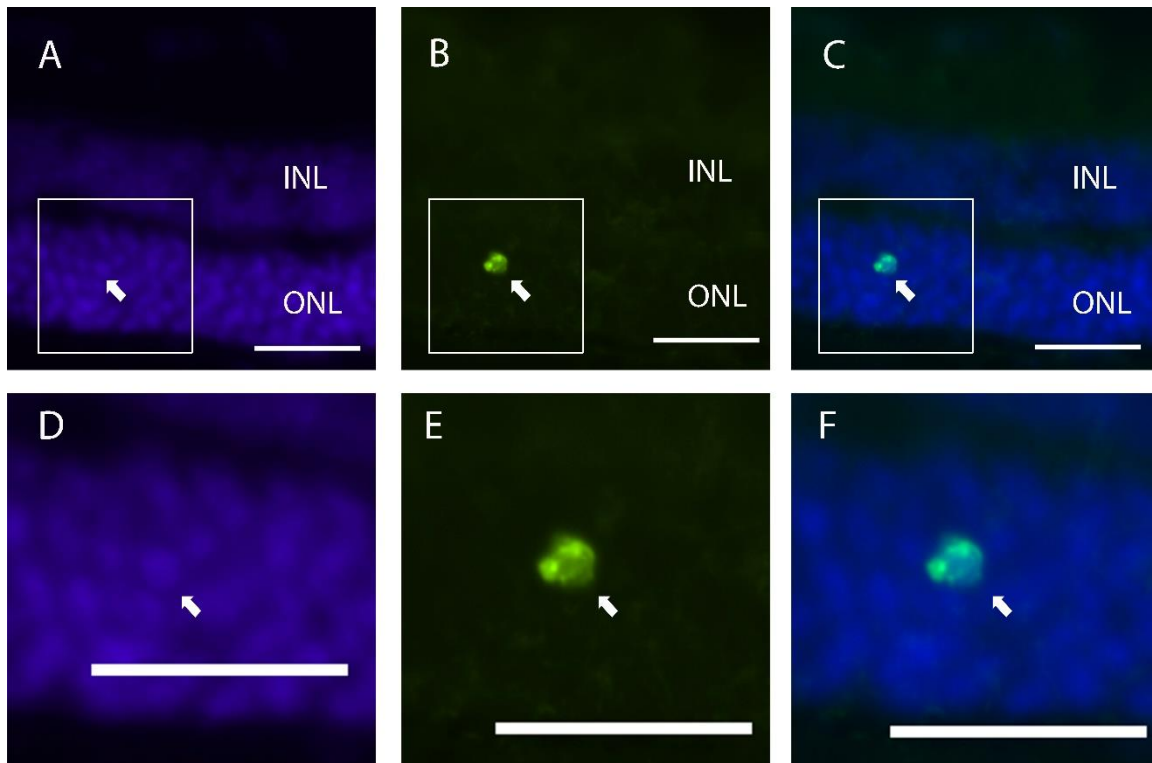
The quantitative measurements on the ONL thickness, ONL ratio as well as photoreceptor nuclei number all confirmed that photoreceptor loss occurs within the first month. By P20, there were fewer than 20% of photoreceptors left. A: Change of ONL thickness against age; B: Change of ONL ratio against age. C: Change in the numbers of photoreceptor nuclei. (\*\*  $p < 0.01$ , data seen in Table 3-1)

Table 3-1 Changes of ONL thickness, ONL ratio and numbers of photoreceptor nuclei against age

Strain	age	n	ONL thickness		ONL ratio		Numbers of nuclei per measurement	
			mean (µm)	SEM	mean (µm)	SEM	mean (µm)	SEM
rd1	P10	3	50.136	0.841	0.325	0.004	11.763	0.291
	P15	3	43.957	1.754	0.281	0.009	9.922	0.462
	P20	3	5.660	0.244	0.069	0.003	1.402	0.070
	P30	3	2.462	1.537	0.026	0.015	0.527	0.068
WT	P10	3	54.782	1.187	0.375	0.004	13.355	0.198
	P15	3	69.134	0.616	0.356	0.004	15.508	0.123
	P20	3	56.189	1.073	0.379	0.010	13.789	0.194
	P30	3	55.776	1.192	0.362	0.005	13.352	0.208

### 3.1.2 Time course of apoptosis in ONL of rd1 retina

Apoptosis is considered to be the main cause of photoreceptor degeneration in RP retina. The apoptotic cells can be identified via morphological assessment such as pyknotic nuclei and biochemical techniques including TUNEL assays. As a result of apoptosis, the cells undergo pyknosis that leads to the condensation and formation of pyknotic nuclei. This can be visualized by light microscope using Haematoxylin and eosin (H&E) staining and by fluorescent microscope using DAPI staining. The apoptotic nuclei are slightly smaller with condensed chromatin comparing to the normal nuclei. TUNEL assay is another widely used method for the detection of apoptotic cells in tissue sections. The principle is to label the 3'-hydroxyl termini in double strand DNA breaks generated during apoptosis.



*Figure 3-3 The fluorescent micrographs of apoptotic cells in P50 Crx retina*

*Cryostat section of a P50 Crx retina stained with DAPI and TUNEL. Under 40× oil magnification, TUNEL +cells overlap with the DAPI stained nuclei and can be easily distinguished from the background (B, C, E and F, Arrow). On the DAPI channel, the apoptotic nucleus is subtly smaller and brighter than the surrounding normal nuclei (A and D, arrow). Green: TUNEL, Blue: DAPI. Scale bar: 25μm.*

To test the sensitivity of these two methods, DAPI staining and TUNEL were applied on retinal sections of P50 Crx mice (Figure 3-3). The results showed that, under 40× oil magnification, the TUNEL labelled cells were restricted within the ONL and were easily distinguished from the background. Although the apoptotic nuclei stained by DAPI tend to be subtly brighter and smaller, it was difficult to differentiate them from other nuclei at 40x magnification. The visualization of the condensed chromatin may require higher magnification or transmission electron microscopy (TEM) to improve the ability to discriminate them from healthy nuclei. Hence, in this study, TUNEL staining was used as the preferred approach to detect apoptotic cells.

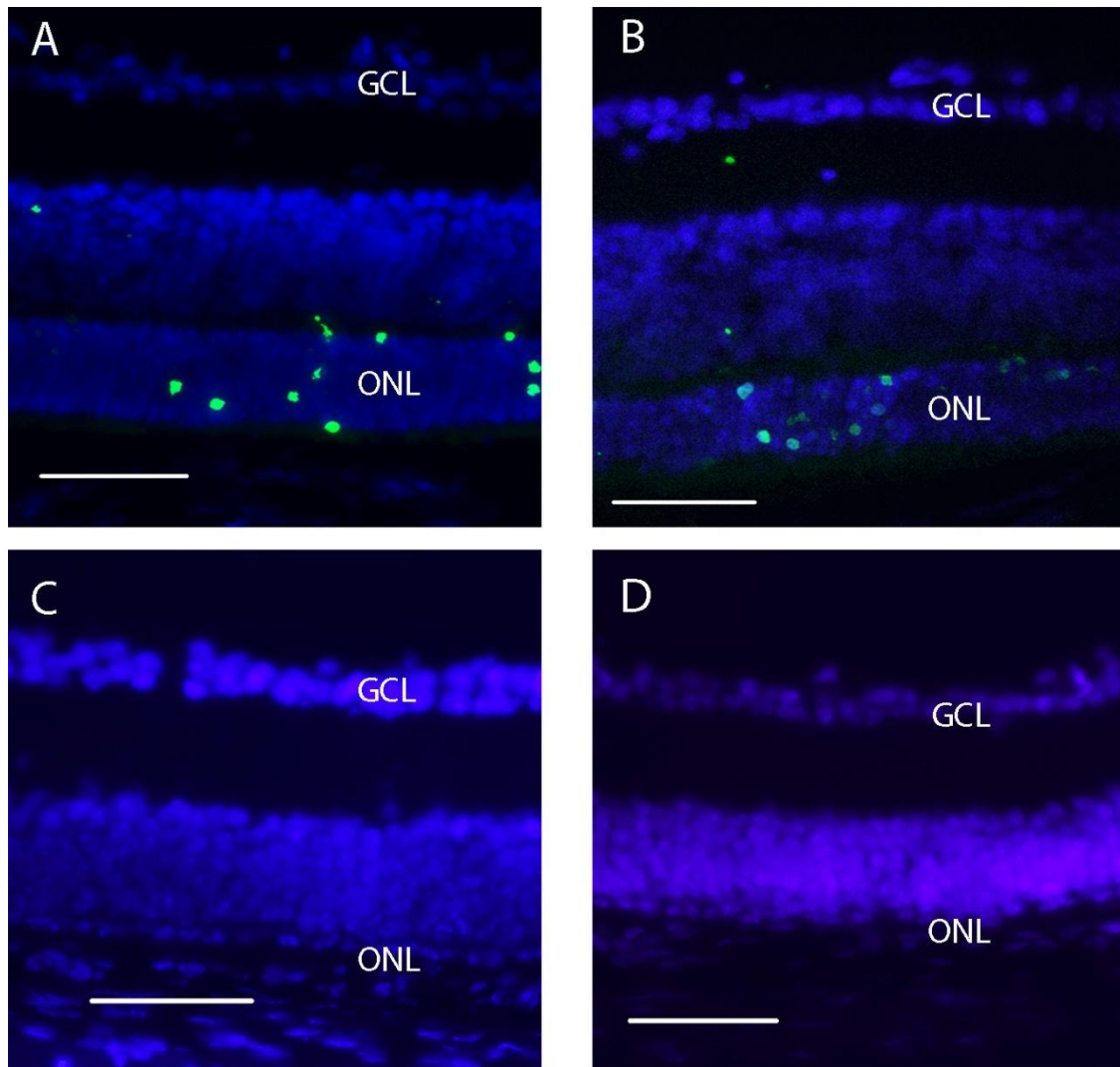


Figure 3-4 Fluorescent micrographs of TUNEL cells (green) in vertical sections of rd1 retina.

The TUNEL+ cells were detectable in the ONL of rd1 retina from P10 and maintained at a high level until P15. The TUNEL+ cells were rarely detected from P20 on. Green: TUNEL; Blue: DAPI. A: P10; B: P15; C: P20; D: P30. Scale bar: 50 $\mu$ m.

To establish the time course of apoptotic activity in rd1 retina, TUNEL staining expression was investigated between P10 and P30. TUNEL+ cells were initially observed at very high density in the ONL between P10 and P15 (Figure 3-4 A and B). By P20, the number of TUNEL+ cells had already decreased significantly, and virtually no TUNEL+ cells were detected after P30 (Figure 3-4 C and D). By contrast, TUNEL+ cells were absent in the WT retina (data not shown).

To determine if the onset of apoptosis matched the timing of ONL thinning, the number of TUNEL+ cells in the ONL was counted (Figure 3-5). The density of TUNEL+ cells was defined as the total number of TUNEL+ cells divided by the corresponding retinal length. TUNEL+ cells were initially observed at a very high density in the ONL at P10, and decreased by 50% between P10-15. By P20, the TUNEL density was only 10% of its value at P10, and no TUNEL+ cells were detected after P30. The results revealed an interesting observation that, although many TUNEL+ cells were detected at

P10-15, the dramatic reduction of ONL thickness occurred after P15, when few apoptotic cells were detected. This suggests that TUNEL+ expression may be a useful approach to detect photoreceptor loss prior to their actual apoptosis.

When analysing the density of TUNEL+ cells and ONL thickness at different retinal eccentricities, it was observed that, the density of TUNEL+ cells was significantly lower in the periphery compared to the central retina (intermediate and perioptic) at the onset of degeneration (Post hoc test: P10, Periphery vs Intermediate:  $p = 0.000$ , Periphery vs Perioptic nerve:  $p = 0.000$ , Dunn's test). However, this difference disappeared at later stages.

In addition, although the absolute ONL thickness was not significantly different at different retinal eccentricities (Two way ANOVA: Age vs Location: effect of location:  $p = 0.624$ , Dunn's test), the ONL ratio was significantly higher in the periphery compared to the other two areas during the early stage of retinal degeneration (Post hoc: P10: Periphery vs Intermediate:  $p = 0.000$ ; P15: Periphery vs Intermediate:  $p = 0.000$ , Periphery vs Perioptic nerve:  $p = 0.000$ , Dunn's test).

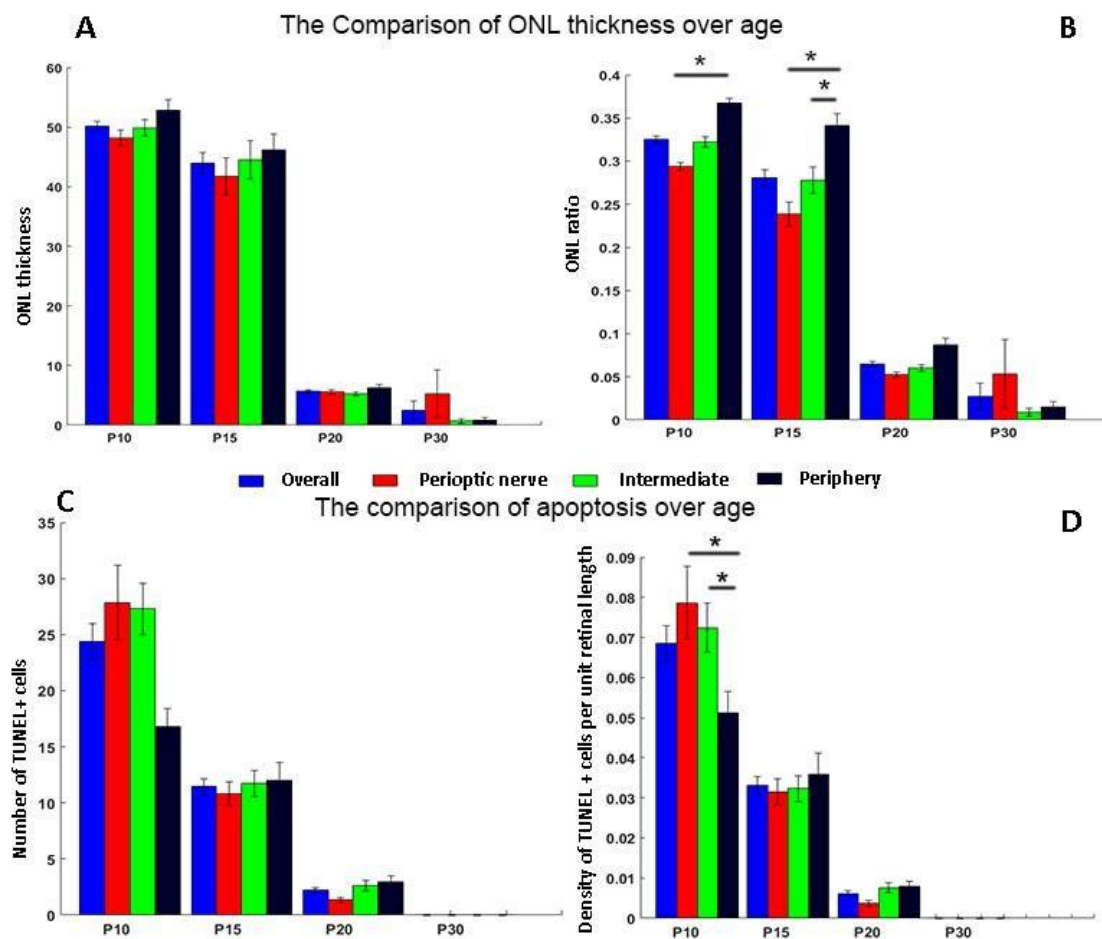


Figure 3-5 Bar chart showing the change of ONL thickness and apoptosis against age in rd1 retina.

*The apoptotic activity was intense between P10-15, while the most remarkable drop of ONL thickness was seen after P15. ,A: Change of absolute ONL thickness against age; B: Change of ONL ratio against age; C: Change of absolute TUNEL+ cells against age; D: Change of TUNEL density against age.*

### 3.1.3 Morphological photoreceptor changes in rd1 retinal sections

Although rods degenerate rapidly in the rd1 retina, surviving cones nevertheless do not exhibit light responses (Chua et al., 2009, Stasheff, 2008). This is presumably due to functional changes reported in glutamatergic synapses between photoreceptors and bipolar cells (Nishiguchi et al., 2015). In order to characterize the remodelling of photoreceptors, immunolabelling for rhodopsin and S Opsin (to label UV cones) was performed on vertical sections to visualize the opsin distribution and morphological details.

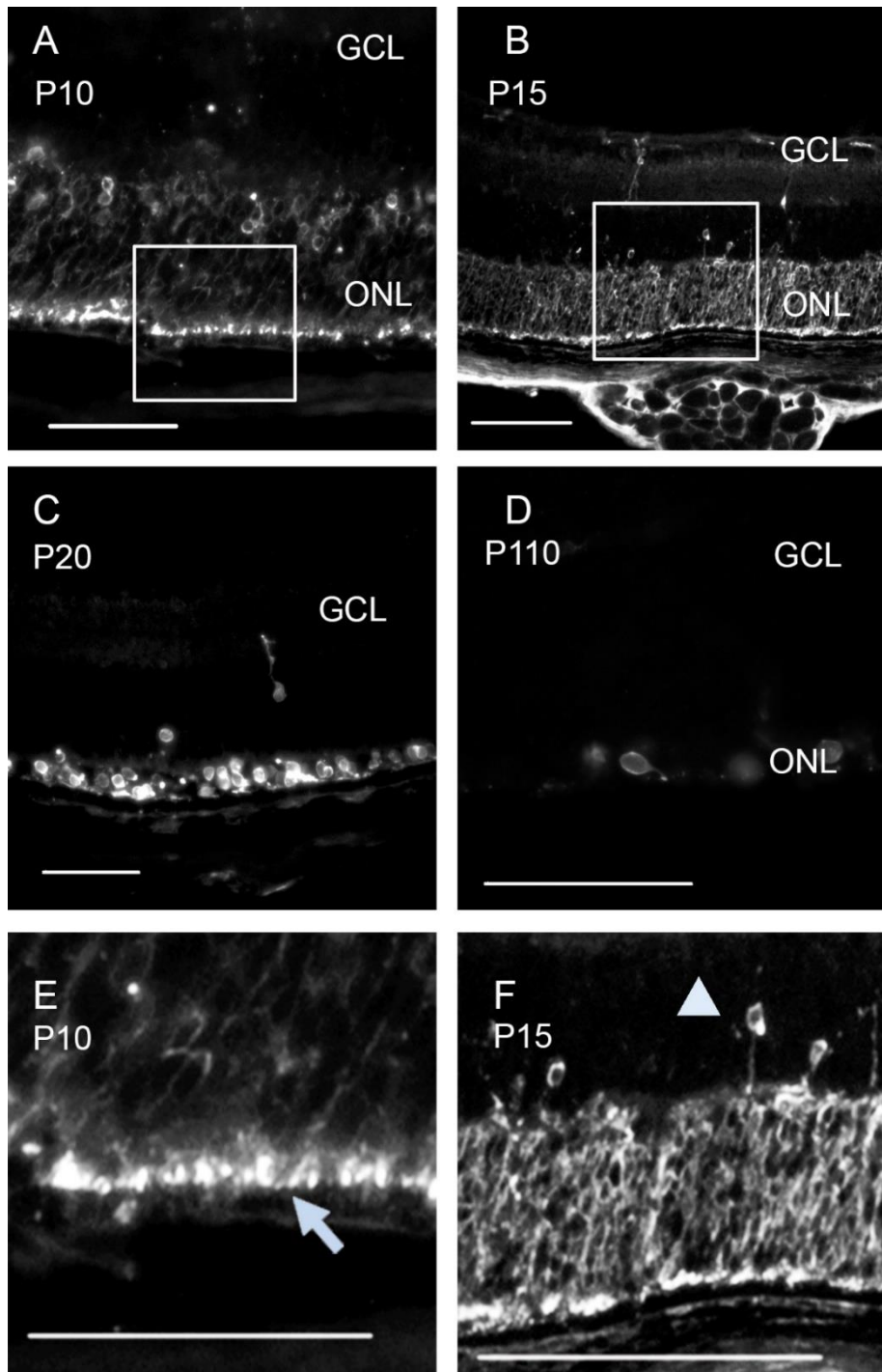


Figure 3-6 Fluorescent micrographs of Rhodopsin in vertical sections of *rd1* retina.

*Rhodopsin* was employed to visualize the remodelling of rods in *rd1* retina. A: *Rhodopsin*+ cells exhibited a round shape and composed the majority of the ONL at P10. B: The *Rhodopsin*+ cells remained vertically aligned at P15. C: Scatters of *Rhodopsin*+ cells were loosely stacked in the ONL at P20. D: *Rhodopsin*+ cells were detectable at P110 at a very low density. E: Selected area from A. The ONL remained relatively intact except for the shortening of the OS (the hyperintensity zone in the outmost of ONL, arrows). F: Selected area from B. Arrow head indicates the processes projecting towards the INL..

In *rd1* retinas, at P10, *Rhodopsin*+ cells were orderly arranged in the ONL with shorter segments (Figure 3-6A), compared to WT retinas. By P15, cells became more disorganized within the ONL (Figure 3-6B). Although in some areas the ONL remained relatively thick, processes were seen

projecting into the inner nuclear layer (INL) (Figure 3-6F, arrow head). These processes disappeared together with the depletion of Rhodopsin+ cells during degeneration. Rhodopsin+ cells were still detectable, but only very sparsely, in vertical sections until P110. with usually 1-2 cells per slice (Figure 3-6D).

In the rd1 retina, S opsin+ cells remained vertically aligned at P10, with shortened outer segments (Figure 3-7A). By P15 the processes were much shorter compared to WT retina (Figure 3-7B), and this was particularly pronounced in the central retina. Cells lost their vertical alignment and were flattened along the ONL after P20 (Figure 3-7C). S opsin expression was still detectable, with only 1-2 cells per slice (Figure 3-7D).

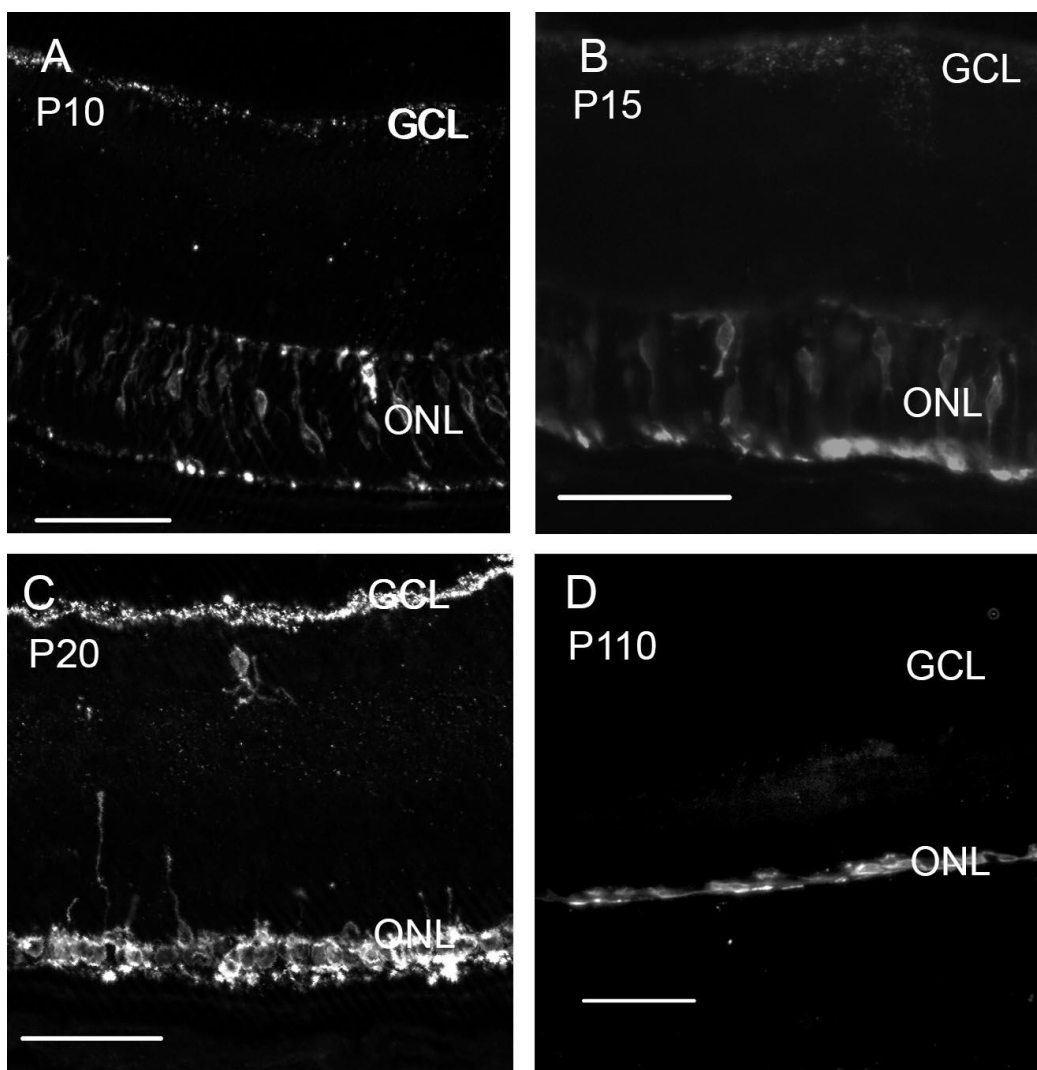


Figure 3-7 Fluorescent micrographs of S opsin in the vertical sections of rd1 retina.

S opsin was employed to visualise the remodelling of the short-wavelength cones. A: At P10, the S opsin+ cells were vertically aligned in the ONL. B: The S opsin cells+ remained vertically arranged but with shortened processes at P15; C: The S opsin+ cells lost their alignment and were stacked more loosely in the ONL. D: The S opsin cells were detectable at P110 with a flattened shape at a very low density. Scale bar: 50µm.

### 3.1.4 The distribution of photoreceptors on whole mount retina of rd1 retina

The results from vertical sections of rd1 retinas revealed that there was a significant change in the overall distribution of surviving photoreceptors, with more surviving cells in the peripheral area and fewer in the central retina, which is consistent with previous studies (Lin et al., 2009). To investigate the distribution pattern of photoreceptors in the rd1 retina, Rhodopsin immunoreactivity was examined on retinal wholemounts at P15 and P20.

When viewing the WT retina from the photoreceptor side, it could be seen that the field was covered with a large number of elongated structure with extensive Rhodopsin expression (Figure 3-8A). In dystrophic retinas at early degeneration stages, rhodopsin expression was also high in the outer/inner segments, however the outer/inner segments appeared as a dot-shape instead of the elongated shape seen in WT, suggesting a shortening of the outer segments (Figure 3-8B). At the later stages of degeneration, rhodopsin expression on cell bodies appeared with the degeneration of the outer/inner segments (Figure 3-8C-F), in agreement with the results from another RP model: the S334ter-line-3 rat (Zhu et al., 2013). Compared to the rod mosaic in WT retina, at P15, although there were fewer rhodopsin+ cells and their outer segments were shorter, at this stage, the distribution of Rhodopsin+ cells remained similar to WT (Figure 3-8). After P20, the number of Rhodopsin+ cells decreased significantly, and only a few scattered cells could be detected. A noticeable difference was seen between the perioptic and peripheral areas, with more rhodopsin expressing cells detected in the periphery, with extended cellular processes oriented towards the central retina. Most surviving rhodopsin+ cells in the central retina were lacking such oriented processes (Figure 3-8C-F).

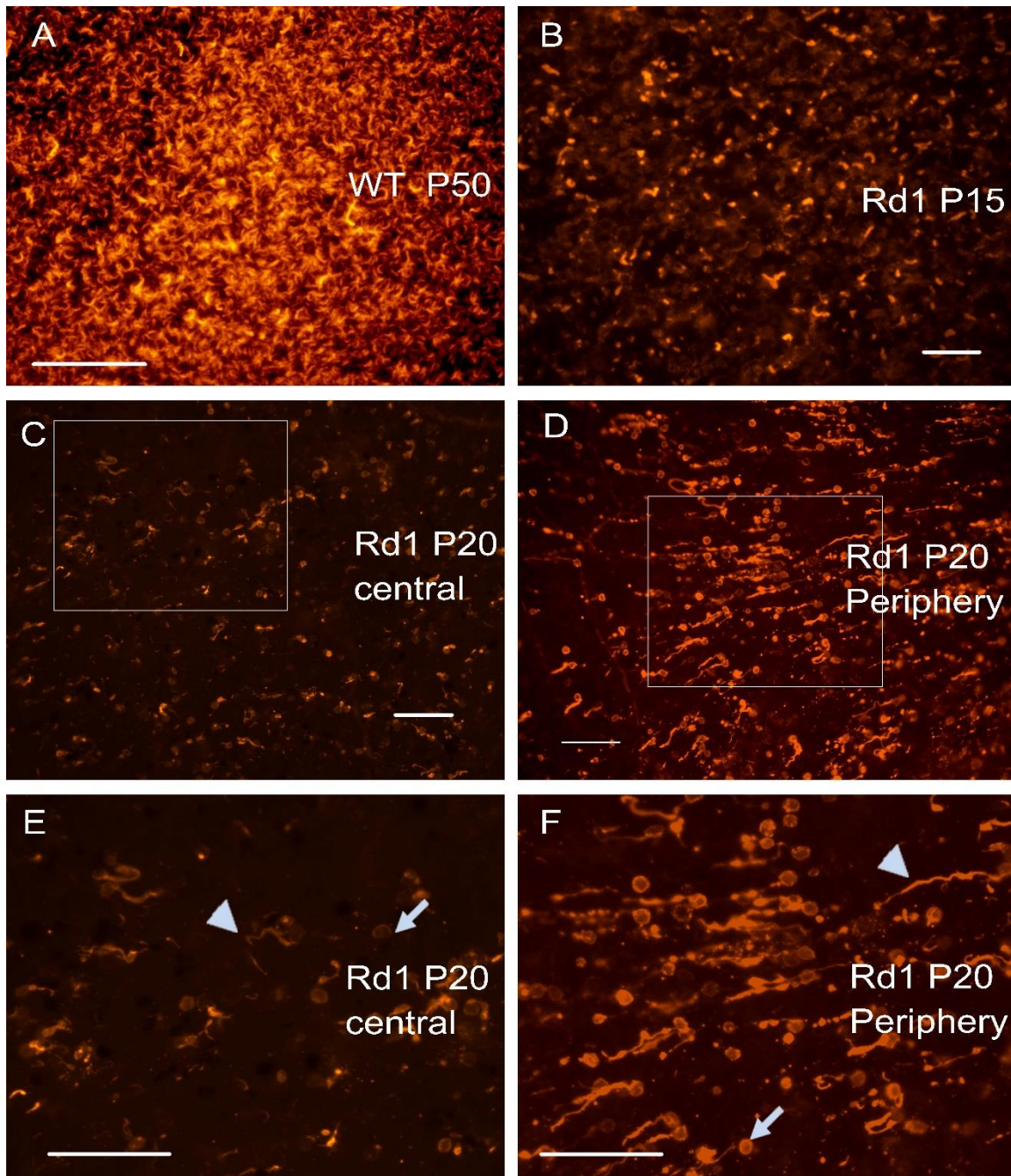


Figure 3-8 Fluorescent micrographs of rhodopsin on wholemount retina

A: In WT retina, extensive expression of Rhodopsin was observed in the OS exhibiting a hyperintense slim-rod shape while the cell bodies were not visible; B: Inrd1 retina at early stage of retinal degeneration, the expression of Rhodopsin was largely reduced. The OS appeared as a dot-shape; C and D: In late degeneration stage of the rd1 retina, there was a discrepancy in the distribution of Rhodopsin+ cells. The density of Rhodopsin cells was high in the periphery but low in the central retina. Meanwhile, the cellular processes of Rhodopsin+ cells in the periphery oriented towards the central area (F arrow), while cells in central area lacked these oriented processes (E arrow), Scale bar: 50 $\mu$ m

## 3.2 Photoreceptor degeneration in Crx retina

### 3.2.1 Changes of ONL thickness in Crx retina

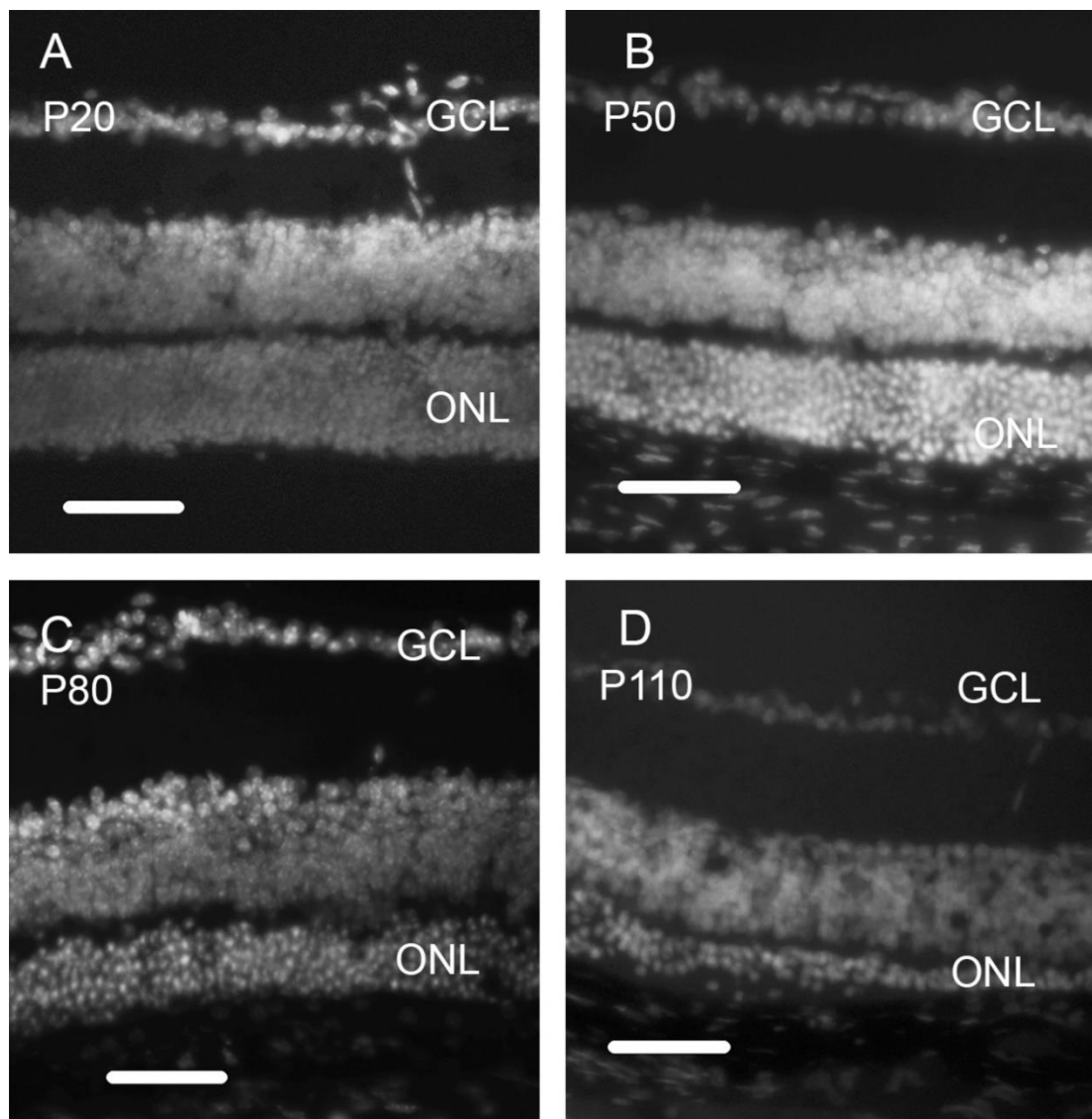


Figure 3-9 Fluorescence micrographs showing the change of ONL thickness against age in Crx retina.

DAPI stained retinal sections from Crx retina between P20-110. In Crx retina, the photoreceptor nuclei remained neatly alignment until P50 and the ONL thickness was only slightly reduced comparing to P20 (A and B). The ONL became disorganised and thickness was decreased sharply by P80 (C). There were only two or three layers of cells left after P110 (D). Images were taken from central area of the retina. Scale bar: 50 $\mu$ m.

Compared to the fast degeneration process in the rd1 retina, degeneration was much slower in Crx retina. When analysing the DAPI stained retinal sections, the ONL was relatively intact up to P50 with only a moderate decrease in the thickness. By P80, the ONL thickness dropped sharply and the nuclei became disorganised. By P110, the ONL became reduced to 2-3 layers, and discontinuity was frequently observed (Figure 3-9).

In order to gain a detailed understanding of the kinetics of photoreceptor degeneration, transverse Crx retinal sections were then examined from a wide range of ages (from P10 to P150), which spans most of the degeneration period (Figure 3-10).

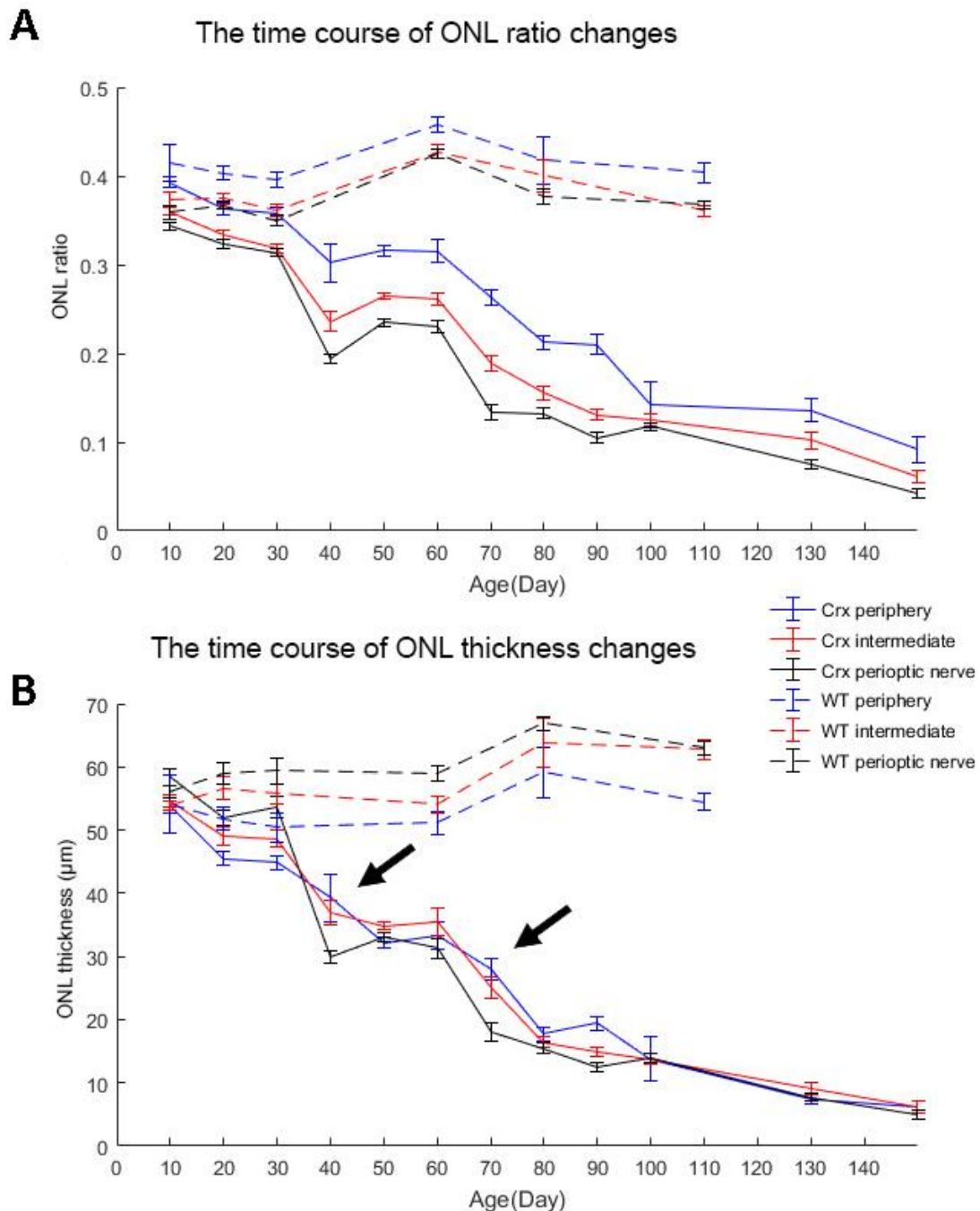


Figure 3-10 Line graph showing group data for the changes of ONL thickness and ONL ratio against age in Crx retina.

Quantitative measurements on the ONL thickness and ONL ratio both indicated that the ONL thickness did not reduce at a constant rate throughout the degenerating process. The ONL thickness was reduced by 40% and 30% during P30-50 and P60-80 respectively. By P80, there was less than 20% of photoreceptors left. A: Changes in ONL ratio with age; B: Changes in absolute ONL thickness with age (data seen in Table 3-2).

Table 3-2 Changes of ONL thickness, ONL ratio and numbers of photoreceptor nuclei against age

Strain	age	n	ONL thickness		ONL ratio		Numbers of nuclei per measurement	
			mean (μm)	SEM	mean (μm)	SEM	mean (μm)	SEM
CRX	P10	3	50.727	0.579	0.351	0.004	10.392	0.147
	P20	3	52.604	1.008	0.339	0.004	11.027	0.188
	P30	3	49.683	0.554	0.318	0.004	11.200	0.165
	P40	3	29.632	0.423	0.255	0.003	6.490	0.101
	P50	3	33.741	0.696	0.260	0.005	6.564	0.137
	P60	3	33.925	1.269	0.262	0.008	6.979	0.254
	P70	3	15.426	1.247	0.161	0.013	3.605	0.371
	P80	3	17.538	0.641	0.166	0.006	3.064	0.120
	P90	3	14.820	0.650	0.139	0.007	2.283	0.144
	P100	3	13.863	0.557	0.123	0.004	1.563	0.157
P130	3	10.383	0.636	0.116	0.007	1.194	0.168	
WT	P10	3	54.782	1.187	0.375	0.004	13.355	0.198
	P20	3	56.189	1.073	0.379	0.010	13.789	0.194
	P30	3	55.776	1.192	0.362	0.005	13.352	0.208
	P60	3	55.190	0.936	0.435	0.004	12.179	0.368
	P80	3	63.821	1.714	0.395	0.010	13.789	0.194
	P110	3	60.940	0.988	0.374	0.005	13.279	0.255

The depletion of ONL was rather slow except for two sharp drops occurring at P30 and P60 respectively (Figure 3-10 B, solid lines, arrows). The ONL thickness decreased by ~33% between P30-40, and decreased further by 50% between P60-70. Although the absolute ONL thickness was similar at different retinal eccentricities during degeneration, there was a clear difference in the ONL ratio for periphery, intermediate and perioptic areas (Figure 3-10 A).

In WT, the ONL ratio was around 11% larger in the periphery than in the central retina (intermediate area and perioptic nerve) at P10, and the difference decreased to 7% by P30 (Figure 3-10 A, dash lines). Despite fluctuations in ONL ratio during development, not much difference was seen at different eccentricities over time in the WT retina.

In the Crx retina, the ONL ratio followed a pattern similar to WT, except that the difference between the perioptic nerve and the other two areas became more pronounced after the two sharp drops described above (Figure 3-10 A, solid lines). At P10, the ONL ratio was 7.6% larger in the central retina than in the periphery. By P30, the ONL ratio decreased by a moderate amount. However, after the first fast cell death wave between P30-40, although the ONL ratio was reduced in all areas, it decreased at a faster rate in the central area than in the periphery, yielding a difference of 0.07 between periphery and central retina (accounts for 20% of the periphery ONL ratio). Another overt change was seen after the second wave of ONL thinning between P60-70, when it dropped from

0.23±0.01 to 0.13±0.01 μm in the perioptic nerve area, whereas in the periphery, it dropped only from 0.31±0.01 μm to 0.26±0.01 μm. The difference became less obvious after P100 when the depletion of photoreceptors had almost completed.

### 3.2.2 Time course of apoptosis in the ONL of Crx retina

To determine the contribution of apoptosis to the two “waves” of photoreceptor degeneration, the number of TUNEL+ cells in the ONL was used to evaluate apoptotic activity and to compare the timing of cell death with the timing of ONL thinning (Figure 3-11). Although the TUNEL+ cells were initially identified in the peripheral retina as early as P30, these apoptotic cells were too sparse to be captured on retinal sections.

The first conspicuous sign of TUNEL + cells was observed at P50, with the average TUNEL density of 9.0±0.76 cells/mm retinal length, and remained at a high level until P70 (8.9±1.10 cells/mm retinal length). Notably, the number of TUNEL+ cells in the intermediate zone was visibly higher than in the periphery between P50-70. The level of TUNEL+ cells dropped by 75% after P70. By P80, the average TUNEL density was only 1.70±0.43 cells/mm retinal length, while the difference in the incidence of TUNEL+ cells between locations was barely detectable, which may be due to the depletion of photoreceptors. At later stages, TUNEL+ cells remained at a very low level and were undetectable on sections at P150, although scattered TUNEL+ cells were still visible until P190. The TUNEL+ cells were completely undetectable after P190, suggesting the end of apoptosis.

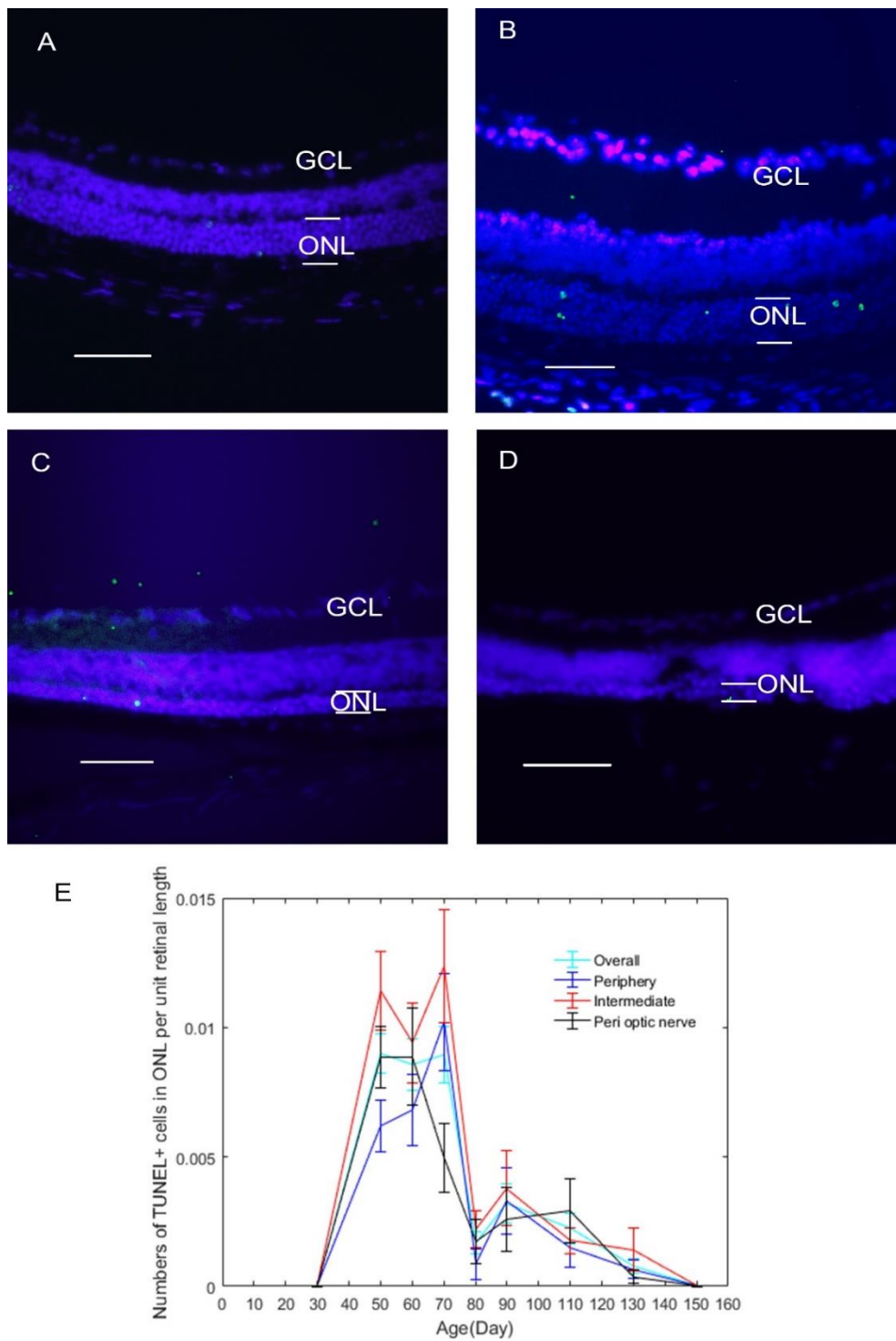


Figure 3-11 Change in the density of TUNEL+ cells in retinal sections of Crx mice against age.

A-D: Fluorescent micrographs of TUNEL+ cells. TUNEL+ cells (Green) were detectable in ONL from P50 and remained at a high level until P70. The number of TUNEL+ cells were largely reduced at P110 and these cells became undetectable by P150. Green: TUNEL; Blue: DAPI. Scale bar: 50 $\mu$ m. E: Line graph showing the change on TUNEL+ cell density in Crx retina with age. The density of TUNEL+ cells was peaked between P50-70 and reduced dramatically after P70.

Table 3-3 The density of TUNEL+ cells in the ONL at different retinal eccentricities

age	n	Periphery			Intermediate			Periopic nerve		
		mean	STD	SEM	mean	STD	SEM	mean	STD	SEM
P30	3	0.000	0.000	0.000	0.000	0.000	0.000	0.000	0.000	0.000
p50	3	6.200	5.500	1.000	11.400	9.300	1.500	8.900	7.800	1.200
p60	3	6.800	5.800	1.400	9.400	7.900	1.600	8.900	10.600	1.900
p70	3	10.200	7.700	1.900	12.400	9.300	2.200	5.000	6.200	1.300
p80	3	0.900	1.800	0.600	2.200	2.500	0.700	1.700	2.900	0.800
p90	3	3.300	3.600	1.300	3.800	5.000	1.400	2.600	4.200	1.200
p110	3	1.500	2.000	0.800	1.800	1.700	0.500	2.900	5.000	1.200
P130	3	0.700	1.300	0.300	1.400	2.900	0.800	0.400	1.000	0.300
P150	3	0.000	0.000	0.000	0.000	0.000	0.000	0.000	0.000	0.000

### 3.2.3 Morphological changes of photoreceptors in vertical sections of Crx retina

Although photoreceptors in the Crx retina are atrophied from the onset, they are able to survive for a relatively long period. Interestingly, after P50 there were areas with focal thinning in the ONL. This focal thinning pattern appeared more frequently with degeneration and became more obvious after P80 (Figure 3-12, arrows).

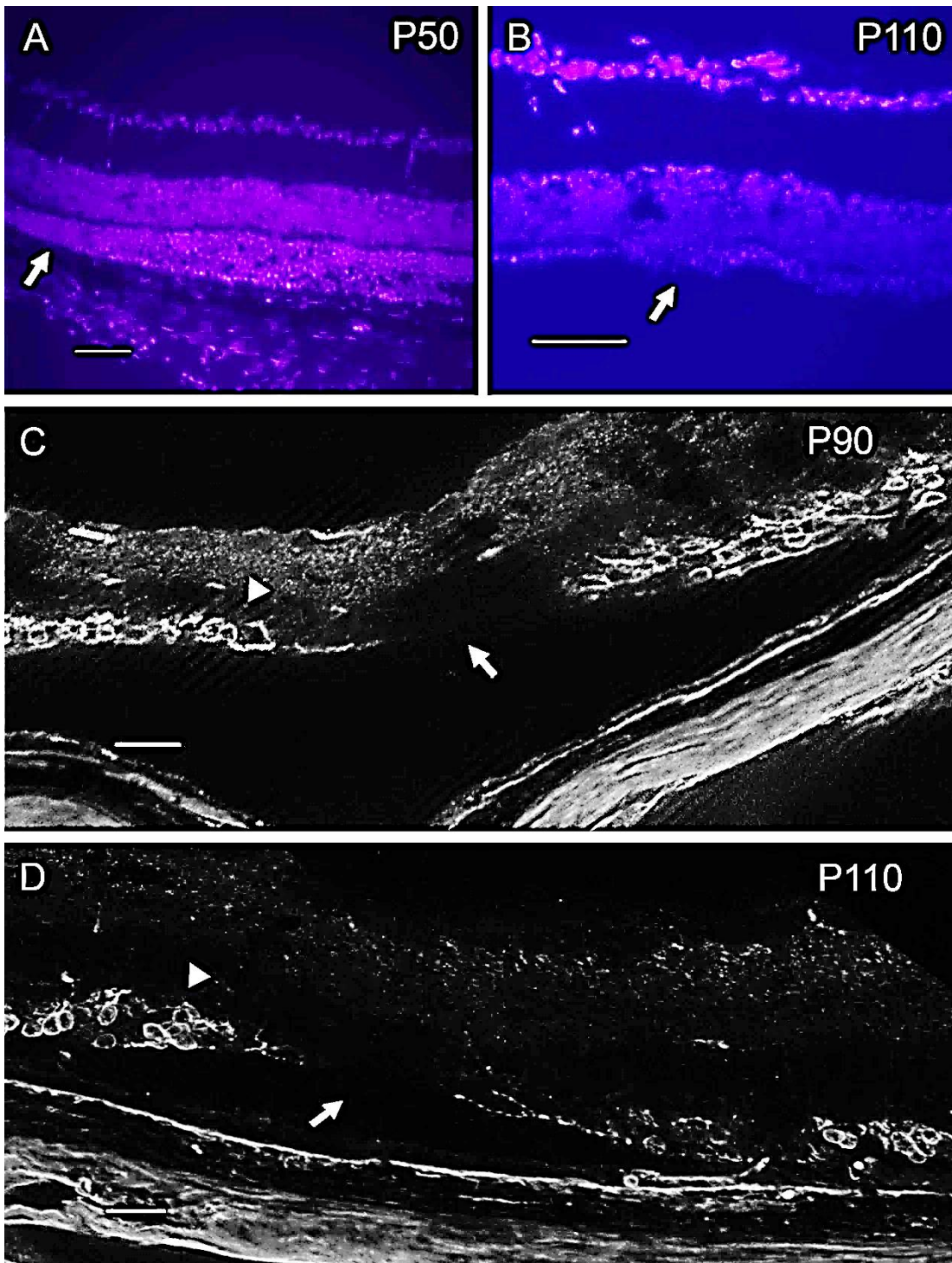


Figure 3-12 Fluorescent micrographs showing focal areas of thinning on retinal section of Crx retina.

*A: P50. Blue: DAPI. Arrow: thinned area. DAPI staining reveals focalized thinning in ONL. B: P110. Blue: DAPI. Arrow: area devoid of nuclei in ONL. DAPI staining reveals discontinuity of ONL. C: P90. Grey: Rhodopsin. Arrow: area that were devoid of rhodopsin+ cells. Arrow heads: area with cluster of cells. D:110. Grey: Rhodopsin. Arrow: area that was devoid of rhodopsin+ cells. Arrow heads: area with cluster of cells. Scale bar: 50µm.*

To characterize the remodelling of photoreceptors during the degenerative process and determine which cells were involved in the thinning pattern, immunolabelling for rhodopsin and S opsin was performed on Crx retinal sections to visualize the opsins' distribution and morphological details.

While the outer segments were absent and only short inner segments were visible (Figure 3-13 A: the overexposed area adjacent to the outermost side of the ONL), the distribution and arrangement of Rhodopsin+ cells remained similar to WT before P20, which is not surprising, given that degeneration did not start until P30. The Rhodopsin+ cells did not change much beyond P50 (Figure 3-13C). Notably, the outer segments had completely disappeared by this stage. Rhodopsin+ cells became less evenly distributed after P80, when there were areas with clusters of Rhodopsin+ cells next to areas that were devoid of cells bodies, with only processes visible (Figure 3-13C and D. Arrows: Areas that were devoid of cells bodies; Arrow head: Areas with cluster of Rhodopsin+ cells). As shown earlier, the rate of ONL thinning became slow after P80, but lasted for up to six months (Furukawa et al., 1999). The expression of Rhodopsin+ cells was in agreement with previous findings, with only one or two remaining cell layers after P110 (Figure 3-13E). However, clusters of Rhodopsin+ cells interspersed with areas devoid of these cells was seen more frequently with age.

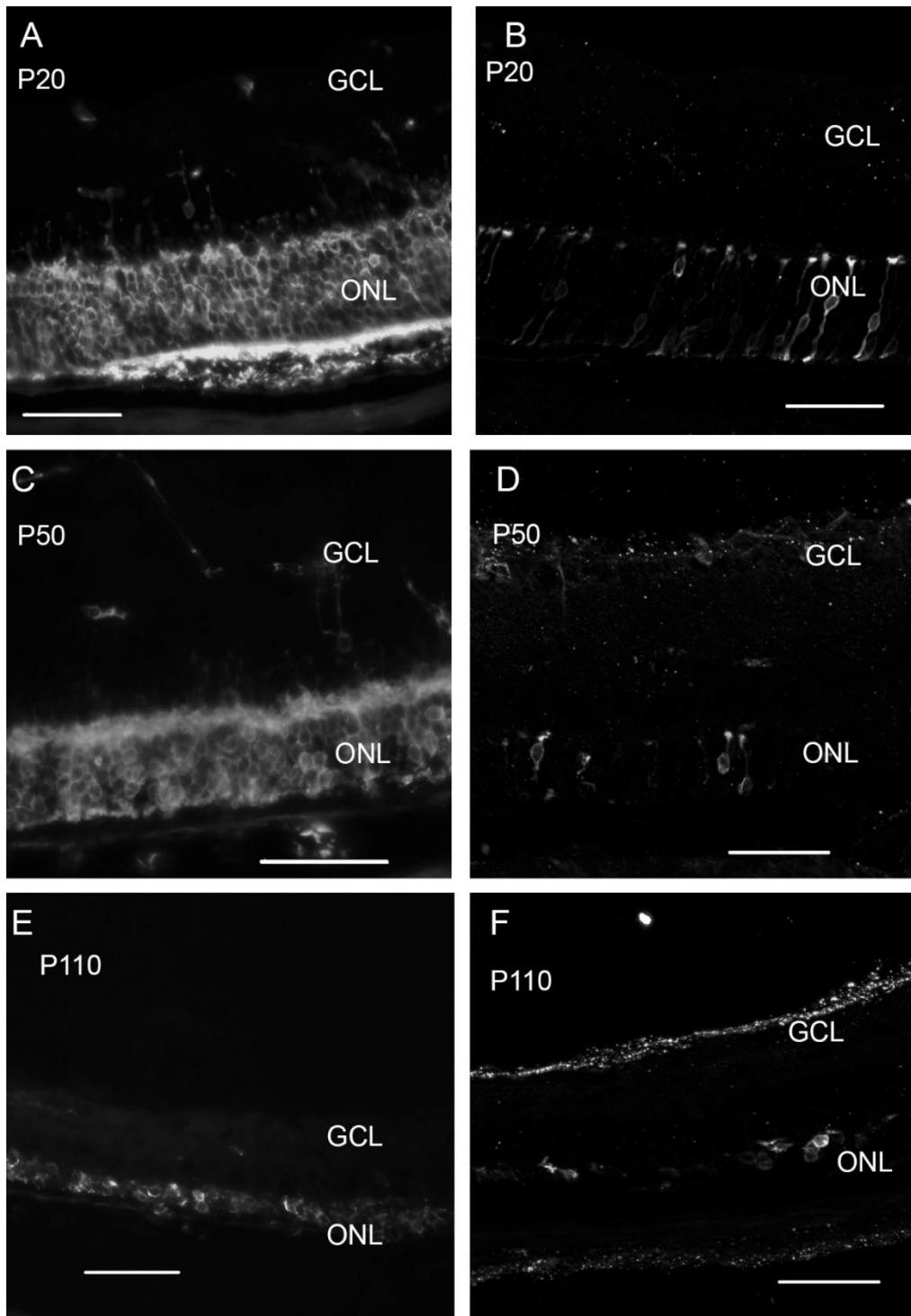


Figure 3-13 Fluorescent micrographs of rhodopsin (A-C) and S opsin (D-F) in Crx retina.

*A, C and E: Fluorescent micrographs of Rhodopsin on Crx retina at different age; The Rhodopsin+ cells arranged in a high density in the ONL before P50. There were remaining OS visible at P20 presenting as the lines with high intensity in the outermost of ONL, while this disappeared completely at P50. B, D and F: Fluorescent micrographs of S opsin on Crx retina at different age; The S opsin+ cells were vertically aligned in the ONL at very low density. The remaining of IS/OS can be observed in the outermost of the cells at P20 presenting as dots with high intensity. This also disappeared by P50. Meanwhile, the number of the S opsin+ cell was largely reduced, and the process of the cells were shortened. Scale bar: 50 $\mu$ m.*

In Crx retina, the distribution of S opsin followed the same pattern as in WT, but there was a distinct change in the morphology. The shortening of OS was conspicuous from the onset of degeneration, while the S opsin+ cells remained vertically aligned (Figure 3-13B). Until P50, the processes of S opsin+ cells became much shorter whereas the characteristic morphology of photoreceptor terminals in the OPL was still visible (Figure 3-13D ). By P110, almost all the cells lost their processes, and only scattered cell bodies could be seen (Figure 3-13F).

#### 3.2.4 The distribution of photoreceptors in Crx retinal wholemounts

To further investigate which cells were attributed to those focalized thinning areas, Rhodopsin and S opsin labelling was performed on Crx retinal wholemounts. At P10, although the elongated structure was absent, the expression of Rhodopsin on wholemount retinas presented in a high density ( Figure 3-14A), while the cell bodies of rhodopsin+ cells were not visible at this stage. By P50, the segments almost disappeared with a high density of round cell bodies left (Figure 3-14B).

Areas with low density of rods, which were compatible with the vertical sections, were commonly seen in the peripheral retina from P80 onwards (Figure 3-14D, arrows: areas that are devoid of cell bodies). Although detected as early as P50, these areas of localised PR defects, which we termed 'holes', were relatively small around P80-100, and became larger with degeneration. After P130, the surviving rhodopsin+ cells became very sparse, making it difficult to distinguish the holes clearly. Notably, these holes presented a unique pattern, with numerous photoreceptors on their rim, but none inside the holes (Figure 3-14D), suggesting cell migration was involved in their formation. On the other hand, although the ONL was confirmed to be much thinner than at P50, the areas that were free of holes maintained their organization, similarly to what we observed at the earlier stages (Figure 3-14B and C). Examination suggested that the distribution of both M opsin+ and S opsin+ cells was independent from the holes.

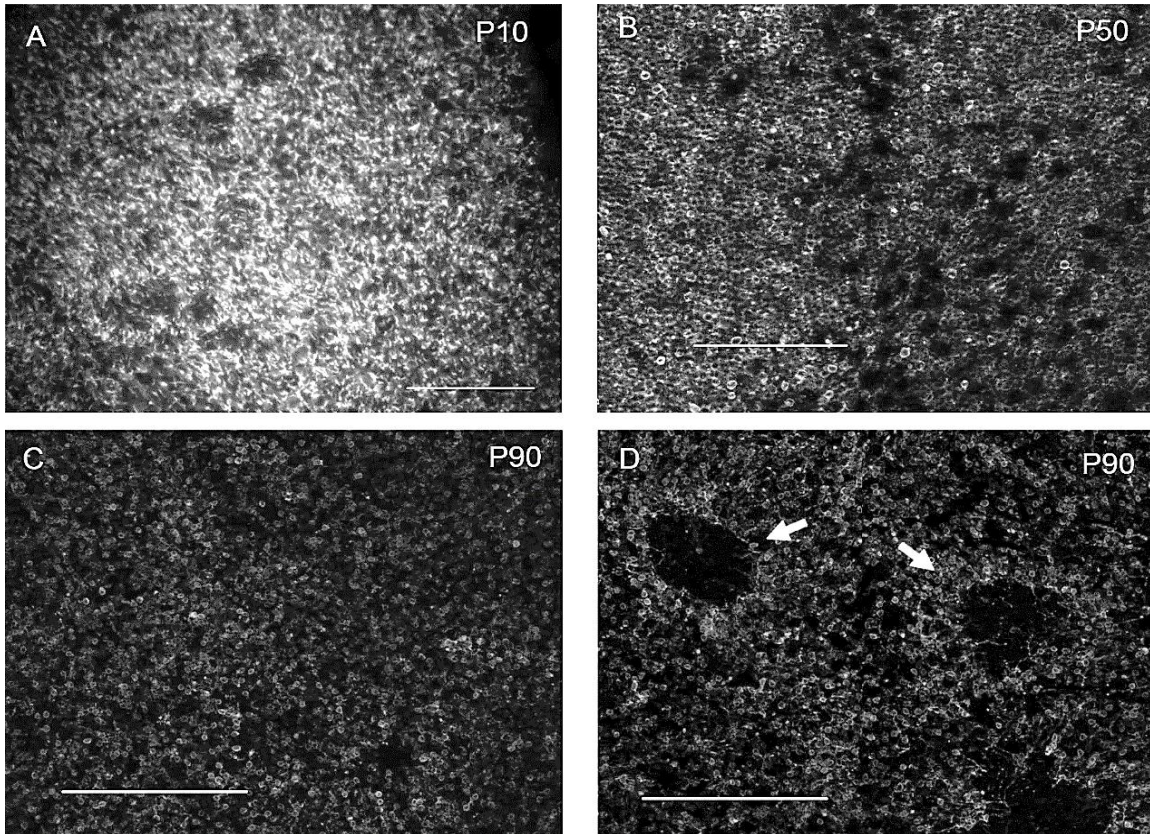


Figure 3-14 Fluorescent micrographs of rhodopsin on whole mount retina of *Crx* mice. Grey: Rhodopsin.

A: P10. The retinas were covered with the remaining IS/OS, which presented as dots or slim lines with high intensity, while the cell bodies were not visible. Scale bar: 100  $\mu\text{m}$ . B: P50. The rhodopsin + outer segments were undetectable at this stage and the round shaped cell bodies can be seen at a high density. Scale bar: 100  $\mu\text{m}$ . C: P90. Hole-free areas. Retinas are covered with the round shaped cell bodies, albeit at a lower density than earlier on. Scale bar: 200  $\mu\text{m}$ . D: P90. Hole of cells. Cell-free zones were observed in some areas of the retina. The holes have abundant cell bodies on their rim. Scale bar: 200  $\mu\text{m}$ . Arrows: Areas that were devoid of cell bodies.

### 3.3 The occurrence of mislocated opsin+ cells in the inner retina associated with degenerating activity

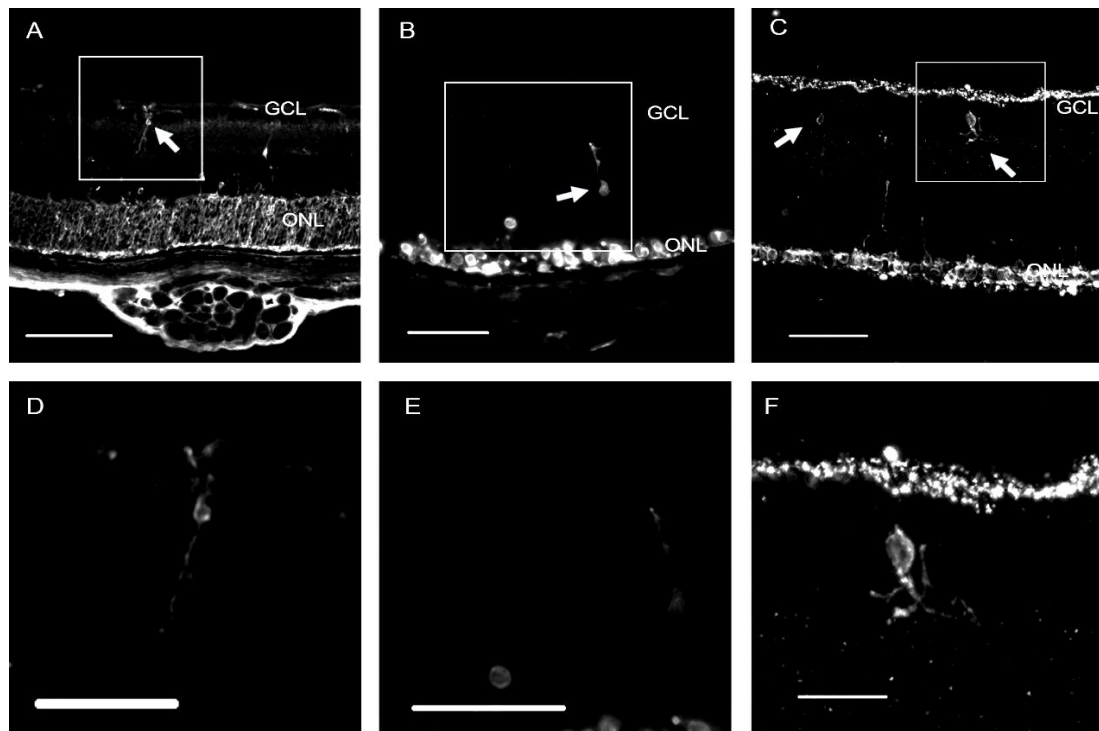


Figure 3-15 Fluorescent micrographs of rhodopsin and S opsin in the inner retina of rd1 mouse

A: P15, grey: Rhodopsin. Scale bar: 50 $\mu$ m. Expression of Rhodopsin was found in the inner retina and displayed a morphology which was different from the Rhodopsin+ cells in the outer retina. Arrows: Rhodopsin+ cells in the inner retina with a round cell body and two processes pointing towards inner and outer retina respectively.; B:P19, grey: Rhodopsin. Scale bar: 50 $\mu$ m. Arrows: Mislocated Rhodopsin+ cells; C: P19, grey: S opsin. Scale bar: 50 $\mu$ m. Arrows: Mislocated S opsin+ cells; D: selected area of A. scale bar: 20  $\mu$ m; E: selected area of B. scale bar: 20  $\mu$ m; F: selected area of C. scale bar: 20  $\mu$ m

An unexpected finding was that scattered cell bodies expressing Rhodopsin and S opsin were observed in the inner retina of both rd1 and Crx retina (from OPL to GCL), whereas the Rhodopsin+ cells and S opsin+ cells were restricted to the ONL in WT retinas. Some of these cells displayed similar morphological features to bipolar cells (Figure 3-15). Mislocated opsin+ cells were detectable from P20-80 in the Crx retina, but were most frequently seen before P50. In the rd1 retina, the mislocated opsin+ cells were detectable between P10-20, and most frequently observed between P15-20, coinciding with the second wave of photoreceptor depletion. They were not detected at later stages. A similar phenomenon has been reported in several rodent models of outer retinal degeneration including the RCS rat and rd1 retina (Semo et al., 2007). Although the morphology of those mislocated opsin+ cells looks similar to bipolar cells, Semo et al (2007) were not able to localise these cells with any other neurons or Müller cells. However, it is clear that the occurrence of mislocated opsin+ cells was highly related to the degenerating activity.

### 3.4 The spatiotemporal relationship of TUNEL+ cells in Crx retina

#### 3.4.1 Correlation between ONL thickness and apoptotic activity

To explore the contribution of apoptosis in the process of photoreceptor degeneration, the time course of ONL thinning and apoptosis was compared in both rd1 retina and Crx retina (Figure 3-16). In rd1 retina, the ONL thickness declined at a fast rate from the onset of photoreceptors degenerate. At that time, the rate of apoptosis is high, as demonstrated by the large incidence of TUNEL+ cells. Apoptotic activity slows down with the depletion of photoreceptors. In Crx retina, the density of TUNEL+ cells was very low at the onset of degeneration. The increase in the incidence of TUNEL+ cells starts immediately after the first wave of photoreceptor degeneration. Large numbers of apoptotic cells were seen throughout the mid-phase of the degeneration process, slowing down beyond P80. The onset of the second wave of photoreceptor death started from the middle phase of intensive apoptosis.

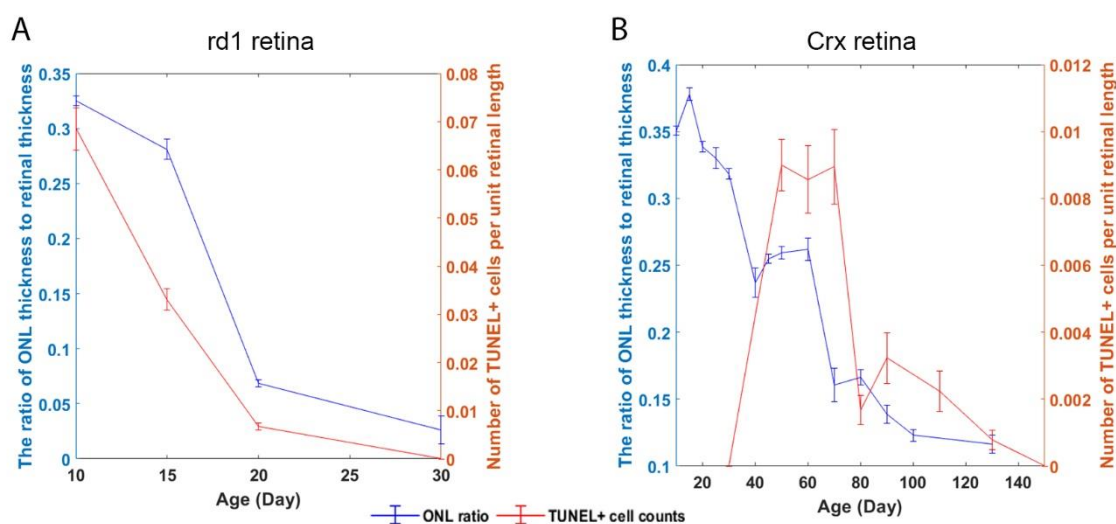


Figure 3-16 Comparison of the time course of apoptotic activity and ONL ratio against age in rd1 and Crx retina

A: The time course of ONL thinning and apoptotic activity in rd1 retina. In rd1 retina, the ONL ratio and number of apoptotic cells peaked at P10 and then reduced over time. B: The time course of ONL thinning and apoptotic activity in Crx retina. While the ONL thickness reduced over time, the number of apoptotic cells was very low before P50. The peak of apoptosis was seen between P50-70 and the number of apoptotic cells dropped rapidly after P70.

It has been reported in S334ter-line3 RP retina that the rods tend to die in clusters, spreading to the adjacent area, generating zones with low density of rods and cones. (Shin et al., 2016). This normally started with clusters of apoptotic cells appearing in the centre of areas with low density of photoreceptors and spread to the adjacent areas leading to further photoreceptor death and migration (Lee et al., 2011). To investigate the clustering pattern in rd1 and Crx retina, vertical sections of rd1 and Crx retinas were inspected during the mid-phase of the degenerating process (P15 for rd1 retina and P50 for Crx retina). As can be seen in Figure 3-17, in some parts of the

periphery and intermediate area of the rd1 retina, the density of apoptotic cells tends to be high. However, this phenomenon was less conspicuous in Crx retina as the density of the apoptotic cells was much lower.

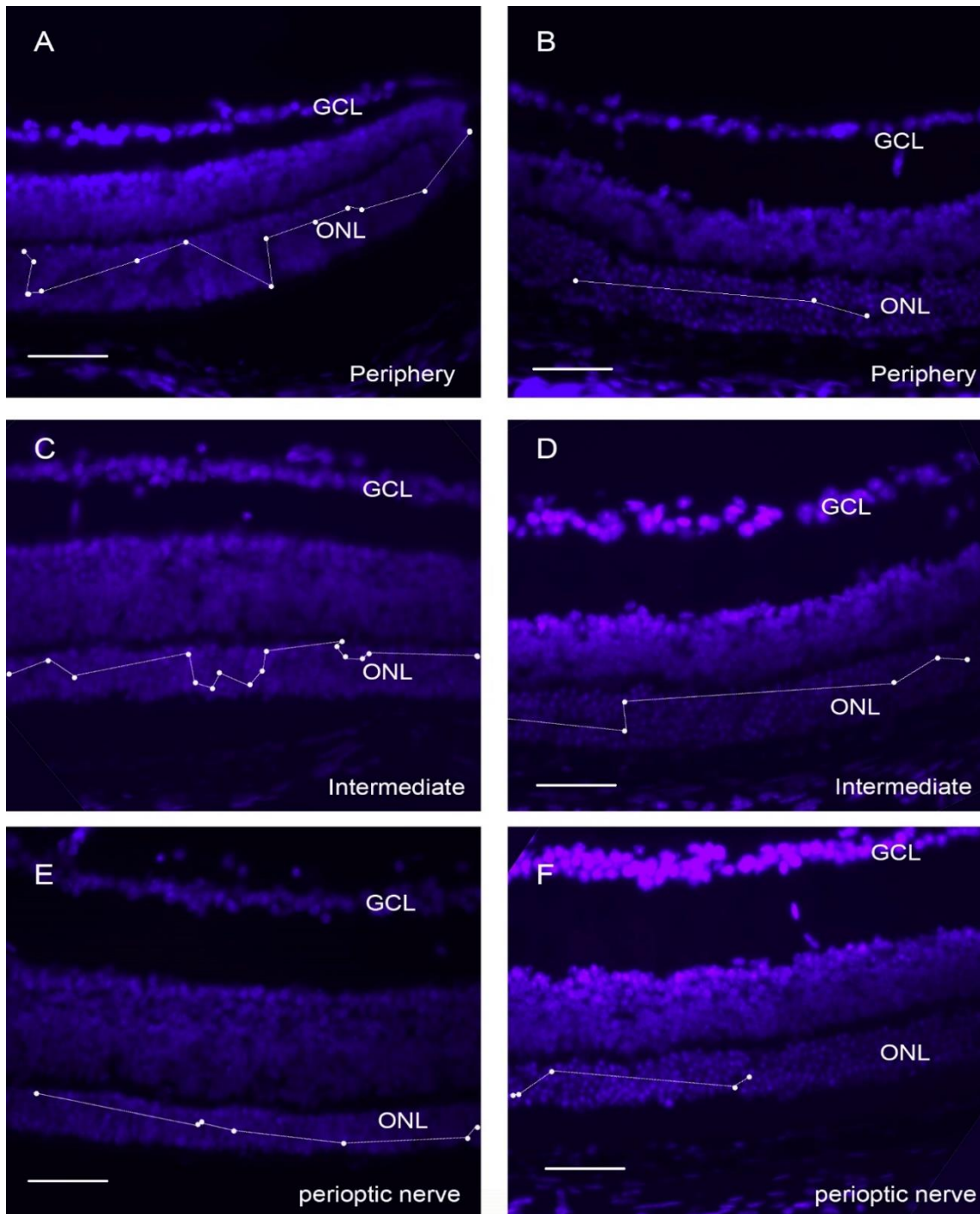


Figure 3-17 Representative images showing the localization of apoptotic cells in rd1 and Crx retina

Fluorescent micrographs of DAPI on P15 rd1 (A, C and E) and P50 Crx retina (B, D and F). White dots represent the position of TUNEL+ cells. A, C and E: The localization of apoptotic cells in P15 rd1 retina. Clusters of apoptotic cells can be seen in the periphery (A) and intermediate (C) area, with some cells tending to be in close proximity. B, D and F: The localization of apoptotic cells in P50 retina. The density of the apoptotic cells was very low in the retinal sections of Crx mouse.

To further investigate the cell-to-cell relationship between apoptotic cells, TUNEL staining was performed on wholemount Crx retinas. Figure 3-18 A-C display the fluorescent micrographs of TUNEL+ cells on wholemount retina, and D-F shows the binary images of Figure 3-18 A-C. The inter-cell distance was calculated between apoptotic cells. The distributions of these values are plotted in Figure 3-18 G-H. From these histograms, it can be seen that cell-to-cell distances have a normal distribution at P40, but shift to a right-skewed distribution at P50, suggesting that more cells were closer to each other. By P70, the cell-to-cell distribution became multimodal, indicating that although many cells tend to be close to each other, the intimate pattern found in P50 was reducing with degenerating process.

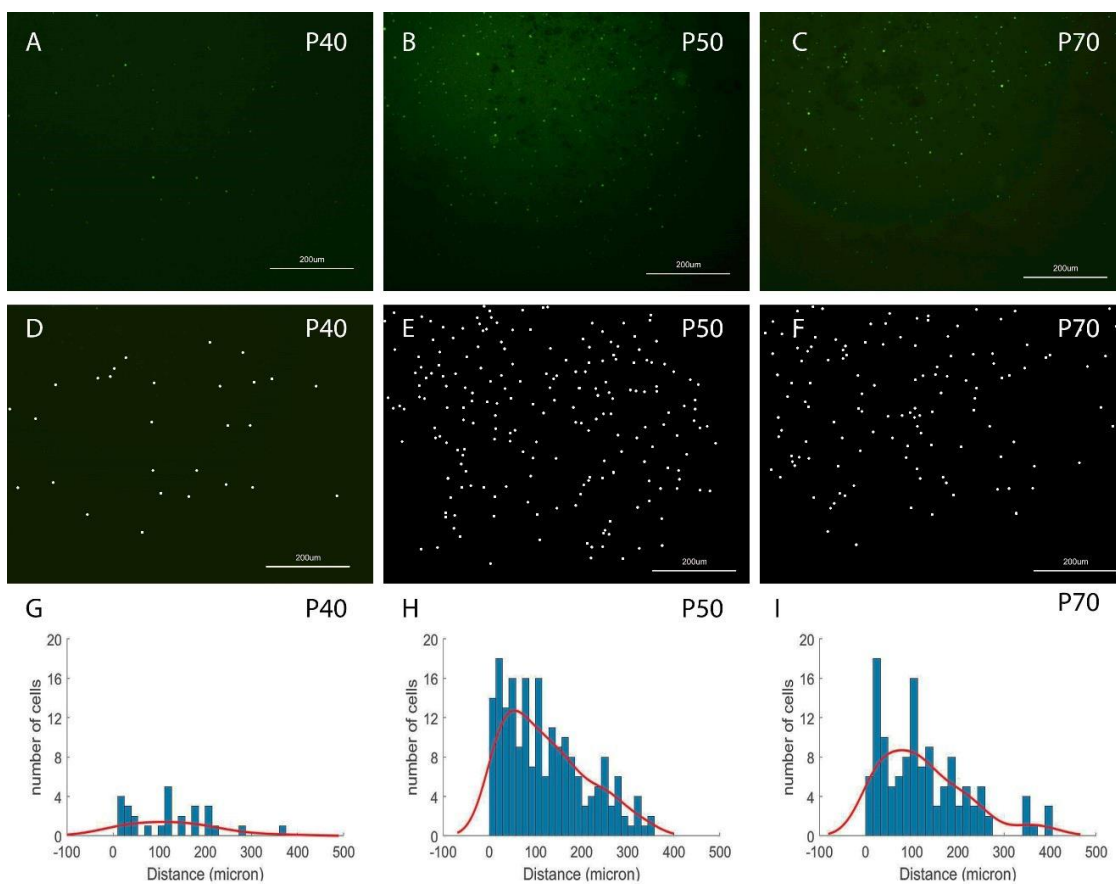


Figure 3-18 The distribution of apoptotic cells in wholemount Crx retina.

A-C The representative fluorescent micrograph of TUNEL+ cells in the wholemount Crx retina at different ages. Images were taken from the central area of the retina with photoreceptor side up. Scale bar: 200µm. D-E The binary images generated from A-C. The density of TUNEL+ cells increased remarkably from P40 to P50 with some cells displayed some apoptotic cells clustering together. G-I Distribution histogram of TUNEL+ cells from D-E. The X axis represents the cell-to-cell distance between a random apoptotic cell to any other apoptotic cell in the image. The Y axis represents the number of cells. The smaller the distance is, the more intimate the cells are. As is shown in the figure, from age P40 to P70, the numbers of cells increased at P50 and then decreased slightly. Meanwhile, a reduced cell-to-cell relationship was seen in P50 (Skewed right histogram) while the histograms from the other two ages display a multimodal distribution.

### 3.5 Parameters to evaluate the remaining photoreceptors

In this study, the ONL thickness and the nuclei counts of ONL were assessed to quantify the surviving photoreceptors. To assess how these two parameters were associated with each other, the correlation between ONL thickness and ONL nuclei counts was analysed. Data from WT, rd1 and Crx retina were assessed separately to determine the power of ONL thickness on evaluating the degenerating process. For all three mouse lines, the relationship between ONL thickness and ONL nuclear counts was linear, as illustrated in Figure 3-19. In all three lines, the Pearson correlation coefficient was high, indicating a linear relationship between the two parameters. Therefore, we may conclude that the ONL thickness and the number of cell nuclei in the ONL are both reliable estimates of ONL degeneration.

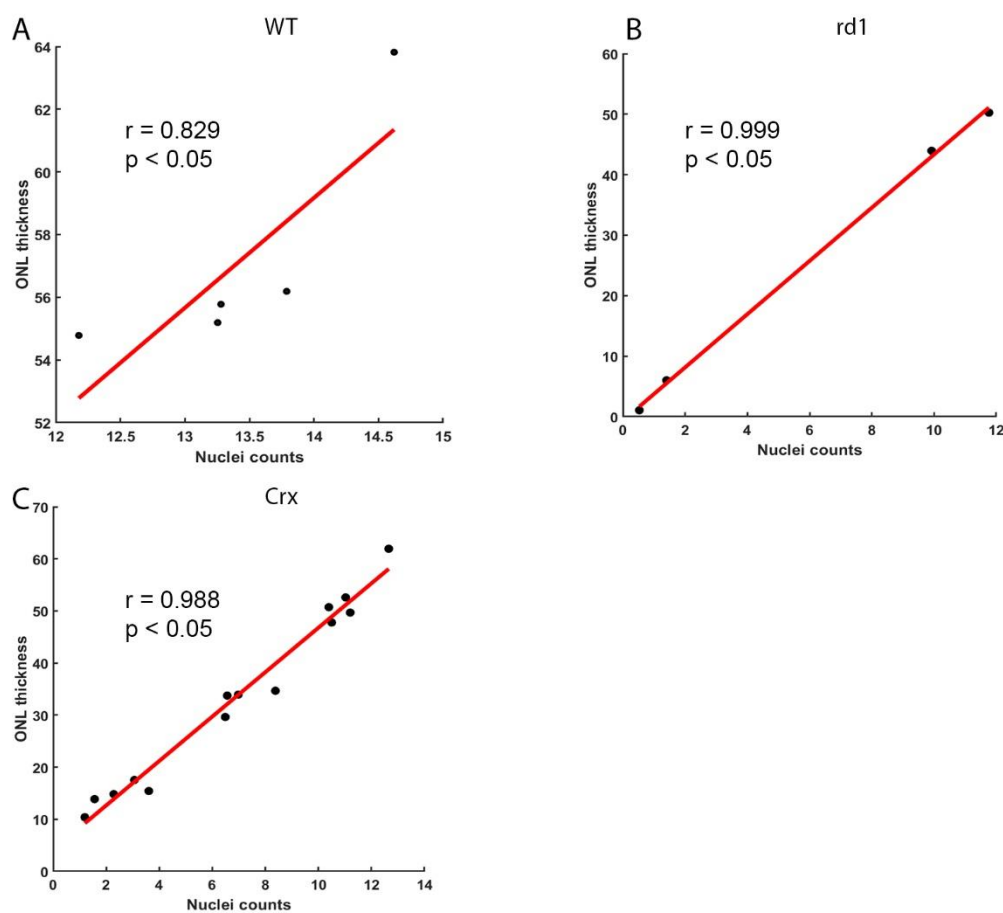


Figure 3-19 The correlation between ONL thickness and ONL nuclei counts in different strains.

There was a high correlation between ONL thickness and ONL nuclei counts in all three strains. The scatter dots were plotted using the average data from each age group. The x value was the average nuclei counts and the y value was the average value of the ONL thickness. A regression line was plotted based on the dots. A: WT retina,  $N = 18$ ; B: rd1 retina,  $N = 12$ ; C: Crx retina,  $N = 42$ .

## 4. Discussion

Results in this chapter presented an investigation into the degeneration process in two different types of animal RP models. Although both models followed a perioptic to peripheral retina degenerating pattern, the time course of the degenerating process was quite different. The rd1 retina followed a fast degenerating process, in which the onset of photoreceptor loss started from P10. The ONL thickness decreased to less than 20% by P20. The Crx retina followed a slow degenerative pattern, in which the onset of photoreceptor loss started from P30. The photoreceptors in the Crx retina survived for a longer period of time and could be detected for up to 7 months.

### 4.1 ONL thickness, ONL nuclei counts and TUNEL+ cells as parameters to evaluate photoreceptor degeneration

Photoreceptor loss during the degenerating process was assessed by measuring the ONL thickness and the nuclei counts identified by DAPI staining of all cell bodies (regardless of photoreceptor subtypes). The correlation between ONL thickness and nuclei counts was compared to validate these two measurements. Although it is assumed that loss of photoreceptors would cause a large variation in nuclei counts while the ONL thickness remain unchanged, the results suggest that decreases in ONL thickness and nuclei counts were highly correlated. That may be because the final value of ONL thickness and nuclei counts was obtained by averaging multiple measurements, and this would be able to compensate for local variation caused by sampling. Hence, we have shown that ONL thickness closely reflects the remaining number of photoreceptor nuclei in these two mice models of retinal degeneration.

The TUNEL assay has been reported as a sensitive method to label dying cells, prior to their actual death (Chang et al., 1993). Once dead, cells are quickly removed by phagocytosis, and therefore TUNEL+ cells do not accumulate in the tissue beyond the period of apoptosis. TUNEL staining is thus an appropriate tool to visualise cells in the process of dying, but it is not useful to detect dead cells. The detection of pyknotic nuclei was also attempted in this study, however, it was found to be challenging to distinguish the pyknotic nuclei from normal ones at the magnification used. Hence, TUNEL staining was used as the method for detecting apoptotic cells.

In WT retina, TUNEL+ cells were frequently seen in the inner retina during the first postnatal week due to programmed cell death in RGCs and amacrine cells (Vecino et al., 2004), but were barely detected at later stages. In this study, we visualised TUNEL+ cells in degenerating photoreceptors. The TUNEL staining was visible only in the ONL in both rd1 and Crx retina.

## 4.2 Photoreceptor degeneration in rd1 and Crx retina

Despite a similar fate in the final stages, the differences in mutations lead to a heterogeneous pathway in the rd1 and Crx retina during the degenerating process, which is in agreement with other studies on RP.

The ONL thickness and nuclei counts in WT retina did not exhibit any conspicuous changes throughout the entire life span studied. In rd1 retina, the change in ONL thickness with age was in accordance with previous publications (Kim et al., 2008).

The results from Crx retina in this study demonstrate a slow degeneration pattern, in agreement with the original publication describing Crx KO mice (Furukawa et al., 1999). Notably, this current study also showed that the ONL thickness does not decrease at a constant rate. Indeed, two periods of rapid degeneration were observed: the first between P30-40, and the second between P60-80, with slower degeneration rate in between.

The results of the TUNEL+ cells from rd1 retina were consistent with previous findings (Portera-Cailliau et al., 1994, Zeng et al., 2005). In rd1 retina, apoptosis played a major part in the first wave of photoreceptor degeneration. TUNEL+ cells were detectable between P10 and P20 and the density of TUNEL+ cells was maintained at a high level up until P15. However, in previous publications, TUNEL+ cells were at a very low level at P10 and reached a peak at around P15, whereas in this current study, the highest TUNEL density was found at P10. Apoptosis in the rd1 retina was only detectable between P10-20 and varies significantly across the retina. It is unclear whether the difference in the peak of apoptosis between this study and previous publications is due to a change in phenotype or purely experimental variability and a low statistical power. A larger sample size combined with transcriptional data would yield further information.

In Crx retinal sections, results from this study showed that TUNEL+ cells were not detectable until P50, whilst apoptosis was noted to start from P30 with sparse TUNEL+ cells observed in the wholemount retina. A possible explanation may be that the first fast degenerating wave takes only about 10 days to complete, whilst the TUNEL+ cells are quickly removed. Hence, sampling at 10-day intervals may not be able to capture fast apoptotic activity during this period. Further study with more frequent sampling may help to establish a more accurate timeline of the apoptotic activity.

Examination of the spatial distribution of TUNEL+ cells in rd1 retina revealed that apoptotic cells appear in clusters in retinal sections, suggesting interactions between the apoptotic cells during degeneration process. The clustering phenomenon was not observed overtly in Crx retinal sections, but this may be due to the lower cell density. Indeed further examination of wholemount retinas

suggested a closer cell-to-cell relationship at P50, suggesting that such interactions may occur in the Crx retina as well.

A unique pattern of rod death, in which holes devoid of cell bodies develop in the retina, has been reported in several slow degeneration rodent models (Zhu et al., 2013, Ma et al., 1998). This study revealed that this same pattern of rod loss is also present in Crx retina. Although these holes can be spotted as early as P50, they are most commonly seen from P80 onwards. A previous study on S334ter-line-3 rats revealed an accumulation of TUNEL+ cells followed by a scattering of microglial cells in the centre of similarly shaped and sized holes during a limited period of degeneration (Lee et al., 2011). The TUNEL+ cells in the holes of the S334ter-line-3 retina were considered to reflect an interaction between activated microglia and dying photoreceptors.

However, in the Crx retina, the highest density of TUNEL+ cells and the closer cell-to-cell relationship was observed at P50, whereas the holes were barely seen at this stage but were more frequently seen at later stages. Although the spatial relationship observed in S334ter-line-3 rats was not seen in Crx retina, it is speculated that the spatial relationship was masked by the concurrent rod and cone death and the clustering pattern of TUNEL+ cells in P50 may have contributed to the formation of the holes later on. Further studies including studying the specific photoreceptor subtype affected may provide a more comprehensive understanding of these cell-to-cell interaction.

## 5. Conclusion

In summary, by comparing the photoreceptor degeneration process in two different mouse models, we found that despite a similar fate in the end stages, there was heterogeneity in the pathways leading to photoreceptor death. Unlike the rd1 mouse that carries a specific rod mutation, where the time course of apoptosis was closely associated with the degeneration process, the Crx retina undergo a more complex degenerating process. While it is challenging to study these events in rd1 retina due to the temporal overlap of development and degeneration periods and the fast degeneration process, the prolonged degeneration process in the CRX mouse provides an opportunity to view and compare the time course of different events. The following studies in this thesis therefore focused on Crx retina, examining the timeline of glial activation in Crx retina and investigating its relationship with the fast degenerating phases.



**Chapter 4. Glial activity is correlated with the  
fast photoreceptor degenerating phases**



## 1. Introduction

As discussed in chapter 1, glial cells play an important role in both the healthy and diseased CNS, maintaining homeostasis of the microenvironment and protecting neurons from all sorts of potential insults.

Glial activation is a prominent feature in neurodegenerative diseases including retinal degeneration, yet the exact role it plays in the degenerative process remains to be elucidated. Glial activation in retinal degeneration is characterized by gliosis and neuroinflammation.

In the retina, gliosis is the term given to the non-specific reactive changes of Müller cells in response to insults, usually involving proliferation and/or hypertrophy, with upregulation of glial fibrillary acidic protein (GFAP), glutamine synthetase (GS) as well as vimentin. Neuroinflammation is an inflammatory process in response to a variety of injuries in the nervous tissue, mediated by the innate immune cell, the microglial cell.

As discussed in Chapter 1, microglial activation is not dependent on the genetic mutation, but relies on local and systematic cytokines, while it is also reported that there is bidirectional communication between Müller cells and microglial cells that regulate the overall response towards insults (Aredo et al., 2015). Hence, fluctuations of the microenvironment during the degenerating process might affect both microglial and Müller cell activity.

It was demonstrated in Chapter 3 that photoreceptor degeneration in the Crx retina occurs mostly during two fast degenerating waves, with much slower degeneration rate in between these two phases. Although the exact mechanism involved in these waves is unclear, it is presumed that some yet-to decipher factors may be involved in accelerating photoreceptor death. These factors, as well as photoreceptor death, may then shift the local or systemic cytokines which may sequentially influence activation of both microglial cells and Müller cells.

This chapter will investigate the characteristics of microglia and Müller cells during photoreceptor degeneration in Crx retina and explore the possible correlation between these events.

## 2. Specific Methods

### 2.1 Animals

The same cohorts of Crx mice and WT mice that were used in Chapter 3 were also used to investigate microglial activation. No less than three mice (one eye per mouse) from each strain were included in each time point.

### 2.2 Tissue collection and immunohistochemistry

Iba1 was used to visualise microglial cells. The diameter of a resting microglial cell (including its processes) is around 15-30  $\mu\text{m}$  (Torres-Platas et al., 2014). Hence, the thickness of retinal sections for examining microglial cells was adjusted to 30  $\mu\text{m}$ . Immunohistochemistry used the protocol described in Chapter 2.

### 2.3 Microscopy

Cryostat sections were scanned using a Nikon NiE upright fluorescence semi-automated microscope with 40 $\times$  oil object. Slices were scanned systematically from the dorsal to ventral ora serrata, while each field of the images was scanned from the top to the bottom using an automated Z drive platform at 3 $\mu\text{m}$  intervals. All raw images were then processed using ImageJ following the same protocol (background subtraction, Z projection and converting into 8 bit) to enhance the images.

For the GFAP filaments analysis, all the GFAP stained images were converted into black and white binary images using ImageJ. Initially, a range of different algorithms for thresholding including the default mode, triangle algorithm and mean mode were compared. The histogram of GFAP stained images displayed a right skewed distribution, in which the best overlap of original image and processed image can be gained using the triangle algorithm (Figure 4-1A-D). Next, the correspondence GFAP and DAPI stained image was used to define the inner margin, the outer margin and the median line of the retinal section (Figure 4-1E and F). The filaments that crossed the median line in the binary images were counted.

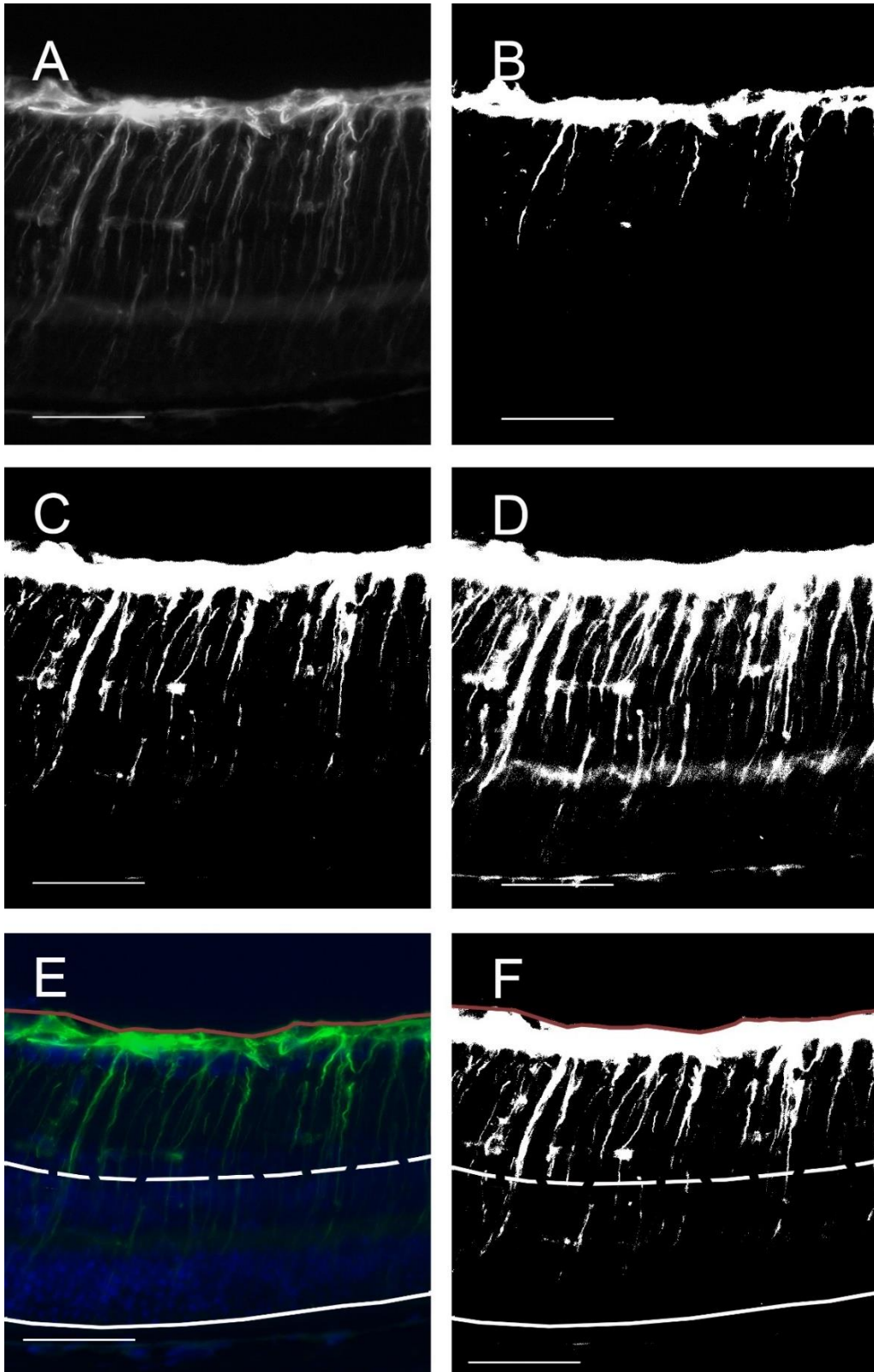


Figure 4-1 Thresholding methods for GFAP filament counts.

A: Representative fluorescent micrograph of GFAP staining. B: Binary image obtained using default mode (modified IsoData algorithm); C: Binary image obtained using triangle algorithm; D: Binary image obtained using mean algorithm. E: The inner margin (red solid line) and outer margin (white solid line) of the retina were defined using the overlay image of GFAP staining and DAPI staining. A virtual median line (white dash line) was drawn

*based on the inner and outer margin. F: The margins defined in overlay image were then applied for GFAP filaments analysis. Image was taken from the central area of the retina. Scale bar: 50  $\mu$ m.*

Image processing, cell counting, data analysis and statistics used the same procedures as described in Chapter 2.

### 3. Results

#### 3.1 The characteristics of Müller cells and microglial cells in WT and Crx retina

##### 3.1.1 Müller cells and microglial cells in WT retina

GFAP is an intermediate filament protein expressed in differentiated astrocytes of the central nervous system. GFAP is considered to be a stress marker for the CNS and upregulation of GFAP in response to injury has been observed in both brain and retina. In the healthy retina, GFAP is normally expressed in astrocytes but is absent from Müller cells. Under normal physiological conditions, GFAP expression is restricted to within the NFL, where the astrocytes are located (Eisenfeld et al., 1984). The results from this study are in agreement with previous publications. In both the developing and adult WT retina, intensive GFAP expression was found on the vitreal surface of the retinal but nowhere else (Figure 4-2 B and E).

In WT retinas, iba+ cells manifested a tiny soma and a ramified structure with large numbers of branching processes (Figure 4-2A and D). Their morphology did not change significantly between P20-80. By P110, the number and size of ramifying processes had significantly decreased. Importantly, iba+1 cells were confined to the inner retina and OPL during the entire period studied, which is in agreement with findings of resting microglial cells as reported previously (Noailles et al., 2016, Wang et al., 2016).

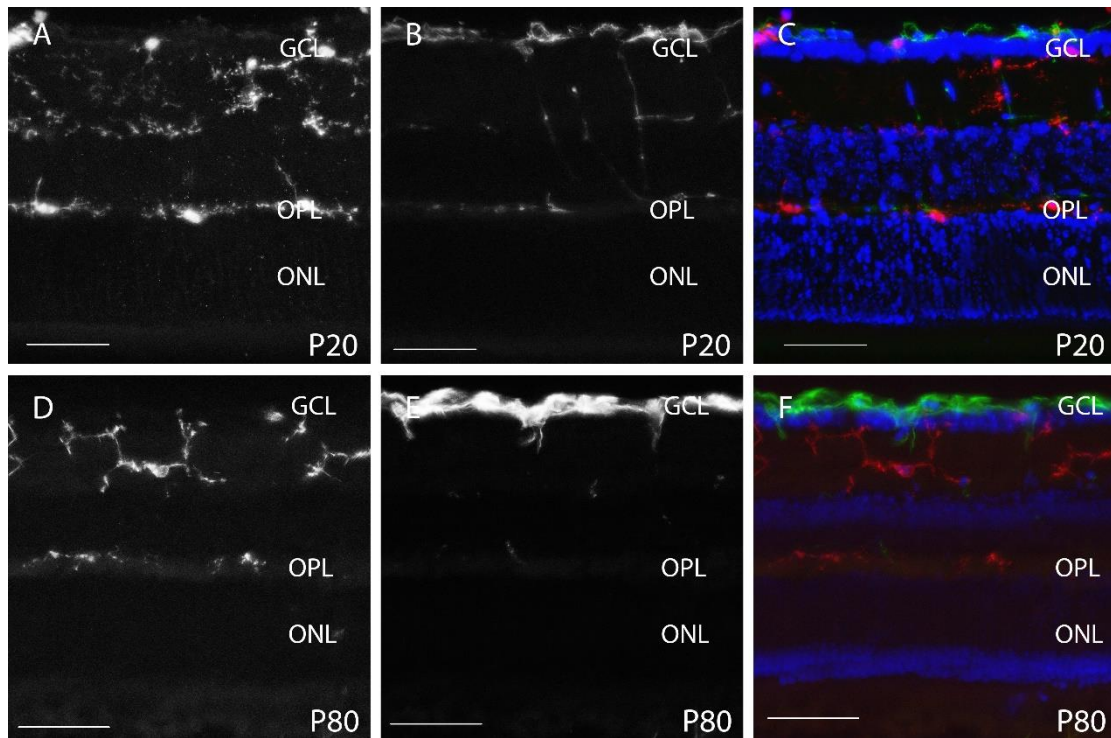


Figure 4-2 Fluorescence micrographs showing the expression of *iba1* in WT retinal sections.

Representative images of retinal section of a P20 and P80 WT retina stained with GFAP, *iba1* and DAPI. The expression of GFAP was strong near the ILM and highly restricted to the inner surface of the retina (NFL and GCL) both in developing and adult retina (B and E). *Iba1*<sup>+</sup> cells exhibited a ramified structure with a tiny soma and numerous long processes. They were distributed across all retinal layers excepted for the ONL (A and D). A-C: P20; A: *iba1*; B: GFAP; C: Overlay: blue: DAPI; red: *iba1*, green: GFAP; D-F: P80; ; A: *iba1*; B: GFAP; C: Overlay: blue: DAPI; red: *iba1*, green: GFAP; Scale bar: 50 $\mu$ m. All images were taken from the central retina.

### 3.1.2 The remodelling of Müller cells during degeneration in the Crx retina

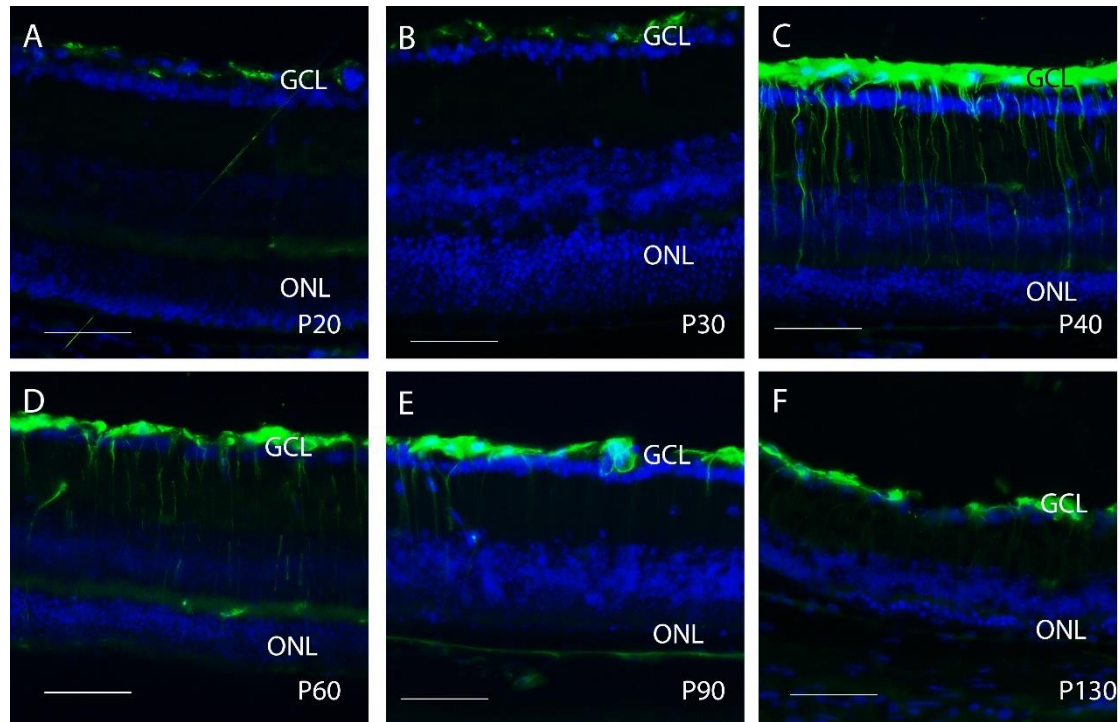


Figure 4-3 Fluorescent micrograph showing the remodelling of Müller cells in Crx retina

Representative images of retinal section of Crx retina stained with GFAP at different ages. The expression of GFAP was low and restricted to the vitreal surface (NFL and GCL) during the first postnatal month in the Crx retina (A and B). At P40, there is a strong increase in GFAP expression of GFAP, appearing as a thick band at the vitreal surface and filaments extending towards the outer retina (C). Expression decreased (band thickness and visible filaments) at P60, P90 and P130 (D, E and F). Images were taken from the central area of the retina. Green: GFAP, Blue: DAPI. Scale bar: 50 $\mu$

In the Crx retina, the expression of GFAP was restricted to within the vitreal surface of the retina at a very low level before P30 (Figure 4-3 A and B). A sharp increase of GFAP expression was observed at P40 in the inner retina, in the vicinity of the GCL and NFL, with long filaments extending towards the outer retina (Figure 4-3C). An interesting phenomenon was that this high expression did not persist with age. Indeed, although the filaments were still visible in some areas, expression was significantly reduced at P60, P90 and P130 compared to P40 (Figure 4-3 D, E and F). The results of the GFAP expression suggested that the gliosis in Crx retina did not maintain at a constant level but fluctuated throughout the degenerating process.

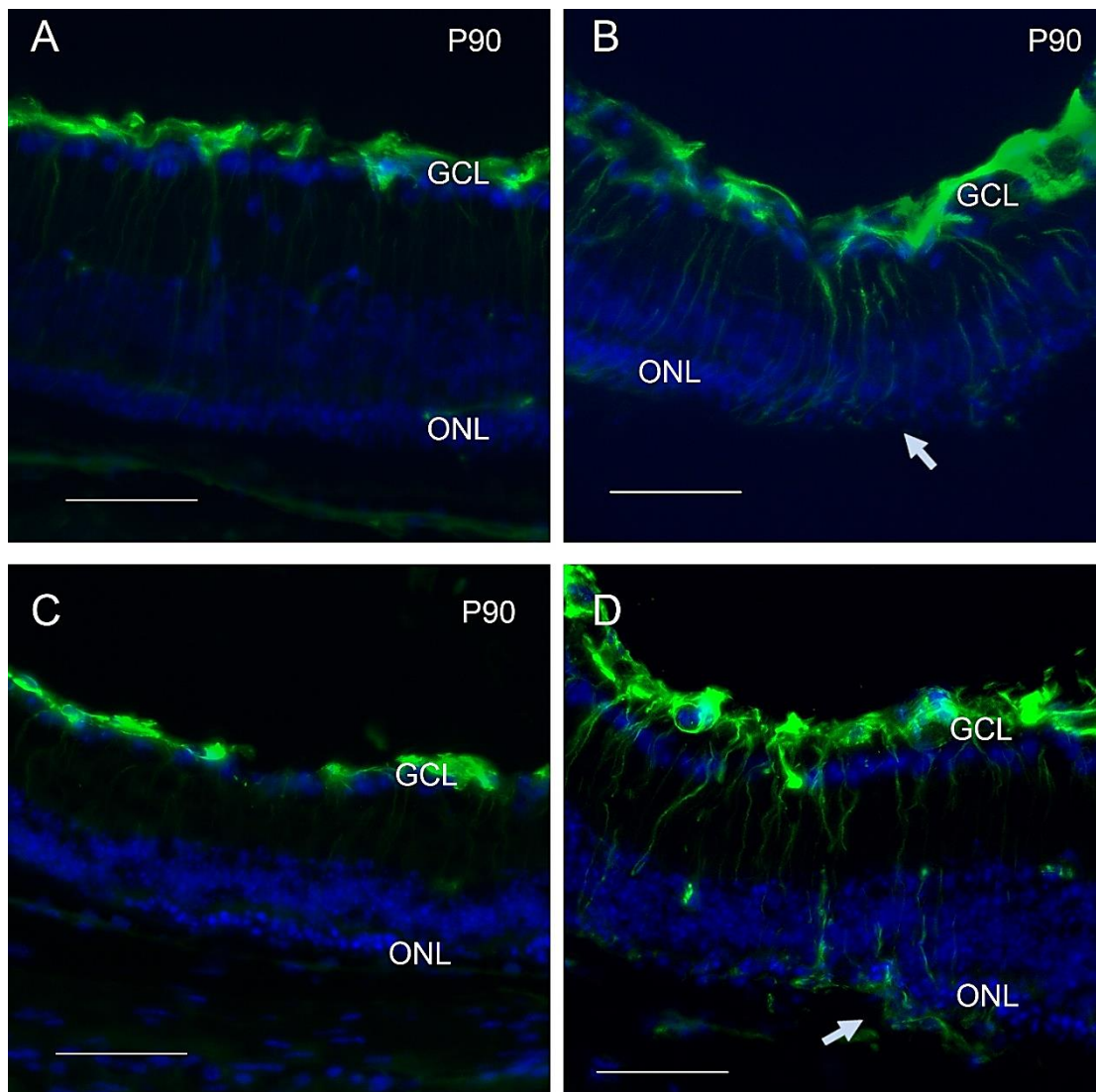


Figure 4-4 Clusters of GFAP+ filaments in the later stages of retinal degeneration in Crx retina.

Representative images of retinal section of Crx retina stained with GFAP showing clusters of GFAP+ filaments. A: P90 Crx retina. Image was taken from central area of the retina. B: P90 Crx retina (the same retina as A). Image was taken from periphery area. Clusters of GFAP+ filaments were found to fill into the area devoid of ONL (arrow). C: P130 Crx retina. Image was taken from central area of the retina. D: P130 Crx retina (the same retina as C). Image was taken from periphery area. Clusters of GFAP+ filaments found in the area devoid of ONL. GFAP+ processes were found expanding to the adjacent area and invading the areas that beyond the outer margin (arrow). Green: GFAP; Blue: DAPI; Scale bar: 50 $\mu$ m.

Notably, after P80, when the areas devoid of photoreceptors were frequently detected, clusters of GFAP+ filaments were found filling into the photoreceptor-free zones (Figure 4-4 B and D). Although, the overall GFAP expression tend to be reduced (Figure 4-4 A and C), the areas with clusters of filaments presented high expression of GFAP. In the later stages, GFAP processes were seen invading the areas that beyond the outer margin.

Visible GFAP filaments were counted at the different ages. Regardless of retinal eccentricity, the changes of filaments counts over age followed a bimodal distribution, with one peak

around P40-50, and a second peak at P70. At later stages, the number of filaments decreased and remained at a stable, lower level (Figure 4-5).

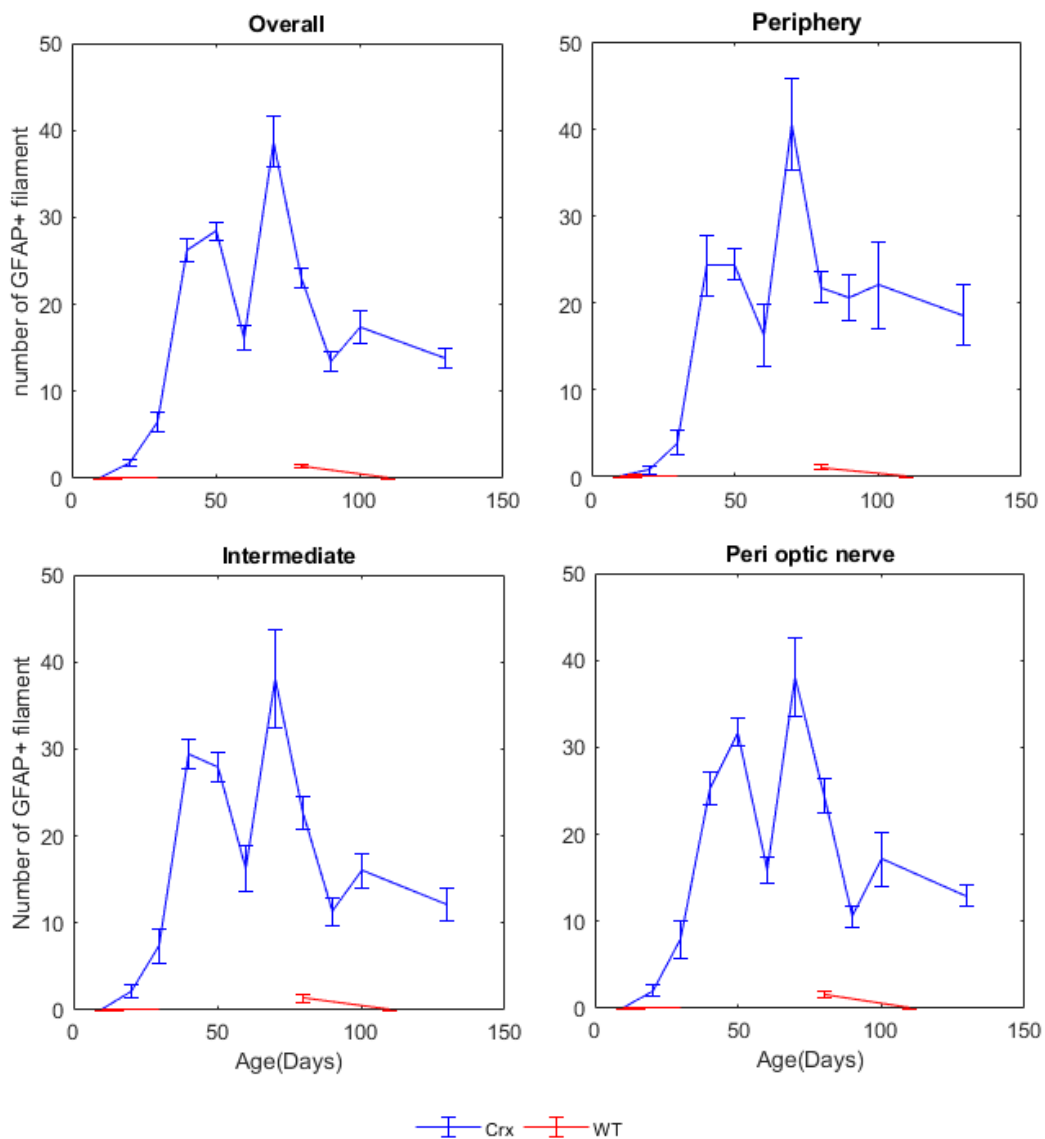


Figure 4-5 Changes in the number of GFAP+ filament against age in Crx and WT retina.

The quantitative measurements on the number of GFAP+ filament indicating that the sharp rise of GFAP filaments density start after P30 and fluctuated during the degenerating process regardless of retinal eccentricity. A: overall number of GFAP+ filaments; B: The number of GFAP+ filaments in the peripheral retina; C: The number of GFAP+ filaments in intermediate retina; D: The number of GFAP filaments in the perioptic nerve. Data seen in Table 4-1.

Table 4-1 The changes of GFAP filament density over age

Strain	age	n	Periphery		Intermediate		Perioptic nerve	
			mean (μm)	SEM	mean (μm)	SEM	mean (μm)	SEM
CRX	P10	3	0.000	0.000	0.000	0.000	0.000	0.000
	P20	3	0.774	0.432	2.139	0.711	2.045	0.620
	P30	3	3.875	1.425	7.360	2.013	7.903	2.100
	P40	3	24.250	3.534	29.333	1.700	25.250	1.867
	P50	3	24.395	1.748	27.922	1.649	31.739	1.664
	P60	3	16.308	3.576	16.200	2.617	15.900	1.549
	P70	3	40.500	5.265	38.083	5.672	38.063	4.585
	P80	3	21.750	1.756	22.629	1.867	24.405	1.988
	P90	3	20.652	2.642	11.323	1.580	10.528	1.240
	P100	3	22	5.000	16.000	2.025	17.111	3.089
P130	3	18.571	3.422	12.154	1.884	12.938	1.270	
WT	P10	3	0.000	0.000	0.000	0.000	0.000	0.000
	P20	3	0.000	0.000	0.000	0.000	0.000	0.000
	P30	3	0.000	0.000	0.000	0.000	0.000	0.000
	P80	3	1.125	0.295	1.333	0.408	1.583	0.336
	P110	3	0.000	0.000	0.000	0.000	0.000	0.000

When reviewing the changes of GFAP filaments in the retinal sections of Crx retina, clusters of GFAP filaments were observed in the areas devoid of photoreceptors as observed in Chapter 3, section 3.3.4, Figure 3-14. To further investigate this phenomenon, wholemount Crx retinas were used at P70, when the holes of photoreceptors were rarely detected, and at P90 when the holes were frequently observed. As shown in Figure 4-6, when double-labelling with the Müller cells specific marker GS and GFAP in areas without photoreceptor holes the end-feet of the GFAP+ filaments were relatively evenly distributed (Figure 4-6 A red signal), while the surface marker GS displayed a porous structure. This is in line with the structure of the activated Müller cells from a transversal view.

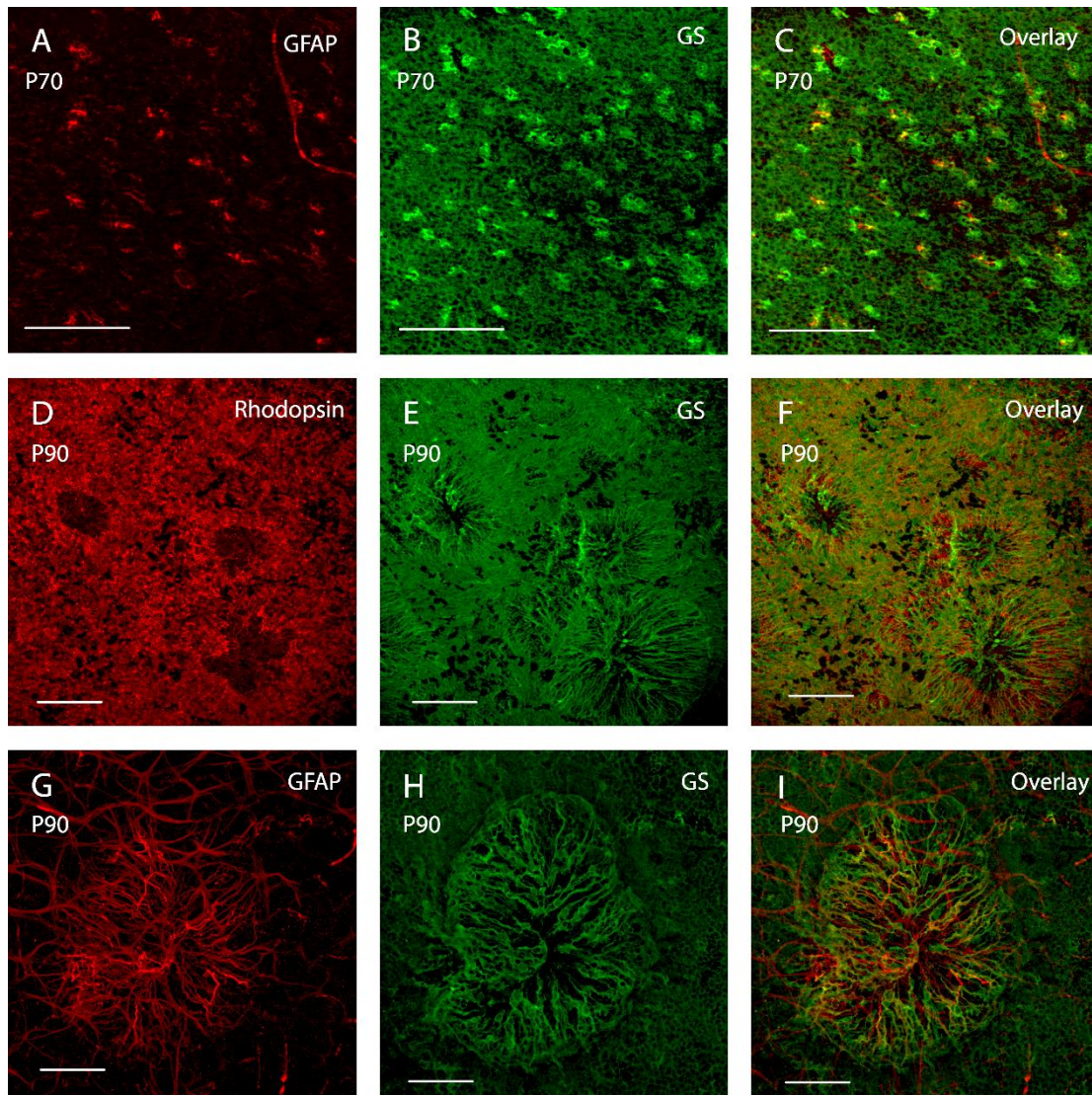


Figure 4-6 Fluorescent micrographs showing the remodelling of Müller cells into the photoreceptors holes.

Representative images wholemount *Crx* retina showing the remodelling of Müller cells associated with the formation of photoreceptor holes. Retinas were viewed from the photoreceptor side up. A-C show the distribution of Müller cells in the absence of photoreceptor holes visualised by GFAP and GS staining. A: GFAP; B: GS, scale bar 100 $\mu$ m. D-F show the co-localization of holes formed by Rhodopsin+ cells and the Müller cells clusters using GS staining. D: Rhodopsin, E: GS, scale bar 150 $\mu$ m. G-I show the detailed structure of the Müller cell cluster using GFAP and GS staining. G: GFAP, H: GS, scale bar 83.35  $\mu$ m.

By contrast, in areas with holes, clusters stained with both GS and GFAP were observed co-localised with the area devoid of rhodopsin+ cells (Figure 4-6 D-I). The GS staining presented round shapes with processes converging towards the centre, whilst the GFAP staining also formed a ‘firework’-like structure (Figure 4-6 G-I). The Double-labelling of GFAP and GS confirmed the remodelling of Müller cells to fill into the photoreceptor-free area.

### 3.1.3 The biological characteristics of iba1+ cells during retinal degeneration in Crx retina

In Crx retinas, iba1+ cells had features similar to WT during the first postnatal month. From P30 on, some iba1+ cells exhibited a larger soma and a reduction in the number of processes. These changes became more pronounced with ageing, and at the same time, there was an overt increase in the number of iba+ cells (Figure 4-7). Notably, while iba1+ cells were absent in the ONL and subretinal area in WT retinas, in Crx there was infiltration of iba1+ cells into the outer retina from P20, prior to the onset of apoptosis (at P30). The accumulation of iba1+ cells in the ONL was observed throughout the entire course of photoreceptor degeneration.

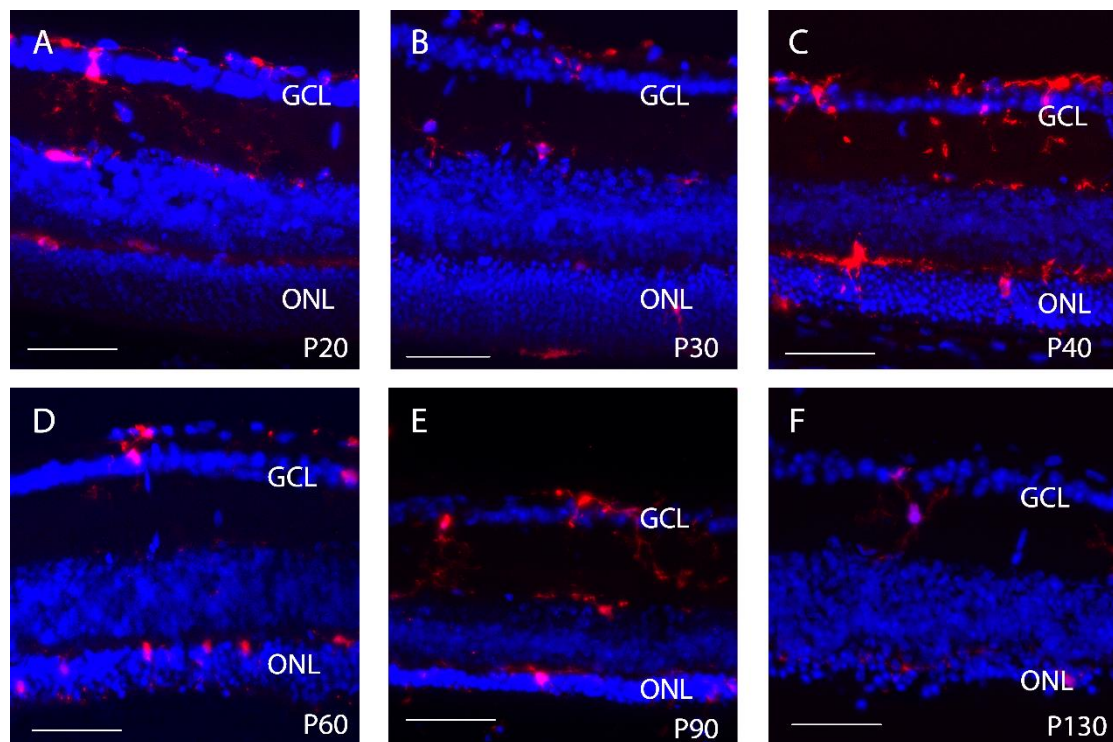


Figure 4-7 Fluorescent micrograph showing microglial activation in Crx retina

Representative images of retinal section of Crx retina stained with iba1 at different ages. The expression of iba1 was very low and restricted in the inner retina in most areas at P20 (A). The infiltration of iba1+ cells into ONL was increased slightly at P30 (B). At P40, the number of iba1+ cells increased in both inner and outer retina. The iba1+ cells also exhibited an amoeboid structure with large soma and fewer processes (C). The expression of iba1 maintained at a high level at both P60 (D) and P90 (E) and were largely reduced at P130 (F).

In the WT retina, microglial cells exhibit a classic ramified structure (Figure 4-8 A and B) with a tiny soma and long, thin processes. Upon activation, they undergo pronounced morphological changes in addition to migration and proliferation (Figure 4-8). Transverse sections reveal that microglial cells in the inner retina exhibit a dendritic shape with their

enlarged somata located within the INL, while numerous short branches emanate from the cell body in the IPL and OPL respectively (Figure 4-8 C and D).

In the ONL, the infiltrated microglial cells presented a similar dendritic structure as the cells seen in the INL, except that they extended abundant processes towards the OPL, and fewer processes towards the RPE (Figure 4-8 E-F). However, the vertical alignment of these cells relied on the architectural support of photoreceptors, and therefore, such vertical alignment disappeared after P80 with the depletion of photoreceptors.

Notably, *iba1*<sup>+</sup> cells with unique morphology were present on the surface of the RPE (Figure 4-8 G and H). Different from *iba1*<sup>+</sup> cells seen in the inner retina and ONL, these cells had an elongated soma without processes.

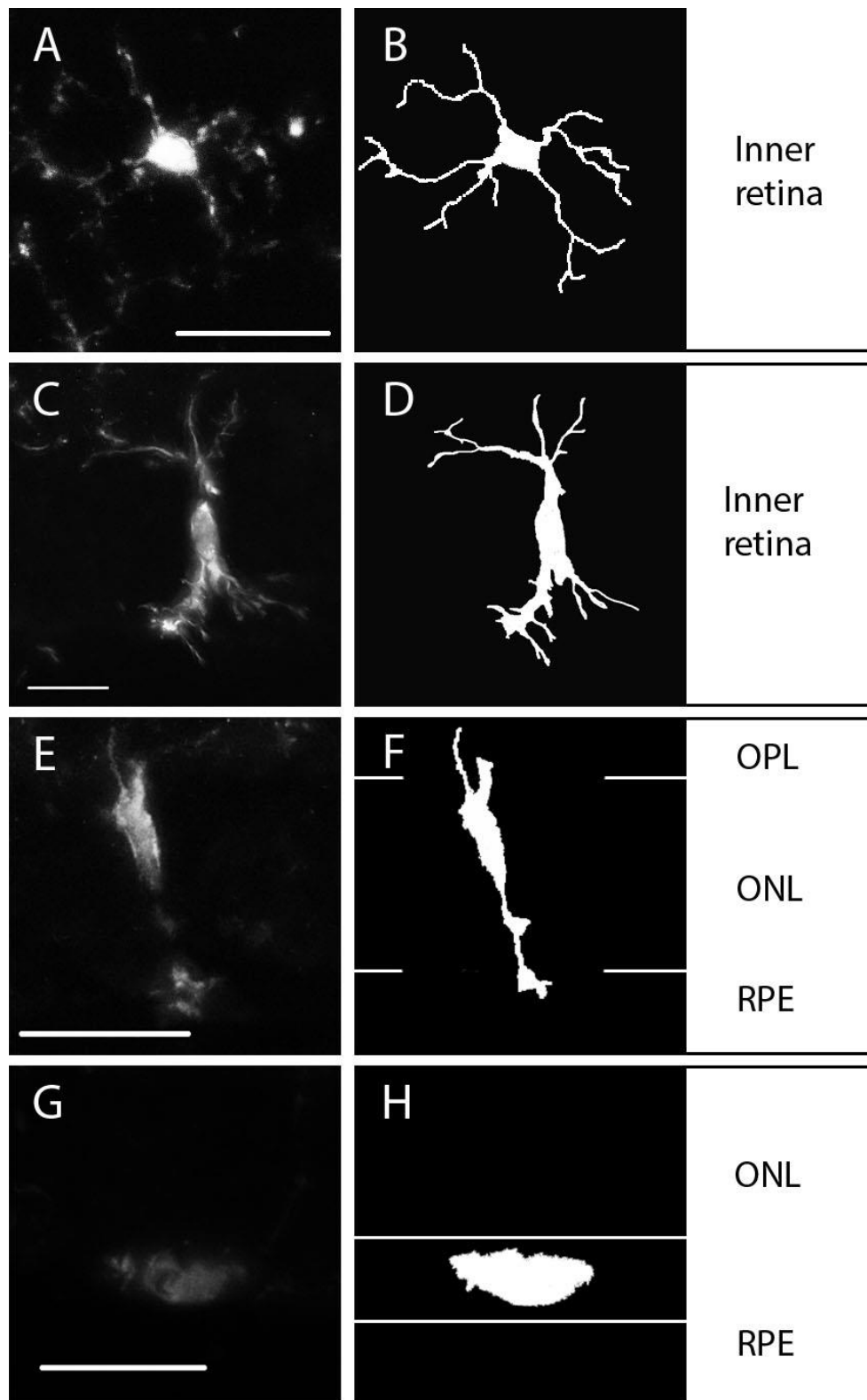


Figure 4-8 Representative micrographs of microglial cells in WT and Crx retina.

The micrographs display the morphological change of microglial cells from resting mode to activated status. In WT retina, microglial cells are restricted within the inner retina presenting a ramified structure with a tiny soma and numerous long branched processes (A and B). In the inner retina, activated microglial cells appear a dendritic shape in a vertical position with enlarged soma and short branches on both side (C and D). Infiltrated microglial cells were also seen in the ONL, which also present in a vertical, dendritic shape with enlarged soma and short

*branches (E and F). A small amount of iba+ cells were seen in the subretinal space, exhibiting a tapered soma with no processes.*

### 3.2 The distribution of iba1+ cells during retinal degeneration

To quantify changes in iba1+ cells numbers over time, the number of iba1+ cells in the inner and outer retina were counted separately. The density of iba1+ cells was initially estimated using the relative number of cells per retinal length, without taking changes in retinal thickness into account.

#### 3.2.1 The distribution of microglial cells in Wt retina

Results obtained from WT retinas were in agreement with previous studies (Paolicelli et al., 2011, Li et al., 2015) (Figure 4-9, dash lines). The average density of iba1+ cells in the inner retina was at a low level at P10 and then increased by five times at P15. The density of iba1+ cells dropped dramatically between P15-20, and the iba1+ cell density was decreased by half at P20. Notably, the high level of iba+ cell density at P15 may be attributed to a transient accumulation of iba1+ cells in the OPL, which may relate to synaptic pruning during development (Tremblay et al., 2010, Schafer et al., 2012). After P30, the incidence of iba+1 cells did not change significantly, with only a slight decrease over three months, which is in agreement with previous studies (Karlstetter and Langmann, 2014). No iba1+ cells were detected in the ONL at any age in WT retinas.

#### 3.2.2 The distribution of microglial cells in Crx retina

At P10, the density of iba1+ cells in the Crx inner retina was significantly higher than in WT (Two way anova: strain vs location, effect of the strain:  $p = 0.000$ ), indicating that the microglial activity may have already shifted at this stage. Notably, the dramatically fluctuation of iba1+ density in the WT inner retina between P10-30 was not observed in the Crx retina. Instead, the iba1+ cell density was decreased by half between P10-15, and maintained at a similar level as it was in adult WT retina from then on (Figure 4-9, solid blue lines). Although there was a significant decrease in the incidence of iba1+ cells in the Crx inner retina at early postnatal stages, differences were much more pronounced in the outer retina. At P10, no iba+1 cells were detected in the ONL. At P20, however, few cells were detected, and their incidence increased between P20-30 and presented in a fluctuating manner during degeneration until P100 (Figure 4-9, red solid lines).

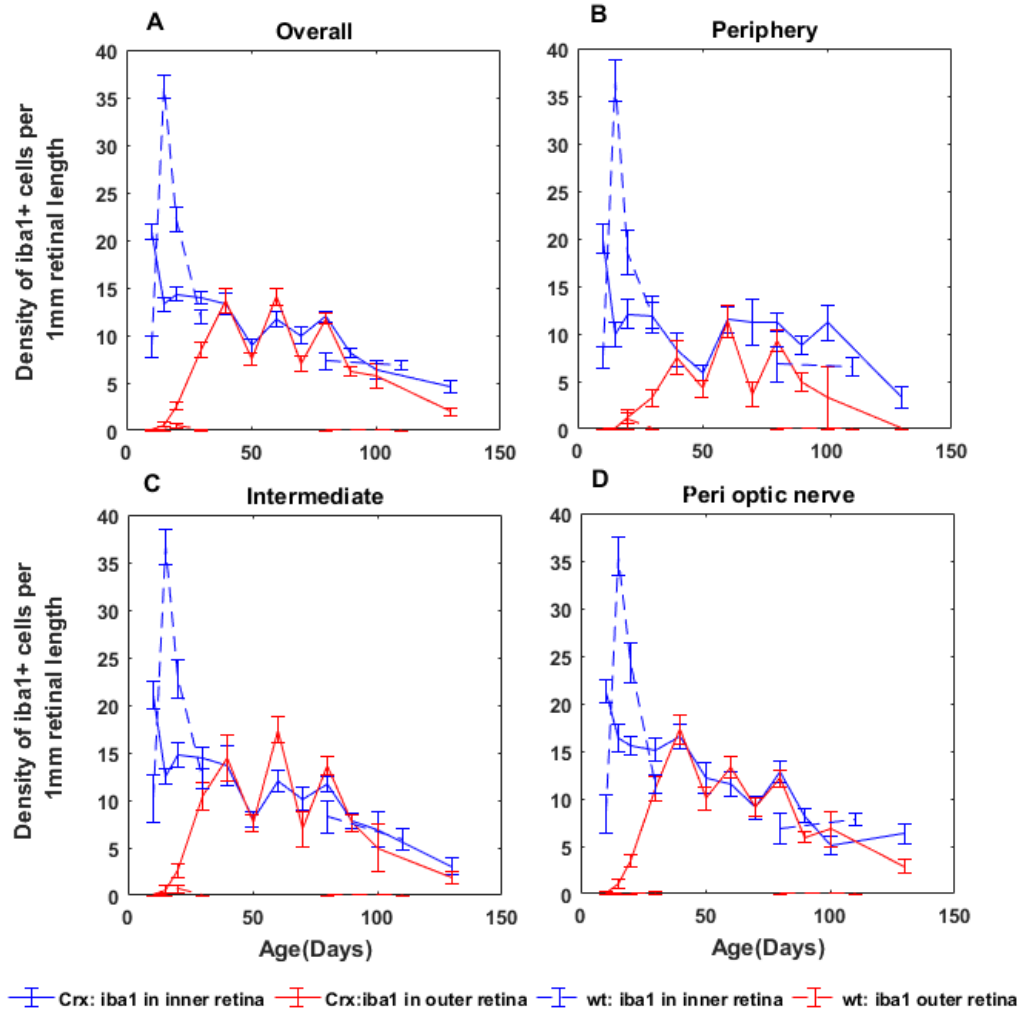


Figure 4-9 Changes in Iba1+ cell density with age in Crx and WT retina

The line graphs display the change of Iba1+ cell density in Crx and WT retina at different locations. The number of Iba1+ cells were normalised by the length of the retinal section to obtain a density per unit retinal length ( $\mu\text{m}$ ). A: Overall density of Iba1+ cells against age; B: Density of Iba1+ cells in periphery against age; C: Density of Iba1+ cells in intermediate area; D: Density of Iba1+ cells in peri optic area against age. Data points: Mean; Error bar: SEM; n = 3 at each time point. Data shown in Table 4-2 and Table 4-3.

Table 4-2 Density of *iba1+* cells in the inner retina of *Crx* and WT retina

Strain	age	n	Periphery		Intermediate		Perioptic nerve	
			mean (cells/mm)	SEM	mean (cells/mm)	SEM	Mean (cells/mm)	SEM
CRX	P10	3	19.969	19.969	19.969	19.969	19.969	19.969
	P20	3	12.092	12.092	12.092	12.092	12.092	12.092
	P30	3	11.931	11.931	11.931	11.931	11.931	11.931
	P40	3	8.359	8.359	8.359	8.359	8.359	8.359
	P50	3	5.896	5.896	5.896	5.896	5.896	5.896
	P60	3	11.481	11.481	11.481	11.481	11.481	11.481
	P70	3	11.159	11.159	11.159	11.159	11.159	11.159
	P80	3	11.181	11.181	11.181	11.181	11.181	11.181
	P90	3	8.729	8.729	8.729	8.729	8.729	8.729
	P100	3	11.188	11.188	11.188	11.188	11.188	11.188
P130	3	3.331	3.331	3.331	3.331	3.331	3.331	
WT	P10	3	7.500	1.100	10.100	2.500	8.400	2.100
	P20	3	18.500	2.300	22.800	2.100	24.300	2.100
	P30	3	12.000	2.000	12.300	1.100	11.500	1.000
	P80	3	6.800	1.800	8.200	1.700	6.800	1.600
	P110	3	6.500	1.000	5.900	1.100	7.800	0.700

Table 4-3 Density of *iba1+* cells in the outer *Crx* retina

age	n	Periphery		Intermediate		Perioptic nerve	
		mean (cells/mm)	SEM	mean (cells/mm)	SEM	Mean (cells/mm)	SEM
P10	3	0.000	0.000	0.000	0.000	0.000	0.000
P20	3	1.167	1.167	1.167	1.167	1.167	1.167
P30	3	3.231	3.231	3.231	3.231	3.231	3.231
P40	3	7.533	7.533	7.533	7.533	7.533	7.533
P50	3	4.224	4.224	4.224	4.224	4.224	4.224
P60	3	11.310	11.310	11.310	11.310	11.310	11.310
P70	3	3.626	3.626	3.626	3.626	3.626	3.626
P80	3	9.255	9.255	9.255	9.255	9.255	9.255
P90	3	4.974	4.974	4.974	4.974	4.974	4.974
P100	3	3.257	3.257	3.257	3.257	3.257	3.257
P130	3	0.000	0.000	0.000	0.000	0.000	0.000

Note: The *iba1+* cells were absent in the outer retina of WT mouse.

Due to the variation of ONL thickness with age and the dynamic nature of microglial cells, it is not clear whether these fluctuations were caused by thinning of the ONL thinning or by changes in microglial activity. While the initial analysis did not take the ONL thickness into account, the density of *iba1+* cells was then corrected by the corresponding area size. Figure 4-10 and Figure 4-11 shows the results after correction. Results from WT retinas were similar to those before correction. In *Crx* retinas, the overall density of *iba1+* cells showed a bimodal curve in both inner and outer retinas (Figure 4-10A and Figure 4-11A, blue lines). In the outer retina, the first peak appears around P40, followed by a 40% drop. The density of *iba1+* cells rose again after P50, and reached peak values at P70 in the inner retina and at P80 in the outer retina. Later on, the density of *iba1+* cells showed a downward trend in all areas, though in the outer retina it continued to be higher than at early stages of degeneration. The

density of iba1+ cells in inner and in the outer retina maintained at a low level after P90, and these changes were concurrent in the inner and outer retina.

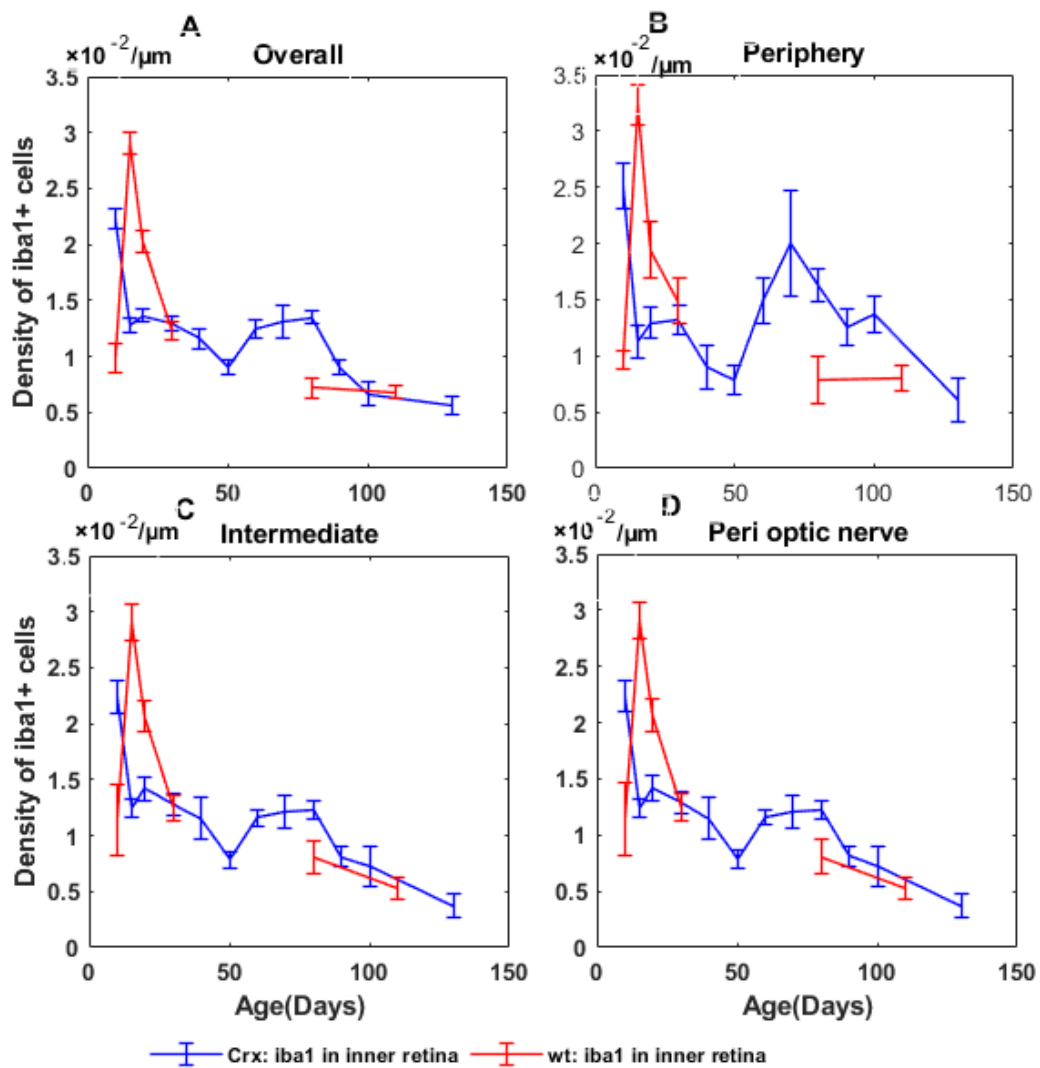


Figure 4-10 Change in iba1+ cell density in the inner Crx and WT retina with age after correction by area size.

The line graphs display the change of iba1+ cell density in Crx and WT retina at different locations after correction by the area size of the inner retina. Unit: Cell per μm<sup>2</sup>. A: Overall density of iba1+ cells against age; B: Density of iba1+ cells in periphery against age; C: Density of iba1+ cells in intermediate area; D: Density of iba1+ cells in peri optic area against age. Data points: Mean; Error bar: SEM; n = 3 at each time point. Data seen in Table 4-4.

Table 4-4 Density of *iba1*+ cells in the inner retina of *Crx* and WT retina after correction

Strain	age	n	Periphery		Intermediate		Peri optic nerve	
			mean ( $\times 10^{-2}/\mu\text{m}^2$ )	SEM	mean ( $\times 10^{-2}/\mu\text{m}^2$ )	SEM	mean ( $\times 10^{-2}/\mu\text{m}^2$ )	SEM
CRX	P10	3	2.511	2.511	2.511	2.511	2.511	2.511
	P20	3	1.290	1.290	1.290	1.290	1.290	1.290
	P30	3	1.321	1.321	1.321	1.321	1.321	1.321
	P40	3	0.902	0.902	0.902	0.902	0.902	0.902
	P50	3	0.785	0.785	0.785	0.785	0.785	0.785
	P60	3	1.493	1.493	1.493	1.493	1.493	1.493
	P70	3	2.002	2.002	2.002	2.002	2.002	2.002
	P80	3	1.631	1.631	1.631	1.631	1.631	1.631
	P90	3	1.249	1.249	1.249	1.249	1.249	1.249
	P100	3	1.369	1.369	1.369	1.369	1.369	1.369
P130	3	0.606	0.606	0.606	0.606	0.606	0.606	
WT	P10	3	0.968	0.078	1.144	0.320	0.831	0.192
	P20	3	1.944	0.249	2.067	0.142	2.055	0.162
	P30	3	1.489	0.205	1.246	0.116	1.036	0.089
	P80	3	0.788	0.214	0.807	0.153	0.605	0.144
	P110	3	0.799	0.117	0.526	0.100	0.731	0.076

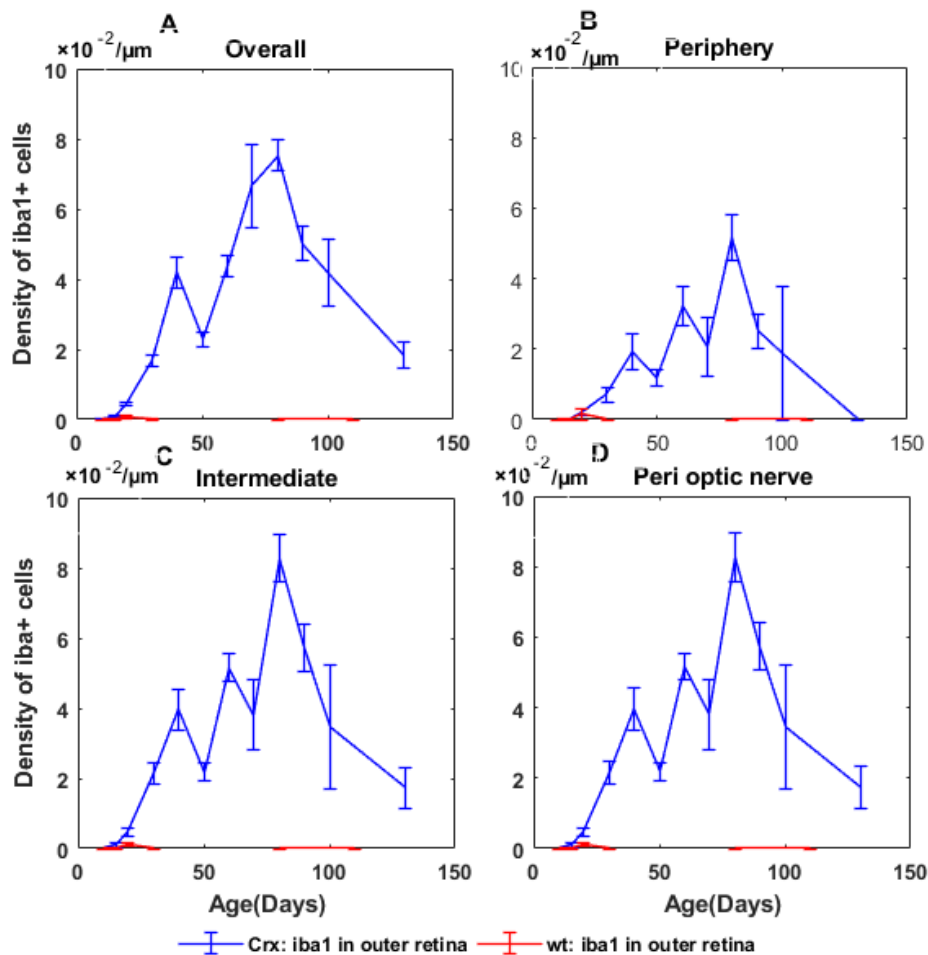


Figure 4-11 Change in *iba1*+ cell density in the outer *Crx* and WT retina with age after correction by area size.

The line graphs display the change of *iba1*+ cell density in *Crx* and WT retina at different locations after correction by the area size of the inner retina. Unit: Cell per  $\mu\text{m}^2$ . A: Overall density of *iba1*+ cells against age; B: Density of

*iba1+* cells in periphery against age; C: Density of *iba1+* cells in intermediate area; D: Density of *iba1+* cells in perioptic area against age. Data points: Mean; Error bar: SEM; n = 3 at each time point. Data seen in Table 4-5

Table 4-5 The density of *iba1+* cells in the outer retina of Crx mice after correction

age	n	Periphery		Intermediate		Perioptic nerve	
		mean ( $\times 10^{-2}/\mu\text{m}^2$ )	SEM	mean ( $\times 10^{-2}/\mu\text{m}^2$ )	SEM	mean ( $\times 10^{-2}/\mu\text{m}^2$ )	SEM
P10	3	0.000	0.000	0.000	0.000	0.000	0.000
P20	3	0.214	0.214	0.214	0.214	0.214	0.214
P30	3	0.696	0.696	0.696	0.696	0.696	0.696
P40	3	1.918	1.918	1.918	1.918	1.918	1.918
P50	3	1.189	1.189	1.189	1.189	1.189	1.189
P60	3	3.205	3.205	3.205	3.205	3.205	3.205
P70	3	2.060	2.060	2.060	2.060	2.060	2.060
P80	3	5.177	5.177	5.177	5.177	5.177	5.177
P90	3	2.506	2.506	2.506	2.506	2.506	2.506
P100	3	1.894	1.894	1.894	1.894	1.894	1.894
P130	3	0.000	0.000	0.000	0.000	0.000	0.000

Note: The *iba1+* cells were absent in the outer retina of WT mouse.

As has been described earlier, there was a subset of unique *iba1+* cells with a flattened soma on the surface of RPE, in the subretinal space. To quantify the presence of those cells over time, their numbers were analysed separately. As shown in Figure 4-12 (red lines), in WT retina, a very small number of these *iba1+* cells were detected within the first postnatal month, and they were present only in the subretinal space in peripheral areas, which is in line with the previous publications indicating that BM derived microglial cells enter the retina via the retinal margin and blood vessels in the ciliary body during development (Santos et al., 2008, Jin et al., 2016).

As for the Crx retina, more of these *iba1+* cells were seen in the subretinal space in central than in peripheral areas (Figure 4-12, blue lines). Furthermore, the presence of these cells fluctuated in line with the degeneration wave and microglial activity, suggesting that the RPE may be a route for the BM derived microglial cells from choroid to enter the subretinal space

in response to photoreceptor degeneration.

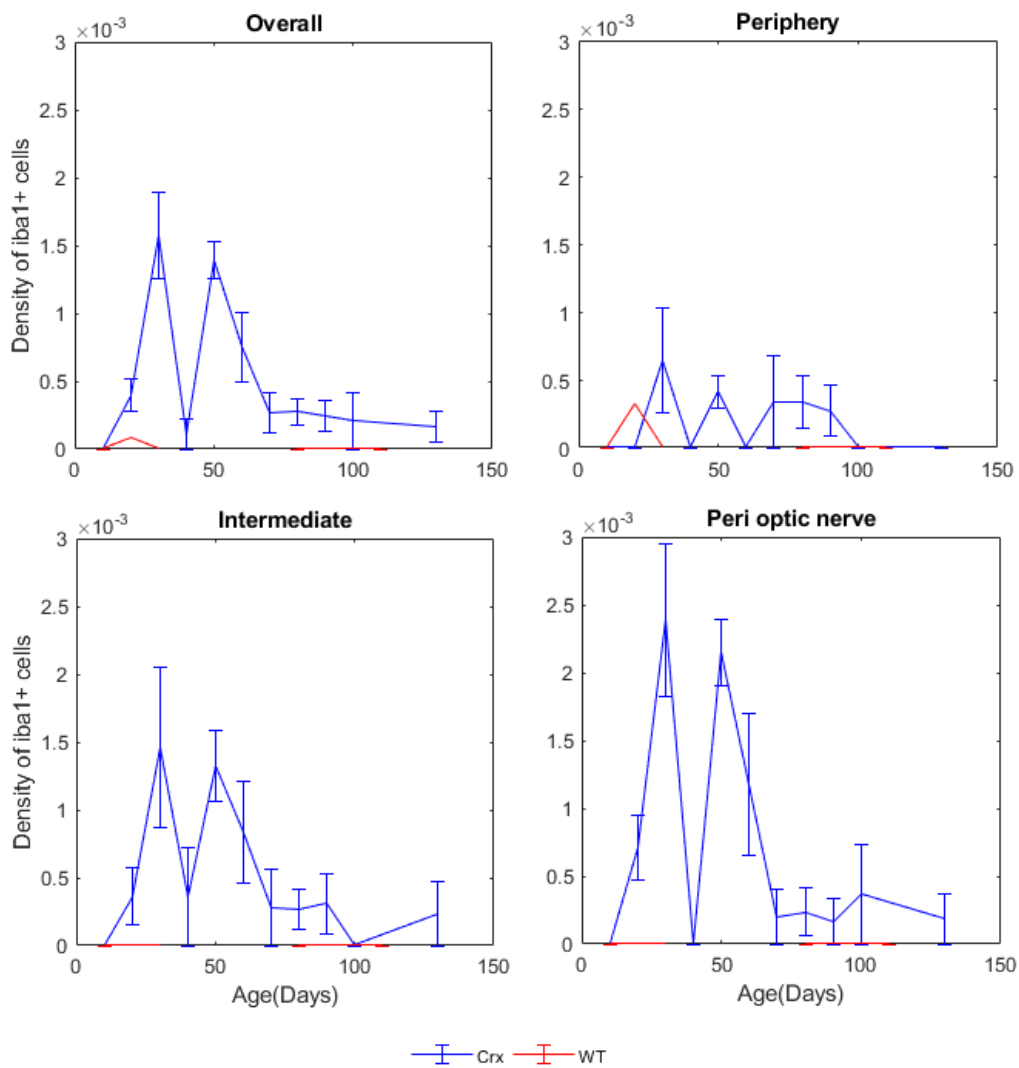


Figure 4-12 The changes in the number of Iba1+ cells in the subretinal space.

The line graphs display the change of Iba1+ cell density in the subretinal space in Crx and WT retina at different location. Unit: Cell per  $\mu\text{m}$ . A: Overall number of Iba1+ cells against age; B: The number of Iba1+ cells in periphery against age; C: The number of Iba1+ cells in intermediate area; D: The number of Iba1+ cells in peri optic area against age. Data points: Mean; Error bar: SEM;  $n = 3$  at each time point. Data seen in Table 4-6.

Table 4-6 The number of iba1+ cells in the subretinal space in Crx retina

age	n	Periphery		Intermediate		Perioptic nerve	
		mean (( $\times 10^{-3}$ cells/mm)	SEM	mean (( $\times 10^{-3}$ cells/mm)	SEM	mean (( $\times 10^{-3}$ cells/mm)	SEM
P10	3	0.000	0.000	0.000	0.000	0.000	0.000
P20	3	0.000	0.000	0.360	0.212	0.708	0.242
P30	3	0.643	0.388	1.460	0.587	2.387	0.566
P40	3	0.000	0.000	0.358	0.358	0.000	0.000
P50	3	0.411	0.117	1.324	0.257	2.150	0.246
P60	3	0.000	0.000	0.838	0.374	1.174	0.524
P70	3	0.338	0.338	0.280	0.280	0.202	0.202
P80	3	0.337	0.189	0.263	0.147	0.236	0.178
P90	3	0.273	0.188	0.307	0.226	0.170	0.170
P100	3	0.000	0.000	0.000	0.000	0.368	0.368
P130	3	0.000	0.000	0.237	0.237	0.183	0.183

### 3.3 The association between microglial activity, gliosis and photoreceptor degeneration in Crx retina.

In order to further investigate the relationship between photoreceptor degeneration, microglial activity and gliosis, the time course of these events were reviewed and compared.

#### 3.3.1 The association between microglial activity and photoreceptor degeneration.

Results presented so far in this chapter demonstrate that there are two waves of microglial activation in the outer retina, and the distribution of iba1+ cells is correlated with photoreceptor degeneration activity. To explore this correlation further, changes in iba1+ cells density in the outer retina were compared with changes in ONL thickness. Figure 4-13A suggests that the changes in iba1+ cell density occurred simultaneously with ONL thinning. The first increase in iba1+ cells occurred during the first wave of photoreceptor degeneration, followed by a 40% drop by the end of that period. The incidence of iba1+ cells then dropped to its lowest values around P50, coinciding with a period of slowing down of ONL thinning. The second wave of photoreceptor degeneration (starting around P60) triggered another increase in the incidence of iba1+ cells, followed by a sharp drop at the end of that second degeneration wave, by P80. The correlation between iba1+ cell density and ONL thickness was calculated from scatter plots of mean values of density of iba1+ cells against mean ONL thickness. Data from the two degeneration were analysed separately (Figure 4-13B and C). Pearson correlation analysis was used to calculate the correlation between these two variables, showing that there was a strong, negative correlation between ONL thickness and the density of iba1+ cells.

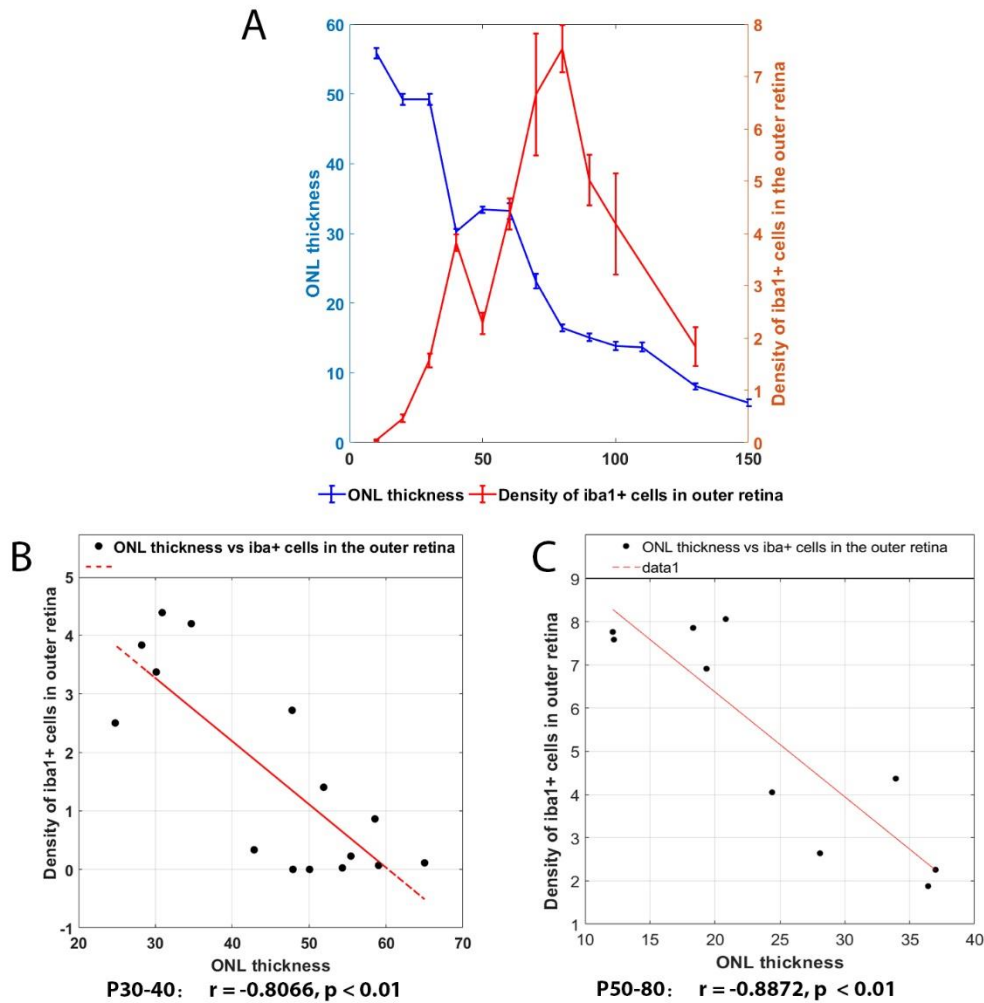


Figure 4-13 Correlation between ONL thinning and microglial activation during retinal degeneration.

A: displays the time course of Iba1+ cell density in the outer retina and ONL thinning. B: Correlation of ONL thickness against density of Iba1+ in outer retina between P10-40. Each dot represent the data from one animal and the red line presents the best fit line of the data points. Pearson correlation:  $r = -0.8066, n=15, p<0.01$ . C: Correlation of ONL thickness against density of Iba1+ in outer retina between P50-80. Each dot represents the data from one animal and the red line presents the best fit line of the data points. Pearson correlation:  $r = -0.8872, n=10, p<0.01$ .

### 3.3.2 The association between gliosis and photoreceptor degeneration.

The results from GFAP filaments also suggested a bimodal distribution during the degenerating process. The timeline of gliosis and photoreceptor loss were therefore compared to determine whether gliosis coincided with photoreceptor degeneration.

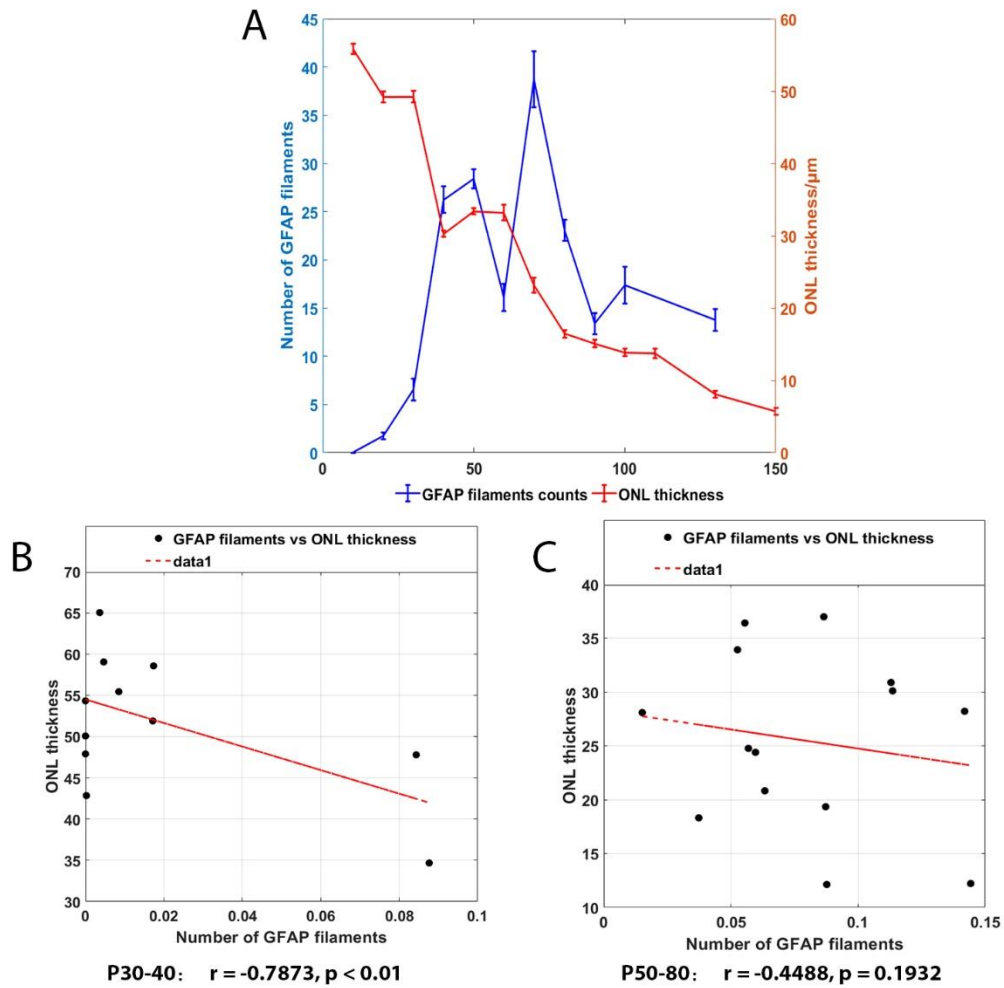


Figure 4-14 Correlation between ONL thinning and gliosis during retinal degeneration.

A: displays the changes in ONL thinning and the GFAP filaments over age. B: Correlation of the number of GFAP filaments and ONL thickness between P10-40. Each dot represent the data from one animal and the red line presents the best fit line of the data points. Pearson correlation:  $r = -0.7873, n=15, p<0.01$ . C: Correlation of the number of GFAP filaments and ONL thickness between P50-80. Each dot represent the data from one animal and the red line presents the best fit line of the data points.. Pearson correlation:  $r = 0.3895, n=10, p = 0.1932$ .

Figure 4-14A reveals that the first wave of GFAP+ filaments rose rapidly and overlapped with the first photoreceptor degeneration wave. However, the high level of GFAP+ filaments was maintained during the first half of the period when the photoreceptor loss slowed down, and dropped during the second half of that period. The second rise of GFAP+ filaments level occurred between P60-80, coinciding with the second degeneration wave. Pearson analysis revealed that there is a significant, negative correlation between ONL thickness and gliosis activity between P30-40, however, this effect was not seen at P50-80.

### 3.3.3 The association between microglial activity and gliosis

Results from Müller cells and microglial activity indicate that both events presented a bimodal distribution during the degenerating process. To further investigate the spatiotemporal relationship between these two events, the timeline of microglial activity and Müller glial activity were compared.

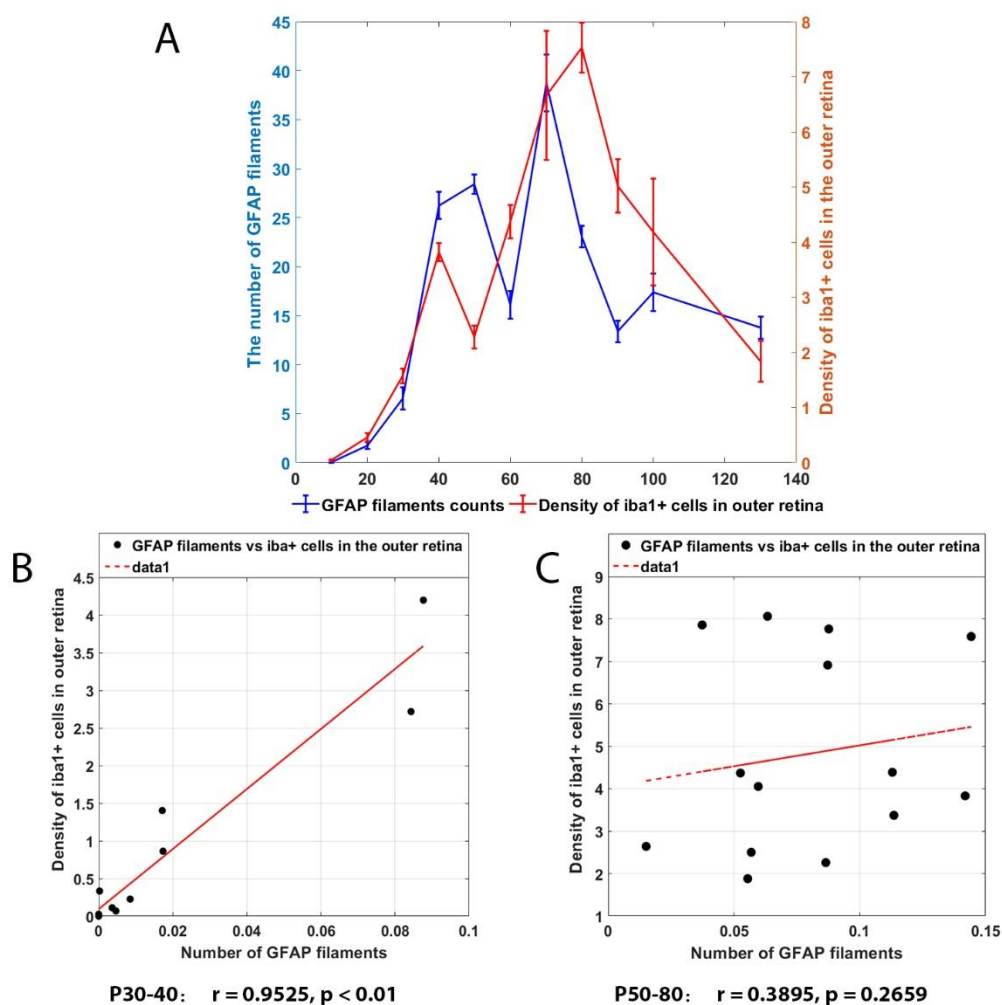


Figure 4-15 Correlation between microglial activity and gliosis during retinal degeneration.

A: displays the changes in the number of Iba1+ cell in the outer retina and the GFAP filaments over age. B: Correlation of the number of GFAP filaments and Iba1+ cells in outer retina between P10-40. Each dot represent the data from one animal and the red line presents the best fit line of the data points. Pearson correlation:  $r = 0.9525$ ,  $n=15$ ,  $p < 0.01$ . C: Correlation of the number of GFAP filaments and Iba1+ cells in outer retina between P50-80. Each dot represent the data from one animal and the red line presents the best fit line of the data points. Pearson correlation:  $r = 0.3895$ ,  $n=10$ ,  $p = 0.2659$ .

As can be seen in Figure 4-15A, the peak of microglial activity coincided with the Müller gliosis activity. However, these events correlated significantly only between P10-40 (Figure 4-15B), during the first wave of degeneration, but not during the second wave, between P50-80 (Figure 4-15C).

## 4. Discussion

In this chapter, the characteristics of resting and activated Müller cells and microglia were demonstrated by comparing GFAP filaments and the distribution and morphology of iba1+ cells in WT and Crx retinas. The results show that in the Crx retina, microglial activity is temporally correlated with photoreceptor degeneration. While there was also an intimate relationship between microglial activity and Müller gliosis during the first degeneration phase, this relationship disappeared at later stages of degeneration.

### 4.1 Remodelling of Müller cells during photoreceptor degeneration in the Crx retina.

Changes in the level of Müller gliosis were evaluated using the sensitive stress marker GFAP. In the healthy retina, GFAP is primarily expressed by astrocytes and its expression is restricted to low levels within the NFL (Eng, 1985). Upregulation of GFAP expression in response to insults is known to be a hallmark of Müller gliosis, characterised by the extension of GFAP+ filaments into the outer retina and the formation of glial scar, which have been reported in a wide range of retinal degenerative diseases including inherited photoreceptor degeneration. It is reported that, in rd1 mouse, the elevation of GFAP expression increases from the start of photoreceptor death and decreases during the subsequent cone degeneration phase (Chua et al., 2013). Recent findings revealed that there is variation of Müller gliosis levels among different RP models and the response is disease-specific (Hippert et al., 2015)

The results on WT retina from this study are in line with previous findings. However, in the Crx retina, although the extension of GFAP+ filaments was observed along with the photoreceptor degeneration process, there was variation in gliosis location in terms of retinal eccentricity and timing during the degeneration process.

In the Crx retina, activated Müller cells exhibited two morphological forms. During the earlier degeneration stages, activated Müller cells had long GFAP+ filaments extending towards the outer retina, while at later stages when there were increasing numbers of photoreceptor “holes” with clusters of firework-like structures co-localising within these holes. Whilst fluctuation in GFAP expression was observed in the extended filaments, GFAP expression in those clusters was sustained once they formed.

The formation of GFAP+ clusters in the photoreceptor ‘holes’ has been reported in other RP models as well, for example in the S334ter-line-3 rat (Ji et al., 2014, Lee et al., 2011) and

P23H rat (Fernandez-Sanchez et al., 2015). Results from this study revealed that in Crx retina, such Müller cell remodelling is associated with rod migration rather than with cone migration in RP models, where rods die before cones. In the Crx retina, rods and cones die concurrently and the rods remain well preserved during the later stage. Hence, the similarity in Crx and RP models is that in both cases, Müller cells clusters appear only at late degeneration stages, although in RP there is cone migration whereas in Crx, rod migration dominates. One hypothesis is that this type of remodelling may be mediated by a unique factor released along with the focal photoreceptor depletion. Further investigation on the crosstalk between Müller cells and photoreceptors may shed some light on the mechanisms of the remodelling process.

#### 4.2 The characteristics of resting microglial cell.

As described in section 5.3 of Chapter 1, there are numerous surface markers and proteins available to label microglial cells. In this study, they were visualised with iba1, which stains all microglial cells, regardless of their activation status and origins. Hence, iba1+ cells represent the entire microglial population, including both innate and extrinsic microglial cells. Although iba1 labelling does not discriminate between resting and reactive microglia, the precise morphology of iba1+ cells can help to determine the status of the cells.

The morphology of iba1+ cells observed in WT retina is consistent with the ramified structure of resting microglial cells illustrated in previous studies (Kierdorf and Prinz, 2017, Nimmerjahn et al., 2005), characterised by a tiny soma and numerous branching processes. This morphology is maintained from 1-3 months postnatal. Notably, fewer processes were observed in iba1+ cells from P110, which might be a sign of priming. However, the expression of MHC II, as well as transcriptional approaches, may be required in order to unequivocally determine the priming status.

The distribution of iba1+ cells in WT retinal layers is also in agreement with the previous publication on resting microglia (Chen et al., 2002). Iba1+ cells are found in small numbers, exclusively in the layers between GCL and OPL, but never in the ONL. Notably, the density of iba1+ cells in the inner retina is relatively high during the first postnatal month, but then decreases beyond P30. In addition, a wave of microglial cells accumulating at the OPL was observed during the second postnatal week, which was in agreement with the previous work on the microglial distribution during development (Santos et al., 2008). As demonstrated in Section 5.2.1.1 of Chapter 1, microglial cells contribute to regulating the development of

synaptic connectivity during retinal development. The high incidence of microglial cells during early development is thus consistent with earlier findings.

### 4.3 The characteristics of Microglial cells during photoreceptor degeneration in the Crx retina

Microglial activation has been widely demonstrated in neurodegenerative diseases including inherited retinal degenerations (Brites and Vaz, 2014, Minett et al., 2016, Zeng et al., 2005). Results from this study are in line with previous studies of microglial activation during photoreceptor degeneration. Indeed, *iba1*<sup>+</sup> cells in the Crx retina underwent morphological changes (from ramified to amoeboid structure) and infiltrated the outer retina with the progression of photoreceptor degeneration.

Notably, in this study, another source of microglial recruitment was also found in the space between RPE and the photoreceptor outer segments. These cells displayed a monocyte structure which was distinct from the structure of microglial cells in the neural retina. This peculiar structure and location may suggest a separate source of those cells, e.g.: bone marrow derived macrophage (BMDM). (Yang et al., 2014) (Benhar et al., 2016)

BMDM recruitment has also been reported in AMD models, in which the onset was prior to RPE apoptosis. It is suggested that, through direct contacting, the BMDMs not only enhance the RPE loss directly by phagocytosis, but also increase the susceptibility of RPE to apoptosis (Devarajan et al., 2016). In this study, the presence of these cells was correlated with the changes in microglial activity within the neural retina, but was more intense in the central area than in the periphery, which may be related to the more intense degeneration in the central area. The interaction with RPE was not investigated, however, the timeline of recruitment found in this study may indicate that it is a secondary process to the changes in the neural retina. Further investigation on the association between the infiltrated microglial cells and RPE may shed some light into the understanding on the disease progression.

Furthermore, retinas were investigated at a 10 day intervals that spanned the major period of photoreceptor degeneration. The results provide a more detailed timeline of microglial activation during photoreceptor degeneration compared to previous studies. In the Crx retina, an increase of *iba1*<sup>+</sup> cell density in the inner retina was initially observed as early as P10. Furthermore, microglial infiltration into the ONL was already detected as early as around P20, in agreement with previous findings on the upregulation of microglial-specific transcripts in the pre-degenerative phase (Gehrig et al., 2007).

Another interesting finding of microglial activity in the developing Crx retina is that the density of iba1+ cells in the inner Crx retina is much lower than it is in the WT retina between P15-20 (See Section 2.6 of Appendix). As discussed earlier, the increase of microglial density in the WT retina may relate to the development of synaptic connectivity, and early neural activity such as visual experience at eye opening (occurring at P12) may be crucial to the regulation of microglial activity. However, in the Crx retina, the mutations result in the failure of elaborating the outer segments of photoreceptors, which leads to a complete lack of light response and may result in low microglial activity levels. Further investigation on the development of synaptic connectivity in Crx retina may provide further insights on the role of microglial regulation in the establishment of synaptic connectivity.

#### 4.4 The correlation between Müller gliosis, microglial activation and photoreceptor degeneration in Crx retina.

Photoreceptor death, Müller gliosis and microglial activation are the common events found in almost all types of outer retinal dystrophies, while how those events interact with each other remains to be elucidated.

It is suggested that in RP, the initial change is that the genetic defects lead to oxidative stress which triggers the alteration of surface proteins in the photoreceptors. These stressed yet viable cells sequentially elicit the initial microglial activation and attract microglial cells to migrate into the outer retina.

The exact sequence of photoreceptor death and microglial activity seems to be variable between disease models. A previous study on the sequential events in the rd1 retina demonstrated that changes in microglial density in the outer retina during degeneration followed a unimodal temporal distribution, with peak density occurring before the peak of apoptosis (Zeng et al., 2005). The authors hypothesized that microglial cells may be an instigator of photoreceptor degeneration, however, the results from another study in the *rd5* retina seem to be contradictory to this assumption. Indeed, although changes in microglial density also followed a unimodal temporal distribution, peak microglial activation occurred at least 5 days after the peak of apoptosis (Hughes et al., 2003).

In this study, we observed a bimodal temporal distribution in the microglial density in the outer Crx retina. The first peak occurred at P40 and the second peak, at P80. The Crx retina has a more severe genetic defect, which affects both rods and cones and the degenerative process is much slower than for both the rd1 and *rd5* models, which provides us with a much

broader temporal margin to investigate and detect various changes. In the Crx retina, photoreceptor death peaks around P50-70, which is exactly in-between the two peaks of microglial activity. Comparison of the correlation of apoptosis and microglial activity between these studies suggests that the latter events may not be directly triggered by apoptosis. Our study further revealed that there was a clear temporal relationship between microglial activation and the rate of photoreceptor degeneration. Microglial activity decreased when the degenerating process slowed between P40-60. These results indicate that there might be an as yet unknown factor that controls microglial activation during the fast degenerating phase, whilst this factor is downregulated between the degeneration waves.

Whilst there was a strong negative correlation between photoreceptor degeneration rate and microglial activity during both degeneration waves, significant correlation between Müller gliosis and other events was detected only the first wave of PR degeneration, but not during the second one.

As described earlier, there were two forms of Müller gliosis, 1) the extension of GFAP+ filaments, which fluctuated along the degeneration process; 2) the formation of firework-like GFAP+ clusters in the later stages, which persisted once formed. Hence, it is hypothesized that the disappearance in the correlation between Müller gliosis and other events may be attributed to the formation of clusters, which is considered to be an irreversible change. Müller gliosis is usually considered to be a response towards injury and is assumed to be induced by photoreceptor death in retinal dystrophies (Chua et al., 2013). However, previous evidence from models of acute retinal degeneration indicate that the extension of Müller filaments may be the guide by activated microglial cells via physical interaction (Wang et al., 2011). The extended filaments may serve as scaffolds for microglial cells to translocate to the lesion site. Microglial cells show great plasticity in response towards changes in the retinal micro-environment and regulate Müller cell activity via neurotrophic factors such as nerve growth factor (NGF) and glial cell line-derived neurotrophic factor (Harada et al., 2002). Meanwhile, Müller cells may in turn feedback onto microglial cells via the TSPO-DBI pathway which reshapes the orientation of microglial processes (Wang et al., 2014). It is proposed that there is dynamic bidirectional communication between Müller cells and microglial cells, which displays huge variation among different pathological conditions. This variation may be an explanation for the disparity in the outcomes of the migration and integration of stem cells post transplantation (Barber et al., 2013). Elucidating

the exact regulatory mechanism will not only help understanding the disease progress, but will also give information on the optimum time windows for therapeutic approaches.

Furthermore, results from this study indicate that, dying photoreceptors during the fast degenerating waves may lead to an accumulation of other chemokines that amplify the inflammatory activity. However, it is unclear whether the exaggerated microglial activity could also accelerate photoreceptor degeneration and Müller gliosis. Another important question that needs to be clarified is whether the mechanisms involved in microglial activation are similar during the entire degeneration period, or whether microglial cells undertake different roles at different degeneration stages. Further experimental approaches to manipulate these factors during the degeneration process may shed light on the mechanisms underlying interactions between microglial activation and photoreceptor death.

## 5. Conclusion

In summary, by comparing the timeline of different events during photoreceptor degeneration in the Crx retina, we found that apoptosis seems to be independent from the fast degeneration waves and microglia activation, suggesting that trying to slow down apoptosis may not be an effective therapeutic strategy. By contrast, the synchronicity of microglial activation and photoreceptor degeneration presents a promising target for protecting photoreceptors. We propose a microglia-based explanation to photoreceptor degeneration and Müller gliosis based on our findings (Figure 4-16). However, it remains to be demonstrated whether microglial activation will ameliorate or exacerbate the degeneration process. In the following chapter, we study the effects of Neurostatin, a microglia inhibitor, on retinal degeneration in an isolated Crx retina model.

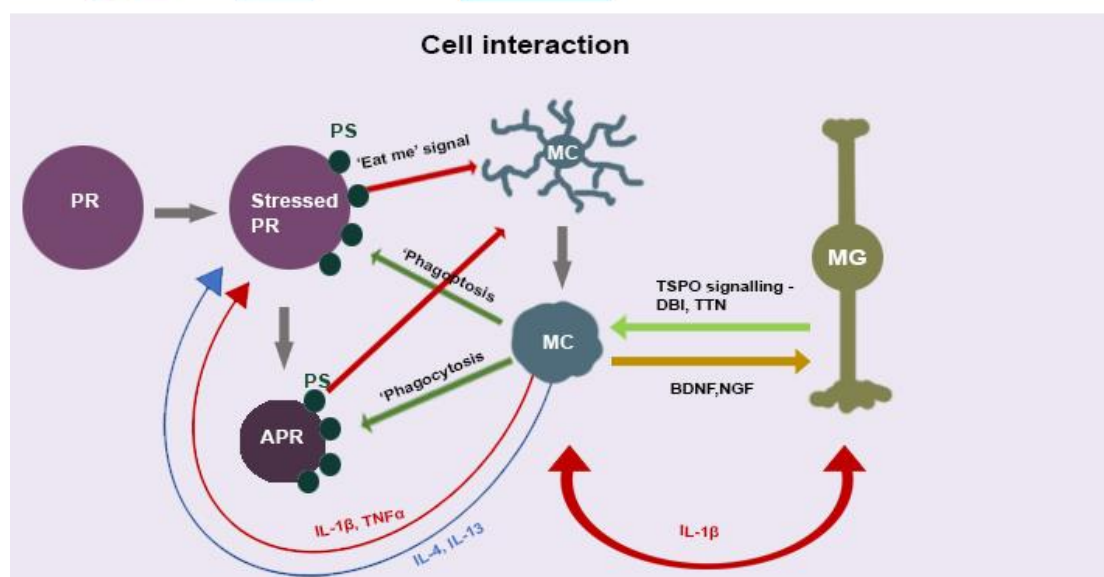
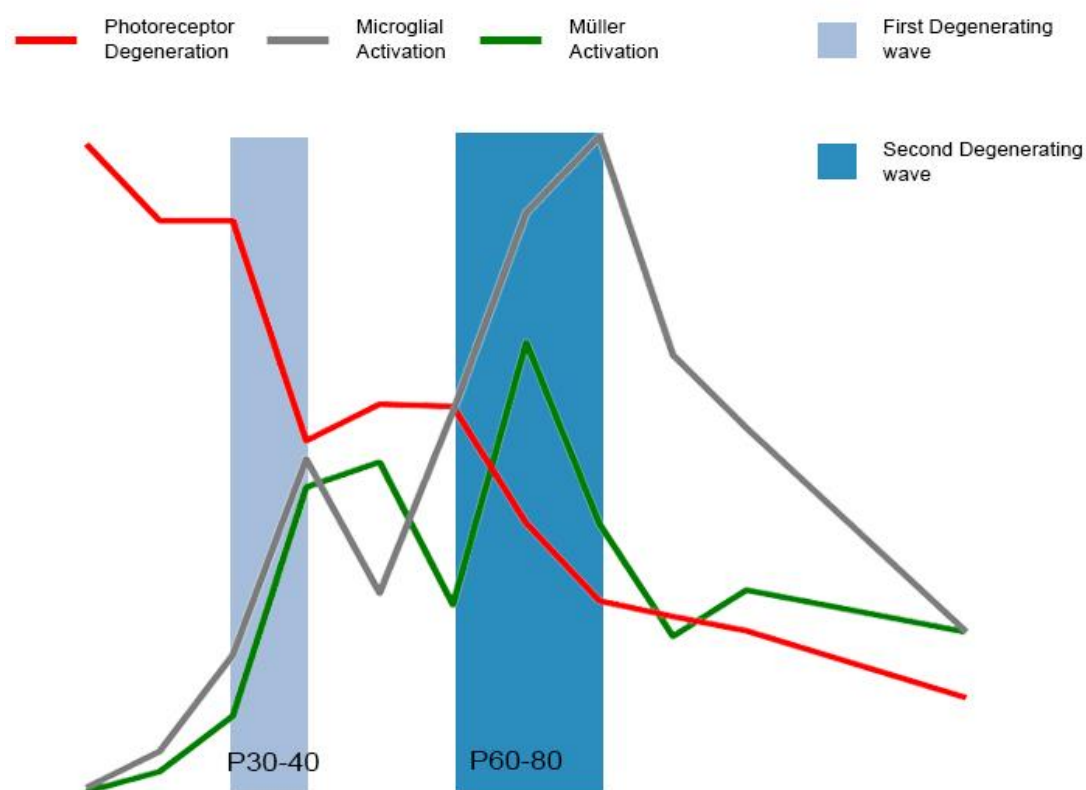


Figure 4-16 Pathological events during photoreceptor degeneration in the Crx retina

Upper panel: Timeline plot of degeneration generated from our experimental observations. The phases defined as fast degenerating waves are highlighted.

Lower panel: Proposed interaction between photoreceptors, microglial cells and Müller cells. Stressed photoreceptors send signals to microglial cells via altering the surface protein PS and transform microglial cells into the activating mode. Upon activation, microglial cells remove apoptotic cells via phagocytosis, however, they can also attack and remove stressed but viable photoreceptors directly via another process called phagoptosis. Microglial cells can accelerate degeneration via releasing proinflammatory factors such as IL-1 $\beta$ , TNF $\alpha$ , but also show protective effect via releasing anti-inflammatory factors such as IL-4, IL-13. During the process, a bidirectional Müller-microglial communication is also set via both releasing and receiving inflammatory factors. Meanwhile, microglial cells modulate the outgrowth of Müller filaments via releasing factors such as BDNF,

*whilst Müller cells can also regulate microglial activity via TSPO signalling. PS: phosphatidylserine; PR: photoreceptor; APR: apoptotic photoreceptor; MC: microglial cell; MG: Müller glia.*

## **Chapter 5. Pharmacological Inhibition of Microglia Cells in Isolated Retina**



## 1. Introduction

The studies outlined in Chapter 3 and Chapter 4 have shown that photoreceptor degeneration in the Crx retina occurs in two main waves, and that strong microglial activation and Müller gliosis occur at the same time, suggesting an intimate relation between these events. The exact mechanism of this interaction remains to be elucidated. Evidence has shown that glial activation is not merely a reactive response towards disease, but can also result in neural cell death via either phagoptosis (phagocytosing viable neurons) or via the release of cytotoxic factors that induce cell death (Flight, 2013, Brown and Neher, 2012, Madeira et al., 2015).

In acute conditions such as infection, activated microglial cells are responsible for phagocytosing pathogens and removing dead neurons to protect the remaining neurons from further damage (Zinkernagel et al., 2013). The contribution of microglial cells during this stage is considered to be protective. By contrast, in chronic disease like retinal degeneration, although high level of anti-inflammatory cytokines such as interleukin – 10(IL-10) have been detected during the photoreceptor death phase (Noailles et al., 2016), microglial cells are considered to be cytotoxic in the long term. Hence, microglial activation is considered to be detrimental in chronic neurodegenerative diseases.

However microglia also play an essential role in the maintenance of functional integrity in both developing and adult retina, and the complete depletion of these cells can be detrimental, leading to the degeneration of photoreceptor synapses and progressively impaired light responses (Wang et al., 2016). Therefore, selectively inhibiting pro-inflammatory pathways, but at the same time without blocking essential physiological function would be the ideal approach to reduce microglia-mediated photoreceptor death and mediate gliosis level. IL-15, the pro-inflammatory cytokine, plays a key role in regulating inflammatory events in the CNS by controlling the response of T and B cells (Gomez-Nicola et al., 2010). It has been reported that overexpression of either endogenous or exogenous IL-15 can lead to infiltration of macrophage and T cells in neurodegenerative disease and trigger a series of inflammatory events such as activation of the NF- $\kappa$ B pathway and the mitogen-activated protein kinase (MAPK) pathway ERK1/2 and p38 (Gomez-Nicola et al., 2008, Gomez-Nicola et al., 2010, Ren and Dubner, 2010). Neurostatin, the O-acetylated form of a sialic acid also called ganglioside, can bind IL-15 with high affinity and therefore inhibit the sequential cascade of inflammation. Neurostatin was

previously reported to selectively inhibit glial activation without disturbing physiological function in a mouse model of drug induced glaucoma (Ganesh and Chintala, 2011).

This chapter presents the results of *in vitro* effects of Neurostatin on microglial activation at different stages of degeneration in the Crx retina.

## 2. Specific Methods

### 2.1 Animals and procedures

To test the efficacy of Neurostatin on inhibiting microglial activation, isolated P10 and P40 Crx retinas were incubated with Neurostatin in oxygenated artificial cerebrospinal fluid (aCSF). We performed these experiments at P10 and P40 because these ages correspond to the pre-activation phase and the activation phase respectively (see Chapter 4). For each animal, one eye was used for Neurostatin incubation, and the other was incubated with plain aCSF as a control. No less than three Crx mice (one eye per animal) were included for each time point. Two WT mice were incubated with plain aCSF using the same protocol to test whether the mere incubation period can induce an inflammatory reaction.

Following cervical dislocation, the eyes were enucleated and kept submerged in a petri dish filled with aCSF (118 mM NaCl, 1 mM NaH<sub>2</sub>PO<sub>4</sub>, 25 mM NaHCO<sub>3</sub>, 3mM KCL, 1 mM MgCl, 2 mM CaCl<sub>2</sub> and 10 mM glucose) continuously bubbled with 95% O<sub>2</sub> and 5% CO<sub>2</sub>. The cornea and lens were gently removed using micro-scissors. Neurostatin shows high affinity to bind IL-15 at concentrations ranging from 200 nM to 5 mM. We chose to use a concentration of 500 nM Neurostatin prepared freshly in oxygenated aCSF on the day of the experiment. The eyecups were moved to a 20 ml centrifuge tube with 6 ml of either drug solution or plain aCSF for incubation. The eyecups were incubated in the centrifuge tube, equilibrating with 95% O<sub>2</sub> and 5% CO<sub>2</sub> at room temperature, and were collected after 8 hours of incubation.

The procedures for tissue fixation, immunohistochemistry, microscopy and data analysis are described in Chapter 2 and Chapter 4.

### 3. Results

3.1 The effect of *in vitro* incubation with aCSF on WT retina.

3.1.1 The morphological change of microglial cells in the WT retina after aCSF incubation.

In order to understand whether incubation with aCSF can activate glial cells in an isolated retina preparation kept *in vitro* for 8 hours, iba1 and GFAP expression was examined in P80 WT retinas.

The morphological examination on iba1+ cells showed that, although the somata of iba1+ cells in the inner retina remained small and round in shape following aCSF incubation, some of these cells exhibited larger processes (Figure 5-1B and C) (from GCL to OPL), except for only one or two cells per slice showing infiltration into the ONL. The infiltrated iba1+ cells exhibited a vertical orientation with their processes extending across the ONL (Figure 5-1F). These infiltrated iba1+ cells could only be detected in the periphery of the incubated retina but were completely absent from the central retina.

Nevertheless, the morphology of iba1+ cells in these acutely treated WT retinas was entirely different from the activated form in age-matched Crx retinas (Figure 5-1H-J). Indeed, none of the iba1+ cells exhibited the same amoeboid features as seen in the Crx retina, suggesting much milder microglia activation than during retinal degeneration.

Next, the expression of GFAP was compared in WT retinas after treatment. As it showed in Figure 5-1K-L, after incubation in aCSF, the expression of GFAP was restricted within GCL at a similar level as observed in untreated age-matched WT retina (Figure 5-1K), which was distinct from the GFAP response seen in Crx retina (Figure 5-1M).

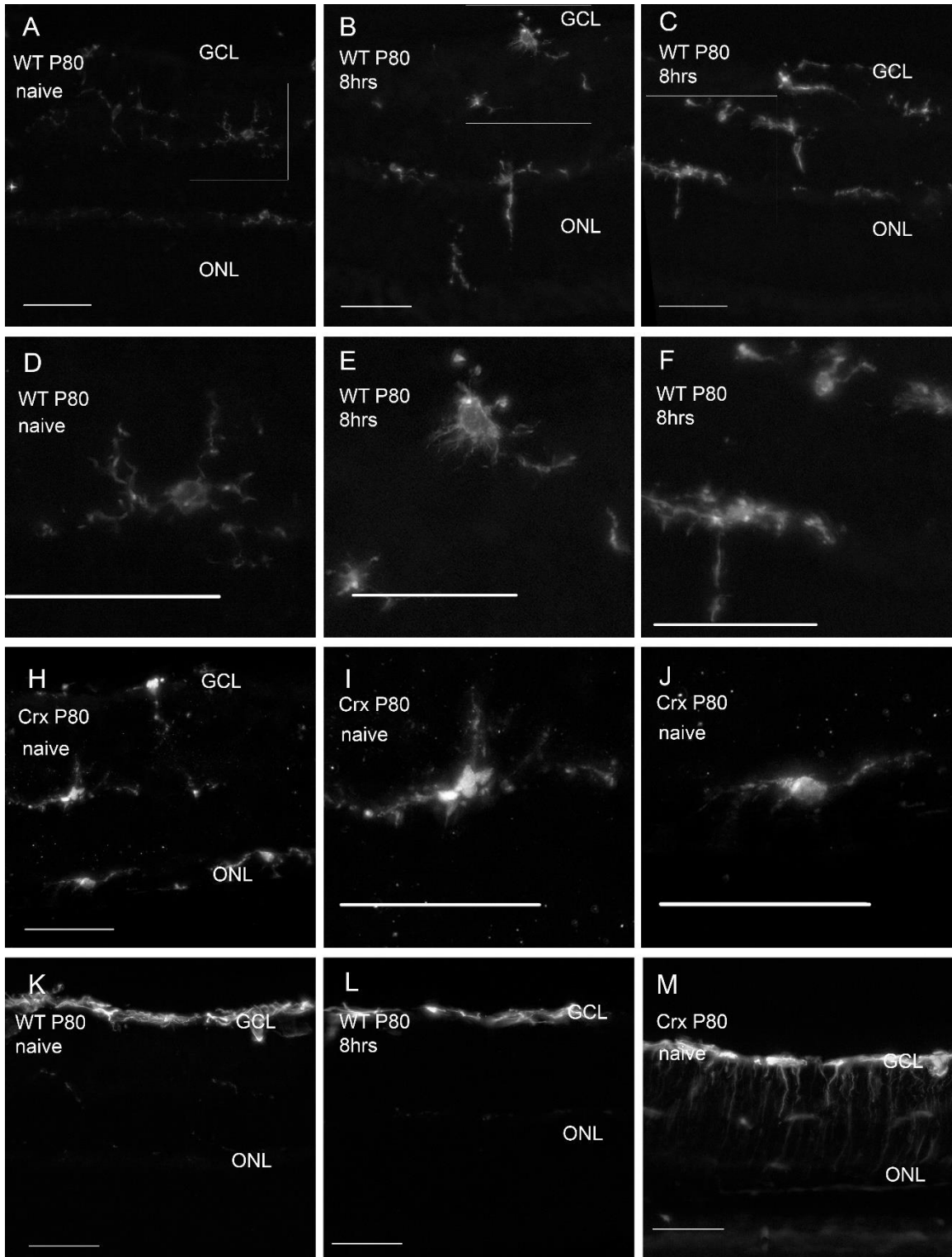


Figure 5-1 Fluorescent micrographs showing the changes in glial cells in the WT retina with/without incubation and in the Crx retina without incubation. Scale bar: 50µm.

A – F: P80 WT retinas without incubation (A, D) and with aCSF incubation for 8hrs (B, C, E, F); D: Iba1+ cell from inner WT retina without incubation; E: Iba1+ cell from inner WT retina with aCSF incubation for 8hrs; F: Iba1+ cell from outer WT retina with aCSF incubation for 8hrs; H – J: P80 Crx retina without incubation. I: Iba1+ cell from inner Crx retina; J:

*Iba1+* cells from outer Crx retina. K-M: changes of GFAP expression. K: expression of GFAP in WT retina without incubation; L: expression of GFAP in WT retina with aCSF incubation for 8hrs; M: GFAP expression in Crx retina without incubation.

### 3.1.2 The distribution of *iba1+* cells and quantification of GFAP expression in WT retina after aCSF incubation

To further evaluate the changes on *iba1+* cells and GFAP expression, the density of *iba1+* cells and GFAP+ filaments were quantified. The data on the density of *iba1+* cells suggested that, there were significantly more *iba1+* cells in inner layers in incubated retinas than in age-matched naïve retinas (Figure 5-2A. Two way ANOVA: The effect of treatment:  $p = 0.001$ ). Meanwhile, the data from GFAP filaments also showed a slight increase (Figure 5-2B. Two way ANOVA: The effect of treatment:  $p = 0.001$ ). These results suggest that the process of isolating the retina together with aCSF incubating can trigger a mild glial activation. However, as presented in Figure 5-2, the glial response caused by incubation was completely different in incubated Crx retinas.

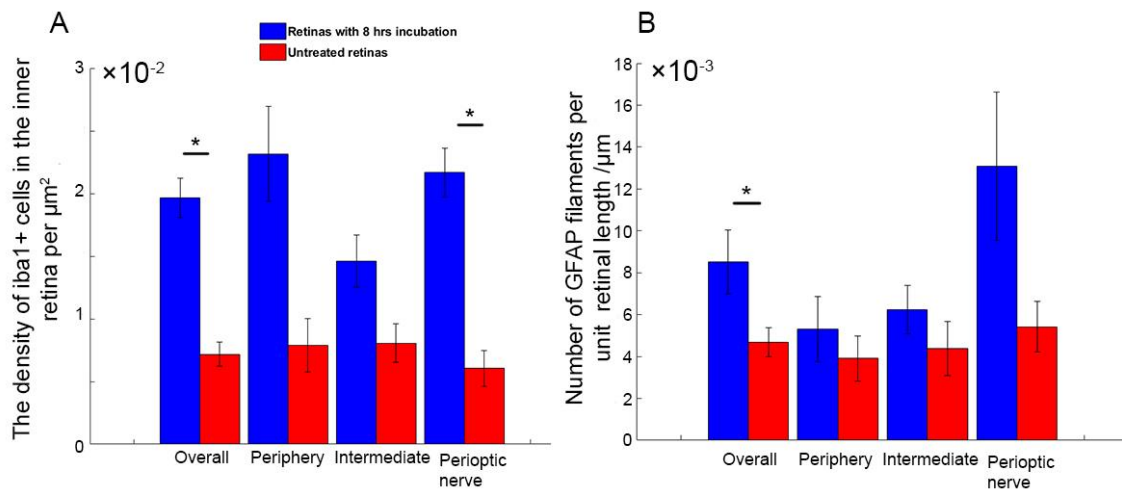


Figure 5-2 The changes of glial cells at different retinal eccentricities with and without incubation.

The figures show detailed information on glial changes after 8hrs aCSF incubation. A: Density of *iba1+* cells in the inner retina after treatment. B: Number of GFAP filaments after treatment. Data points: Mean; Error bar: SEM;  $n = 2$  at each time point. Data seen in Table 5-1.

Table 5-1 Changes of glial cells at different retinal eccentricities after treatment

	Location	n	aCSF incubation		Untreated	
			mean	SEM	mean	SEM
Density of iba1+ cells ( $\times 10^{-2}/\mu\text{m}^2$ )	Perioptic area	2	1.41	0.21	0.79	0.21
	Intermediate	2	1.02	0.12	0.81	0.15
	Periphery	2	1.40	0.12	0.60	0.14
Number of GFAP filaments( $\times 10^{-3}/\mu\text{m}$ )	Perioptic area	2	5.31	1.55	3.91	1.08
	Intermediate	2	6.24	1.15	4.39	1.29
	Periphery	2	13.10	3.53	5.43	1.22

### 3.2 The effect of Neurostatin on microglia in Crx retina

#### 3.2.1 The effect of Neurostatin on retinas in the pre-degenerating phase

To determine the effect of Neurostatin on microglial cells, the morphology and density of iba1+ cells were assessed following 8 hours incubation with Neurostatin. As demonstrated in Chapter 4, although more iba1+ cells were observed in the inner layers of Crx retinas at P10 (see Figure 4-7 in Chapter 4) than in age-matched WT retinas, there were no visible morphological changes in the iba1+ cells, and the microglial cells did not exhibit signs of infiltration in the ONL before P20.

After 8 hrs incubation with plain aCSF, iba1+ cells in the P10 Crx retina were still restricted to inner layers and did not infiltrate into the ONL (Figure 5-3B). These iba1+ cells displayed a typical ramified structure with a tiny soma and numerous processes (Figure 5-3D, E). However, comparing to the age matched naive retina, the density of iba1+ cells in the inner Crx retina were significantly decreased after incubation regardless of either Neurostatin or plain aCSF incubated retinas (Two way ANOVA, location vs treatment, effect of treatment,  $p = 0.000$ ). In the retinas incubated with Neurostatin, there were fewer but yet not significant iba1+ cells in the inner layers than in retinas incubated with plain aCSF (Post hoc: Neurostatin vs Control: Periphery:  $p = 0.864$ , Intermediate:  $p = 0.948$ , Perioptic area:  $p = 0.972$ , Dunn's test). There was, however, no distinct morphological change in the iba1+ cells in Neurostatin treated retinas.

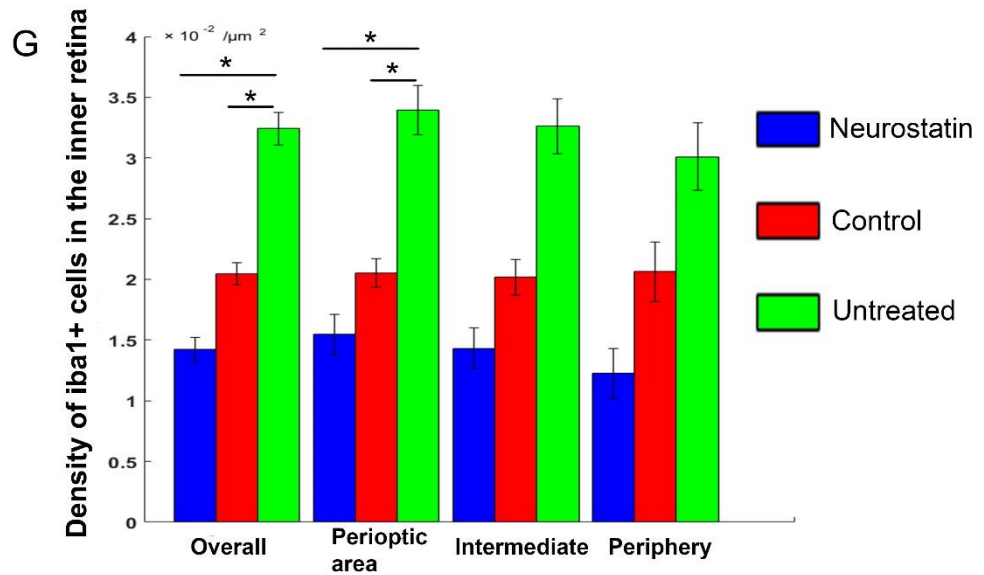
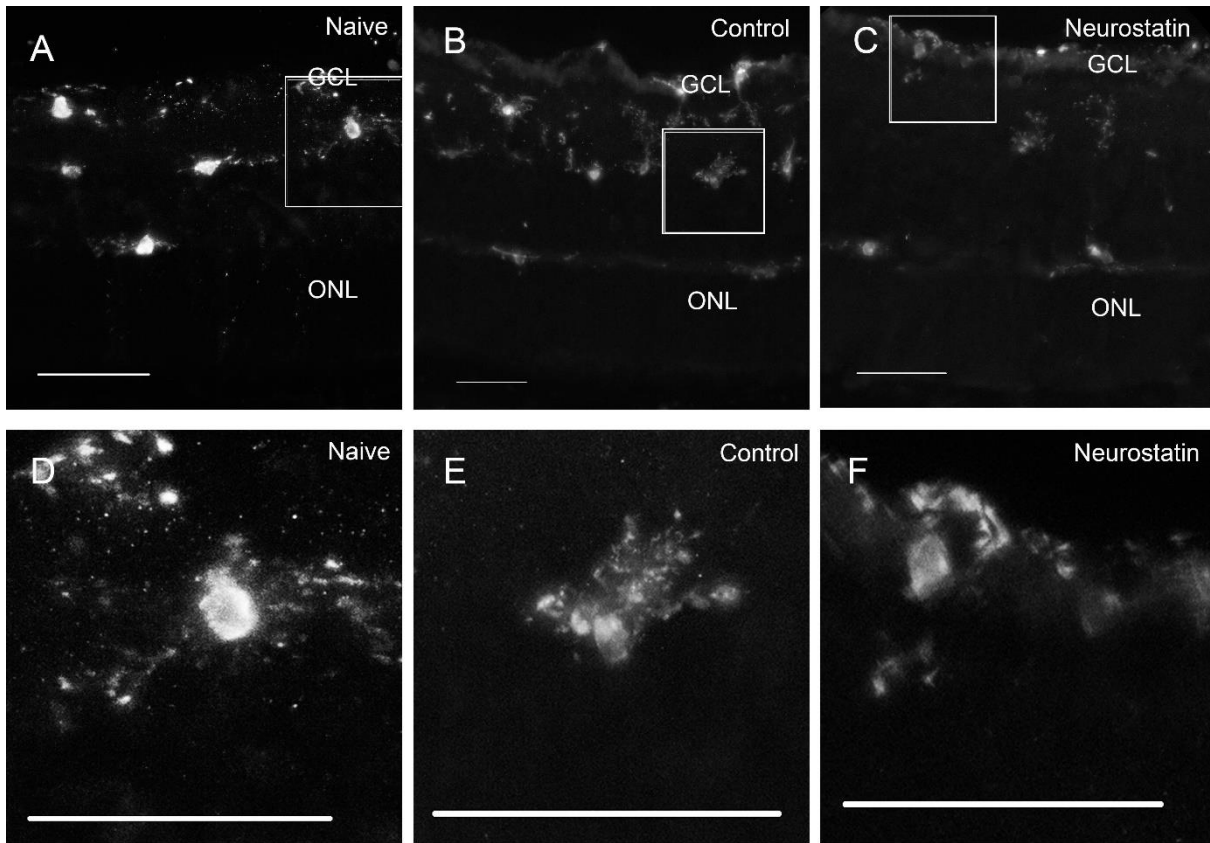


Figure 5-3 The effect of Neurostatin on iba1+ expression in P10 inner Crx retina

A – F: Fluorescent micrographs showing the expression of iba1+ in the P10 Crx retinas. Scale bar: 50 $\mu$ m. A: Naive; B: Control; C: Neurostatin. D: Selected area of A, white square; E: Selected area of B, white square; F: Selected area of C, white square; G: The density of iba1+ cells in the inner retina among different groups. Data points: Mean; Error bar: SEM; n = 3 at each time point. Data seen in Table 5-2

Table 5-2 The effect of Neurostatin on iba1+ density in P10 Crx retina

Location	n	Neurostatin		aCSF incubation		untreated	
		mean ( $\times 10^{-2}/\mu\text{m}^2$ )	SEM	mean ( $\times 10^{-2}/\mu\text{m}^2$ )	SEM	mean ( $\times 10^{-2}/\mu\text{m}^2$ )	SEM
Perioptic area	3	1.55	0.17	2.05	0.12	3.39	0.20
Intermediate	3	1.43	0.17	2.02	0.15	3.26	0.22
Periphery	3	1.23	0.21	2.06	0.25	3.01	0.28

Next, the effect of Neurostatin on GFAP expression was investigated. As seen in Figure 5-4 A-C, the expression of GFAP was low and there was no conspicuous changes in GFAP expression after treatment with Neurostatin. Surprisingly, further analysis on the number of GFAP filaments suggested that there was a slight increase yet not significant on the GFAP filaments after Neurostatin treatment (Two way ANOVA, location vs treatment, effect of treatment,  $p = 0.7996$ ).

Altogether, the results on iba1 and GFAP expression indicate that, in P10 Crx retina, incubation with Neurostatin may have a mild effect on reducing microglial cells in the inner retina, and it may trigger an upregulation on GFAP expression.

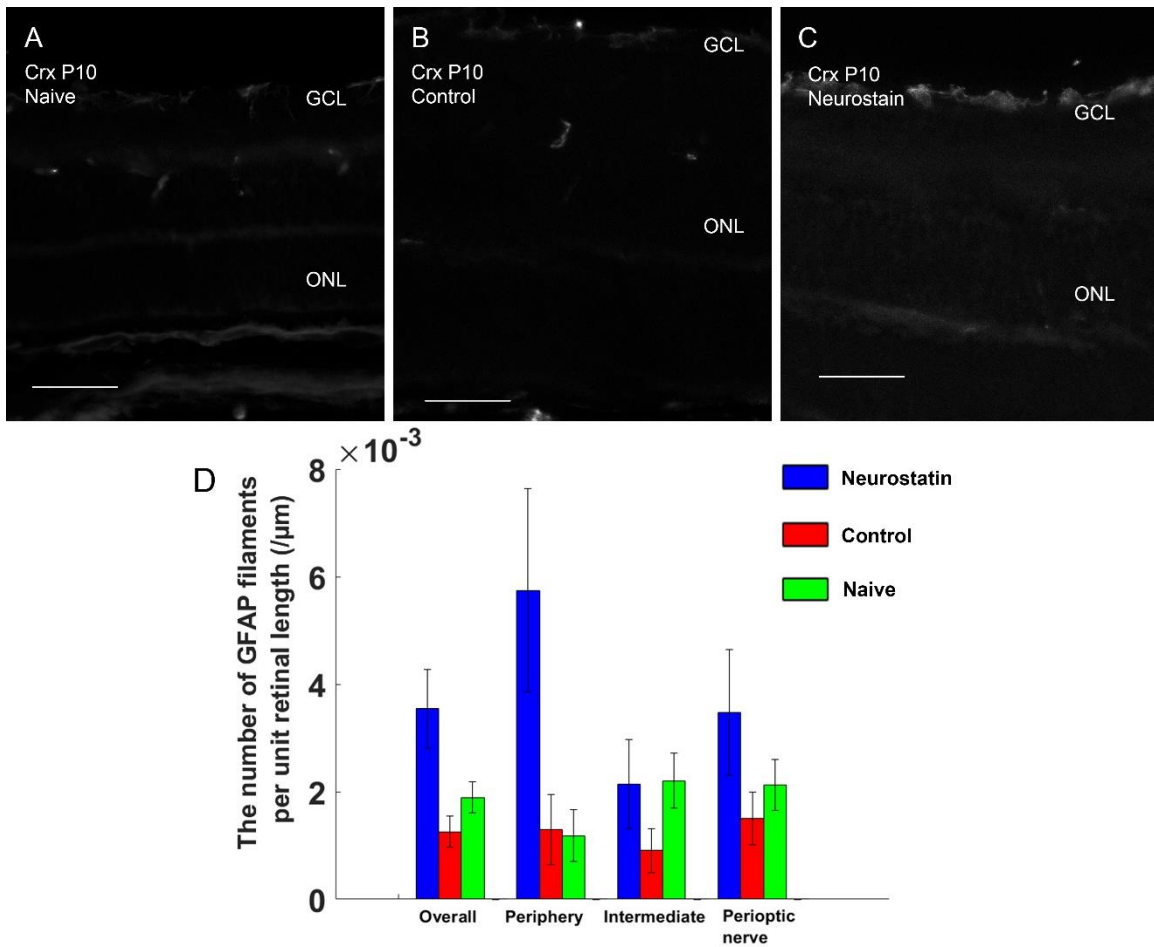


Figure 5-4 The effect of Neurostatin on GFAP expression in P10 inner Crx retina.

A – C: Fluorescent micrographs showing the expression of GFAP in the P10 Crx retinas. Scale bar:  $50\mu\text{m}$ . A: Naive; B: Control; C: Neurostatin. G. The number of GFAP filaments in different groups. Data points: Mean; Error bar: SEM;  $n = 3$  at each time point. Data seen in Table 5-3

Table 5-3 The effect of Neurostatin on GFAP filaments in P10 Crx retina

Location	n	Neurostatin		aCSF incubation		untreated	
		mean ( $\times 10^{-3}/\mu\text{m}$ )	SEM	mean ( $\times 10^{-3}/\mu\text{m}$ )	SEM	mean ( $\times 10^{-3}/\mu\text{m}$ )	SEM
Perioptic area	3	3.48	1.17	1.51	0.59	2.13	0.48
Intermediate	3	2.14	0.82	1.07	0.36	2.20	0.51
Periphery	3	5.75	1.89	1.31	0.44	1.18	0.48

### 3.2.2 The effect of Neurostatin on retinas in the microglial activating phase

The results presented in Chapter 4 have illustrated that microglial activation and gliosis reached its first peak at P40. Almost all the iba1+ cells turned into the amoeboid mode, with an enlarged

soma and short processes. Infiltration of iba1+ cells in the ONL was commonly seen during this stage. Extended GFAP+ filaments were detectable across the retinas. To investigate the effect of Neurostatin on microglial activation during this first wave of degeneration, P40 retinas were incubated following the same methodology as in previous sections.

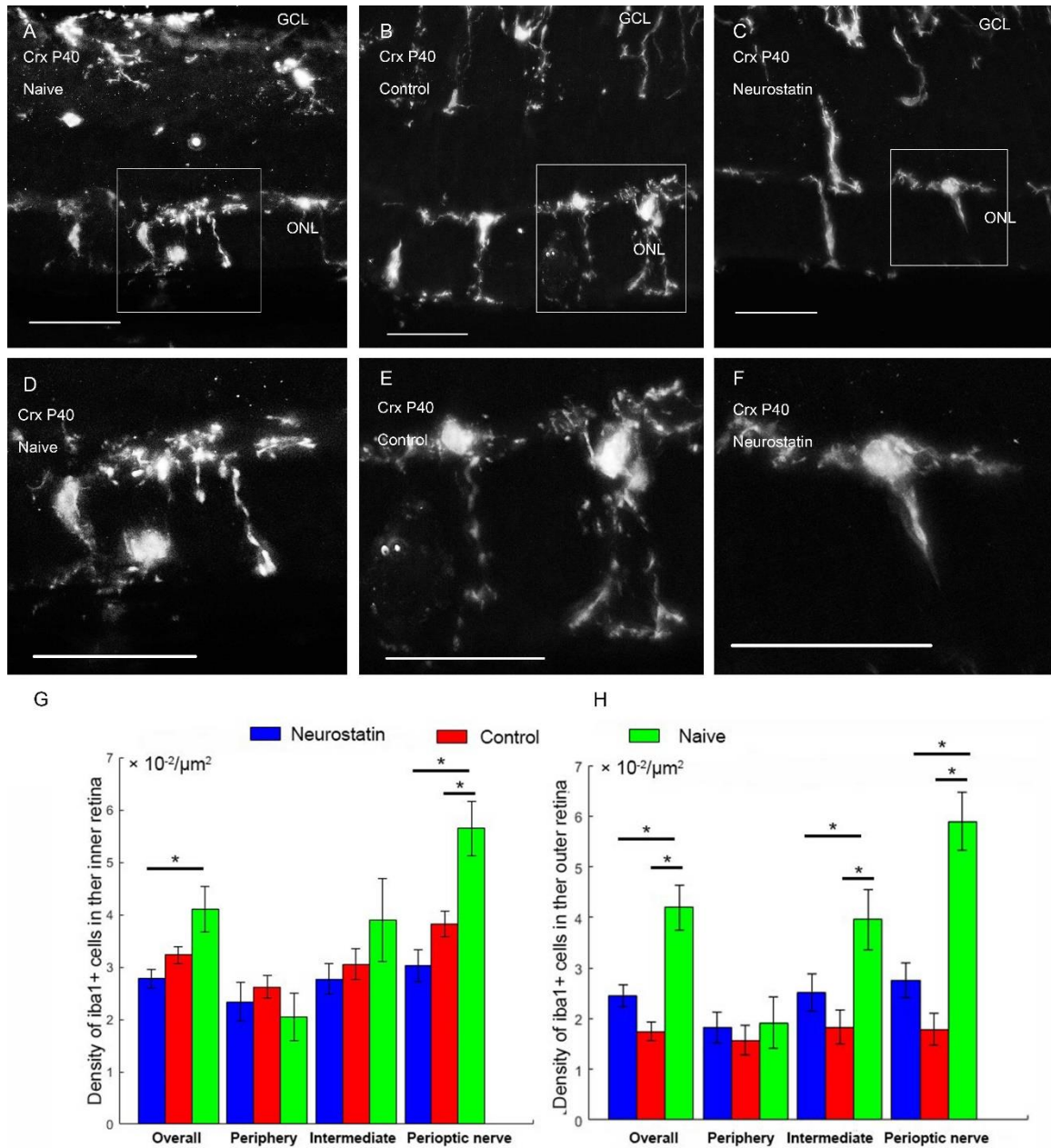


Figure 5-5 The effect of Neurostatin on iba1+ cells in P40 Crx retina

A – F: Fluorescent micrographs showing the expression of iba1+ in the P40 Crx retinas. Scale bar: 50 $\mu\text{m}$ . A: Naive; B: Control; C: Neurostatin. D: Selected area of A, white square; E: Selected area of B, white square; F: Selected area of C, white square; G: The density of iba1+ cells in the inner retina among different groups. H: The density of iba1+ cells in

the outer retina among different groups. Data points: Mean; Error bar: SEM; n = 3 at each time point. Data seen in Table 5-4

Table 5-4 The effect of Neurostatin on iba1+ cell density in P40 Crx retina

	Location	n	Neurostatin		aCSF incubation		Untreated	
			mean ( $\times 10^{-2}/\mu\text{m}^2$ )	SEM	mean ( $\times 10^{-2}/\mu\text{m}^2$ )	SEM	mean ( $\times 10^{-2}/\mu\text{m}^2$ )	SEM
Inner retina	Perioptic area	3	1.27	0.09	1.85	0.09	5.64	0.52
	Intermediate	3	1.30	0.10	1.70	0.12	3.90	0.79
	Periphery	3	1.21	0.15	1.73	0.13	2.05	0.45
Outer retina	Perioptic area	3	2.75	0.35	2.89	0.28	5.90	0.58
	Intermediate	3	2.51	0.37	2.85	0.31	3.96	0.60
	Periphery	3	1.82	0.31	2.39	0.26	1.92	0.50

In the incubated retinas either with or without Neurostatin, most of the iba1+ cells remained in the amoeboid form across the retina (Figure 5-5B, C), and infiltration of iba1+ cells into the ONL was widely seen in both groups (Figure 5-5E and F).

Similar to the findings in the P10 retina, comparing to the age matched naive retina, there was a significant decrease in the density of iba1+ cells in the inner layers in all incubated retinas, regardless of whether incubated with Neurostatin and in those incubated with plain aCSF, although the density was comparably lower in the Neurostatin treated samples (Two way ANOVA: Treatment vs Location, Effect of treatment,  $p = 0.000$ ).

There were also significantly fewer iba1+ cells in the ONL in both incubated groups compared to untreated retinas ( Two way ANOVA: Treatment vs Location, Effect of treatment,  $p = 0.001$ ). However, compared to retinas incubated with plain aCSF, Neurostatin did not decrease the density of iba1+ cells in the outer retina.

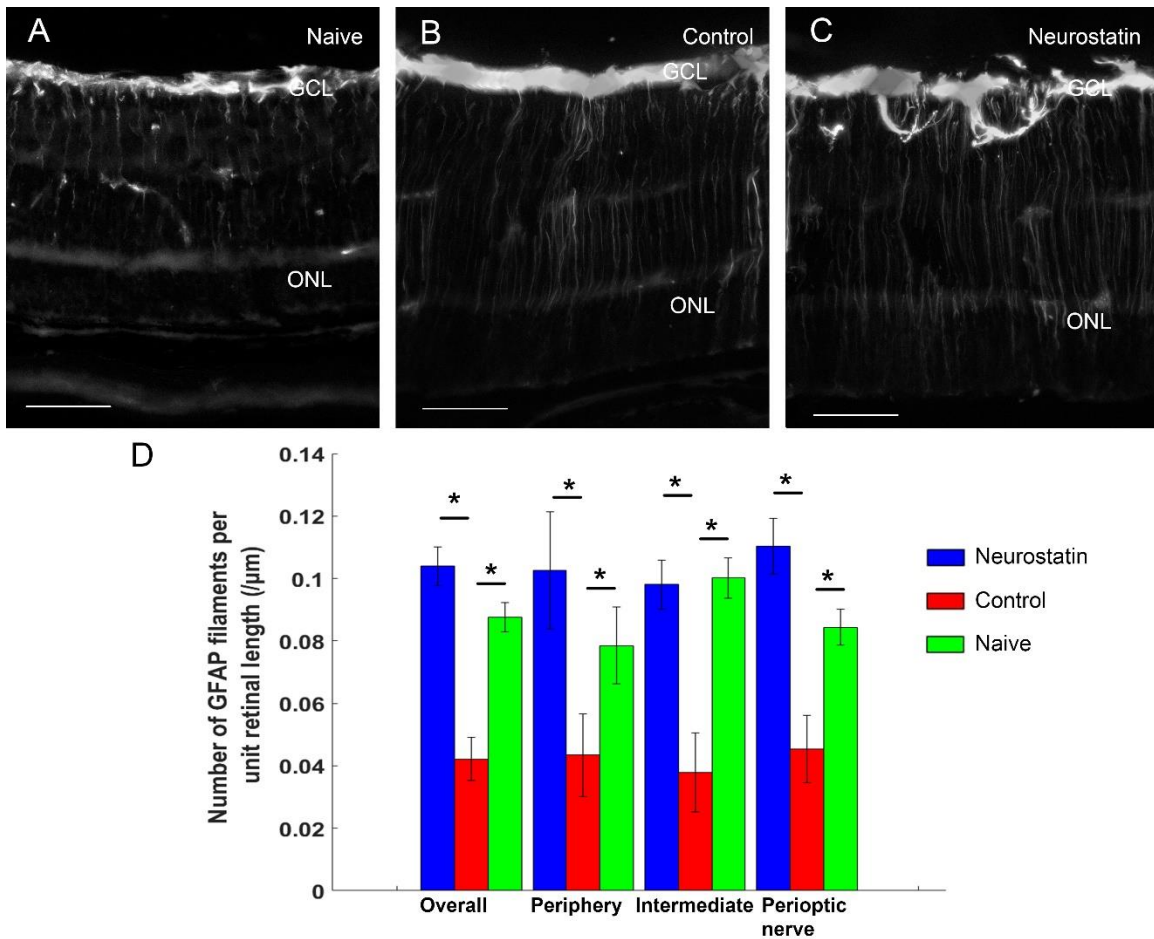


Figure 5-6 The effect of Neurostatin on GFAP in P40 Crx retina

A – C: Fluorescent micrographs showing the expression of GFAP in the P40 Crx retinas. Scale bar: 50µm. A: Naive; B: Control; C: Neurostatin. D: The number of GFAP filaments in P40 Crx retina. Data points: Mean; Error bar: SEM; n = 3 at each time point. Data seen in Table 5-5

Table 5-5 The number of GFAP filaments in P40 Crx retina

Location	n	Neurostatin		aCSF incubation		Untreated	
		mean ( $\times 10^{-2}/\mu\text{m}$ )	SEM	mean ( $\times 10^{-2}/\mu\text{m}$ )	SEM	mean ( $\times 10^{-2}/\mu\text{m}$ )	SEM
Perioptic area	3	11.03	0.89	4.54	1.08	8.44	0.58
Intermediate	3	9.81	0.78	3.78	1.27	10.01	0.65
Periphery	3	10.26	1.88	4.34	1.32	7.86	1.23

Next, the effect of Neurostatin on GFAP expression were investigated. The extension of GFAP filaments were detectable in all three groups (Figure 5-6). However, analysis on the number of

GFAP+ filaments revealed that, compared to the untreated retina, the number of GFAP filaments was significantly reduced after incubation in plain aCSF. However, the number of GFAP filaments was significantly increased after treatment with Neurostatin, indicating that incubation of Neurostatin may paradoxically upregulate GFAP expression in the isolated environment.

### 3.3 Summary

Table 5-6 demonstrates the differences in the glial response among different strains and treatments. In WT mice, the microglial response and the Müller response were consistent in both developing and adult retina following aCSF incubation. There was a mild increase in the Iba1+ cell density in the inner retina and the number of GFAP filaments, however, the incubation did not lead to the rise of Iba1+ cells in the outer retina.

In Crx mice, following aCSF incubation, a decrease of Iba1+ density in the inner retina and GFAP filament number were detected in both P10 and P40 retina, whilst there was a variation in the microglial response observed in the outer retina at different ages. The Iba1+ cell density was largely reduced in the outer retina of P40 after incubated in aCSF, the treatment did not trigger any changes in the outer retina of P10.

Comparing with aCSF treatment, there was no much difference in the microglial response in Crx retina following Neurostatin incubation, except for a slighter larger reduction in the Iba1+ density in the inner retina. However, as opposed to reduction of GFAP filament number after aCSF incubation, the number of GFAP filaments was increased after Neurostatin treatment in both P10 and P40 Crx retina.

*Table 5-6 Summary of the responses toward treatment.*

	WT P10	WT P80	Crx P10		Crx P40	
	aCSF	aCSF	aCSF	Neurostatin	aCSF	Neurostatin
Iba1 in IR	↑	↑	↓	↓↓	↓	↓↓
Iba1 in OR	→	→	→	→	↓↓	↓
GFAP	↑	↑	↓	↑	↓	↑

*IR: GCL to OPL; OR: outer retina; ↑: mild to moderate increase; ↓: mild to moderate decrease; →: no change; ↓↓: moderate to severe decrease. The changes were evaluated by comparing with the age-matched untreated retina.*

## 4. Discussion:

This study sought to test the effect of Neurostatin on glial cells in isolated Crx retina. The results showed that Neurostatin has a mild effect on reducing the density of iba1+ cells in the inner layers of isolated Crx retinas at both P10 and P40, but triggered a rise of GFAP expression at P40. In addition, the assessment on the response of microglial cells suggested that there was heterogeneity in microglial reactions in response to different insults.

### 4.1 The glial response in the isolated retina under aCSF incubation

It is known that microglial cells are highly sensitive to environmental changes and can provide immediate response and transform from a resting mode to a reactive mode in such conditions. Furthermore, microglial cells exhibit heterogeneous responses to different types of injuries (Gertig and Hanisch, 2014). Therefore, this current study first investigated whether the isolated retinal preparation together with aCSF incubation can trigger microglial activation and Müller gliosis.

A previous study on the isolated rat retina with aCSF incubation revealed that there was an increased release of lactate dehydrogenase (LDH) (an indicator of neural damage) over time during incubation with aCSF (Tokuda et al., 2004, Romano et al., 1995). Another study using organotypic cultures of retinal wholemounts revealed that there was sustained microglial activation during in these cultures. However, the activation did not cause cytokine release, nor did it lead to additional apoptosis other than axotomy-induced apoptosis in the INL following retinal isolation preparation (Bauer et al., 2016).

In this current study, the observed changes in iba1+ cells were in agreement with microglial activation observed in these earlier studies. Iba1+ cells displayed subtle morphological changes following incubation with a modest increase in cell density in the inner retina. Iba1+ cells were restricted to the inner retina and remained absent from the ONL. It should be noted that the increase in microglial density observed is probably due to cell proliferation of the innate microglial population, as there is no recruitment of BM-derived macrophage in the isolated retina. In addition, the morphology of iba1+ cells here was clearly distinct from iba1+ cells observed during the photoreceptor death phase of Crx retina. Furthermore, Bauer et al. (2016) demonstrated that the onset of microglial activation following incubation did not present until day 3, whilst the GFAP expression at day 0 was similar to the *in vivo* pattern. The results from

this study are in line with Bauer's findings. Despite a mild increase in the number of GFAP filaments, the expression of GFAP in incubated retina was indistinguishable from the untreated retinas.

Therefore, our results are in line with those previous studies; there is a mild microglial activation in the isolated retina during aCSF incubation which is quite distinct from the microglial activation during photoreceptor degeneration. The microglial activation in the inner retina here may be a combined effect of axotomy-induced Ganglion cell death and environment change caused by incubation. However, the activated microglial cells do not lead to further apoptosis and cytokine release, nor Müller gliosis.

#### 4.2 The glial response in the isolated Crx retina

Maintaining isolated retinas in aCSF over time induces mild glial activation. Furthermore, Bauer et al (2016) suggested that the combination of culturing isolated retinas and LPS stimulation (classic M1 stimulation) can trigger microglial activation, characterized by increased production of TNF- $\alpha$ , IL-2 and IL-6, while the total number of microglial cells remained at the same level as they were without LPS stimulation. The authors suggested that LPS exposure produces a model that is similar to the neurodegeneration process.

This current study investigated whether microglial activation in Crx retina is altered in the isolated retina under incubation. Our results show that, following 8 hours incubation in aCSF, the density of iba1+ cells in the inner layers of both P10 and P40 Crx retina decreased. Furthermore, there was also a sharp drop on the GFAP filaments in P40 Crx retina. As discussed in Chapter 4, an increase of microglial density was observed at P10 Crx retina, and microglial density reached its peak at P40 during the first activation wave. A study on microglial repopulation suggested that, the repopulation of microglial cells is mainly attributed to the proliferation of innate microglial cells (Huang et al., 2018). It is postulated that a continuous supply of stimulating factors may be necessary for glial activity during retinal degeneration. Incubation of isolated retinas in vitro for 8 hours may cause a decrease in the presence of these factors, resulting in fewer glial proliferation and explaining our findings.

#### 4.3 The effect of Neurostatin in isolated Crx retina

Neurostatin has been previously reported to reduce the classical microglial activation, the p38 and ERK1/2 activation, via blockade of IL-15 activity in cell culture (Gomez-Nicola et al., 2010). In

this present study, isolated Crx retinas were incubated with Neurostatin for 8 hrs to investigate the effect of Neurostatin on microglial activation.

In the P10 Crx retina, comparing to the control group, there was a significant reduction of iba1+ cell density in the inner retina after Neurostatin treatment. However, the effect was less pronounced at P40. Although the density of iba1+ cells was slightly lower in the inner retina after incubation with Neurostatin, in the outer retina, it was higher in the Neurostatin group. As discussed previously, microglial activation in the P10 Crx retina may be a response towards incubation, whereas at P40 Crx retina, microglial activation is associated with photoreceptor degeneration.

Furthermore, at P40, the most remarkable change in microglial cells in the inner retina was the proliferation of resident microglia. By contrast, the increase of microglial density in the outer retina was caused by the migration and infiltration of microglial cells from the inner retina into the outer retina. The recruitment of microglial cells into the outer retina is considered to be a result of changes in local cytokines and the alteration of the surface proteins on photoreceptors (Brown and Neher, 2012). The differences in the effect of Neurostatin on microglial activation between the inner and outer retina may indicate that Neurostatin interferes more with pathways involved in cell proliferation, than with cell migration.

However, the effect of Neurostatin on GFAP expression seems to be contradictory to the microglial response, as the gliosis would normally be expected to be positively correlated with the reduction of microglial activity via JAK-STAT signaling (Kim et al., 2002). One of the possible explanation is that, the iba1+ cell density could not accurately reflect the activity of specific microglial subsets being involved. Furthermore, it has been suggested that Neurostatin could directly regulate GFAP expression in the CNS via the ERK1/2 MAPK pathway, however, the response of GFAP may vary among different location of the brain. For instance, treatment with Neurostatin (GM1 subtype) is able to cause a significant attenuation of GFAP increment in hippocampus, but shows no effect in the spetum (Oderfeld-Nowak et al., 1993). A limitation of the present study is that downstream effects, such as changes in cytokine levels, and the communication between microglia and Müller cells were not assessed. Hence, the exact pathways that were affected and the communication between glial cells were unknown . Further investigation into the effect of Neurostatin on microglial activation will require investigating a large number of possible downstream pathways.

## 5. Conclusion

The results presented in this chapter showed that Neurostatin has a mild effect on reducing the density of iba1+ cells in the inner Crx retina both at P10 and at P40. Moreover, it may alter microglial activation status although the evidence for this is less clear. The data suggests, however, that the experimental conditions may have affected the results. Moreover, it is clear that *ex vivo* retinal preparations cannot provide information on the interaction between microglial activation and photoreceptor survival for a long period. The next set of studies therefore sought to investigate whether Neurostatin could provide a long term protective effect on photoreceptors in the Crx retina at different stages of degeneration.



**Chapter 6. The Effect of Neurostatin on Microglial  
Activation and Photoreceptor Survival in Crx  
Retina**



## 1. Introduction

Chapter 5 has shown that Neurostatin has a mild effect on reducing inner retinal microglial cell proliferation and increasing GFAP expression in an *in vitro* preparation of the Crx retina. However, Chapter 5 also shows that glial activation patterns are different *in vitro* and *in vivo*. One possibility is that microglia activation *in vitro* may result from a combination of the effects of RGC axotomy and inherent photoreceptor degeneration. An additional issue is that the supply of BM-derived microglial cells is impaired in isolated retinal preparations. Hence, *in vitro* approaches cannot provide reliable information on how manipulating glial activity can protect photoreceptors in the long-term.

As described in Chapter 1, the states of microglial activation can be divided into two categories: M1 microglia, responsible for the neurotoxic response; M2 microglia, responsible for the neuroprotective response. Although these two states temporally overlap, microglial activation is considered to be cytotoxic in the long term.

Earlier chapters in this thesis have shown that in the Crx retina, there are two waves of glial activation during photoreceptor degeneration, and these events are intimately related. Although the exact mechanism underlying this relationship is unknown, such temporal correlation between these two events raised the question whether it is indeed microglial and Müller activation that accelerates ensuing photoreceptor death, or whether it is the other way around, with glial activity resulting from fast photoreceptor degeneration.

We hypothesized that dying photoreceptors during the fast degenerating waves may amplify inflammatory activity, and glial hyperactivity may in turn further accelerate photoreceptor degeneration. Therefore, manipulating glial activation may help to slow down the photoreceptor degenerating process.

In this light, the aim of the study presented in this chapter was to investigate the long-term effects of microglial activation on photoreceptor loss at different degeneration stages, and to determine whether inhibiting microglial activity could improve photoreceptor survival.

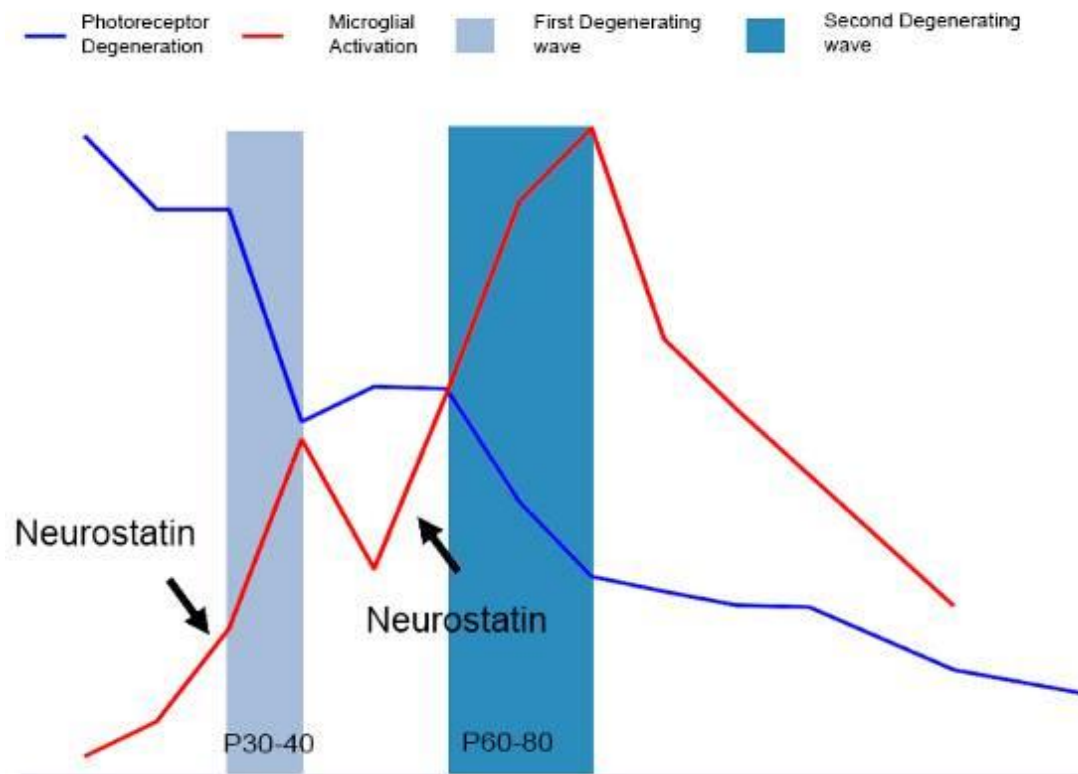


Figure 6-1 Schematic diagram of the events during photoreceptor degeneration in the Crx retina  
 Black arrows show the time points when Neurostatin was administered.

## 2. Specific Methods:

### 2.1 Animals and surgical procedures

Neurostatin was applied via intravitreal injection at the beginning of the first activation wave and P55 the beginning of the second activation wave (Figure 6-1). The time points of Neurostatin administration were chosen according to the time course of microglial activation in Crx retina (see previous chapters). The effect of Neurostatin was assessed from 7 days to two months post-injection.

A P25 and a P55 cohort of Crx mice were used, respectively corresponding to the beginning of the first and second activation waves. For each animal, the left eye was used for intraocular injection, while the right eye was not injected.

Due to their invasive nature, even intravitreal injections with plain phosphate-buffered saline (PBS) can cause a reactive change in both Müller and microglial cells within 24 hrs, but then the

effect becomes less pronounced after 7 days (Seitz and Tamm, 2014). To exclude this potentially confounding effect, the earliest tissue collection was determined to be at 7 days post-injection (DPI).

For the P25 cohort, retinas were collected at 7 days (n = 2 for each group), 15 days (n = 5), 30 days (n=5) and 60 days (n = 4) post-injection (P25-7DPI, P25-15DPI, P25-30DPI, P25-60DPI, DPI: Days post-injection), while for the P55 cohort, retinas were collected at 15 days (n = 4) and 30 days (n = 4) post-injection (P55-15DPI, P55-30DPI).

The procedures for tissue fixation, immunohistochemistry, microscopy and data analysis are described in Chapter 2 and Chapter 4.

## 2.2 Intravitreal injection and drug preparation

Once under general anaesthesia (10% Domitor and 7.5% Ketamine, 100ul/10g body weight. Intraperitoneal injection), the left eye was treated with topical anaesthetic (oxybuprocain, Bausch & Lomb, UK) and mydriatic eye drops (cyclopentolate hydrochloride, Bausch & Lomb, UK). 2% carbomer eye gel (Bausch & Lomb, UK) was then generously applied on both eyes. A 20 second interval was allowed between each drug.

Prior to the injection, a cover slip was placed on the cornea of the left eye to view the fundus using direct microscopy. An incision was made in the ventral scleral limbus, using a 30-gauge needle. A 34-gauge Hamilton syringe (Hamilton CO. USA) was gently inserted through the incision into the vitreous cavity (Figure 6-2A). 1  $\mu$ l of drug/placebo was injected while the fundus was monitored (Figure 6-2B). Eyes with signs of complications, such as haemorrhage, retinal detachment, or injuries to the lens or iris, were excluded.

Trypan blue, which is widely used as a dye in intraocular surgeries, was added to visualise the solution injected in order to facilitate the injection procedure. In an ocular toxicity study of trypan blue in rabbit, it has been shown that intravitreal injection of a 0.2% trypan blue solution can lead to rhodopsin loss in the ventral retina, even though there was no functional change in ERG test. By contrast, no sign of retinal toxicity could be detected when using only 0.06% trypan blue in the solution (Veckeneer et al., 2001), suggesting that it is safe at this low concentration. In this study, we managed to visualise the injected solution at the much lower concentration of 0.001%, and this is what we used for all our experiments.

5 mM Neurostatin solution (dissolved in distilled water with 0.001% trypan blue) was freshly prepared on the day of injection. The distilled water with 0.001% trypan blue was injected into animals in the control groups, as a vehicle control (placebo).

Previous studies have suggested that, phosphate buffered saline (PBS) is not toxic to mouse retina and is considered to be the ideal agent for intraocular injection (Hombrebueno et al., 2014). However, due to the chemical nature of Neurostatin, which can only reach the desired concentration in distilled water, hence distilled water was used as the agent in this study.

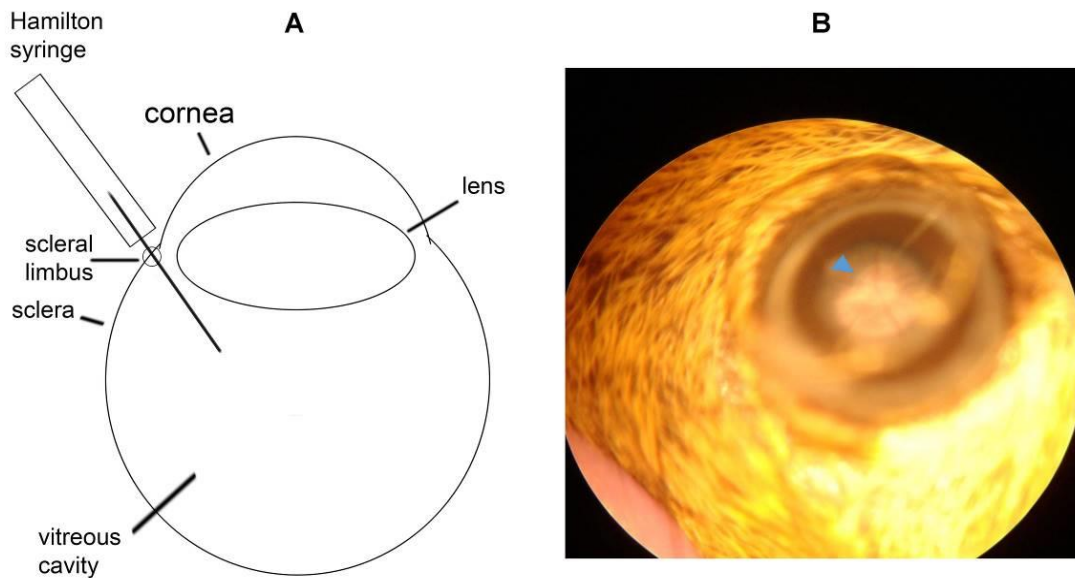


Figure 6-2 Schematic graph of intravitreal injection and fundus image of mouse eye.

A: The Hamilton syringe was inserted into the vitreous cavity through an incision made in the scleral limbus. B: mouse fundus. Blue arrowhead: optic nerve.

### 3. Results

#### 3.1 The effect of Neurostatin on the first activation wave.

Chapter 4 has shown that *iba1*<sup>+</sup> cells exhibit a typical “activated” morphology, with enlarged soma and shorter processes. These changes become conspicuous from P30 and the infiltration of *iba1*<sup>+</sup> cells into the ONL is detectable as early as P20, while the onset of photoreceptor loss is not detectable before P30. The Müller cells activation manifested itself as the extension of GFAP filaments towards the outer retina. The changes occurred from P40 and fluctuated throughout the degenerating process. In the later stage, stellate patterns of GFAP filaments were also observed to form into the focal photoreceptor defects.

To investigate the effect of Neurostatin on glial activity and photoreceptor survival in the Crx retina, Neurostatin was applied via intravitreal injection at P25, which corresponds to the beginning of the first activation wave. Retinas were collected at 7DPI, 15DPI, DPI 30 and 60DPI to investigate the short-term and long-term effects of Neurostatin.

### 3.1.1 The effect of Neurostatin on glial activity following intravitreal injection.

The morphology and incidence of iba1+ cells was investigated at P25-7DPI, P25-15DPI, P25-30DPI and P25-60DPI. Iba1+ cells in the inner retina exhibited enlarged somata in both Neurostatin and control groups at P25-7DPI and P25-15DPI (Figure 6-3 A, D, G and J, arrows). The infiltration of iba1+ cells into the ONL was observed in both groups at P25-7DPI (Figure 6-3A and D, arrow heads). In addition, more iba1+ cells were present in both groups at P25-15DPI (Figure 6-3 G and J, arrowheads). These morphological changes are similar to those observed in age-matched untreated Crx retinas, suggesting that they reflect the age-related microglial proliferation.

At P25-30DPI, amoeboid-shaped iba1+ cells were observed in both groups (Figure 6-4 A and D, arrows). Infiltration of iba1+ cells into the ONL was still detectable in both groups as well, although there were slightly fewer iba1+ cells in the ONL of the Neurostatin group (Figure 6-4A and D, arrowheads). At P25-60DPI, significantly fewer iba1+ cells could be detected in the inner retina in both groups (Figure 6-4 G and J), which may be a result of ageing rather than treatment.

The investigation on GFAP expression showed that, there was a variation on the GFAP expression at different time point after treatment. At P25-7DPI, an obvious rise in GFAP+ filaments was observed in both groups (Figure 6-3B and E), followed by a decrease at P25-15DPI (Figure 6-3 H and K). The changes between these periods showed no difference between Neurostatin and control. Nevertheless, the occurrence of GFAP+ upregulation found here was much earlier than what has been found in the Crx retina in Chapter 4, whilst the downregulation of GFAP later on presented at the first peak of glial activation wave, indicating that this might be an effect of the injection itself.

However, a month following injection, an effect of Neurostatin was detected. Comparing to the control groups, an clear increase was seen in GFAP+ filaments in retinas treated with

Neurostatin at both P25-30DPI (Figure 6-4B and E) and P25-60DPI (Figure 6-4 H and L), suggesting that Neurostatin may also have a long term effect on increasing Müller activity.

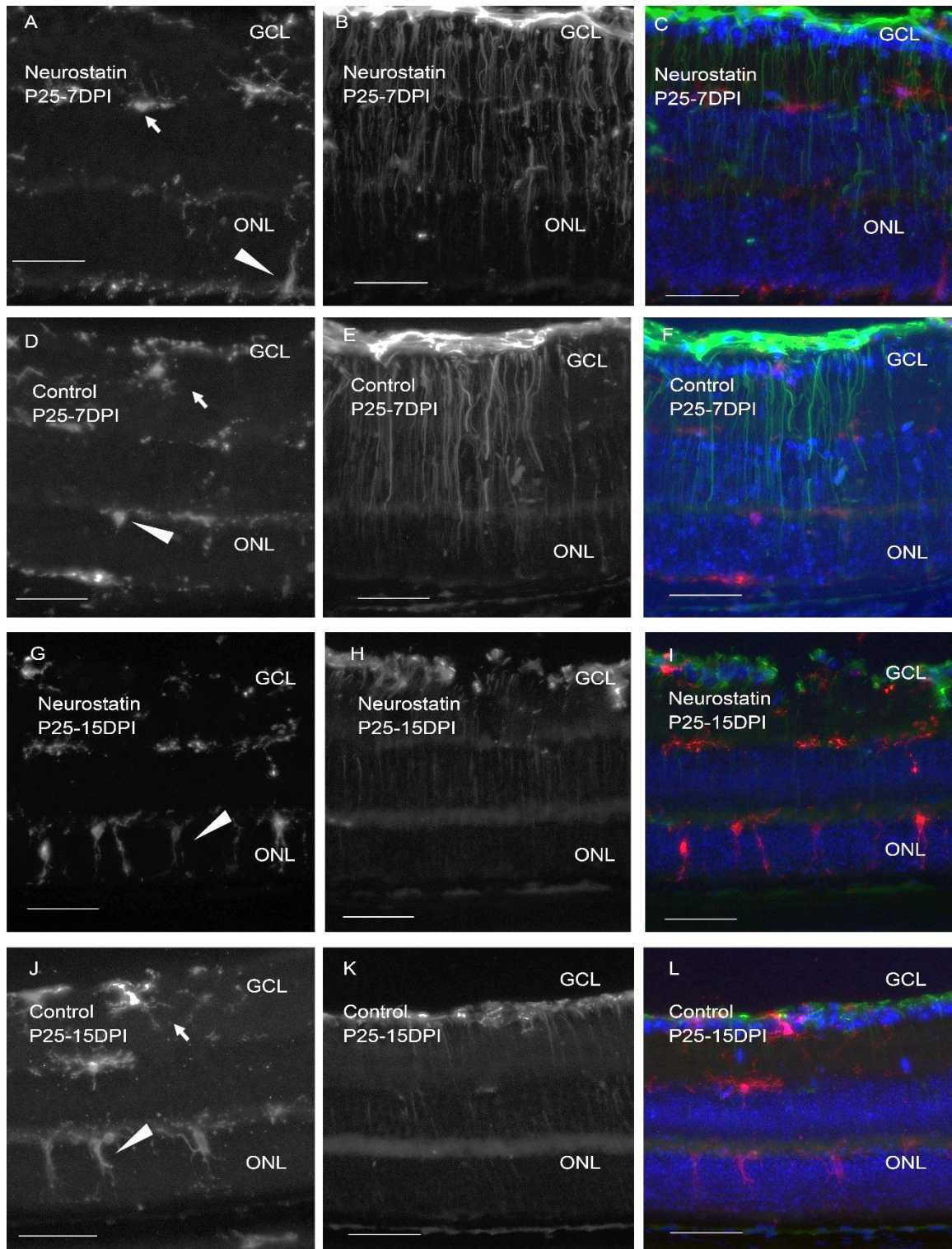


Figure 6-3 Fluorescent micrographs of glial cells following Neurostatin treatment in early stages

Representative images showing the response of glial cells at different time point following Neurostatin treatment. A, D, G, J: Iba1; B,E,H,K: GFAP; C, F, I, L: Red: Iba1, Blue: DAPI. Green: GFAP. Images were taken from central area of the retina. Scale bar: 50µm

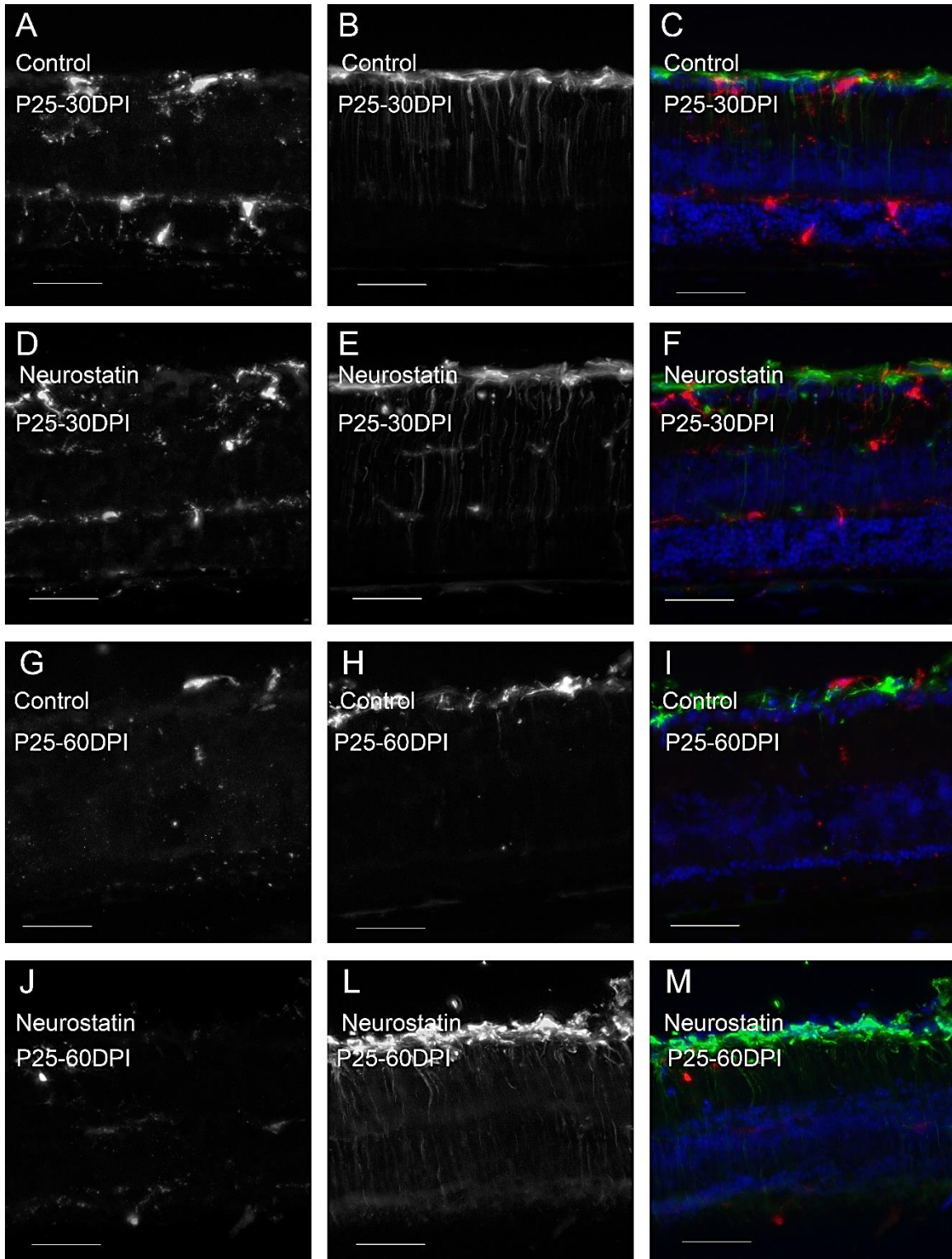


Figure 6-4 Fluorescent micrographs of glial cells following Neurostatin treatment in later stages

Representative images showing the response of glial cells at different time point following Neurostatin treatment. A, D, G, J: Iba1; B,E,H,K: GFAP; C, F, I, L: Red: iba1, Blue: DAPI. Green: GFAP. Images were taken from central area of the retina. Scale bar: 50µm

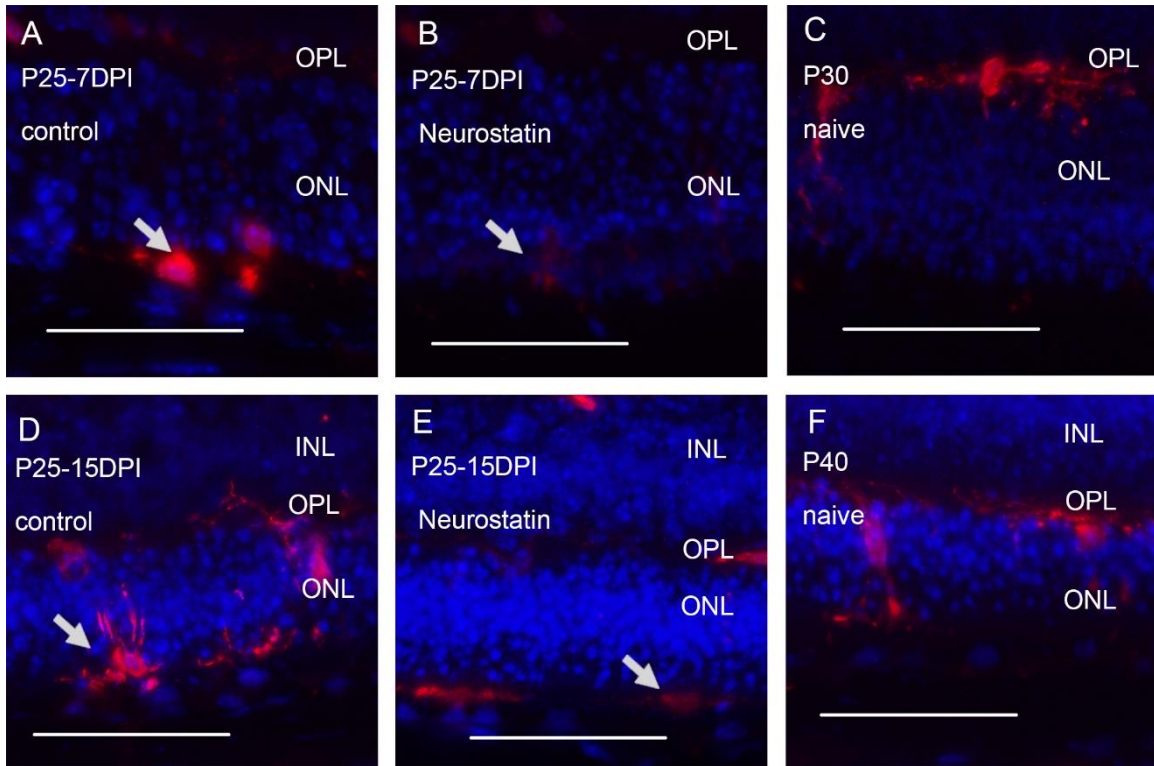


Figure 6-5 Fluorescent micrographs of Iba1+ cells in the outer most of ONL following intravitreal injection.

Representative images showing the expression of Iba1 in the outer most of ONL within the first two weeks following intravitreal injection. Red: Iba1; Blue: DAPI; Images were taken from central area of the retina. Scale bar: 50µm

In addition, an accumulation of Iba1+ cell in the outermost part of ONL was seen in both groups at P25-7DPI and P25-15DPI (Figure 6-5 A-B and D-E arrows), which was not commonly seen in age-matched untreated retinas (Figure 6-5 C and F). These cells disappeared after a month post-injection, suggesting that their appearance may have been related to the intravitreal injection procedure.

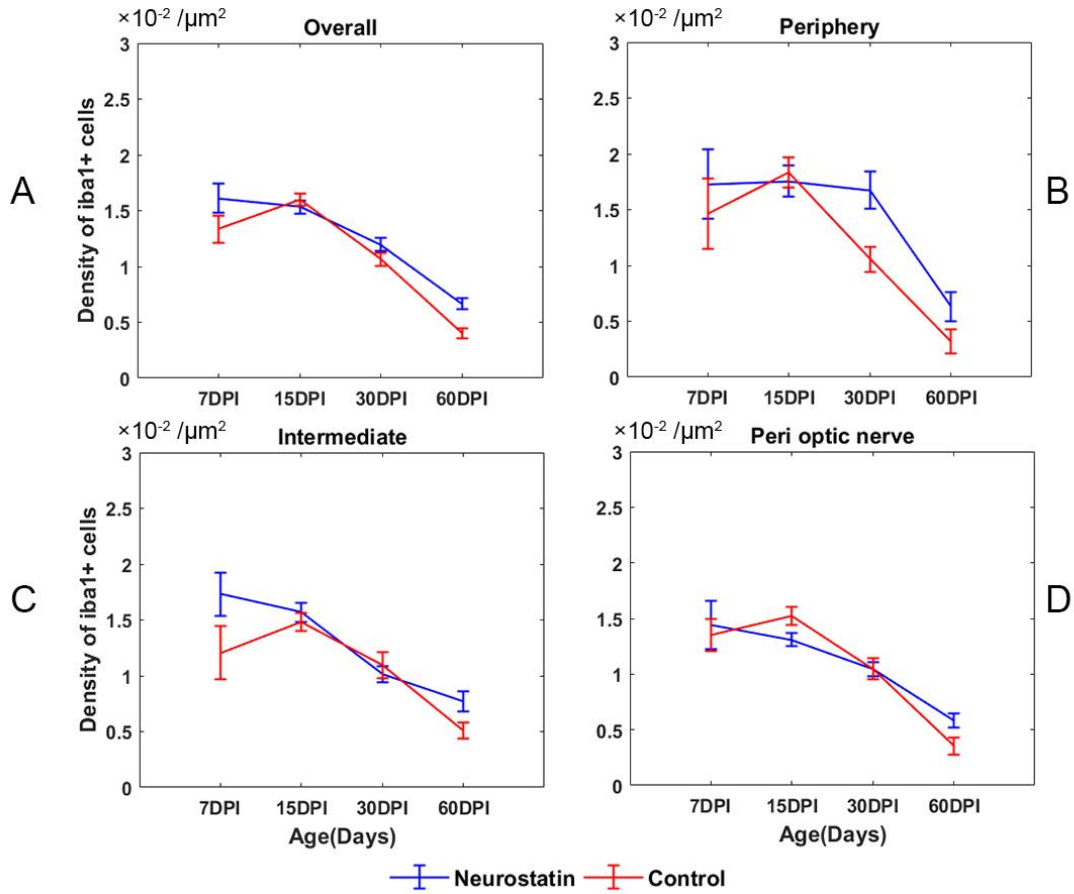


Figure 6-6 Changes of Iba1+ cell density in the inner retina over time following treatment with Neurostatin.

The figures show detailed information on microglial changes in the inner retina following treatment with Neurostatin. A: The overall density; B: The density in the peripheral retina; C: The density in intermediate retina; D: The density in the peri optic nerve. Data points: Mean; Error bar: SEM; 7DPI (n = 2), P25-15DPI (n = 5), P25-30DPI (n = 5), P25-60DPI (n = 4). Data seen in Table 6-1.

Table 6-1 Changes of iba1+ cell density in the inner retina over time following treatment with Neurostatin

Treatment	DPI	N	Perioptic nerve		Intermediate		Periphery	
			mean ( $\times 10^{-2}/\mu\text{m}^2$ )	SEM	mean ( $\times 10^{-2}/\mu\text{m}^2$ )	SEM	mean ( $\times 10^{-2}/\mu\text{m}^2$ )	SEM
Neurostatin	P25-7DPI	2	1.441	0.220	1.734	0.220	1.729	0.313
	P25-15DPI	5	1.309	0.058	1.569	0.058	1.756	0.141
	P25-30DPI	5	1.042	0.066	1.012	0.066	1.675	0.167
	P25-60DPI	4	0.580	0.064	0.770	0.064	0.632	0.128
Control	P25-7DPI	2	1.350	0.146	1.207	0.146	1.465	0.318
	P25-15DPI	5	1.519	0.082	1.480	0.082	1.832	0.133
	P25-30DPI	5	1.045	0.094	1.093	0.094	1.054	0.111
	P25-60DPI	4	0.354	0.075	0.508	0.075	0.324	0.108

In order to quantify the changes in iba1+ cell density following Neurostatin treatment, the density of iba1+ cells in the inner retina and outer retina was assessed at different DPI. Figure 6-6 illustrates changes in iba1+ cell density in the inner retina. In contrast with the data from ex vivo experiment in Chapter 5, the results showed that there was a significant increase of iba1+ cell density in the inner retina after treatment with Neurostatin (Two way ANOVA: Treatment vs DPI: Effect of treatment:  $p = 0.018$ ). By contrast, data on the outer retina showed that the overall effect of Neurostatin on the iba1+ cells was not significant (Figure 6-7. Two way ANOVA: Treatment vs DPI: Effect of treatment:  $p = 0.786$ ).

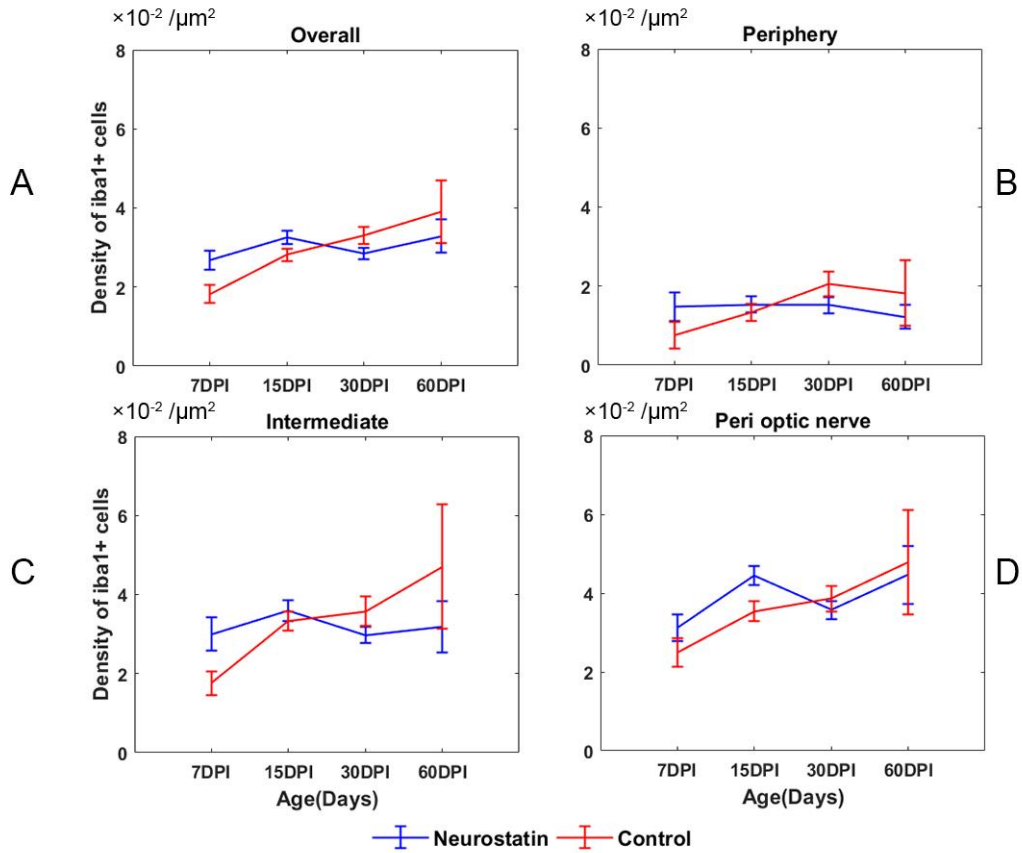


Figure 6-7 Changes of iba1+ cell density in the outer retina over time following treatment with Neurostatin.

The figures show detailed information on microglial changes in the outer retina following treatment with Neurostatin. A: The overall density; B: The density in the peripheral retina; C: The density in intermediate retina; D: The density in the perioptic nerve. Data points: Mean; Error bar: SEM; 7DPI (n = 2), P25-15DPI (n = 5), P25-30DPI (n = 5), P25-60DPI (n = 4). Data seen in Table 6-2.

Table 6-2 Changes of iba1+ cell density in the outer retina over time following treatment with Neurostatin.

Treatment	DPI	N	Perioptic nerve		Intermediate		Periphery	
			mean ( $\times 10^{-2}/\mu\text{m}^2$ )	SEM	mean ( $\times 10^{-2}/\mu\text{m}^2$ )	SEM	mean ( $\times 10^{-2}/\mu\text{m}^2$ )	SEM
Neurostatin	P25-7DPI	2	3.110	0.337	3.003	0.412	1.484	0.366
	P25-15DPI	5	4.438	0.243	3.582	0.264	1.536	0.197
	P25-30DPI	5	3.569	0.223	2.978	0.211	1.515	0.206
	P25-60DPI	4	4.458	0.742	3.178	0.653	1.222	0.308
Control	P25-7DPI	2	2.495	0.361	1.759	0.299	0.753	0.335
	P25-15DPI	5	3.537	0.259	3.326	0.237	1.340	0.212
	P25-30DPI	5	3.859	0.326	3.570	0.372	2.059	0.313
	P25-60DPI	4	4.782	1.317	4.707	1.584	1.821	0.825

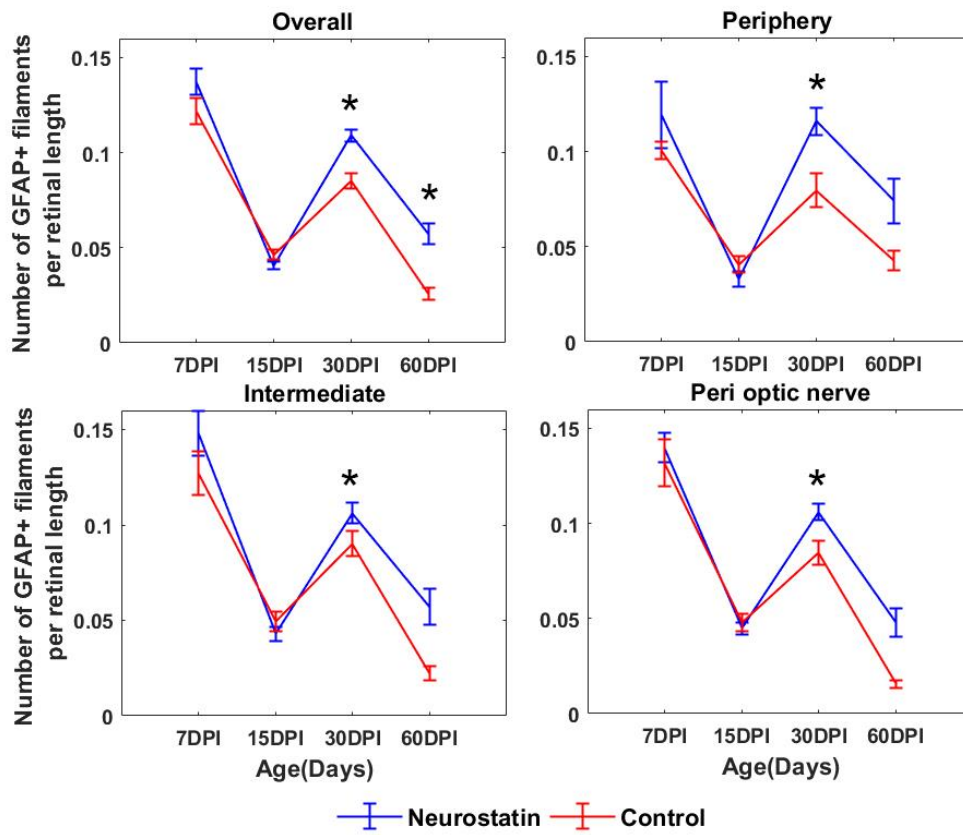


Figure 6-8 Changes of the number of GFAP+ filaments following treatment with Neurostatin.

The figures show detailed information on the changes of Müller cells following treatment with Neurostatin. A: The overall number of GFAP+ filaments; B: The number of GFAP filaments in the peripheral retina; C: The number of GFAP+ filaments in intermediate retina; D: The number of GFAP+ filaments in the peri optic nerve. Data points: Mean; Error bar: SEM; 7DPI (n = 2), P25-15DPI (n = 5), P25-30DPI (n = 5), P25-60DPI (n = 4). Data seen in Table 6-3

Table 6-3 Changes of the number of GFAP+ filaments following treatment with Neurostatin.

Treatment	DPI	N	Perioptic nerve		Intermediate		Periphery	
			mean ( $\times 10^{-2}/\mu\text{m}^2$ )	SEM	mean ( $\times 10^{-2}/\mu\text{m}^2$ )	SEM	mean ( $\times 10^{-2}/\mu\text{m}^2$ )	SEM
Neurostatin	P25-7DPI	2	0.119	0.008	0.119	0.012	0.119	0.018
	P25-15DPI	5	0.033	0.003	0.033	0.004	0.033	0.004
	P25-30DPI	5	0.116	0.004	0.116	0.006	0.116	0.007
	P25-60DPI	4	0.074	0.007	0.074	0.009	0.074	0.012
Control	P25-7DPI	2	0.132	0.012	0.127	0.011	0.101	0.005
	P25-15DPI	5	0.048	0.005	0.050	0.005	0.041	0.004
	P25-30DPI	5	0.085	0.006	0.090	0.007	0.080	0.009
	P25-60DPI	4	0.016	0.002	0.022	0.004	0.043	0.005

Next, the number of GFAP+ filaments was analysed. The number of GFAP+ filaments fluctuated during the recorded period. At 7DPI and 15DPI, the changes on the number of GFAP+ filaments were concurrent between Neurostatin and control groups. However, a significant increase of overall GFAP+ filament number was seen at both 30DPI and 60DPI (Figure 6-8, Two way ANOVA: Treatment vs DPI: Effect of treatment:  $p = 0.000$ ). The results indicated that intravitreal injection with Neurostatin may have a delayed effect on upregulation of GFAP expression.

### 3.1.2 The effect of intravitreal Neurostatin injection on ONL thickness.

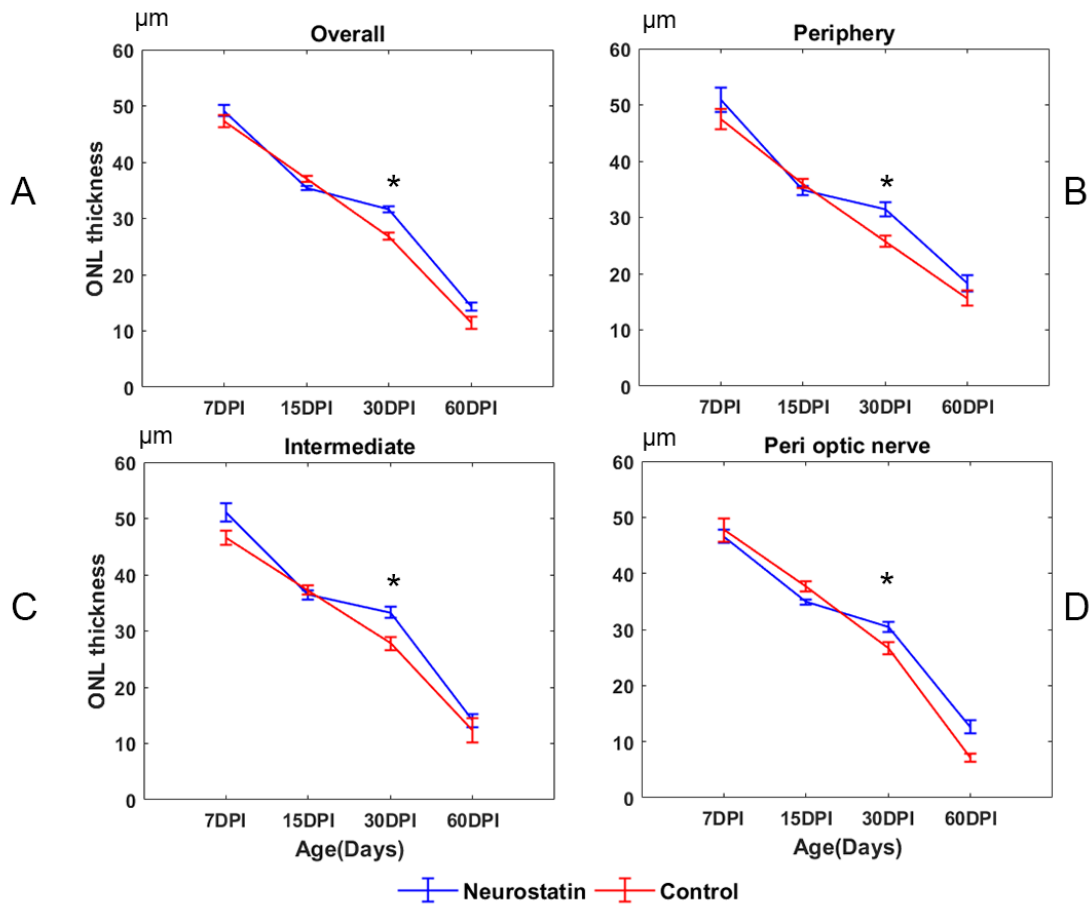


Figure 6-9 Changes in ONL thickness over time following treatment with Neurostatin.

The figures show detailed information on ONL thickness following treatment with Neurostatin. A: The overall ONL thickness; B: The ONL thickness in the peripheral retina; C: The ONL thickness in intermediate retina; D: The ONL thickness in the peri optic nerve. Data points: Mean; Error bar: SEM; 7DPI (n = 2), P25-15DPI (n = 5), P25-30DPI (n = 5), P25-60DPI (n = 4). Data seen in Table 6-4.

Table 6-4 Changes in ONL thickness over time following treatment with Neurostatin.

Treatment	DPI	N	Perioptic nerve		Intermediate		Periphery	
			mean (μm)	SEM	mean (μm)	SEM	mean (μm)	SEM
Neurostatin	P25-7DPI	2	46.621	1.149	51.063	1.649	50.873	2.130
	P25-15DPI	5	34.911	0.506	36.400	0.739	34.807	0.794
	P25-30DPI	5	30.419	0.918	33.293	1.001	31.452	1.243
	P25-60DPI	4	12.621	1.122	14.086	1.221	18.227	1.424
Control	P25-7DPI	2	47.718	2.125	46.567	1.282	47.440	1.779
	P25-15DPI	5	37.696	0.945	37.245	0.808	35.954	0.809
	P25-30DPI	5	26.671	1.044	27.782	1.207	25.740	1.025
	P25-60DPI	4	7.180	0.740	12.320	2.138	15.600	1.353

The thickness of the ONL was then examined to investigate whether the treatment of Neurostatin could improve photoreceptor survival (Figure 6-9). These results show that the ONL thickness was significantly higher at around 30DPI (Two-way ANOVA: Treatment vs DPI: Effect of treatment:  $p = 0.001$ ), suggesting that Neurostatin has a modest positive effect on photoreceptor survival, an effect that is perhaps mediated by affecting the microglial activation during the first activation wave. However, the ONL thinned out by ~75%, between 7DPI and 60DPI in both the Neurostatin and control groups, indicating that treatment with Neurostatin alone may not be able to stop the degenerating process.

### 3.1.3 The effect of Neurostatin on photoreceptor death

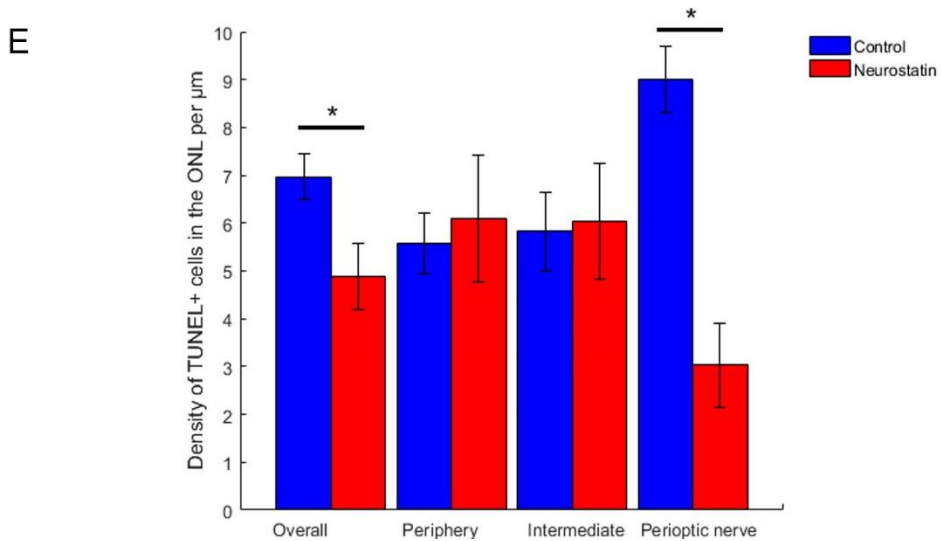
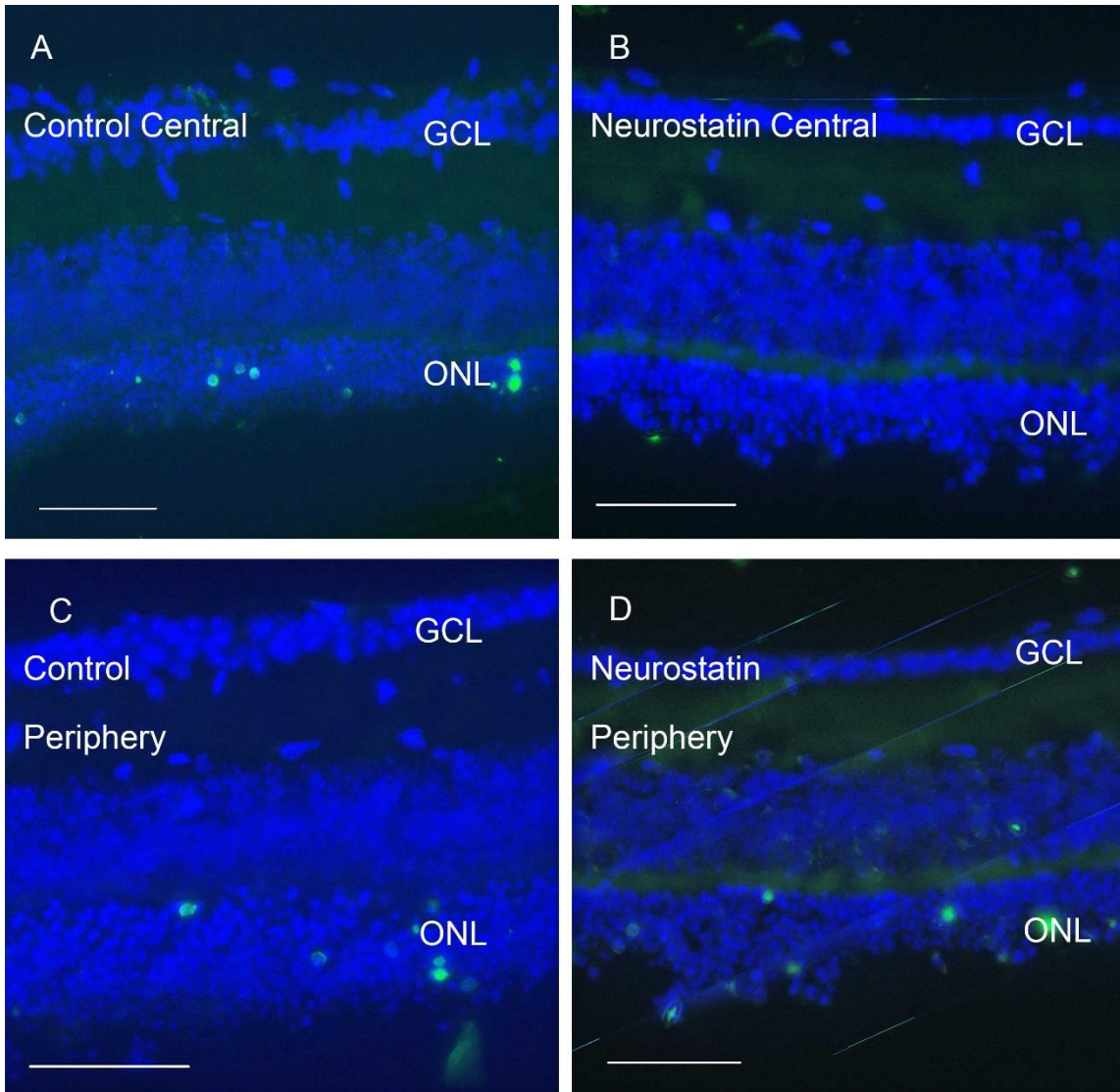


Figure 6-10 Effect of Neurostatin treatment on photoreceptor death

A-D: Representative images showing fluorescent micrographs of TUNEL+ cells. Green: TUNEL; Blue: DAPI. Images were taken from central area of the retina. Scale bar: 50µm. E: Bar chart showing the effect of Neurostatin on TUNEL+ cell density at P25-30DPI. Data points: Mean; Error bar: SEM; n = 2. Data seen in Table 6-5.

Table 6-5 The effect of Neurostatin on TUNEL+ cell density at P25-30DPI

Treatment	location	N	Mean ×10 <sup>-2</sup> cells/µm <sup>2</sup>	STD	SEM
Neurostatin	Perioptic nerve	2	3.027	2.787	0.881
	intermediate	2	6.035	3.445	1.218
	Periphery	2	6.092	3.782	1.337
Control	Perioptic nerve	2	8.998	2.758	0.689
	intermediate	2	5.828	3.079	0.823
	Periphery	2	5.581	2.173	0.627

As shown in Chapter 3, apoptosis is highly active between P50–70 in the Crx outer retina. To determine whether the level of apoptotic activity can be modified by Neurostatin, the density of TUNEL+ cells was quantified at P25-30DPI (Figure 6-10 A-D). The results revealed that significantly fewer TUNEL+ cells were detected following Neurostatin treatment (Figure 6-10 E). Closer inspection of the results according to retinal eccentricity revealed that the effect was much more pronounced in the central retina than in the periphery. These results suggest that Neurostatin may protect photoreceptor from dying. However, the effect is confined to the central retina.

### 3.2 The effect of Neurostatin during the second activation wave.

To determine whether Neurostatin has an effect during the second activation wave, the drug was injected into the vitreous at P55, and retinas were harvested at 15DPI and 30DPI.

#### 3.2.1 The effect of intravitreal Neurostatin on glial cells

No obvious morphological changes were detected in iba1+ cells after treatment with Neurostatin (Figure 6-11). Importantly, at 30DPI, the morphology of iba1+ cells from both groups was characteristic of ageing tissue undergoing degeneration (von Bernhardt et al., 2015), with a small soma and few processes (Figure 6-11 G).

Results on GFAP staining showed that, although the expression of GFAP was similar between the Neurostatin and control group at 15DPI, there was a distinct difference seen at 30DPI, as much more GFAP+ filaments were found in the group treated with Neurostatin.

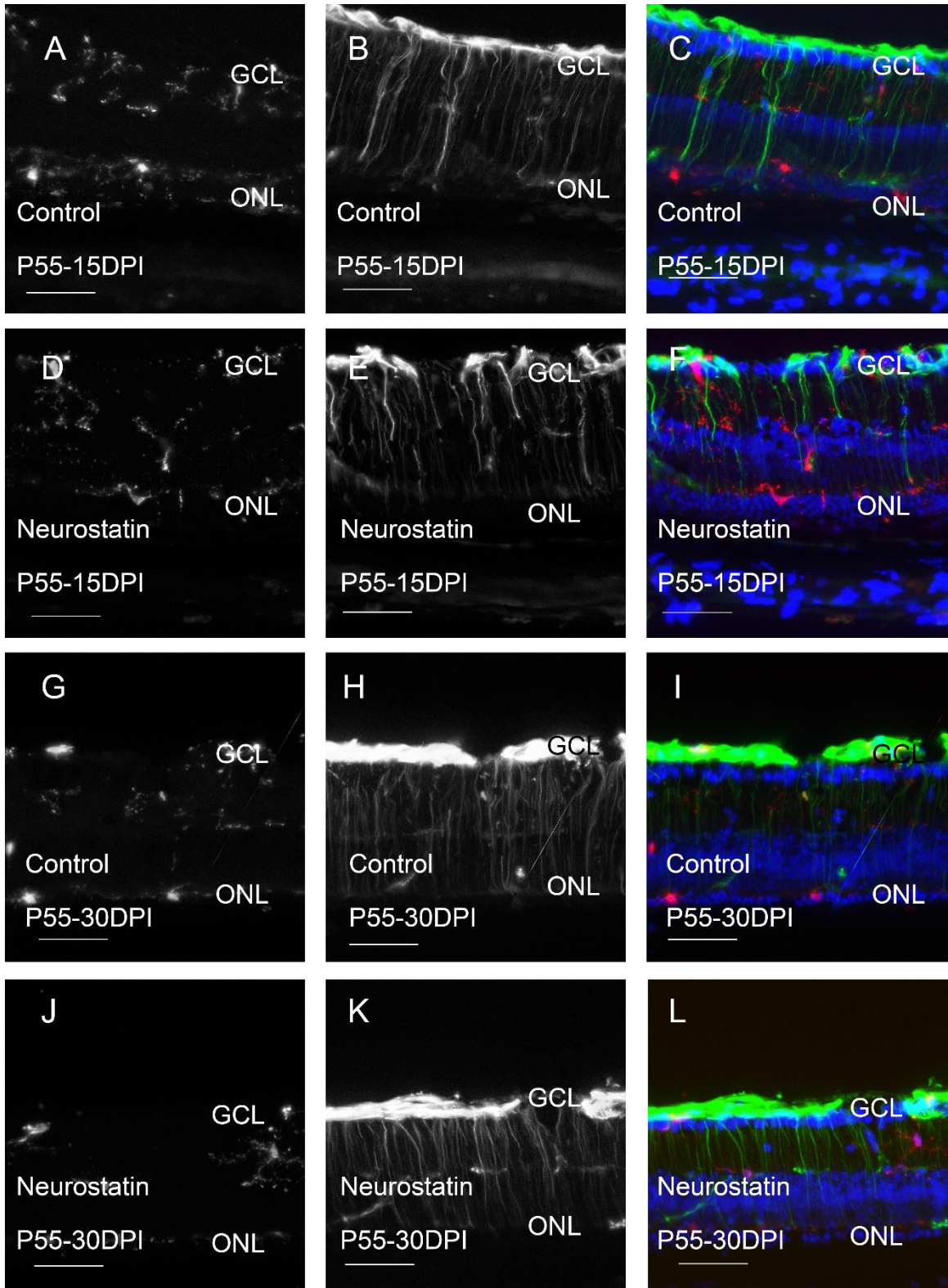


Figure 6-11 Fluorescent micrographs of glial cells following treatment with Neurostatin during the second activation wave

Representative images showing the response of glial cells at different time point following Neurostatin treatment. A, D, G, J: Iba1; B,E,H,K: GFAP; C, F, I, L: Red: Iba1, Blue: DAPI. Green: GFAP. Images were taken from central area of the retina. Scale bar: 50µm

Next, the effect of Neurostatin on the density of Iba1+ cells in different retinal layers was quantified. Overall, there were significantly fewer Iba1+ cells in the inner retina at 15DPI (Figure 6-12. Two-way ANOVA: Treatment vs DPI,  $p = 0.0321$ ). Notably, this effect was more obvious in the perioptic area than other areas. However, no difference was detected between control and Neurostatin treated retinas at 30DPI.

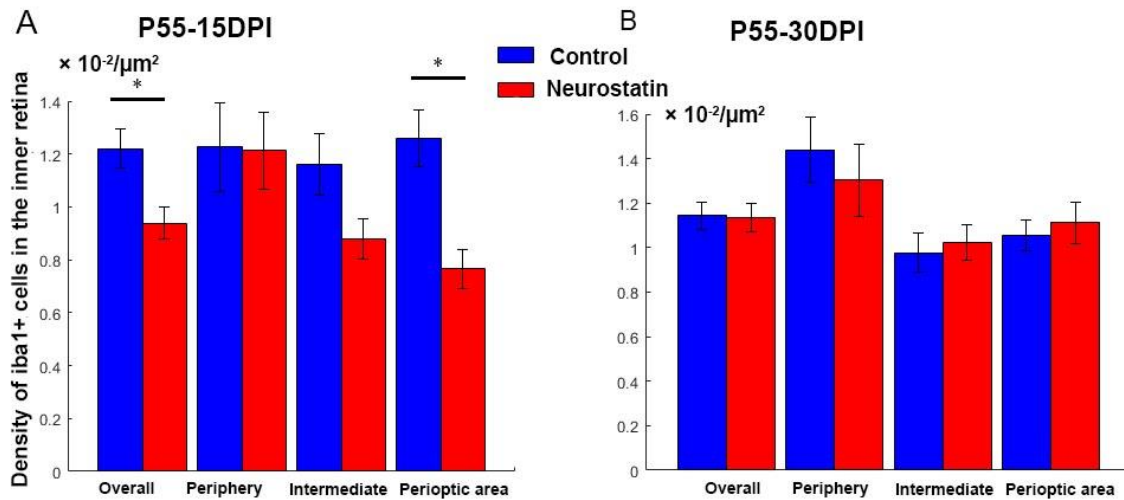


Figure 6-12 Bar chart showing the density changes of Iba1+ cells in the inner retina following Neurostatin treatment during the second activation wave.

The figures show detailed information on the effect of Neurostatin on the Iba1+ cells at the second activation wave. A: Density of Iba1+ cells in the inner retina at 15 days after treatment. B: Density of Iba1+ cells in the inner retina at 30 days after treatment. Data points: Mean; Error bar: SEM;  $n = 4$  at each time point. Data seen in Table 6-6.

Table 6-6 The effect of Neurostatin on Iba1+ cells in the inner retina at the second activation wave.

Treatment	DPI	N	Perioptic nerve		Intermediate		Periphery	
			Mean/ ×10 <sup>-2</sup> cells/µm <sup>2</sup>	SEM	Mean/ ×10 <sup>-2</sup> cells/µm <sup>2</sup>	SEM	Mean/ ×10 <sup>-2</sup> cells/µm <sup>2</sup>	SEM
Neurostatin	P55-15DPI	4	0.766	0.074	0.880	0.077	0.938	0.060
	P55-30DPI	4	1.111	0.095	1.024	0.080	1.135	0.064
Control	P55-15DPI	4	1.259	0.108	1.161	0.116	1.219	0.074
	P55-30DPI	4	1.056	0.069	0.977	0.087	1.144	0.060

Interestingly, *iba1*<sup>+</sup> cell density changes took longer to develop following Neurostatin treatment in the outer retina than in the inner retina. Indeed, no changes were seen earlier than 30DPI (Figure 6-13), and even then, they were not significant (Figure 6-13: Two-way ANOVA: Treatment vs DPI: Effect of treatment:  $p = 0.158$ ).

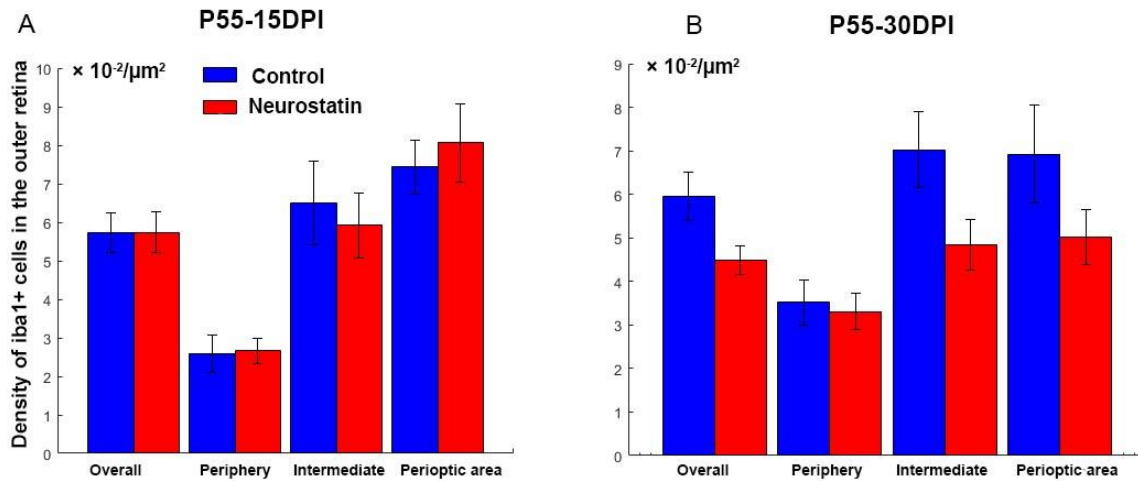


Figure 6-13 Changes in *iba1*<sup>+</sup> cells density in the outer retina following Neurostatin treatment during the second activation wave.

The figures show detailed information on the effect of Neurostatin on the *iba1*<sup>+</sup> cells at the second activation wave. A: Density of *iba1*<sup>+</sup> cells in the outer retina at 15 days after treatment. B: Density of *iba1*<sup>+</sup> cells in the outer retina at 30 days after treatment. Data points: Mean; Error bar: SEM;  $n = 4$  at each time point. Data seen in Table 6-7.

Table 6-7 The effect of Neurostatin on *iba1*<sup>+</sup> cells in the outer retina at the second activation wave

Treatment	DPI	N	Perioptic nerve		Intermediate		Periphery	
			Mean/ $\times 10^{-2}$ cells/ $\mu\text{m}^2$	SEM	Mean/ $\times 10^{-2}$ cells/ $\mu\text{m}^2$	SEM	Mean/ $\times 10^{-2}$ cells/ $\mu\text{m}^2$	SEM
Neurostatin	P55-15DPI	4	8.062	1.009	5.915	0.845	2.658	0.339
	P55-30DPI	4	5.017	0.627	4.843	0.583	3.310	0.418
Control	P55-15DPI	4	7.434	0.702	6.503	1.075	2.580	0.488
	P55-30DPI	4	6.924	1.120	7.027	0.881	3.515	0.522

The quantitative analysis also suggests that there was an overt increase on GFAP expression following treatment with Neurostatin. At 15DPI, the differences on the number of GFAP<sup>+</sup> filaments was only detectable in the central area of the retina, whilst the effect was more obvious in the periphery and intermediate area at 30DPI, indicating that the Neurostatin may

initially take effect in the central retina and spread to the periphery over time (Figure 6-14: Two-way ANOVA: Treatment vs DPI: Effect of treatment:  $p = 0.000$ ).

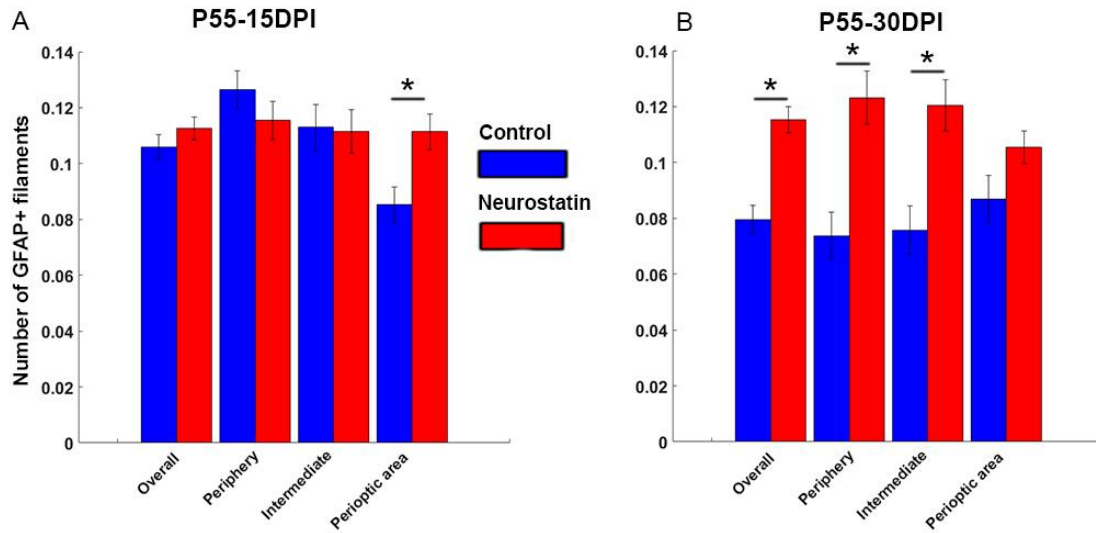


Figure 6-14 Changes in GFAP filament number following Neurostatin treatment during the second activation wave.

The figures show detailed information on the effect of Neurostatin on GFAP+ filaments at the second activation wave. A: Number of GFAP filaments at 15 days after treatment. B: Number of GFAP+ filaments at 30 days after treatment. Data points: Mean; Error bar: SEM;  $n = 4$  at each time point.. Data seen in Table 6-8.

Table 6-8 The effect of Neurostatin on GFAP filaments at the second activation wave

Treatment	DPI	N	Perioptic nerve		Intermediate		Periphery	
			Mean/ $\mu\text{m}$	SEM	Mean/ $\mu\text{m}$	SEM	Mean/ $\mu\text{m}$	SEM
Neurostatin	P55-15DPI	4	0.116	0.007	0.116	0.008	0.114	0.006
	P55-30DPI	4	0.123	0.008	0.120	0.009	0.105	0.009
Control	P55-15DPI	4	0.127	0.007	0.113	0.008	0.085	0.006
	P55-30DPI	4	0.074	0.008	0.076	0.009	0.087	0.009

3.2.2 The effect of Neurostatin on ONL thickness following intravitreal injection.

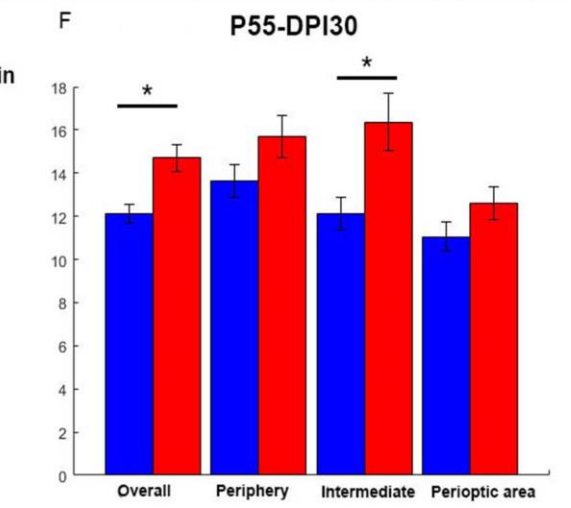
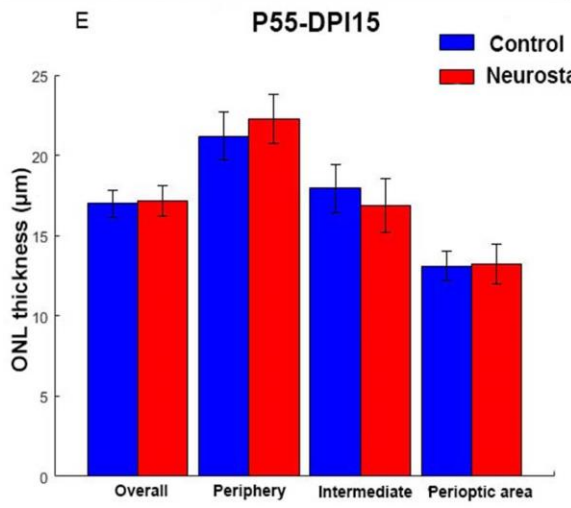
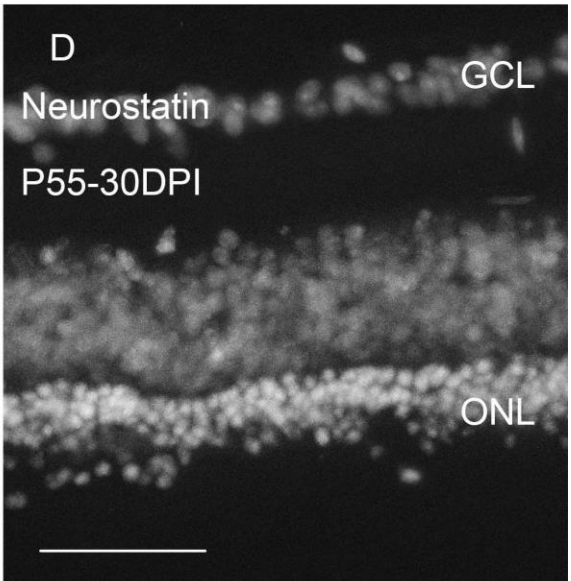
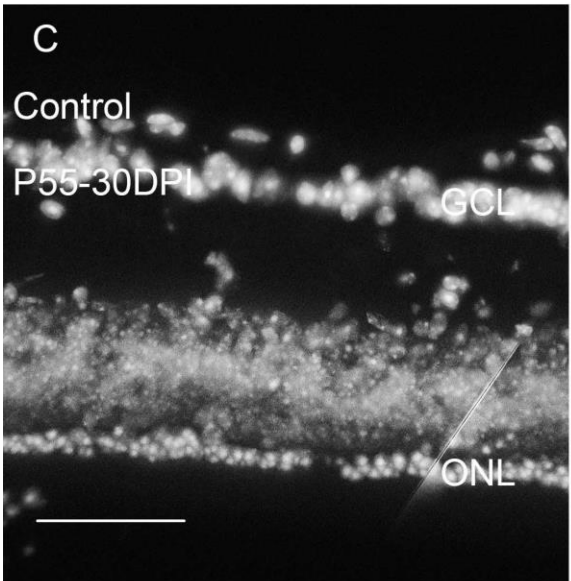
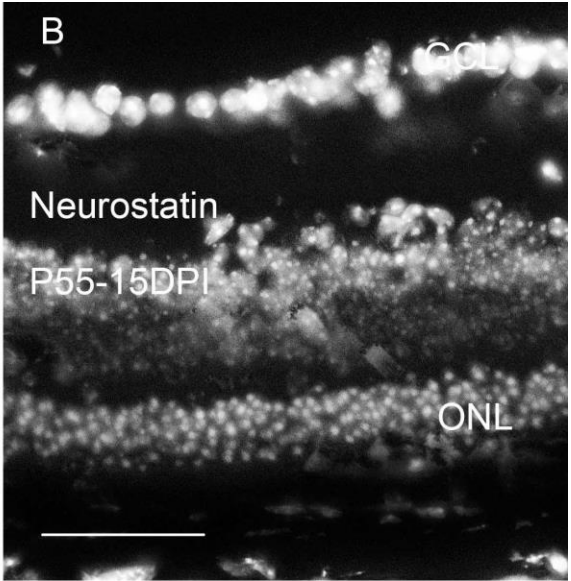
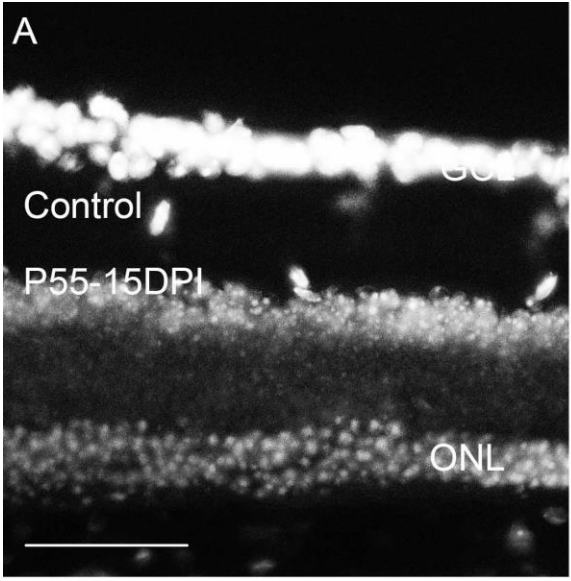


Figure 6-15 The change of ONL thickness after treated with Neurostatin at the second activation wave.

A-D: Fluorescent micrographs showing the expression of DAPI (grey) in the retinal section following treatment. Scale bar 50µm. Images taken from central area of the retina. E: Bar chart showing the ONL thickness on different location of retina at 15DPI .F: Bar chart showing the ONL thickness on different location of retina at 30DPI. Data seen in Table 6-9

Table 6-9 The effect of Neurostatin on ONL thickness in the second activation wave.

Treatment	DPI	N	Perioptic nerve		Intermediate		Periphery	
			Mean/µm	SEM	Mean/µm	SEM	Mean/µm	SEM
Neurostatin	P55-15DPI	4	13.232	1.264	16.881	1.682	22.296	1.534
	P55-30DPI	4	12.604	0.755	16.362	1.313	15.697	0.959
Control	P55-15DPI	4	13.119	0.890	17.943	1.509	21.200	1.504
	P55-30DPI	4	11.048	0.686	12.108	0.764	13.632	0.754

The ONL thickness was then measured at both 15DPI and 30 DPI, to investigate whether Neurostatin also has a protective effect on photoreceptors when applied during the second activation wave. The results show that, although there was no overt change at 15DPI, it prevents ONL thinning at 30DPI (Figure 6-15 E and F: Two-way ANOVA: Treatment vs DPI: Effect of treatment,  $p = 0.0489$ ).

### 3.3 Treatment at different time-points leads to different microglial density levels, but the outcome is still photoreceptor preservation.

Neurostatin has a protective effect on ONL thickness when applied at either P25 or P55. To investigate whether the timing of treatment could influence the long-term outcome, the density of iba1+ cells in different retinal layers, the number of GFAP+ filaments and the ONL thickness of P25-60DPI and P55-30DPI were compared.

There was a significant increase in the density of iba1+ cells in the inner retina in both Neurostatin and control groups of P55-30DPI (Figure 6-16 A. Two-way ANOVA: Treatment vs DPI: Effect of DPI:  $p = 0.000$ ).

A similar effect was also observed with the density of iba1+ cells in the outer retina, where it was significantly higher in both Neurostatin and control groups when treated at P55 (Figure 6-16 B.: Two-way ANOVA: Treatment vs DPI: Effect of DPI:  $p = 0.009$ )

Analysis on GFAP+ filaments displayed an effect that was similar to iba1+ cells. The number of GFAP filaments was significantly higher in both Neurostatin and control group at P55-30DPI (Figure 6-16 D: Two-way ANOVA: Treatment vs DPI: Effect of DPI:  $p = 0.000$ ).

However, for ONL thickness there was no difference between treatments at P25 and P55 (Figure 6-16 C: Two-way ANOVA Treatment vs DPI: Effect of DPI:  $p = 0.4919$ ), suggesting that the long-term protective effect of Neurostatin on the ONL thickness was not dependent on whether the drug was administered during the first or the second activation wave.

In summary, although the effect of Neurostatin on glial activity may differ during the first or second activation wave, overall the exact timing of administering the drug does not affect its long-term protective effect on photoreceptor survival.

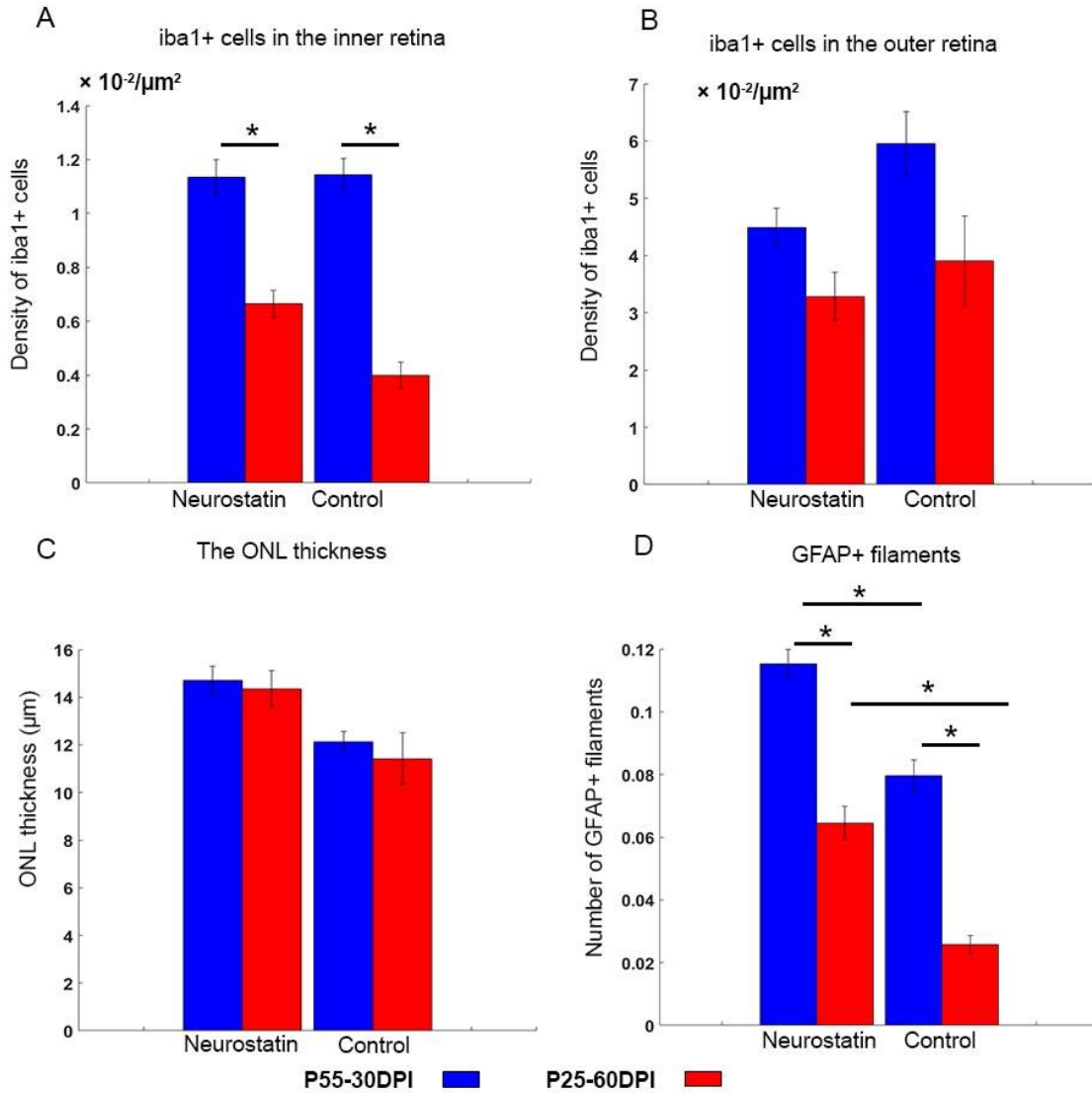


Figure 6-16 Bar chart showing the comparison of the effect on the iba1+ cells and ONL between P25-60DPI and P55-30DPI.

A. The density of iba1+ cells in the inner retina at different DPI. B. The density of iba1+ cells in the outer retina at different DPI. C. The ONL thickness at different DPI. D. The number of GFAP+ filaments at different DPI. Data points: Mean; Error bar: SEM.

## 4. Discussion

This study sought to investigate the effect of Neurostatin on glial activation and photoreceptor loss at different degenerative stages. The results show that intravitreal Neurostatin injection somewhat prolongs photoreceptor survival. However, a single treatment with Neurostatin may not be sufficient to prevent photoreceptor depletion.

#### 4.1 The modulation of glial activity in retinal degeneration.

Previous studies have shown that microglial activation contributes to photoreceptor loss (Madeira et al., 2015, Zabel et al., 2016). Modulation of the immune activity can provide neuroprotective effects in several animal models of retinal degeneration (Roche et al., 2016, Syeda et al., 2015). A previous study has shown that depletion of MyD88 can reduce photoreceptor loss in the rd1 retina by interfering with the TLR/IL-1R pathway (Syeda et al., 2015). Similarly, regulation of fractaline-CX3CR1 signalling via intravitreal injection of progesterone has a neuroprotective effect in the rd10 retina (Roche et al., 2016).

Neurostatin has previously been reported to inhibit microglial activation via the NFkB, MARK/ERK pathways (Gomez-Nicola et al., 2010). Activity regulation of the NFkB and MARK/ERK is known to be correlated with the production of pro-inflammatory mediators. Furthermore, the MARK/ERK pathway is also known to be responsible for regulating the infiltration of immune cells and the cytokine production under pathological conditions (Lu et al., 2007). Blocking the MARK/ERK pathways is considered to be an effective way to attenuate microglial activation.

A previous study on the xenotransplant of glioma in nude mice revealed that, intratumoral injection of Neurostatin can effectively inhibit the activation of epidermal growth factor receptor (EGFR), which further controls the activation of the downstream MAPK/ERK pathways by reducing the expression of ERK1 and ERK2 (Valle-Argos et al., 2010).

This study is the first to present the effect of Neurostatin on microglial activation and photoreceptor survival in inherited retinal dystrophies.

Both our *in vitro* and *in vivo* experiments show that microglial cells did not undergo major morphological changes following Neurostatin treatment, indicating that the drug may not be able to revert microglial cells to their resting mode. Furthermore, although a moderate reduction of iba1+ cell density was observed in isolated retinas, there were no conspicuous changes *in vivo*. It should be noted that retinas incubated *in vitro* were collected for fixation immediately after the incubation without washout, whereas for the *in vivo* experiments, the earliest examination was conducted at 7DPI. Due to the dynamic nature of microglial cells, it would not be surprising that the status of microglial cells changes over a period of time after treatment.

Furthermore, as the iba1 labelling can only reflect the overall microglial population without discriminating between different functional subsets, the density and the morphology of the iba1+ cells alone may not be able to fully reveal the changes in microglial cells caused by Neurostatin. As discussed in Chapter 1, it is likely that the microglial population consists of several different functional subsets, each of which is responsible for reacting towards a specific stimulus. Hence, it is presumed that during photoreceptor degeneration, although all of microglial cells become activated, only one or several of these subsets contribute to initiate the downstream pathways.

Neurostatin is known to block the downstream pathways that are triggered by IL-15. Hence, it is reasonable to assume that IL-15 expressing microglial cells are sensitive to the Neurostatin treatment. Hence, the effect of Neurostatin on microglial activity should not be ruled out based on the data from iba1 labelling only. Further studies to investigate the functional subsets involved in microglial activation in Crx retina are therefore necessary to demonstrate this possibility.

Downstream signalling molecules such as cytokines and chemokines may be more sensitive to changes in microglial activity. Furthermore, statistical power may be affected by the limited sample size used in this study, which may also influence the sensitivity of the parameters assessed, demonstrating the need for further studies.

In a previous study on gliomas, Neurostatin was suggested to interfere with cell proliferation leading to a downregulation of GFAP, via inhibiting the expression of cell cycle promoters and the EGFR pathway, and via blocking the activation of MARKs and PI3K pathway (Valle-Argos et al., 2011). Another study on a mouse model of drug-induced glaucoma showed that intravitreal injection of Neurostatin could reduce RGC death by attenuating reactive gliosis (Ganesh and Chintala, 2011). In this study, Neurostatin showed an effect of upregulating GFAP expression in both *in vitro* and *in vivo* experiments, which contradicts the two previous studies. Neurostatin, also known as gangliosides, are sialic acid-containing glycosphingolipids which are abundant in the central nervous system. A wide spectrum of structures have been found in the chains of gangliosides, which result in a diversity in their functionality. In mammal, GM1, GD1a, GD1b, and GT1b are the most common structures. It is reported that, the effect of ganglioside GM1 on the level of GFAP varies between septum and hippocampus (Oderfeld-Nowak et al., 1993), whilst a variation among different structure was also found in the effect of cell proliferation in the

glioma model. In this study, disialoganglioside GD1b was employed, which was identical to that used in the drug-induced glaucoma model. However, in the glaucoma model, ganglion cells were most affected whilst photoreceptors were well preserved, which may have resulted in a different glial reactivity. The different outcomes of these studies demonstrates the complexity of the underlying mechanism for glial activation and the diversity of response towards modulation, which highlights the need for a better understanding of glial activity in order to design effective therapies. Nonetheless, the upregulation in GFAP expression did not weaken the protective effect on photoreceptors, indicating that the changes on GFAP level may be the result rather than the initiator of microglial activity and photoreceptor degeneration.

#### 4.2 The long-term effect of Neurostatin on photoreceptor survival

Although the data presented in this chapter did not provide sufficient direct evidence that Neurostatin can indeed revert microglial cells to their resting state, results do show that the drug can, to a certain extent, protect photoreceptors from dying, and that this holds regardless of whether the treatment is administered during the first or second wave of degeneration. The comparison of ONL thickness at the late stage of photoreceptor degeneration between groups treated at different time (P25-60DPI vs P55-30DPI) suggested that the timing of treatment does not affect the long-term overall outcome of photoreceptor survival.

However, in the group treated during the first activation wave, preventing ONL thinning was more efficient in the group kept for 30DPI than in the group kept for 60DPI, which coincides with the second activation wave. The kinetics of Neurostatin in the vitreous cavity are not known, and it is plausible that the weaker effect of the drug after more prolonged post injection periods is due to complete intraocular disappearance of the drug. Hence a second treatment (or perhaps a continuous intraocular supply of the drug) is probably necessary to achieve better photoreceptor survival.

It is important to note that, the Neurostatin treatment was not able to prevent the overall ONL thinning, in line with other studies on the modulation of microglial activation. It is perhaps not surprising since Neurostatin may only interfere with inflammatory pathways, whilst the genetic defects are not fixed. Hence this treatment may only contribute to reduce the amount of microglial-associated photoreceptor death. However, previous studies have shown that microglia may affect the turnover and cell replacement of retinal progenitors by

immunosuppression (Dick, 2009). Combining microglial modulation with other approaches such as stem cell transplantation may provide a more promising outcome.

## 5. Conclusion

The results present in this chapter demonstrated that a single intravitreal injection of Neurostatin in Crx mice can slow down the progression of photoreceptor loss, suggesting that microglial activation may normally contribute to photoreceptor loss during retinal degeneration. Although our results cannot provide sufficient insights about underlying mechanisms involved, this study paves the way to understand how photoreceptors respond to glial modulation at different stages of degeneration. Future work should aim to elucidate the specific functional subsets and downstream pathways that are involved.



## **Chapter 7.      General Discussion**



The findings presented in this thesis document the dynamics of glial activity during photoreceptor degeneration in the Crx retina. Specifically, microglial and Müller activation in the Crx retina occurs in two waves, concurrent with the waves of photoreceptor death. These findings reveal that microglial activity and photoreceptor degeneration are intimately related. The results also suggest that, Müller cell activity is only associated with microglial activity and photoreceptor degeneration during the first degenerating wave, indicating that Müller cell activation may have entered an irreversible state during or after the second activation wave, in which they do not respond towards microglial modulation. Finally, this study has suggested that microglial activation may have detrimental effects during the degeneration process, whilst Müller gliosis could be a result of degeneration rather than an initiator, suggesting that being able to control microglial activity may have potential benefits on photoreceptor survival. In addition, this thesis has investigated the contribution of glial activation to photoreceptor survival different stages of degeneration. It demonstrated that intraocular injection with Neurostatin can slow down photoreceptor death regardless of whether the treatment is administered during the first or second degeneration wave, however, it also has an effect of increasing GFAP expression.

## 1. Glial activity during photoreceptor degeneration

Glial activation has been reported in a wide range of retinal disorders, but how exactly activated glia interact with neurons remains to be elucidated. However, it is widely accepted that there are many different patterns of microglial and Müller cell activation, depending on the specific stimuli and microenvironment linked to the onset of degeneration.

The data from this study established a timeline of microglial activity according to the changes in the density of iba1+ cells in different retinal layers and Müller activity according to the changes in GFAP expression, demonstrating dynamic changes in the activity patterns.

Previous studies in the rd1 and rd10 retina have attempted to explore a possible relationship between microglial activation and photoreceptor death assessed according to apoptosis (Zeng et al., 2005, Hughes et al., 2003), but could not demonstrate such correlation. Our results in the Crx retina corroborate these findings.

As discussed previously, iba1 labelling can only reflect the overall microglial population. Studying dynamic changes in microglial gene expression in response to photoreceptor loss could help reveal some of the mechanisms involved in the microglial-neuron interaction.

Nevertheless, the changes in iba1+ expression described provides a basis for future studies that could focus more specifically on subsets of microglial cells.

As opposed to the intimate relationship between microglial activity and photoreceptor degeneration, there seems to be a functional variation between different waves of Müller activation. Müller activity only correlates with microglial activity and photoreceptor degeneration during the first wave, whilst the correlation disappears in the second wave.

Recent findings have suggested that, in the brain, microglial cells are able to transform astrocytes into either neuroprotective or neurodegenerative phenotypes according to different insults (Shinozaki et al., 2017), which is in line with the M1 and M2 polarization in microglial cells. As the unique macroglia in the retina, Müller cells carry a similar functional responsibility as the astrocytes in the brain. Hence, it is speculated that the variation of Müller response may be related to the polarization of activated microglial cells. Further investigation on microglial - Müller communication may help to provide valuable information for effective therapies.

## **2. Future implications and potential therapeutic strategies**

Although retinal dystrophies remains untreatable, with the introduction of advanced technologies, several new potential therapies are becoming available. Retinal prosthetic devices are being developed, aiming to circumvent photoreceptors and stimulate surviving neurons. Stem cell transplantation, on the other hand, aim to replace dead photoreceptors with newly generated ones, at the same time providing trophic support for the remaining cells against further photoreceptor degeneration (Ng et al., 2014).

To date, Argus II is the only clinically approved retinal prosthetic model, and they provide only very limited vision for blind patients (Stingl et al., 2013). Stem cell therapy is still in its infancy, with still many challenges to overcome before becoming clinically efficient. Therefore, rather than trying to replace or circumvent dead photoreceptors, it is very important to develop effective therapeutic strategies that can rescue remaining photoreceptors, if the intervention is done early enough, such as gene therapy. Hopefully, controlling glial activity during the critical phases of degeneration will, in the future, help rescue photoreceptors as well.

Previous studies have shown that, microglial activation contributes to photoreceptor death directly via phagocytosing viable photoreceptors, but also indirectly, by accelerating the rate of degeneration via releasing cytotoxic factors. Our results revealed that, although the application of Neurostatin showed a protective effect during both activation waves, it had a stronger protective effect against photoreceptor death (assessed by measuring the ONL thickness) when administered during the first activation wave, suggesting that early intervention of microglial activity may lead to a more successful outcome.

Hence, it would be interesting to examine whether continuous administration of Neurostatin from the onset of retinal degeneration would improve photoreceptor survival further. To achieve this, it will be necessary to devise an approach to continuously deliver the drug to the retina at effective dosage. Oral or topical administration may encourage compliance especially for the treatment of the early stage of the diseases (Jin et al., 2008). However, to get molecules like Neurostatin to pass through either the cornea/sclera or blood-retinal barrier in order to reach the retina remains challenging. On the other hand, although direct intraocular injections would help controlling the amount of drug reaching the retina, due to its invasive nature, repeated injections are undesirable. One possible approach would be to design a controlled drug release solution such as slow release from polymer nanoparticles. Nanoparticles have previously been reported to be successful for ocular applications (Conley and Naash, 2010). An experimental design using nanoparticles for slow release of Neurostatin may help to boost our understanding of the role of glial activity in retinal degeneration.

Another promising approach is to combine microglial modulation with stem cell therapy. Microglial modulation may support stem cell therapy in three aspects. In the early stage of retinal degeneration, stem cells can serve as a trophic mediator to enhance survival of the remaining photoreceptors (Caplan and Dennis, 2006), whilst modulation of microglial activation can also slow down photoreceptor degeneration. In addition, immunological rejection and gliosis remain serious barriers to successful stem cell therapy. As the innate immune cells, microglial cells play an important role in both the immune response and the regulation of gliosis. . It would be very interesting to investigate whether the combination of these two treatments would amplify the outcome. (Garg et al., 2017). Furthermore, recent studies have reported that microglial cells can regulate differentiation of retinal progenitors (Dick, 2009). Modulation of the microglial activity can control photoreceptor regeneration kinetics via regulating the response of Müller cells towards cell death (White et al., 2017). Therefore, microglial modulation may help to facilitate stem cell therapy to restore retinal function.



## References:

- AKAISHI, K., ISHIGURO, S., DURLU, Y. K. & TAMAI, M. 1998. Quantitative analysis of major histocompatibility complex class II-positive cells in posterior segment of Royal College of Surgeons rat eyes. *Jpn J Ophthalmol*, 42, 357-62.
- ALLIOT, F., GODIN, I. & PESSAC, B. 1999. Microglia derive from progenitors, originating from the yolk sac, and which proliferate in the brain. *Brain Res Dev Brain Res*, 117, 145-52.
- APPLEBURY, M., ANTOCH, M., BAXTER, L., CHUN, L., FALK, J., FARHANGFAR, F., KAGE, K., KRZYSTOLIK, M., LYASS, L. & ROBBINS, J. 2000. The murine cone photoreceptor: a single cone type expresses both S and M opsins with retinal spatial patterning. *Neuron*, 27, 513-523.
- AREDO, B., ZHANG, K., CHEN, X., WANG, C. X., LI, T. & UFRET-VINCENY, R. L. 2015. Differences in the distribution, phenotype and gene expression of subretinal microglia/macrophages in C57BL/6N (Crb1 rd8/rd8) versus C57BL6/J (Crb1 wt/wt) mice. *J Neuroinflammation*, 12, 6.
- ARNOLD, T. & BETSHOLTZ, C. 2013. The importance of microglia in the development of the vasculature in the central nervous system. *Vasc Cell*, 5, 4.
- ARNOUX, I. & AUDINAT, E. 2015. Fractalkine Signaling and Microglia Functions in the Developing Brain. *Neural Plast*, 2015, 689404.
- BALMER, J., JI, R., RAY, T. A., SELBER, F., GASSMANN, M., PEACHEY, N. S., GREGG, R. G. & ENZMANN, V. 2013. Presence of the Gpr179(nob5) allele in a C3H-derived transgenic mouse. *Mol Vis*, 19, 2615-25.
- BARBER, A. C., HIPPERT, C., DURAN, Y., WEST, E. L., BAINBRIDGE, J. W., WARRE-CORNISH, K., LUHMANN, U. F., LAKOWSKI, J., SOWDEN, J. C., ALI, R. R. & PEARSON, R. A. 2013. Repair of the degenerate retina by photoreceptor transplantation. *Proc Natl Acad Sci U S A*, 110, 354-9.
- BARNETT, N. L., POW, D. V. & ROBINSON, S. R. 2000. Inhibition of Muller cell glutamine synthetase rapidly impairs the retinal response to light. *Glia*, 30, 64-73.
- BAUER, P. M., ZALIS, M. C., ABDSHILL, H., DEIERBORG, T., JOHANSSON, F. & ENGLUND-JOHANSSON, U. 2016. Inflamed In Vitro Retina: Cytotoxic Neuroinflammation and Galectin-3 Expression. *PLoS One*, 11, e0161723.
- BAYES, M., GIORDANO, M., BALCELLS, S., GRINBERG, D., VILAGELIU, L., MARTINEZ, I., AYUSO, C., BENITEZ, J., RAMOSARROYO, M. A., CHIVELET, P., SOLANS, T., VALVERDE, D., AMSELEM, S., GOOSSENS, M., BAIGET, M., GONZALEZDUARTE, R. & BESMOND, C. 1995. Homozygous Tandem Duplication within the Gene Encoding the Beta-Subunit of Rod Phosphodiesterase as a Cause for Autosomal Recessive Retinitis-Pigmentosa. *Human Mutation*, 5, 228-234.
- BENHAR, I., REEMST, K., KALCHENKO, V. & SCHWARTZ, M. 2016. The retinal pigment epithelium as a gateway for monocyte trafficking into the eye. *The EMBO journal*, 35, 1219-1235.
- BIALAS, A. R. & STEVENS, B. 2013. TGF-beta signaling regulates neuronal C1q expression and developmental synaptic refinement. *Nat Neurosci*, 16, 1773-82.
- BIEDERMANN, B., BRINGMANN, A. & REICHENBACH, A. 2002. High-affinity GABA uptake in retinal glial (Muller) cells of the guinea pig: electrophysiological characterization, immunohistochemical localization, and modeling of efficiency. *Glia*, 39, 217-28.
- BOWES, C., LI, T. S., DANCIGER, M., BAXTER, L. C., APPLEBURY, M. L. & FARBER, D. B. 1990. Retinal Degeneration in the Rd Mouse Is Caused by a Defect in the Beta-Subunit of Rod Cgmp-Phosphodiesterase. *Nature*, 347, 677-680.
- BRINGMANN, A., GROSCHE, A., PANNICKE, T. & REICHENBACH, A. 2013. GABA and Glutamate Uptake and Metabolism in Retinal Glial (Muller) Cells. *Front Endocrinol (Lausanne)*, 4, 48.
- BRINGMANN, A., PANNICKE, T., GROSCHE, J., FRANCKE, M., WIEDEMANN, P., SKATCHKOV, S. N., OSBORNE, N. N. & REICHENBACH, A. 2006. Muller cells in the healthy and diseased retina. *Prog Retin Eye Res*, 25, 397-424.
- BRINGMANN, A., REICHENBACH, A. & WIEDEMANN, P. 2004. Pathomechanisms of cystoid macular edema. *Ophthalmic Res*, 36, 241-9.

- BRINGMANN, A. & WIEDEMANN, P. 2012. Muller glial cells in retinal disease. *Ophthalmologica*, 227, 1-19.
- Brites, D. & Vaz, A. R. 2014. Microglia centered pathogenesis in ALS: insights in cell interconnectivity. *Front Cell Neurosci*, 8, 117.
- BROWN, G. C. & NEHER, J. J. 2012. Eaten alive! Cell death by primary phagocytosis: 'phagoptosis'. *Trends Biochem Sci*, 37, 325-32.
- BROWN, G. C. & NEHER, J. J. 2014. Microglial phagocytosis of live neurons. *Nat Rev Neurosci*, 15, 209-16.
- CAPLAN, A. I. & DENNIS, J. E. 2006. Mesenchymal stem cells as trophic mediators. *Journal of cellular biochemistry*, 98, 1076-1084.
- CHANG, B. 2015. Survey of the nob5 mutation in C3H substrains. *Mol Vis*, 21, 1101-5.
- CHANG, B., HAWES, N. L., HURD, R. E., DAVISSON, M. T., NUSINOWITZ, S. & HECKENLIVELY, J. R. 2002. Retinal degeneration mutants in the mouse. *Vision Res*, 42, 517-25.
- CHANG, B., HAWES, N. L., PARDUE, M. T., GERMAN, A. M., HURD, R. E., DAVISSON, M. T., NUSINOWITZ, S., RENGARAJAN, K., BOYD, A. P., SIDNEY, S. S., PHILLIPS, M. J., STEWART, R. E., CHAUDHURY, R., NICKERSON, J. M., HECKENLIVELY, J. R. & BOATRIGHT, J. H. 2007. Two mouse retinal degenerations caused by missense mutations in the beta-subunit of rod cGMP phosphodiesterase gene. *Vision Res*, 47, 624-33.
- CHANG, G. Q., HAO, Y. & WONG, F. 1993. Apoptosis: final common pathway of photoreceptor death in rd, rds, and rhodopsin mutant mice. *Neuron*, 11, 595-605.
- CHEN, L., YANG, P. & KIJLSTRA, A. 2002. Distribution, markers, and functions of retinal microglia. *Ocul Immunol Inflamm*, 10, 27-39.
- CHERRY, J. D., OLSCHOWKA, J. A. & O'BANION, M. K. 2014. Neuroinflammation and M2 microglia: the good, the bad, and the inflamed. *J Neuroinflammation*, 11, 98.
- CHHOR, V., LE CHARPENTIER, T., LEBON, S., ORE, M. V., CELADOR, I. L., JOSSERAND, J., DEGOS, V., JACOTOT, E., HAGBERG, H., SAVMAN, K., MALLARD, C., GRESSENS, P. & FLEISS, B. 2013. Characterization of phenotype markers and neuronotoxic potential of polarised primary microglia in vitro. *Brain Behav Immun*, 32, 70-85.
- CHUA, J., FLETCHER, E. L. & KALLONIATIS, M. 2009. Functional remodeling of glutamate receptors by inner retinal neurons occurs from an early stage of retinal degeneration. *J Comp Neurol*, 514, 473-91.
- CHUA, J., NIVISON-SMITH, L., FLETCHER, E. L., TRENHOLM, S., AWATRAMANI, G. B. & KALLONIATIS, M. 2013. Early remodeling of Muller cells in the rd/rd mouse model of retinal dystrophy. *J Comp Neurol*, 521, 2439-53.
- CONLEY, S. M. & NAASH, M. I. 2010. Nanoparticles for retinal gene therapy. *Prog Retin Eye Res*, 29, 376-97.
- COTTET, S. & SCHORDERET, D. F. 2009. Mechanisms of apoptosis in retinitis pigmentosa. *Curr Mol Med*, 9, 375-83.
- DAVALOS, D., GRUTZENDLER, J., YANG, G., KIM, J. V., ZUO, Y., JUNG, S., LITTMAN, D. R., DUSTIN, M. L. & GAN, W. B. 2005. ATP mediates rapid microglial response to local brain injury in vivo. *Nat Neurosci*, 8, 752-8.
- DEN HOLLANDER, A. I., HECKENLIVELY, J. R., VAN DEN BORN, L. I., DE KOK, Y. J., VAN DER VELDE-VISSER, S. D., KELLNER, U., JURKLIES, B., VAN SCHOONEVELD, M. J., BLANKENAGEL, A., ROHRSCHEIDER, K., WISSINGER, B., CRUYSBURG, J. R., DEUTMAN, A. F., BRUNNER, H. G., APFELSTEDT-SYLLA, E., HOYNG, C. B. & CREMERS, F. P. 2001. Leber congenital amaurosis and retinitis pigmentosa with Coats-like exudative vasculopathy are associated with mutations in the crumbs homologue 1 (CRB1) gene. *Am J Hum Genet*, 69, 198-203.
- DEVARAJAN, G., NIVEN, J., FORRESTER, J. V. & CRANE, I. J. 2016. Retinal Pigment Epithelial Cell Apoptosis is Influenced by a Combination of Macrophages and Soluble Mediators Present in Age-Related Macular Degeneration. *Curr Eye Res*, 1-10.

- DHEEN, S. T., KAUR, C. & LING, E. A. 2007. Microglial activation and its implications in the brain diseases. *Curr Med Chem*, 14, 1189-97.
- DICK, A. D. 2009. Influence of microglia on retinal progenitor cell turnover and cell replacement. *Eye (Lond)*, 23, 1939-45.
- EBERT, S., WEIGELT, K., WALCZAK, Y., DROBNIK, W., MAUERER, R., HUME, D. A., WEBER, B. H. & LANGMANN, T. 2009. Docosahexaenoic acid attenuates microglial activation and delays early retinal degeneration. *J Neurochem*, 110, 1863-75.
- EISENFELD, A. J., BUNT-MILAM, A. H. & SARTHY, P. V. 1984. Muller cell expression of glial fibrillary acidic protein after genetic and experimental photoreceptor degeneration in the rat retina. *Invest Ophthalmol Vis Sci*, 25, 1321-8.
- ENG, L. F. 1985. Glial fibrillary acidic protein (GFAP): the major protein of glial intermediate filaments in differentiated astrocytes. *J Neuroimmunol*, 8, 203-14.
- FENN, A. M., SMITH, K. M., LOVETT-RACKE, A. E., GUERAU-DE-ARELLANO, M., WHITACRE, C. C. & GODBOUT, J. P. 2013. Increased micro-RNA 29b in the aged brain correlates with the reduction of insulin-like growth factor-1 and fractalkine ligand. *Neurobiol Aging*, 34, 2748-58.
- FERNANDEZ-SANCHEZ, L., LAX, P., CAMPELLO, L., PINILLA, I. & CUENCA, N. 2015. Astrocytes and Muller Cell Alterations During Retinal Degeneration in a Transgenic Rat Model of Retinitis Pigmentosa. *Front Cell Neurosci*, 9, 484.
- FERRARI, S., DI IORIO, E., BARBARO, V., PONZIN, D., SORRENTINO, F. S. & PARMEGGIANI, F. 2011. Retinitis pigmentosa: genes and disease mechanisms. *Curr Genomics*, 12, 238-49.
- FERREIRA, R. & BERNARDINO, L. 2015. Dual role of microglia in health and disease: pushing the balance toward repair. *Front Cell Neurosci*, 9, 51.
- FERRI, K. F. & KROEMER, G. 2001. Organelle-specific initiation of cell death pathways. *Nat Cell Biol*, 3, E255-63.
- FLETCHER, E. L. & KALLONIATIS, M. 1996. Neurochemical architecture of the normal and degenerating rat retina. *J Comp Neurol*, 376, 343-60.
- FLIGHT, M. H. 2013. Neurological disorders: Eaten alive! *Nat Rev Neurosci*, 14, 816-7.
- FRANCIS, P. J. 2006. Genetics of inherited retinal disease. *J R Soc Med*, 99, 189-91.
- FU, Y. 1995. Phototransduction in Rods and Cones. In: KOLB, H., FERNANDEZ, E. & NELSON, R. (eds.) *Webvision: The Organization of the Retina and Visual System*. Salt Lake City (UT).
- FURUKAWA, T., MORROW, E. M. & CEPKO, C. L. 1997. Crx, a novel otx-like homeobox gene, shows photoreceptor-specific expression and regulates photoreceptor differentiation. *Cell*, 91, 531-41.
- FURUKAWA, T., MORROW, E. M., LI, T., DAVIS, F. C. & CEPKO, C. L. 1999. Retinopathy and attenuated circadian entrainment in Crx-deficient mice. *Nat Genet*, 23, 466-70.
- GANESH, B. S. & CHINTALA, S. K. 2011. Inhibition of reactive gliosis attenuates excitotoxicity-mediated death of retinal ganglion cells. *PLoS One*, 6, e18305.
- GARG, A., YANG, J., LEE, W. & TSANG, S. H. 2017. Stem Cell Therapies in Retinal Disorders. *Cells*, 6.
- GARGINI, C., TERZIBASI, E., MAZZONI, F. & STRETTOI, E. 2007. Retinal organization in the retinal degeneration 10 (rd10) mutant mouse: a morphological and ERG study. *J Comp Neurol*, 500, 222-38.
- GEHRIG, A., LANGMANN, T., HORLING, F., JANSSEN, A., BONIN, M., WALTER, M., POTHS, S. & WEBER, B. H. 2007. Genome-wide expression profiling of the retinoschisin-deficient retina in early postnatal mouse development. *Invest Ophthalmol Vis Sci*, 48, 891-900.
- GERMAN, O. L., AGNOLAZZA, D. L., POLITI, L. E. & ROTSTEIN, N. P. 2015. Light, lipids and photoreceptor survival: live or let die? *Photochem Photobiol Sci*, 14, 1737-53.
- GERTIG, U. & HANISCH, U. K. 2014. Microglial diversity by responses and responders. *Front Cell Neurosci*, 8, 101.

- GINHOUX, F., GRETER, M., LEOEUF, M., NANDI, S., SEE, P., GOKHAN, S., MEHLER, M. F., CONWAY, S. J., NG, L. G. & STANLEY, E. R. 2010. Fate mapping analysis reveals that adult microglia derive from primitive macrophages. *Science*, 330, 841-845.
- GODBOUT, J. P., CHEN, J., ABRAHAM, J., RICHWINE, A. F., BERG, B. M., KELLEY, K. W. & JOHNSON, R. W. 2005. Exaggerated neuroinflammation and sickness behavior in aged mice following activation of the peripheral innate immune system. *FASEB J*, 19, 1329-31.
- GOLDMANN, T., WIEGHOFER, P., JORDAO, M. J., PRUTEK, F., HAGEMEYER, N., FRENZEL, K., AMANN, L., STASZEWSKI, O., KIERDORF, K., KRUEGER, M., LOCATELLI, G., HOCHGERNER, H., ZEISER, R., EPELMAN, S., GEISSMANN, F., PRILLER, J., ROSSI, F. M., BECHMANN, I., KERSCHENSTEINER, M., LINNARSSON, S., JUNG, S. & PRINZ, M. 2016. Origin, fate and dynamics of macrophages at central nervous system interfaces. *Nat Immunol*, 17, 797-805.
- GOMES-LEAL, W. 2012. Microglial physiopathology: how to explain the dual role of microglia after acute neural disorders? *Brain Behav*, 2, 345-56.
- GOMEZ-NICOLA, D. & PERRY, V. H. 2015. Microglial dynamics and role in the healthy and diseased brain: a paradigm of functional plasticity. *Neuroscientist*, 21, 169-84.
- GOMEZ-NICOLA, D., VALLE-ARGOS, B. & NIETO-SAMPEDRO, M. 2010. Blockade of IL-15 activity inhibits microglial activation through the NFkappaB, p38, and ERK1/2 pathways, reducing cytokine and chemokine release. *Glia*, 58, 264-76.
- GOMEZ-NICOLA, D., VALLE-ARGOS, B., SUARDIAZ, M., TAYLOR, J. S. & NIETO-SAMPEDRO, M. 2008. Role of IL-15 in spinal cord and sciatic nerve after chronic constriction injury: regulation of macrophage and T-cell infiltration. *J Neurochem*, 107, 1741-52.
- GORDON, S. 2003. Alternative activation of macrophages. *Nat Rev Immunol*, 3, 23-35.
- GORDON, S. 2007. The macrophage: past, present and future. *Eur J Immunol*, 37 Suppl 1, S9-17.
- GREENBERG, D. A. & JIN, K. 2005. From angiogenesis to neuropathology. *Nature*, 438, 954-9.
- HAMEL, C. 2006. Retinitis pigmentosa. *Orphanet J Rare Dis*, 1, 40.
- HAMEL, C. P. 2007. Cone rod dystrophies. *Orphanet J Rare Dis*, 2, 7.
- HANISCH, U. K. 2013. Functional diversity of microglia - how heterogeneous are they to begin with? *Front Cell Neurosci*, 7, 65.
- HARADA, T., HARADA, C., KOHSAKA, S., WADA, E., YOSHIDA, K., OHNO, S., MAMADA, H., TANAKA, K., PARADA, L. F. & WADA, K. 2002. Microglia-Muller glia cell interactions control neurotrophic factor production during light-induced retinal degeneration. *J Neurosci*, 22, 9228-36.
- HARADA, T., HARADA, C., NAKAYAMA, N., OKUYAMA, S., YOSHIDA, K., KOHSAKA, S., MATSUDA, H. & WADA, K. 2000. Modification of glial-neuronal cell interactions prevents photoreceptor apoptosis during light-induced retinal degeneration. *Neuron*, 26, 533-41.
- HILDEBRAND, G. D. & FIELDER, A. R. 2011. Anatomy and Physiology of the Retina. *Pediatric retina*. Springer.
- HIPPERT, C., GRACA, A. B., BARBER, A. C., WEST, E. L., SMITH, A. J., ALI, R. R. & PEARSON, R. A. 2015. Muller glia activation in response to inherited retinal degeneration is highly varied and disease-specific. *PLoS One*, 10, e0120415.
- HOEFFEL, G., CHEN, J., LAVIN, Y., LOW, D., ALMEIDA, F. F., SEE, P., BEAUDIN, A. E., LUM, J., LOW, I., FORSBERG, E. C., POIDINGER, M., ZOLEZZI, F., LARBI, A., NG, L. G., CHAN, J. K., GRETER, M., BECHER, B., SAMOKHVALOV, I. M., MERAD, M. & GINHOUX, F. 2015. C-Myb(+) erythro-myeloid progenitor-derived fetal monocytes give rise to adult tissue-resident macrophages. *Immunity*, 42, 665-78.
- HOMBREBUENO, J. R., LUO, C., GUO, L., CHEN, M. & XU, H. 2014. Intravitreal Injection of Normal Saline Induces Retinal Degeneration in the C57BL/6J Mouse. *Transl Vis Sci Technol*, 3, 3.
- HUANG, Y., XU, Z., XIONG, S., SUN, F., QIN, G., HU, G., WANG, J., ZHAO, L., LIANG, Y. X., WU, T., LU, Z., HUMAYUN, M. S., SO, K. F., PAN, Y., LI, N., YUAN, T. F., RAO, Y. & PENG, B. 2018. Repopulated microglia are solely derived from the proliferation of residual microglia after acute depletion. *Nat Neurosci*, 21, 530-540.

- HUGHES, E. H., SCHLICHTENBREDE, F. C., MURPHY, C. C., SARRA, G. M., LUTHERT, P. J., ALI, R. R. & DICK, A. D. 2003. Generation of activated sialoadhesin-positive microglia during retinal degeneration. *Invest Ophthalmol Vis Sci*, 44, 2229-34.
- INDIK, Z. K., HUNTER, S., HUANG, M. M., PAN, X. Q., CHIEN, P., KELLY, C., LEVINSON, A. I., KIMBERLY, R. P. & SCHREIBER, A. D. 1994. The high affinity Fc gamma receptor (CD64) induces phagocytosis in the absence of its cytoplasmic domain: the gamma subunit of Fc gamma RIIIA imparts phagocytic function to Fc gamma RI. *Exp Hematol*, 22, 599-606.
- ITO, D., IMAI, Y., OHSAWA, K., NAKAJIMA, K., FUKUUCHI, Y. & KOHSAKA, S. 1998. Microglia-specific localisation of a novel calcium binding protein, Iba1. *Molecular brain research*, 57, 1-9.
- JAKUBZICK, C. V., RANDOLPH, G. J. & HENSON, P. M. 2017. Monocyte differentiation and antigen-presenting functions. *Nat Rev Immunol*, 17, 349-362.
- JEON, C. J., STRETTOI, E. & MASLAND, R. H. 1998. The major cell populations of the mouse retina. *J Neurosci*, 18, 8936-46.
- JI, Y., YU, W. Q., EOM, Y. S., BRUCE, F., CRAFT, C. M., GRZYWACZ, N. M. & LEE, E. J. 2014. The effect of TIMP-1 on the cone mosaic in the retina of the rat model of retinitis pigmentosa. *Invest Ophthalmol Vis Sci*, 56, 352-64.
- JIN, J., SKLAR, G. E., OH, V. M. S. & LI, S. C. 2008. Factors affecting therapeutic compliance: A review from the patient's perspective. *Therapeutics and clinical risk management*, 4, 269.
- JIN, N., GAO, L., FAN, X. & XU, H. 2016. Friend or Foe? Resident Microglia vs Bone Marrow-Derived Microglia and Their Roles in the Retinal Degeneration. *Mol Neurobiol*.
- JOHANSSON, A. C., APPELQVIST, H., NILSSON, C., KAGEDAL, K., ROBERG, K. & OLLINGER, K. 2010. Regulation of apoptosis-associated lysosomal membrane permeabilization. *Apoptosis*, 15, 527-40.
- JONES, B. W. & MARC, R. E. 2005. Retinal remodeling during retinal degeneration. *Exp Eye Res*, 81, 123-37.
- KACIMI, R., GIFFARD, R. G. & YENARI, M. A. 2011. Endotoxin-activated microglia injure brain derived endothelial cells via NF-kappaB, JAK-STAT and JNK stress kinase pathways. *J Inflamm (Lond)*, 8, 7.
- KANEKO, H., NISHIGUCHI, K. M., NAKAMURA, M., KACHI, S. & TERASAKI, H. 2008. Characteristics of bone marrow-derived microglia in the normal and injured retina. *Investigative ophthalmology & visual science*, 49, 4162-4168.
- KARLSTETTER, M. & LANGMANN, T. 2014. Microglia in the aging retina. *Adv Exp Med Biol*, 801, 207-12.
- KARLSTETTER, M., NOTHDURFTER, C., ASLANIDIS, A., MOELLER, K., HORN, F., SCHOLZ, R., NEUMANN, H., WEBER, B. H., RUPPRECHT, R. & LANGMANN, T. 2014. Translocator protein (18 kDa) (TSPO) is expressed in reactive retinal microglia and modulates microglial inflammation and phagocytosis. *J Neuroinflammation*, 11, 3.
- KARLSTETTER, M., SCHOLZ, R., RUTAR, M., WONG, W. T., PROVVIS, J. M. & LANGMANN, T. 2015. Retinal microglia: just bystander or target for therapy? *Prog Retin Eye Res*, 45, 30-57.
- KEVANY, B. M. & PALCZEWSKI, K. 2010. Phagocytosis of retinal rod and cone photoreceptors. *Physiology (Bethesda)*, 25, 8-15.
- KIELIAN, T. 2006. Toll-like receptors in central nervous system glial inflammation and homeostasis. *J Neurosci Res*, 83, 711-30.
- KIERDORF, K. & PRINZ, M. 2017. Microglia in steady state. *J Clin Invest*.
- KIM, K. H., PUORIS'HAAG, M., MAGULURI, G. N., UMINO, Y., CUSATO, K., BARLOW, R. B. & DE BOER, J. F. 2008. Monitoring mouse retinal degeneration with high-resolution spectral-domain optical coherence tomography. *J Vis*, 8, 17 1-11.
- KIM, O. S., PARK, E. J., JOE, E. H. & JOU, I. 2002. JAK-STAT signaling mediates gangliosides-induced inflammatory responses in brain microglial cells. *J Biol Chem*, 277, 40594-601.
- KOENENKOOP, R. K. 2004. An overview of Leber congenital amaurosis: a model to understand human retinal development. *Surv Ophthalmol*, 49, 379-98.

- KOENEKOOP, R. K. 2009. Why do cone photoreceptors die in rod-specific forms of retinal degenerations? *Ophthalmic Genet*, 30, 152-4.
- KOHNO, H., CHEN, Y., KEVANY, B. M., PEARLMAN, E., MIYAGI, M., MAEDA, T., PALCZEWSKI, K. & MAEDA, A. 2013. Photoreceptor proteins initiate microglial activation via Toll-like receptor 4 in retinal degeneration mediated by all-trans-retinal. *J Biol Chem*, 288, 15326-41.
- LAWSON, L. J., PERRY, V. H., DRI, P. & GORDON, S. 1990. Heterogeneity in the distribution and morphology of microglia in the normal adult mouse brain. *Neuroscience*, 39, 151-70.
- LEE, E. J., JI, Y., ZHU, C. L. & GRZYWACZ, N. M. 2011. Role of Muller cells in cone mosaic rearrangement in a rat model of retinitis pigmentosa. *Glia*, 59, 1107-17.
- LEE, Y. S., MORINAGA, H., KIM, J. J., LAGAKOS, W., TAYLOR, S., KESHWANI, M., PERKINS, G., DONG, H., KAYALI, A. G., SWEET, I. R. & OLEFSKY, J. 2013. The fractalkine/CX3CR1 system regulates beta cell function and insulin secretion. *Cell*, 153, 413-25.
- LEWIS, G. P. & FISHER, S. K. 2003. Up-regulation of glial fibrillary acidic protein in response to retinal injury: its potential role in glial remodeling and a comparison to vimentin expression. *Int Rev Cytol*, 230, 263-90.
- LI, L., ETER, N. & HEIDUSCHKA, P. 2015. The microglia in healthy and diseased retina. *Exp Eye Res*, 136, 116-30.
- LI, Q. & BARRES, B. A. 2018. Microglia and macrophages in brain homeostasis and disease. *Nat Rev Immunol*, 18, 225-242.
- LIN, B., MASLAND, R. H. & STRETTOI, E. 2009. Remodeling of cone photoreceptor cells after rod degeneration in rd mice. *Exp Eye Res*, 88, 589-99.
- LIN, H. H., STACEY, M., STEIN-STREILEIN, J. & GORDON, S. 2010. F4/80: the macrophage-specific adhesion-GPCR and its role in immunoregulation. *Adv Exp Med Biol*, 706, 149-56.
- LINDQVIST, N., LIU, Q., ZAJADACZ, J., FRANZE, K. & REICHENBACH, A. 2010. Retinal glial (Muller ) cells: sensing and responding to tissue stretch. *Invest Ophthalmol Vis Sci*, 51, 1683-90.
- LIU, X., BULGAKOV, O. V., WEN, X. H., WOODRUFF, M. L., PAWLYK, B., YANG, J., FAIN, G. L., SANDBERG, M. A., MAKINO, C. L. & LI, T. 2004. AIPL1, the protein that is defective in Leber congenital amaurosis, is essential for the biosynthesis of retinal rod cGMP phosphodiesterase. *Proc Natl Acad Sci U S A*, 101, 13903-8.
- LIU, X., YE, F., XIONG, H., HU, D.-N., LIMB, G. A., XIE, T., PENG, L., ZHANG, P., WEI, Y. & ZHANG, W. 2015. IL-1 $\beta$  induces IL-6 production in retinal Müller cells predominantly through the activation of p38 MAPK/NF- $\kappa$ B signaling pathway. *Experimental Cell Research*, 331, 223-231.
- LORENZ, B., GYURUS, P., PREISING, M., BREMSER, D., GU, S., ANDRASSI, M., GERTH, C. & GAL, A. 2000. Early-onset severe rod-cone dystrophy in young children with RPE65 mutations. *Invest Ophthalmol Vis Sci*, 41, 2735-42.
- LU, K., CHO, C. L., LIANG, C. L., CHEN, S. D., LILIANG, P. C., WANG, S. Y. & CHEN, H. J. 2007. Inhibition of the MEK/ERK pathway reduces microglial activation and interleukin-1-beta expression in spinal cord ischemia/reperfusion injury in rats. *J Thorac Cardiovasc Surg*, 133, 934-41.
- LU, Y. B., FRANZE, K., SEIFERT, G., STEINHAUSER, C., KIRCHHOFF, F., WOLBURG, H., GUCK, J., JANMEY, P., WEI, E. Q., KAS, J. & REICHENBACH, A. 2006. Viscoelastic properties of individual glial cells and neurons in the CNS. *Proc Natl Acad Sci U S A*, 103, 17759-64.
- LU, Y. B., IANDIEV, I., HOLLBORN, M., KORBER, N., ULBRICHT, E., HIRRLINGER, P. G., PANNICKE, T., WEI, E. Q., BRINGMANN, A., WOLBURG, H., WILHELMSSON, U., PEKNY, M., WIEDEMANN, P., REICHENBACH, A. & KAS, J. A. 2011. Reactive glial cells: increased stiffness correlates with increased intermediate filament expression. *FASEB J*, 25, 624-31.
- LU, Y. B., PANNICKE, T., WEI, E. Q., BRINGMANN, A., WIEDEMANN, P., HABERMANN, G., BUSE, E., KAS, J. A. & REICHENBACH, A. 2013. Biomechanical properties of retinal glial cells: comparative and developmental data. *Exp Eye Res*, 113, 60-5.
- MA, C., PAPERMASTER, D. & CEPKO, C. L. 1998. A unique pattern of photoreceptor degeneration in cyclin D1 mutant mice. *Proc Natl Acad Sci U S A*, 95, 9938-43.

- MADEIRA, M. H., BOIA, R., SANTOS, P. F., AMBROSIO, A. F. & SANTIAGO, A. R. 2015. Contribution of microglia-mediated neuroinflammation to retinal degenerative diseases. *Mediators Inflamm*, 2015, 673090.
- MANTEGAZZA, A. R., MAGALHAES, J. G., AMIGORENA, S. & MARKS, M. S. 2013. Presentation of phagocytosed antigens by MHC class I and II. *Traffic*, 14, 135-52.
- MARTIN, C. A., LONGMAN, E., WOODING, C., HOOSDALLY, S. J., ALI, S., AITMAN, T. J., GUTMANN, D. A., FREEMONT, P. S., BYRNE, B. & LINTON, K. J. 2007. Cd36, a class B scavenger receptor, functions as a monomer to bind acetylated and oxidized low-density lipoproteins. *Protein Sci*, 16, 2531-41.
- MARTINEZ, F. O. & GORDON, S. 2014. The M1 and M2 paradigm of macrophage activation: time for reassessment. *F1000Prime Rep*, 6, 13.
- MASLAND, R. H. 2012. The neuronal organization of the retina. *Neuron*, 76, 266-80.
- MILLS, C. D., KINCAID, K., ALT, J. M., HEILMAN, M. J. & HILL, A. M. 2000. M-1/M-2 macrophages and the Th1/Th2 paradigm. *J Immunol*, 164, 6166-73.
- MINETT, T., CLASSEY, J., MATTHEWS, F. E., FAHRENHOLD, M., TAGA, M., BRAYNE, C., INCE, P. G., NICOLL, J. A., BOCHE, D. & MRC, C. 2016. Microglial immunophenotype in dementia with Alzheimer's pathology. *J Neuroinflammation*, 13, 135.
- MORGANTI, J. M., NASH, K. R., GRIMMIG, B. A., RANJIT, S., SMALL, B., BICKFORD, P. C. & GEMMA, C. 2012. The soluble isoform of CX3CL1 is necessary for neuroprotection in a mouse model of Parkinson's disease. *J Neurosci*, 32, 14592-601.
- MORROW, E. M., FURUKAWA, T., RAVIOLA, E. & CEPKO, C. L. 2005. Synaptogenesis and outer segment formation are perturbed in the neural retina of Crx mutant mice. *BMC Neurosci*, 6, 5.
- NG, T. K., FORTINO, V. R., PELAEZ, D. & CHEUNG, H. S. 2014. Progress of mesenchymal stem cell therapy for neural and retinal diseases. *World J Stem Cells*, 6, 111-9.
- NIMMERJAHN, A., KIRCHHOFF, F. & HELMCHEN, F. 2005. Resting microglial cells are highly dynamic surveillants of brain parenchyma in vivo. *Science*, 308, 1314-8.
- NISHIGUCHI, K. M., CARVALHO, L. S., RIZZI, M., POWELL, K., HOLTHAUS, S. M., AZAM, S. A., DURAN, Y., RIBEIRO, J., LUHMANN, U. F., BAINBRIDGE, J. W., SMITH, A. J. & ALI, R. R. 2015. Gene therapy restores vision in rd1 mice after removal of a confounding mutation in Gpr179. *Nat Commun*, 6, 6006.
- NOAILLES, A., FERNANDEZ-SANCHEZ, L., LAX, P. & CUENCA, N. 2014. Microglia activation in a model of retinal degeneration and TUDCA neuroprotective effects. *J Neuroinflammation*, 11, 186.
- NOAILLES, A., MANEU, V., CAMPELLO, L., GOMEZ-VICENTE, V., LAX, P. & CUENCA, N. 2016. Persistent inflammatory state after photoreceptor loss in an animal model of retinal degeneration. *Sci Rep*, 6, 33356.
- NORDEN, D. M., MUCCIGROSSO, M. M. & GODBOUT, J. P. 2015. Microglial priming and enhanced reactivity to secondary insult in aging, and traumatic CNS injury, and neurodegenerative disease. *Neuropharmacology*, 96, 29-41.
- ODERFELD-NOWAK, B., JEGLINSKI, W., SKUP, M., SKANGIEL-KRAMSKA, J., ZAREMBA, M. & KOCZYK, D. 1993. Differential effects of GM1 ganglioside treatment on glial fibrillary acidic protein content in the rat septum and hippocampus after partial interruption of their connections. *J Neurochem*, 61, 116-9.
- ODERFELD-NOWAK, B., JEGLIŃSKI, W., SKUP, M., SKANGIEL-KRAMSKA, J., ZAREMBA, M. & KOCZYK, D. 1993. Differential effects of GM1 ganglioside treatment on glial fibrillary acidic protein content in the rat septum and hippocampus after partial interruption of their connections. *Journal of neurochemistry*, 61, 116-119.
- ORTIN-MARTINEZ, A., NADAL-NICOLAS, F. M., JIMENEZ-LOPEZ, M., ALBURQUERQUE-BEJAR, J. J., NIETO-LOPEZ, L., GARCIA-AYUSO, D., VILLEGAS-PEREZ, M. P., VIDAL-SANZ, M. & AGUDO-BARRIUSO, M. 2014. Number and distribution of mouse retinal cone photoreceptors:

- differences between an albino (Swiss) and a pigmented (C57/BL6) strain. *PLoS One*, 9, e102392.
- OTERO, K., TURNBULL, I. R., POLIANI, P. L., VERMI, W., CERUTTI, E., AOSHI, T., TASSI, I., TAKAI, T., STANLEY, S. L., MILLER, M., SHAW, A. S. & COLONNA, M. 2009. Macrophage colony-stimulating factor induces the proliferation and survival of macrophages via a pathway involving DAP12 and beta-catenin. *Nat Immunol*, 10, 734-43.
- PAOLICELLI, R. C., BOLASCO, G., PAGANI, F., MAGGI, L., SCIANNI, M., PANZANELLI, P., GIUSTETTO, M., FERREIRA, T. A., GUIDUCCI, E. & DUMAS, L. 2011. Synaptic pruning by microglia is necessary for normal brain development. *science*, 333, 1456-1458.
- PATEL, A. R., RITZEL, R., MCCULLOUGH, L. D. & LIU, F. 2013. Microglia and ischemic stroke: a double-edged sword. *Int J Physiol Pathophysiol Pharmacol*, 5, 73-90.
- PELLIKKA, M., TANENTZAPF, G., PINTO, M., SMITH, C., MCGLADE, C. J., READY, D. F. & TEPASS, U. 2002. Crumbs, the Drosophila homologue of human CRB1/RP12, is essential for photoreceptor morphogenesis. *Nature*, 416, 143-9.
- PENFOLD, P. L., LIEW, S. C., MADIGAN, M. C. & PROVIS, J. M. 1997. Modulation of major histocompatibility complex class II expression in retinas with age-related macular degeneration. *Invest Ophthalmol Vis Sci*, 38, 2125-33.
- PENN, J. S., NAASH, M. I. & ANDERSON, R. E. 1987. Effect of light history on retinal antioxidants and light damage susceptibility in the rat. *Exp Eye Res*, 44, 779-88.
- PENNESI, M. E., MICHAELS, K. V., MAGEE, S. S., MARICLE, A., DAVIN, S. P., GARG, A. K., GALE, M. J., TU, D. C., WEN, Y., ERKER, L. R. & FRANCIS, P. J. 2012. Long-term characterization of retinal degeneration in rd1 and rd10 mice using spectral domain optical coherence tomography. *Invest Ophthalmol Vis Sci*, 53, 4644-56.
- PERRY, V. H. & TEELING, J. 2013. Microglia and macrophages of the central nervous system: the contribution of microglia priming and systemic inflammation to chronic neurodegeneration. *Semin Immunopathol*, 35, 601-12.
- PIGNATELLI, V., CEPKO, C. L. & STRETTOI, E. 2004. Inner retinal abnormalities in a mouse model of Leber's congenital amaurosis. *J Comp Neurol*, 469, 351-9.
- PORTERA-CAILLIAU, C., SUNG, C. H., NATHANS, J. & ADLER, R. 1994. Apoptotic photoreceptor cell death in mouse models of retinitis pigmentosa. *Proc Natl Acad Sci U S A*, 91, 974-8.
- PORTO, F. B., PERRAULT, I., HICKS, D., ROZET, J. M., HANOTEAU, N., HANEIN, S., KAPLAN, J. & SAHEL, J. A. 2002. Prenatal human ocular degeneration occurs in Leber's congenital amaurosis (LCA2). *J Gene Med*, 4, 390-6.
- PORTO, F. B., PERRAULT, I., HICKS, D., ROZET, J. M., HANOTEAU, N., HANEIN, S., KAPLAN, J. & SAHEL, J. A. 2003. Prenatal human ocular degeneration occurs in Leber's Congenital Amaurosis (LCA1 and 2). *Adv Exp Med Biol*, 533, 59-68.
- PRINZ, M., ERNY, D. & HAGEMEYER, N. 2017. Ontogeny and homeostasis of CNS myeloid cells. *Nat Immunol*, 18, 385-392.
- PROVIS, J. M. 2001. Development of the primate retinal vasculature. *Prog Retin Eye Res*, 20, 799-821.
- PUNZO, C. & CEPKO, C. 2007. Cellular responses to photoreceptor death in the rd1 mouse model of retinal degeneration. *Invest Ophthalmol Vis Sci*, 48, 849-57.
- PUNZO, C., KORNACKER, K. & CEPKO, C. L. 2009. Stimulation of the insulin/mTOR pathway delays cone death in a mouse model of retinitis pigmentosa. *Nat Neurosci*, 12, 44-52.
- RANSOHOFF, R. M. 2016. How neuroinflammation contributes to neurodegeneration. *Science*, 353, 777-83.
- REDMOND, T. M., YU, S., LEE, E., BOK, D., HAMASAKI, D., CHEN, N., GOLETZ, P., MA, J. X., CROUCH, R. K. & PFEIFER, K. 1998. Rpe65 is necessary for production of 11-cis-vitamin A in the retinal visual cycle. *Nat Genet*, 20, 344-51.
- REN, K. & DUBNER, R. 2010. Interactions between the immune and nervous systems in pain. *Nature medicine*, 16, 1267-1276.

- ROCHE, S. L., WYSE-JACKSON, A. C., GOMEZ-VICENTE, V., LAX, P., RUIZ-LOPEZ, A. M., BYRNE, A. M., CUENCA, N. & COTTER, T. G. 2016. Progesterone Attenuates Microglial-Driven Retinal Degeneration and Stimulates Protective Fractalkine-CX3CR1 Signaling. *PLoS One*, 11, e0165197.
- ROHRER, B., PINTO, F. R., HULSE, K. E., LOHR, H. R., ZHANG, L. & ALMEIDA, J. S. 2004. Multidestructive pathways triggered in photoreceptor cell death of the rd mouse as determined through gene expression profiling. *J Biol Chem*, 279, 41903-10.
- ROMANO, C., PRICE, M. T. & OLNEY, J. W. 1995. Delayed excitotoxic neurodegeneration induced by excitatory amino acid agonists in isolated retina. *J Neurochem*, 65, 59-67.
- ROOSING, S., THIADENS, A. A., HOYNG, C. B., KLAVER, C. C., DEN HOLLANDER, A. I. & CREMERS, F. P. 2014. Causes and consequences of inherited cone disorders. *Prog Retin Eye Res*, 42, 1-26.
- RYMO, S. F., GERHARDT, H., SAND, F. W., LANG, R., UV, A. & BETSHOLTZ, C. 2011. A two-way communication between microglial cells and angiogenic sprouts regulates angiogenesis in aortic ring cultures. *PloS one*, 6, e15846.
- SANTOS, A. M., CALVENTE, R., TASSI, M., CARRASCO, M. C., MARTIN-OLIVA, D., MARIN-TEVA, J. L., NAVASCUES, J. & CUADROS, M. A. 2008. Embryonic and postnatal development of microglial cells in the mouse retina. *J Comp Neurol*, 506, 224-39.
- SASAHARA, M., OTANI, A., OISHI, A., KOJIMA, H., YODOI, Y., KAMEDA, T., NAKAMURA, H. & YOSHIMURA, N. 2008. Activation of bone marrow-derived microglia promotes photoreceptor survival in inherited retinal degeneration. *Am J Pathol*, 172, 1693-703.
- SCHAFER, D. P., LEHRMAN, E. K., KAUTZMAN, A. G., KOYAMA, R., MARDINLY, A. R., YAMASAKI, R., RANSOHOFF, R. M., GREENBERG, M. E., BARRES, B. A. & STEVENS, B. 2012. Microglia sculpt postnatal neural circuits in an activity and complement-dependent manner. *Neuron*, 74, 691-705.
- SCHIETROMA, C., PARAIN, K., ESTIVALET, A., AGHAIE, A., BOUTET DE MONVEL, J., PICAUD, S., SAHEL, J. A., PERRON, M., EL-AMRAOUI, A. & PETIT, C. 2017. Usher syndrome type 1-associated cadherins shape the photoreceptor outer segment. *J Cell Biol*, 216, 1849-1864.
- SEITZ, R. & TAMM, E. R. 2014. Muller cells and microglia of the mouse eye react throughout the entire retina in response to the procedure of an intravitreal injection. *Adv Exp Med Biol*, 801, 347-53.
- SEMO, M. A., VUGLER, A. A. & JEFFERY, G. 2007. Paradoxical opsin expressing cells in the inner retina that are augmented following retinal degeneration. *European Journal of Neuroscience*, 25, 2296-2306.
- SERNAGOR, E. 2006. *Retinal development*, Cambridge University Press.
- SHEN, W., FRUTTIGER, M., ZHU, L., CHUNG, S. H., BARNETT, N. L., KIRK, J. K., LEE, S., COOREY, N. J., KILLINGSWORTH, M., SHERMAN, L. S. & GILLIES, M. C. 2012. Conditional Muller cell ablation causes independent neuronal and vascular pathologies in a novel transgenic model. *J Neurosci*, 32, 15715-27.
- SHIN, J. A., KIM, H. S., VARGAS, A., YU, W. Q., EOM, Y. S., CRAFT, C. M. & LEE, E. J. 2016. Inhibition of Matrix Metalloproteinase 9 Enhances Rod Survival in the S334ter-line3 Retinitis Pigmentosa Model. *PLoS One*, 11, e0167102.
- SHINOZAKI, Y., SHIBATA, K., YOSHIDA, K., SHIGETOMI, E., GACHET, C., IKENAKA, K., TANAKA, K. F. & KOIZUMI, S. 2017. Transformation of Astrocytes to a Neuroprotective Phenotype by Microglia via P2Y1 Receptor Downregulation. *Cell Rep*, 19, 1151-1164.
- STASHEFF, S. F. 2008. Emergence of sustained spontaneous hyperactivity and temporary preservation of OFF responses in ganglion cells of the retinal degeneration (rd1) mouse. *J Neurophysiol*, 99, 1408-21.
- STINGL, K., BARTZ-SCHMIDT, K. U., BESCH, D., BRAUN, A., BRUCKMANN, A., GEKELER, F., GREPPMAIER, U., HIPPEL, S., HORTDORFER, G., KERNSTOCK, C., KOITSCHIEV, A., KUSNYERIK, A., SACHS, H., SCHATZ, A., STINGL, K. T., PETERS, T., WILHELM, B. & ZRENNER, E. 2013. Artificial

- vision with wirelessly powered subretinal electronic implant alpha-IMS. *Proc Biol Sci*, 280, 20130077.
- STREIT, W. J., SAMMONS, N. W., KUHNS, A. J. & SPARKS, D. L. 2004. Dystrophic microglia in the aging human brain. *Glia*, 45, 208-12.
- SYEDA, S., PATEL, A. K., LEE, T. & HACKAM, A. S. 2015. Reduced photoreceptor death and improved retinal function during retinal degeneration in mice lacking innate immunity adaptor protein MyD88. *Exp Neurol*, 267, 1-12.
- SZEL, A., ROHLICH, P., CAFFE, A. R., JULIUSSON, B., AGUIRRE, G. & VAN VEEN, T. 1992. Unique topographic separation of two spectral classes of cones in the mouse retina. *J Comp Neurol*, 325, 327-42.
- THANOS, S. 1992. Sick photoreceptors attract activated microglia from the ganglion cell layer: a model to study the inflammatory cascades in rats with inherited retinal dystrophy. *Brain Res*, 588, 21-8.
- THANOS, S. & RICHTER, W. 1993. The migratory potential of vitally labelled microglial cells within the retina of rats with hereditary photoreceptor dystrophy. *Int J Dev Neurosci*, 11, 671-80.
- TOKUDA, K., TSUKAMOTO, T., FUJISAWA, S. & MATSUBARA, M. 2004. Evaluation of toxicity due to vital stains in isolated rat retinas. *Acta Ophthalmol Scand*, 82, 189-94.
- TORRES-PLATAS, S. G., COMEAU, S., RACHALSKI, A., BO, G. D., CRUCEANU, C., TURECKI, G., GIROS, B. & MECHAWAR, N. 2014. Morphometric characterization of microglial phenotypes in human cerebral cortex. *J Neuroinflammation*, 11, 12.
- TREMBLAY, M. E., LOWERY, R. L. & MAJEWSKA, A. K. 2010. Microglial interactions with synapses are modulated by visual experience. *PLoS Biol*, 8, e1000527.
- TUCKER, C. L., RAMAMURTHY, V., PINA, A. L., LOYER, M., DHARMARAJ, S., LI, Y., MAUMENEE, I. H., HURLEY, J. B. & KOENKOOP, R. K. 2004. Functional analyses of mutant recessive GUCY2D alleles identified in Leber congenital amaurosis patients: protein domain comparisons and dominant negative effects. *Mol Vis*, 10, 297-303.
- VALLE-ARGOS, B., GOMEZ-NICOLA, D. & NIETO-SAMPEDRO, M. 2010. Glioma growth inhibition by neurostatin and O-But GD1b. *Neuro Oncol*, 12, 1135-46.
- VALLE-ARGOS, B., GOMEZ-NICOLA, D. & NIETO-SAMPEDRO, M. 2011. Neurostatin blocks glioma cell cycle progression by inhibiting EGFR activation. *Mol Cell Neurosci*, 46, 89-100.
- VAN HUET, R. A., ESTRADA-CUZCANO, A., BANIN, E., ROTENSTREICH, Y., HIPPEL, S., KOHL, S., HOYNG, C. B., DEN HOLLANDER, A. I., COLLIN, R. W. & KLEVERING, B. J. 2013. Clinical characteristics of rod and cone photoreceptor dystrophies in patients with mutations in the C8orf37 gene. *Invest Ophthalmol Vis Sci*, 54, 4683-90.
- VECINO, E., HERNANDEZ, M. & GARCIA, M. 2004. Cell death in the developing vertebrate retina. *Int J Dev Biol*, 48, 965-74.
- VECKENEER, M., OVERDAM, K., MONZER, J., KOBUCH, K., MARLE, W., SPEKREIJSE, H. & MEURS, J. 2001. Ocular toxicity study of trypan blue injected into the vitreous cavity of rabbit eyes. *Graefe's archive for clinical and experimental ophthalmology*, 239, 698-704.
- VERBAKEL, S. K., VAN HUET, R. A. C., BOON, C. J. F., DEN HOLLANDER, A. I., COLLIN, R. W. J., KLAVER, C. C. W., HOYNG, C. B., ROEPMAN, R. & KLEVERING, B. J. 2018. Non-syndromic retinitis pigmentosa. *Prog Retin Eye Res*, 66, 157-186.
- VOGLER, S., PANNICKE, T., HOLLBORN, M., GROSCHE, A., BUSCH, S., HOFFMANN, S., WIEDEMANN, P., REICHENBACH, A., HAMMES, H. P. & BRINGMANN, A. 2013. Muller cell reactivity in response to photoreceptor degeneration in rats with defective polycystin-2. *PLoS One*, 8, e61631.
- VON BERNHARDI, R., EUGENIN-VON BERNHARDI, L. & EUGENIN, J. 2015. Microglial cell dysregulation in brain aging and neurodegeneration. *Front Aging Neurosci*, 7, 124.
- WANG, M., MA, W., ZHAO, L., FARISS, R. N. & WONG, W. T. 2011. Adaptive Muller cell responses to microglial activation mediate neuroprotection and coordinate inflammation in the retina. *J Neuroinflammation*, 8, 173.

- WANG, M., WANG, X., ZHAO, L., MA, W., RODRIGUEZ, I. R., FARISS, R. N. & WONG, W. T. 2014. Macroglia-microglia interactions via TSP0 signaling regulates microglial activation in the mouse retina. *J Neurosci*, 34, 3793-806.
- WANG, X., ZHAO, L., ZHANG, J., FARISS, R. N., MA, W., KRETSCHMER, F., WANG, M., QIAN, H. H., BADEA, T. C., DIAMOND, J. S., GAN, W. B., ROGER, J. E. & WONG, W. T. 2016. Requirement for Microglia for the Maintenance of Synaptic Function and Integrity in the Mature Retina. *J Neurosci*, 36, 2827-42.
- WEIGELT, K., ERNST, W., WALCZAK, Y., EBERT, S., LOENHARDT, T., KLUG, M., REHLI, M., WEBER, B. H. & LANGMANN, T. 2007. Dap12 expression in activated microglia from retinoschisin-deficient retina and its PU.1-dependent promoter regulation. *J Leukoc Biol*, 82, 1564-74.
- WHITE, D. T., SENGUPTA, S., SAXENA, M. T., XU, Q., HANES, J., DING, D., JI, H. & MUMM, J. S. 2017. Immunomodulation-accelerated neuronal regeneration following selective rod photoreceptor cell ablation in the zebrafish retina. *Proc Natl Acad Sci U S A*, 114, E3719-E3728.
- WINKLER, B. S., ARNOLD, M. J., BRASSELL, M. A. & PURO, D. G. 2000. Energy metabolism in human retinal Muller cells. *Invest Ophthalmol Vis Sci*, 41, 3183-90.
- WONG-RILEY, M. T. 2010. Energy metabolism of the visual system. *Eye Brain*, 2, 99-116.
- XU, H., CHEN, M., MAYER, E. J., FORRESTER, J. V. & DICK, A. D. 2007. Turnover of resident retinal microglia in the normal adult mouse. *Glia*, 55, 1189-98.
- YANG, J., ZHANG, L., YU, C., YANG, X.-F. & WANG, H. 2014. Monocyte and macrophage differentiation: circulation inflammatory monocyte as biomarker for inflammatory diseases. *Biomarker research*, 2, 1.
- YOSHIDA, N., IKEDA, Y., NOTOMI, S., ISHIKAWA, K., MURAKAMI, Y., HISATOMI, T., ENAIDA, H. & ISHIBASHI, T. 2013. Laboratory evidence of sustained chronic inflammatory reaction in retinitis pigmentosa. *Ophthalmology*, 120, e5-12.
- YOUM, Y. H., GRANT, R. W., MCCABE, L. R., ALBARADO, D. C., NGUYEN, K. Y., RAVUSSIN, A., PISTELL, P., NEWMAN, S., CARTER, R., LAQUE, A., MUNZBERG, H., ROSEN, C. J., INGRAM, D. K., SALBAUM, J. M. & DIXIT, V. D. 2013. Canonical Nlrp3 inflammasome links systemic low-grade inflammation to functional decline in aging. *Cell Metab*, 18, 519-32.
- ZABEL, M. K., ZHAO, L., ZHANG, Y., GONZALEZ, S. R., MA, W., WANG, X., FARISS, R. N. & WONG, W. T. 2016. Microglial phagocytosis and activation underlying photoreceptor degeneration is regulated by CX3CL1-CX3CR1 signaling in a mouse model of retinitis pigmentosa. *Glia*, 64, 1479-91.
- ZENG, H. Y., ZHU, X. A., ZHANG, C., YANG, L. P., WU, L. M. & TSO, M. O. 2005. Identification of sequential events and factors associated with microglial activation, migration, and cytotoxicity in retinal degeneration in rd mice. *Invest Ophthalmol Vis Sci*, 46, 2992-9.
- ZHAO, L., ZABEL, M. K., WANG, X., MA, W., SHAH, P., FARISS, R. N., QIAN, H., PARKHURST, C. N., GAN, W. B. & WONG, W. T. 2015. Microglial phagocytosis of living photoreceptors contributes to inherited retinal degeneration. *EMBO Mol Med*, 7, 1179-97.
- ZHAO, T., LI, Y., WENG, C. & YIN, Z. 2012. The changes of potassium currents in RCS rat Muller cell during retinal degeneration. *Brain Res*, 1427, 78-87.
- ZHAO, Y., HONG, D. H., PAWLYK, B., YUE, G., ADAMIAN, M., GRYNBERG, M., GODZIK, A. & LI, T. 2003. The retinitis pigmentosa GTPase regulator (RPGR)- interacting protein: subserving RPGR function and participating in disk morphogenesis. *Proc Natl Acad Sci U S A*, 100, 3965-70.
- ZHU, C. L., JI, Y., LEE, E. J. & GRZYWACZ, N. M. 2013. Spatiotemporal pattern of rod degeneration in the S334ter-line-3 rat model of retinitis pigmentosa. *Cell Tissue Res*, 351, 29-40.
- ZIEBELL, J. M. & MORGANTI-KOSSMANN, M. C. 2010. Involvement of pro- and anti-inflammatory cytokines and chemokines in the pathophysiology of traumatic brain injury. *Neurotherapeutics*, 7, 22-30.
- ZINKERNAGEL, M. S., CHINNERY, H. R., ONG, M. L., PETITJEAN, C., VOIGT, V., MCLENACHAN, S., MCMENAMIN, P. G., HILL, G. R., FORRESTER, J. V., WIKSTROM, M. E. & DEGLI-ESPOSTI, M. A.

2013. Interferon gamma-dependent migration of microglial cells in the retina after systemic cytomegalovirus infection. *Am J Pathol*, 182, 875-85.